Fortschritt-Berichte VDI

VDI

Reihe 5

Grund- und Werkstoffe/ Kunststoffe

Nr. 760

Dipl.-Chem. Ludmilla Derr, Bremen

# Interactions between enzymes and oxide colloidal particles and their influence on enzymatic activity

# Interactions between enzymes and oxide colloidal particles and their influence on enzymatic activity

Dem Fachbereich Produktionstechnik

der

UNIVERSITÄT BREMEN

zur Erlangung des Grades
Doktor-Ingenieur
vorgelegte

Dissertation

von

Diplom-Chemikerin

Ludmilla Derr

Gutachter:
Prof. Dr.-Ing. Kurosch Rezwan, Universität Bremen
Prof. Dr.-Ing. Jorg Thöming, Universität Bremen

Tag der mündlichen Prüfung: 11. März 2016

Fortschritt-Berichte VDI

Reihe 5

Grund- und Werkstoffe/ Kunststoffe

Dipl.-Chem. Ludmilla Derr, Bremen

Nr. 760

# Interactions between enzymes and oxide colloidal particles and their influence on enzymatic activity

VDI verlag

Derr, Ludmilla
**Interactions between enzymes and oxide colloidal particles and their influence on enzymatic activity**
Fortschr.-Ber. VDI Reihe 5 Nr. 760. Düsseldorf: VDI Verlag 2016.
210 Seiten, 66 Bilder, 9 Tabellen.
ISBN 978-3-18-376005-3, ISSN 0178-952X,
€ 76,00/VDI-Mitgliederpreis € 68,40.

**Keywords:** α-chymotrypsin – Adsorption – Colloidal particles – Physisorption – Covalent immobilization – Enzyme immobilization – Enzymatic activity – Alumina – Silica – Titania

Enzyme immobilization on inorganic oxide particles is a widely employed technique that permits the reuse of costly enzymes in catalytic processes. The aim of this study was to investigate the effects of adsorption on ceramic particles on the catalytic activities of enzymes. The adsorption of the proteolytic enzyme α-chymotrypsin on silica, alumina, and titania was studied. The enzyme adsorption was specifically investigated by material characterization before and after adsorption, quantification of the adsorbed enzyme and detailed enzymatic activity measurements. Furthermore, the experimental results were interpreted based on complementary simulations. Covalent enzyme immobilization on amino-functionalized alumina and silica was also performed. Its effects on the enzymatic activity of α-chymotrypsin were additionally investigated by employing matrix-assisted laser desorption ionization time-of-flight mass spectroscopy.

**Bibliographische Information der Deutschen Bibliothek**
Die Deutsche Bibliothek verzeichnet diese Publikation in der Deutschen Nationalbibliographie; detaillierte bibliographische Daten sind im Internet unter http://dnb.ddb.de abrufbar.

**Bibliographic information published by the Deutsche Bibliothek**
(German National Library)
The Deutsche Bibliothek lists this publication in the Deutsche Nationalbibliographie (German National Bibliography); detailed bibliographic data is available via Internet at http://dnb.ddb.de.

Dissertation Universität Bremen



ISSN 0178-952X
ISBN 978-3-18-376005-3

# Acknowledgments

I would like to acknowledge my thesis supervisor, Prof. Kurosch Rezwan, for the opportunity to complete this PhD thesis project and for the scientific freedom that he gave me during the years of my PhD studies.

I would also like to express my gratitude to my co-supervisor Prof. Jorg Thöming for being the co-examiner of this thesis.

Moreover, I would like to give special thanks to my collaborators Prof. Ralf Dringen, Prof. Lucio Colombi Ciacchi, Dr. Susan Köppen and Nils Hildebrand for motivating and valuable discussions.

Thanks to all colleagues from the working groups of Prof. Dringen and Prof. Colombi Ciacchi for their assistance, fruitful discussions and friendly collaboration over the course of numerous days in the laboratory.

Thanks to my officemates and friends Eduardo Meller, Karoline Pardun and Alieh Aminian for their support, for numerous scientific discussions and for a wonderfully friendly atmosphere in the office.

Furthermore, I would like to thank my colleagues Cristian Nuortila, Christian Ellenberg and Gabriela Berger for wonderful non-scientific discussions. Many thanks to all of my colleagues from the Advanced Ceramics Group for the friendly working atmosphere and their interest in my work.

I would like to thank my parents Tamara and Sergej Derr, my friends and my Kung Fu family for their support and their trust in me throughout the years of my PhD studies.

Last but certainly not least, I would like to thank Peter for his support, his motivation, his serenity, great discussions, and his constant trust in me over the last few years.

Ludmilla

*"Life can only be understood backwards; but it must be lived forwards."*

*Søren Kierkegaard*

*To M. F. C.*

# Contents

# List of abbreviations and symbols

*Abbreviations:*

| | |
|---|---|
| AFM | Atomic force microscopy |
| $Al_2O_3$ | α-$Al_2O_3$, alumina |
| Al-OH | Hydroxyl groups on alumina surface |
| APBS | Adaptive Poisson-Boltzmann Solver |
| Asp | Aspartic acid |
| BCA | Bicinchoninic acid |
| BCA assay | Bicinchoninic acid protein assay |
| BET equation | Brunauer, Emmet, and Teller equation |
| CD | Circular dichroism |
| -COOH | Carboxyl group |
| $Cu^{2+}$, $Cu^{+}$ | Cuprous cations |
| CVD | Chemical vapor deposition |
| CVI | Colloidal vibration current |
| $d_{50}$ | Median of particle size |
| Da | Dalton, atomic mass unit (1 Da = 1 g $mol^{-1}$) |
| $ddH_2O$ | Double deionized water |
| DLS | Dynamic light scattering |
| DLVO theory | Derjaguin, Landau, Verwey, and Overbeck theory |
| DSSP | Define Secondary Structure of Proteins method |
| FT-IR | Fourier transform infrared spectroscopy |
| GRCEL | Glycylarginylcysteinylglutamylleucine |
| HCl | Hydrochloric acid |
| HR-TEM | High-resolution transmission electron microscopy |
| E | Enzyme |
| ES | Enzyme-substrate complex |
| His | Histidine |
| IEP | Isoelectric point |
| ITC | Isothermal titration calorimetry |
| KBr | Potassium bromide |
| KOH | Potassium hydroxide |
| LEaP | Link, Edit and Parm program |
| LINCS | 'Linear constraint solver' algorithm |
| MALDI-ToF-MS | Matrix-assisted laser desorption ionization time-of-flight mass spectroscopy |
| MD | Molecular Dynamics simulations |
| MRSL | Methionylarginylserinylleucine |

| | |
|---|---|
| MRW | Mean residue weight |
| MS | Mass spectroscopy |
| MUSIC | Multi site complexation model |
| $-NH_2$ | Amino group |
| NMR | Nuclear magnetic resonance spectroscopy |
| -OH | Hydroxyl group |
| P | Product |
| $PAA_{SEM}$ | Theoretical protein accessible area based on SEM images |
| PDB | Brookhaven Protein Database |
| PZC | Point of zero charge |
| RDF | Radial distribution function |
| RSA | Random sequential adsorption |
| S | Substrate |
| SD | Standard deviation |
| SDS-PAGE | Sodium dodecyl sulfate-polyacrylamide gel electrophoresis |
| SEM | Scanning electron microscopy |
| Ser | Serine |
| $SiO_2$ | Silicon dioxide, silica |
| SPR | Surface Plasmon resonance |
| $SSA_{BET}$ | Specific surface area calculated using BET equation |
| TEM | Transmission electron microscopy |
| TIP3P | Water model |
| $TiO_2$ | Titanium dioxide, titania |
| UV-Vis | Ultraviolet-visible |
| VMD | Visual Molecular Dynamics |

*Symbols:*

| | |
|---|---|
| Å | Ångström, 1 Å = 0.1 nm |
| A | Absorption in Lambert-Beer law |
| $K_a$ | Acid dissociation constant |
| $Z_S$ | Acoustic impedances of the suspension |
| $Z_T$ | Acoustic impedances of the transducer |
| A (ω) | Acoustic wave frequency |
| N | Avogadro's number ($6.02214129 * 10^{23}$ $mol^{-1}$) |
| $k_B$ | Boltzmann constant ($1.3806488 * 10^{-23}$ $m^2$ kg $s^{-2}$ $K^{-1}$) |

| | |
|---|---|
| ψ | Bond between the α-carbon and the carbonyl carbon in proteins |
| Φ | Bond between the nitrogen and the α-carbon in proteins |
| x, y, and z | Cartesian coordinates |
| $[E_{free}]$ | Concentration of free enzyme |
| $c_i^0$ | Concentration of ion i in the bulk medium |
| c′ | Concentration of the optically active substance |
| θ | Coverage of the surface with proteins |
| α | Cross-sectional area of a gas nitrogen molecule |
| $x_D$ | Debye-Huckel length |
| ρ | Density |
| $\rho_m$ | Density of the medium |
| $\rho_p$ | Density of the particles |
| $K_d$ | Dissociation constant |
| x | Distance from particle surface |
| $W_{DLVO}$ | DLVO interaction energy |
| $\mu_D$ | Dynamic electrophoretic mobility of the particles |
| $I_n$ | Electric current, which compensates for $I_s$ |
| $K^\infty$ | Electrical conductivity of the medium |
| $W_{DL}$ | Electrostatic interaction energy |
| ψ | Electrostatic potential at a given position in the diffuse layer |
| e | Elementary charge |
| Θ | Ellipticity |
| H | Enthalpy |
| S | Entropy |
| K | Equilibrium constant |
| E | Extinction |
| ε | Extinction coefficient |
| $S_0$ | Free adsorption sites |
| M | Frequency of the acoustic wave |
| p | Gas pressure |
| G | Gibbs energy |
| A | Hamaker constant |
| h | Hour |
| $v_0$ | Initial velocity |
| $I_0$ | Intensity of incident light |
| I | Intensity of transmitted light |
| I | Ionic strength |
| v | Kinematic viscosity |

| | |
|---|---|
| $K_L$ | Langmuir constant |
| $c_i$ | Local ion density |
| $p_e$ | Local electric charge density in the diffuse layer |
| $\beta_{ii}$ | London-van der Waals constant |
| $W_{vdW}$ | London-van der Waals interaction potential |
| m/ z | Mass-to-charge ratio |
| $\Gamma_{max}$ | Maximal adsorbed protein amount |
| $V_{max}$ | Maximum velocity of the reaction |
| $[\Theta]_{MRW}$ | Mean molar ellipticity |
| $K_M$ | Michaelis-Menten constant |
| $[\Theta]$ | Molar ellipticity |
| M | Molecular weight of the adsorbate |
| $pK_a$ | Negative decimal logarithm of the acid dissociation constant |
| $S_{ads}$ | Number of adsorption sites occupied with proteins or the adsorbed protein concentration |
| $n_i$ | Number of atoms per unit volume |
| $S_B$ | Number of binding sites |
| v | Orbit frequency of the electron |
| $r_1$, $r_2$ | Particle radii |
| $R_1$, $R_2$ | Particle radius |
| $\Psi_0$ | Particle surface potential |
| $\varphi$ | Particle volume fraction |
| H | Particles' separation distance |
| l | Pathlength |
| $\varepsilon_0$ | Permittivity of free space ($8.854187 * 10^{-12}$ F $m^{-1}$) |
| $pH_{PZC}$ | pH of point of zero charge |
| n | Pi |
| h | Planck constant ($6.62606957 * 10^{-34}$ $m^2$ kg $s^{-1}$) |
| $\alpha$ | Polarizability of the material |
| c | Protein concentration in solution |
| $[H^+]$ | Proton activity in mol $m^{-3}$ |
| r | Radial distance at any point in the double layer from the center of the particle |
| $R_S$ | Radius of the spherical particle |
| $k_{ads}$ and $k_{des}$ | Rate constants for adsorption and desorption |
| $\kappa$ | Reciprocal Debye-Huckel length |
| K | Reciprocal of the Langmuir constant |
| $\varepsilon_r$ | Relative permittivity of the medium |
| $p_0$ | Saturation gas pressure |

| | |
|---|---|
| R | Side chain of an amino acid |
| Si-OH | Silanol group |
| Si-O-Si | Siloxane group |
| [Ψ] | Specific ellipticity |
| $\Delta_{ads} G^0$ | Standard Gibbs energy of adsorption |
| [S] | Substrate concentration |
| $\sigma_0$ | Surface charge density |
| [MOH], $MO^-$], $[MOH_2^+]$ | Surface concentrations of the corresponding surface groups |
| $K_S$ | Surface conductivity of the double layer |
| $I_S$ | Surface current |
| $N_S$ | Surface density of reactive sites (sites per $m^2$) |
| T | Temperature |
| t | Time |
| $[E_{total}]$ | Total enzyme concentration |
| $k_{cat}$ | Turnover number of the enzyme |
| $z_i$ | Valence of the ion i |
| η | Viscosity |
| $V_m$ | Volume of gas building a monolayer on the particle surface |
| $W_i$ | Work required to bring the *i*th ion to the position with the potential Ψ |
| ζ | Zeta potential |
| $\Psi_\zeta$ | Zeta potential of particles after protein adsorption |

# Summary

The aim of this study was to investigate the effects of adsorption on ceramic particles on the catalytic activities of enzymes. Although the key interaction forces that govern protein adsorption on inorganic particles are known, their influence on enzymatic activity has been poorly evaluated and difficult to predict. Enzyme immobilization on inorganic oxide particles is a widely employed technique that permits the reuse of costly enzymes in catalytic processes. An understanding of the major factors that control protein adsorption and their impact on the catalytic activities of enzymes will lead to more individualized immobilization with increased enzymatic activity after immobilization.

The adsorption of the proteolytic enzyme α-chymotrypsin on silica ($SiO_2$), alumina ($Al_2O_3$), and two types of titania ($TiO_2$) was studied. The enzyme adsorption process was specifically investigated by extensive material characterization before and after adsorption, quantification of the adsorbed enzyme and detailed enzymatic activity measurements. The assays required to investigate the enzymatic activity of the adsorbed chymotrypsin were optimized and adapted for specific application to oxide colloidal particles based on known assays for dissolved enzymes. Furthermore, the experimental results were interpreted based on complementary simulations. Covalent enzyme immobilization on amino-functionalized $Al_2O_3$ and $SiO_2$ was also performed. The effects of immobilization on the enzymatic activity of α-chymotrypsin were additionally investigated by employing matrix-assisted laser desorption ionization time-of-flight mass spectroscopy (MALDI-ToF-MS) using lysozyme as the enzyme substrate to analyze multiple lysozyme-derived peptides after proteolytic digestion. The main findings of this thesis are as follows:

*Physisorption:*

- Chymotrypsin adsorbed efficiently on all tested colloidal particles in a concentration- and pH-dependent manner; adsorption increased with increasing pH.
- Adsorption increased as the hydrophobicity of the particles increased.
- The highest adsorption affinities were exhibited by the two types of $TiO_2$, followed by $Al_2O_3$ and then $SiO_2$.

- An activity assay for adsorbed enzymes was established as a simple, rapid method to determine the changes in the catalytic activities of adsorbed enzymes.
- A substantial loss in enzymatic activity was observed after adsorption for all tested colloidal particles.
- For chymotrypsin adsorbed on $TiO_2$ (rutile), an increase in the $K_M$ value for the artificial substrate p-nitrophenyl acetate (p-NPA) was analyzed and potentially attributed to blockage of the active site or conformational changes due to adsorption.
- Lateral enzyme-enzyme interactions appeared to have little influence on enzymatic activity, which was similar for all colloidal particles and was largely independent of the surface density of the adsorbed enzymes.

*Covalent immobilization:*

- The formation of lysozyme-derived peptides was induced by covalently immobilized chymotrypsin on the surface of particles.
- Kinetic studies revealed that chymotrypsin bound to colloidal particles remained active longer than unbound chymotrypsin.
- A reduction in enzymatic activity and slower digestion kinetics were observed after immobilization to both $Al_2O_3$ and $SiO_2$ particle types.
- The loss of enzymatic activity was more pronounced for $SiO_2$ than for $Al_2O_3$ in cyclic reusability studies, likely due to differences in the digestion reaction and possible steric hindrance.
- Both materials retained lysozyme digestion activity after 7 weeks of storage at room temperature.

# Zusammenfassung

Das Ziel dieser Arbeit war die Untersuchung der Auswirkungen der Enzymadsorption auf keramischen Partikeln auf die katalytische Aktivität der Enzyme. Obwohl die wichtigen Wechselwirkungen, die die Proteinadsorption auf Oxidpartikeln beeinflussen, bekannt sind, ihr Einfluss auf die enzymatische Aktivität ist wenig untersucht und unzureichend vorhersehbar. Enzymimmobilisierung auf anorganischen Oxidpartikeln ist eine weit verbreitete Methode um die Wiederverwendbarkeit der kostspieligen Enzyme in katalytischen Prozessen zu ermöglichen. Das Verstehen der Hauptfaktoren, die die Adsorption steuern und deren Einfluss auf die katalytische Aktivität der Enzyme kann zur Auswahl einer individuelleren Immobilisierungsmethode und somit zu einer gesteigerten enzymatischen Aktivität nach der Immobilisierung führen.

Die Adsorption des proteolytischen Enzyms α-Chymotrypsin auf Siliciumoxid ($SiO_2$), Aluminiumoxid ($Al_2O_3$) und auf zwei Arten von Titanoxid ($TiO_2$) wurde erforscht. Der Prozess der Enzymadsorption wurde mit Hilfe der ausführlichen Materialcharakterisierung vor und nach der Adsorption, der Bestimmung der adsorbierten Enzymmenge und der detaillierten Messungen der enzymatischen Aktivität untersucht. Die Analysemethoden, die für die Untersuchung der katalytischen Aktivität des adsorbierten Chymotrypsin nötig waren, wurden im Rahmen dieser Arbeit für die spezielle Anwendung mit kolloidalen Oxidpartikeln basierend auf bekannter Untersuchungsmethode für gelöste Enzyme optimiert und weiterentwickelt. Desweiteren wurden die experimentellen Ergebnisse basierend auf ergänzenden Simulationen interpretiert. Zusätzlich wurde die Methode der kovalenten Enzymimmobilisierung auf aminofunktionalisierten $Al_2O_3$- und $SiO_2$-Partikeln angewendet. Die Auswirkung auf die katalytische Aktivität von α-Chymotrypsin wurde mit MALDI-ToF-MS untersucht, indem die Peptide aus dem proteolytischen Verdau des Substrates Lysozym analysiert wurden. Die Hauptergebnisse dieser Arbeit sind folgende:

*Physisorption:*

- Chymotrypsin adsorbierte auf allen getesteten kolloidalen Partikeln und wies dabei Konzentrations- und pH-Abhängigkeit auf, wobei die Adsorption mit steigendem pH gestiegen ist.
- Höhere Adsorption wurde für hydrophobere Oberflächen beobachtet.

- Beide Arten von $TiO_2$ zeigten die höchste Adsorptionsaffinität, gefolgt von $Al_2O_3$ und zuletzt von $SiO_2$.
- Aktivitätstest für adsorbierte Enzyme wurde etabliert und diente als einfache und schnelle Methode zur Bestimmung der Änderungen der katalytischen Aktivität von adsorbierten Enzymen.
- Erheblicher Verlust der enzymatischen Aktivität wurde nach der Adsorption auf allen getesteten kolloidalen Partikeln beobachtet.
- Für das adsorbierte Chymotrypsin auf $TiO_2$ (Rutil): Anstieg des $K_M$ Wertes für das künstliche Substrat p-Nitrophenylacetat (p-NPA) wurde festgestellt, wobei die Blockierung des Aktivitätszentrums oder die Konformationsänderungen wahrscheinliche Ursachen dafür waren.
- Seitliche Wechselwirkungen der benachbarten adsorbierten Enzyme schienen die enzymatische Aktivität kaum zu beeinflussen, da diese für alle kolloidalen Partikel größtenteils unabhängig von der Dichte der adsorbierten Enzyme auf der Oberfläche blieb.

*Kovalente Immobilisierung:*

- Die Entstehung der Peptide, die Lysozym zugeordnet wurden, wurde durch die Präsenz des kovalent immobilisierten Chymotrypsins auf der Partikeloberfläche herbeigeführt.
- Kinetische Untersuchungen: Chymotrypsin, das auf Partikeln immobilisiert wurde, blieb länger aktiv als das nicht immobilisierte Chymotrypsin.
- Verringerung der enzymatischen Aktivität und langsamere Kinetik der Verdauung wurden nach der Immobilisierung auf $Al_2O_3$ und $SiO_2$ beobachtet.
- Die Verringerung der enzymatischen Aktivität bei den Wiederverwendungsstudien war mehr ausgeprägt für $SiO_2$ als für $Al_2O_3$ und war am wahrscheinlichsten durch die Verdaureaktion und die möglichen sterischen Hinderungen zu erklären.

Beide Materialien waren aktiv bei dem Verdau von Lysozym nach 7 Wochen Lagerung bei Raumtemperatur.

# 1 Introduction

*ABSTRACT: This chapter provides an introduction to the aims and motivation and describes the key questions of the completed study.*

## 1.1 Aims and motivation

Colloidal nano- and submicron-sized ceramic materials are widely used due to their advantageous and unique properties, such as customizable surface chemistry, high surface area, and biocompatibility[1, 2]. Based on the strengths of these characteristics, these materials have been employed in many different biological, biotechnological, and biomedical applications, such as implants, biosensors, bioreactors, drug delivery systems, biomolecule separation and purification systems, enzyme carriers, and proteomic applications[2-5]. Various applications include protein immobilization either in the form of uncontrolled protein adsorption in the case of protein corona formation on implants and biomaterials or in the form of artificially covalently immobilized proteins for biosensors, purification systems, and lab-on-a-chip reactors[3-9].

Since the first demonstration of an immobilized enzyme in 1950[3], numerous studies have been performed with the aim of understanding the processes underlying the interactions between proteins and carrier materials. Another challenging topic in this research field is the investigation of protein adsorption on colloidal particles exposed to biological environments, such as cell cultures, cell lysates, and blood[5, 10]. Because the particles interact with proteins from the surrounding environment and build an uncontrolled protein layer, this newly formed particle surface becomes the interface at which subsequent interactions between the particles and the biological system occur. More detailed and fundamental investigation of the protein-ceramic interface is therefore needed in biomaterials research.

A special emphasis in biomaterials research is enzyme immobilization, which offers advantages such as increased stability, higher catalytic activity, continuous operation, and resistance to environmental changes such as pH and temperature[7, 11-18]. Because enzymes are costly components of catalysis processes and the recovery of dissolved enzymes

is extremely expensive and time-consuming, enzyme immobilization offers a welcome simplification of the separation and recovery processes[7, 11-18].

Various enzyme immobilization strategies have been employed for numerous applications. Four key methods can be highlighted: i) physical adsorption or physisorption; ii) covalent binding; iii) physical entrapment, such as in a polymeric matrix or mesoporous $SiO_2$; and iv) affinity methods, e.g., using avidin, biotin or metal chelation[3, 7, 15, 19]. Each immobilization strategy has both advantages and disadvantages. Physisorption is the mildest immobilization method due to the absence of additional chemical substances. Hence, physisorption has the greatest potential to preserve the native structure of the active site of the immobilized enzyme[3, 4]. However, the immobilized enzymes are theoretically in equilibrium with the medium and can be desorbed upon changes in pH, temperature, and ionic strength or by the addition of other competing proteins[4, 9, 20-25]. Covalent immobilization strategies and affinity methods often result in an immobilized enzyme that is more stable against environmental changes. The main disadvantage of covalent immobilization is the involvement of additional linkers, spacers, and other coupling substances, which can promote unwelcome side reactions and decrease catalytic activity. Furthermore, the immobilized enzymes, which are entrapped within a highly cross-linked polymer matrix or encapsulated within a membrane, can exhibit limitations in terms of the diffusion of both analytes and products[3, 15, 26]. To minimize the disadvantages of each immobilization method, it is essential to carefully select the experimental conditions for the immobilization, to maximize the immobilization rate, and to strike a balance between the structural stability of the enzyme and the stability of the immobilized layer.

General trends in protein adsorption as a basic process involving interactions between the carrier material and proteins have been identified. Protein adsorption is influenced by pH, ionic strength and temperature[4, 9, 20-25]. Proteins generally adsorb more readily on hydrophobic surfaces, promoting the release of water molecules and increasing entropy[4, 9, 27-29]. Protein adsorption and orientation are also governed by electrostatic forces between the carrier material and the proteins[3, 4, 20-23, 27, 30-33]. The surface and curvature of the carrier material influence adsorption[9, 20, 34, 35]. However, the mechanisms underlying the adsorption process and the complex interplay of the multiple driving forces are not well understood and require further clarification. Further

investigation may also improve enzyme immobilization strategies and applications based on immobilized enzymes.

A key goal of this thesis is to analyze the effects of colloidal ceramic particles on the enzymatic activities of adsorbed or covalently immobilized enzymes (see Figure 1.1). Given the full complexity of the interactions between enzymes and colloidal particles, a simple model system is preferred. A serine protease, α-chymotrypsin, was chosen as a model enzyme. α-Chymotrypsin is a well-known protease with a well-characterized structure, thoroughly investigated enzymatic activity and a wide range of possible applications. Two key immobilization strategies, physisorption and covalent binding, were examined in this work, and four types of colloidal materials, specifically $Al_2O_3$, $SiO_2$ and two types of $TiO_2$, were used depending on experimental requirements. Physisorption is the most straightforward and mild method of immobilization[3, 4, 7, 17]. Alterations in activity caused by linkers and additional chemical substances can be excluded because no additional reagents are required for this process. However, desorption processes must be examined and prevented for the physisorption method[3, 4, 7, 17]. Because of the limitations of physisorption in terms of desorption processes in some technical applications, covalent binding was employed as an alternative immobilization method.

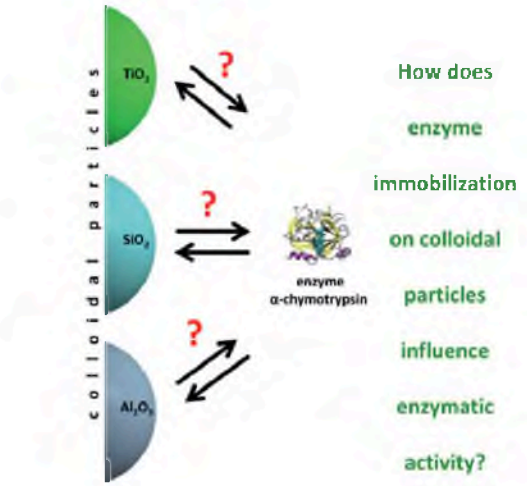


Figure 1.1 Graphical representation of the primary question of this thesis.

The driving forces for enzyme adsorption were determined for the chosen colloidal systems. For this purpose, factors such as pH, ionic strength, and temperature were controlled. Various analyses, such as protein adsorption experiments, dynamic light scattering measurements, circular dichroism measurements, and zeta potential measurements, were performed and investigated in detail. Scanning electron microscopy, transmission electron microscopy, and volumetric measurements of gas adsorption isotherms to determine specific surface area and hydrophobic/ hydrophilic properties were employed to further characterize the carrier materials.

The main focus of this work is the assessment of the enzymatic activities of immobilized enzymes. These data can be difficult to obtain because enzymatic activity may be altered by various factors, including orientation on the surface, denaturation, and steric hindrance[4, 15, 16, 21, 29, 36-38]. In addition, the total number of particles in a particle-containing solution and/ or the number of enzyme molecules bound to each particle may be unknown. Conventional assays for the direct measurement of the activities of dissolved enzymes are often based on UV/ Vis spectrometry and are thus not applicable for enzymes immobilized on colloidal particles because these particles increase light scattering and consequently produce false results. To circumvent these problems, a method to measure the activity of dissolved enzymes using p-nitrophenyl acetate (p-NPA)[39-41] as the enzyme substrate was adapted to allow its use for adsorbed enzymes. Within the frame of this work, the optimized procedure and methodology will be demonstrated in detail. Because coupling substances that are used for covalent immobilization interfere with this optimized assay, the enzymatic activity of covalently immobilized chymotrypsin was estimated by matrix-assisted laser desorption/ ionization time-of-flight mass spectroscopy (MALDI-ToF-MS) using lysozyme as an enzyme substrate.

Finally, the experimental results will be discussed in the context of the results of representative simulations. These simulations were performed under the same conditions as in the adsorption experiments within a collaborative project involving the Advanced Ceramics Group (Faculty of Production Engineering, University of Bremen, Germany), the Center for Biomolecular Interactions Bremen (Faculty of Biology/ Chemistry, University of Bremen, Germany), and the Hybrid Materials Interfaces Group (Faculty of Production Engineering and Bremen Center for Computational Materials Science, University of Bremen, Germany).

# 2 Interactions between colloidal particles in aqueous suspension

*ABSTRACT: Chapter 2 provides an introduction to the major non-covalent interaction forces essential for the interactions between particles and proteins and between colloidal particles in aqueous media. van der Waals and electrostatic interactions are explained in detail, including explanations of the Hamaker constant, particle surface charge, particle zeta potential, the electric double layer, and the role of the medium's ionic strength and pH. The Derjaguin, Landau, Verwey, and Overbeck (DLVO) theory is introduced to estimate the interaction potential between colloidal particles. Non-DLVO forces are also briefly presented with a focus on hydrogen bonding and hydrophobic interactions.*

## 2.1 Van der Waals forces

To explain the fundamental interaction forces between colloidal particles and between proteins and colloidal particles, both proteins and colloidal particles are assumed to be spherical particles for the entirety of Chapter 2. The interaction forces between two spherical particles originate from the interplay between the molecules in the particles and the medium that surrounds and separates the particles. The van der Waals forces result in dipole-dipole interactions between the molecules in the particles and produce strong attractive forces. An outstanding demonstration of these forces is the feet of the gecko, which allow climbing on smooth surfaces and even walking upside-down on the ceiling due to van der Waals interactions[42].

Three different types of van der Waals interaction forces have been identified[43]: i) dipole-dipole interactions (also called orientation forces, introduced by Keesom[44]); ii) dipole-induced dipole interactions (also referred to as induction forces, introduced by Debye[45]); and iii) fluctuating dipole-induced dipole interactions (also referred to as dispersion forces, introduced by London[46]). The total van der Waals interaction force is the sum of these three forces. The London-van der Waals force is typically dominant compared to the other forces. Mathematical details for all three contributions are discussed in physical chemistry books as described in the indicated references[42, 43, 47-50]. This model was first developed for

intermolecular microscopic interactions and was expanded and applied to macroscopic bodies such as colloidal particles by summing the forces between the molecules in the particles. Based on this model, Hamaker described the dependency of the London-van der Waals interaction potential $W_{vdW}$ of two spherical particles with radii $r_1$ and $r_2$ on the separation distance $H$ of the particles as follows[51]:

$$W_{vdW}(H) = -\frac{A}{6}\left(\frac{2r_1r_2}{m} + \frac{2r_1r_2}{m+4r_1r_2} + ln\frac{m}{m+4r_1r_2}\right) \quad (2.1)$$

where $m = H^2 + 2(r_1 + r_2)H$. The Hamaker constant $A$ describes the pairwise additive interaction forces between the molecules in a given system. The Hamaker constant $A_{ii}$ for the interaction of two components of a material $i$ can be calculated for London-van der Waals interactions for short distances and in a vacuum as follows[43]:

$$A_{ii} = \pi^2 n_i^2 \beta_{ii} \quad (2.2)$$

where $n_i$ is the number of atoms per unit volume and $\beta_{ii}$ is the London van der Waals constant, which is given by equation $\beta_{ii} = \frac{3}{4}\alpha^2 h\nu$. $\nu$ is the orbit frequency of the electron, $\alpha$ is the polarizability of the material, and $h$ is Planck's constant. The Hamaker constant ($A_{132}$) for the interaction between two particles composed of material 1 and material 2 in medium 3 can be calculated as a function of the Hamaker constant for the interaction between the atoms of the particle composed of material 1 ($A_{11}$), between the atoms of the particle composed of material 2 ($A_{22}$), and between the atoms in medium 3 ($A_{33}$)[43]:

$$A_{132} = \left(\sqrt{A_{11}} - \sqrt{A_{33}}\right)\left(\sqrt{A_{22}} - \sqrt{A_{33}}\right) \quad (2.3)$$

Table 2.1 presents the Hamaker constants of selected metal oxides and the enzyme $\alpha$-chymotrypsin in water ($A_{particle\text{-}water\text{-}particle}$ and $A_{enzyme\text{-}water\text{-}enzyme}$, respectively). All data were obtained from the indicated references[52-54]. An approximation of $A_{particle\text{-}water\text{-}enzyme}$ is given by the

equation[42] $A_{132} \approx \sqrt{A_{131} * A_{232}}$. The Hamaker constant can be determined experimentally from surface force measurements using a surface force apparatus or atomic force microscopy[52-54].

Table 2.1 Hamaker constants of metal oxides and $\alpha$-chymotrypsin in water[52-54].

| Material | α-Chymotrypsin | $Al_2O_3$ | $SiO_2$ | $TiO_2$ (rutile) | $TiO_2$ (anatase) |
|---|---|---|---|---|---|
| Hamaker constant A ($10^{-21}$ J) | 41.1 | 27.5 | 1.6 | 60 | 37 |

Using the Hamaker constants given in Table 2.1, the London-van der Waals interparticle interaction potentials can be determined for these selected materials using equation (2.1), as illustrated in Figure 2.1.

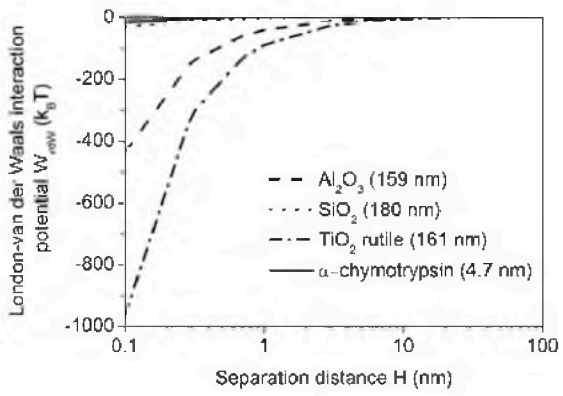


Figure 2.1 London-van der Waals interparticle interaction potential between two spherical particles of the same material in water at 25 °C. For $\alpha$-chymotrypsin, a molecule diameter of 4.7 nm was used. For $Al_2O_3$, $SiO_2$, and $TiO_2$ (rutile), particle diameters of 159, 180, and 161 nm, respectively, were used. T is the temperature, $k_B$ is the Boltzmann constant, and 1 $k_BT$ equals $4.11*10^{-21}$ J.

The London-van der Waals interaction decreases steeply with decreasing particle distance, and the interaction is nearly zero for distances greater than 10 nm. The calculation of the van der Waals interaction potential to determine the influence of neighboring atoms on interactions was

discussed in detail by Lifshitz and coworkers[43, 55]. Neighboring atoms can influence the polarizability of two interacting molecules and change the precise calculation of the Hamaker constant. However, the distance dependence trends of the van der Waals interaction remain unchanged[42]. Comprehensive discussions of van der Waals forces and the Hamaker constant are provided in the indicated references[42, 43, 49, 50, 55].

## 2.2 Electrostatic double layer forces

Both proteins and inorganic colloidal particles have surface charges in aqueous media, leading to attractive or repulsive interaction forces between the particles, which are referred to as electrostatic interactions or electrostatic double layer forces. Electrostatic interactions exert strong effects despite large distances between colloidal particles and are important driving forces in many biological interactions and adsorption processes[47, 49]. The next subchapter, 2.2.1, explains the origin of the surface charge of a colloid system; this discussion is essential for understanding electrostatic interactions.

### 2.2.1 Surface charge

The surface charge on colloidal particles in aqueous environments originates from a variety of processes, e.g., the adsorption and dissociation of ions on the particle surface and the protonation and dissociation of particle surface groups. Amino ($-NH_2$) and carboxyl ($-COOH$) groups on protein surfaces can be protonated or deprotonated, leading to positively charged $-NH_3^+$ or negatively charged $-COO^-$ groups, respectively[42, 48]. In addition, oxide particles (e.g., $Al_2O_3$, $SiO_2$ and $TiO_2$) have hydroxyl groups ($-OH$) on their surfaces that can be deprotonated ($-O^-$, negatively charged) or protonated ($-OH_2^+$, positively charged). These processes are dependent on the pH of the environment[42, 47]. Figure 2.2 illustrates the protonation/ deprotonation of surface groups on proteins and metal oxide particles.

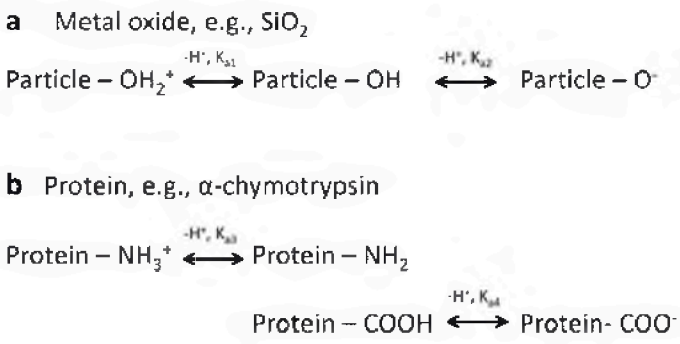


Figure 2.2 Protonation and deprotonation of surface groups on (a) metal oxide particles and (b) proteins.

The pH at which the metal oxide groups dissociate can be determined using the mass balance equation of the equilibrium reaction in Figure 2.2a. The acid dissociation constants for the protonation, $K_{a1}$, and the deprotonation, $K_{a2}$, of the amphoteric hydroxyl groups (corresponding to MOH) on metal oxide particles can be calculated as follows[56]:

$$K_{MOH_2^+} = K_{a1} = \frac{[MOH][H^+]}{[MOH_2^+]} \tag{2.4}$$

$$K_{MOH} = K_{a2} = \frac{[MO^-][H^+]}{[MOH]} \tag{2.5}$$

where $[MOH]$, $[MO^-]$ and $[MOH_2^+]$ are the surface concentrations of the corresponding surface groups in mol $m^{-2}$ and $[H^+]$ is the proton activity in mol $m^{-3}$. The equilibrium constants of the –COOH and $-NH_2$ protein surface groups can be analogously obtained using equations (2.4) and (2.5). Dissociation constants are usually expressed as the negative decimal logarithm or $pK_a$ value, which corresponds to the pH at which half of the sites are deprotonated:

$$pK_a = -log_{10}(K_a) \tag{2.6}$$

The surface density of the reactive sites, $N_S$, which is given as sites per $m^2$, can be determined via equation (2.7)[56]:

$$N_S = [MOH] + [MO^-] + [MOH_2^+] \tag{2.7}$$

Based on equations (2.4), (2.5), and (2.6), three terms can be obtained to describe the concentrations of the different ionization states that are dependent on $[H^+]$. $[H^+]$ is an approximate of the concentration of protons in the medium ($[H^+] \approx 10^{-pH}$):

$$[MOH] = \frac{N_S[H^+]K_{a1}}{[H^+]K_{a1} + K_{a1}K_{a2} + [H^+]^2} \tag{2.8}$$

$$[\mathrm{MO^-}] = \frac{N_S K_{a1}K_{a2}}{[H^+]K_{a1} + K_{a1}K_{a2} + [H^+]^2} \tag{2.9}$$

$$[MOH_2^+] = \frac{N_S[H^+]^2}{[H^+]K_{a1} + K_{a1}K_{a2} + [H^+]^2} \tag{2.10}$$

Because the concentrations of charged sites on the particle surface are a function of pH, the surface charge density $\sigma_0$ can be calculated as follows[56]:

$$\sigma_0 = eN_S(\theta_+ - \theta_-) \tag{2.11}$$

where $e$ is the elementary charge, $\theta_+ = \frac{[MOH_2^+]}{N_S}$, and $\theta_- = \frac{[MO^-]}{N_S}$. Thus, $[MOH]$ is greatest when $[MOH_2^+]$ and $[MO^-]$ are in equilibrium. The point of zero charge (PZC) is a material constant defined as the pH at which the net

surface charge and thus the surface potential are zero. The PZC can be written in logarithmic form as follows[57, 58]:

$$PZC = \frac{1}{2}(pK_{a1} + pK_{a2}) \tag{2.12}$$

For this calculation, the amphoteric surface hydroxyl group is assumed to have two $pK_a$ values (2-pK model)[56, 58]. Replacing the equilibrium reaction in Figure 2.2a with $[MOH^{0.5-}] + H^+ \leftrightarrow [MOH_2^{0.5+}]$, a model with one $pK_a$ (1-pK model)[58, 59] can be applied for metal oxides. According to equation (2.12), the PZC is equal to the $pK_a$ of the reaction. The 2-pK and 1-pK models are controversial in the literature[58] but generate similar results under select conditions[58]. Further information can be found in the references[56, 58-60].

### 2.2.2 Zeta potential

The surface charges on colloidal particles create an electric field in aqueous media. This electric field attracts a layer of oppositely charged counterions, forming the electric double layer[42, 47, 48, 50]. Figure 2.3 depicts the formation of a layer of counterions on a positively charged particle surface.

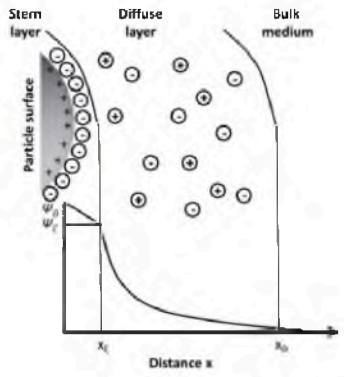


Figure 2.3 Electric double layer of a charged colloidal particle in aqueous medium at a low ion concentration. The diffuse layer contains mobile negatively charged counterions and positively charged co-ions. Counterions are adsorbed on the particle surface, called the

Stern layer. The particle surface potential is $\Psi_0$ and decreases with increasing distance from the particle surface. The zeta potential $\Psi_\zeta$ is measured at the shear plane of the Stern and diffuse layers. $x_D$ is referred to as the Debye-Hückel length. $\Psi_\zeta$ and $x_D$ are explained in this chapter.

A layer of counterions adsorbs on the particle surface to form the Stern layer, which is also known as the Helmholtz layer. The Stern layer is typically immobile, but ongoing exchange with ions in solution occurs[49, 50, 61]. The resulting diffuse layer consists of mobile co-ions and counterions that are in thermal motion. Both layers counteract the particle's surface charge. The electrostatic potential determines the distribution of ions in the layers and is maximal at the particle surface. It decreases linearly in the Stern layer and exponentially in the diffuse layer with increasing distance from the particle surface, as shown in Figure 2.3[49, 50, 61]. The zeta potential $\Psi_\zeta$ is the potential at the shear plane, where the Stern layer ends and the mobile diffuse layer begins. The zeta potential can be determined by electrokinetic measurements, which are described in Chapter 7. Analogous to the surface charge, the zeta potential is a function of the pH of the medium. The pH at which the zeta potential of colloidal particles is zero is referred to as the isoelectric point (IEP). The zeta potentials of colloidal $Al_2O_3$, $SiO_2$ and two types of $TiO_2$ particles as a function of pH are presented in Figure 2.4. For an ideal electrolyte-free system, the previously described PZC would be equivalent to the IEP[61].

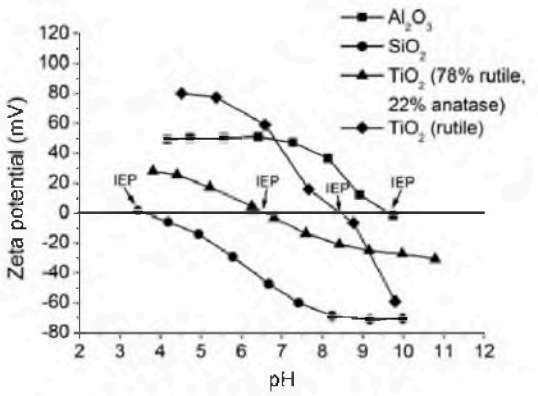


Figure 2.4 Zeta potentials of colloidal $Al_2O_3$, $SiO_2$ and two types of $TiO_2$ particles as a function of pH. Electroacoustic spectroscopy measurements were performed in double-deionized water at an initial ionic strength of 3 mM adjusted with KCl. The IEP is the pH at which the zeta potential is zero. The average IEPs of $Al_2O_3$, $SiO_2$, $TiO_2$ (78% rutile, 22%

anatase), and $TiO_2$ (rutile) are approximately 9.9 ± 0.1, 2.7 ± 0.1, 6.6 ± 0.1, and 8.3 ± 0.3, respectively.

### 2.2.3 The Poisson-Boltzmann equation

The Poisson-Boltzmann equation enables the calculation of the potential distribution in the diffuse layer as a function of the distance from the particle surface. This equation is essential for understanding electrostatic interactions in biological and colloid systems[42, 48-50]. The following mathematical considerations were primarily obtained from references[42, 48-50] with additional modifications and comments. The Poisson equation describes the relationship between the electrostatic potential $\Psi$ in the diffuse layer and the local charge density[47]:

$$\nabla^2\Psi = \frac{\partial^2\Psi}{\partial x^2} + \frac{\partial^2\Psi}{\partial y^2} + \frac{\partial^2\Psi}{\partial z^2} = -\frac{\rho_e}{\varepsilon_r \varepsilon_0} \tag{2.13}$$

where $\rho_e$ is the local electric charge density in C $m^{-3}$, $\varepsilon_r$ is the relative permittivity of the medium, and $\varepsilon_0$ is the permittivity of free space. x, y, and z are the Cartesian coordinates indicating the location of $\Psi$. The local ion density $c_i$ can be derived using the Boltzmann equation[47]:

$$c_i = c_i^0 e^{-W_i/k_B T} \tag{2.14}$$

$c_i^0$ is the concentration of ion $i$ in the bulk medium in units of ions per $m^3$, $k_B$ is the Boltzmann constant, and $T$ is the temperature. $W_i$ is the work required to move the $i$th ion in solution from an infinite distance to a position near the particle surface at which the potential is $\Psi$. For the next step, an assumption is made that the work required to displace other molecules can be neglected and only electric work is needed to move the ion. This electric work needed to move a charged ion to the position of $\Psi$ is $W_i = z_i e\Psi$, where $z_i$ is the valence of the ions. The local charge density $\rho_e$ is calculated as the sum of all ions[50, 62]:

$$\rho_e = \sum_i c_i z_i e \tag{2.15}$$

Combining equations (2.13), (2.14), and (2.15) leads to the Poisson-Boltzmann equation[50, 63]:

$$\nabla^2 \Psi = -\frac{1}{\varepsilon_r \varepsilon_0} \sum_i c_i^0 z_i e e^{-z_i e \Psi / k_B T} \tag{2.16}$$

The simplest solution for the Poisson-Boltzmann equation is for an infinitely extended planar surface because the potential cannot change in the y and z directions because of symmetry[47]. This condition eliminates the y and z coordinates in the Poisson-Boltzmann equation. Based on the assumption that $e|\Psi| \ll k_B T$, which corresponds to a potential of approximately 25 mV at 25 °C, the 'linearized Poisson-Boltzmann equation' can be derived[47]:

$$\frac{d^2 \Psi}{dx^2} = \Psi \left( \frac{e^2 \sum_i z_i^2 c_i^0}{\varepsilon_r \varepsilon_0 k_B T} \right) \tag{2.17}$$

For many applications, the result is valid even for higher potentials up to 50-80 mV[42, 47]. The term in brackets in equation (2.17) is the square of the reciprocal Debye-Hückel length, κ, which is depicted in Figure 2.3 and is given by the following:

$$\kappa = \frac{1}{x_D} = \sqrt{\frac{e^2 \sum_i z_i^2 c_i^0}{\varepsilon_r \varepsilon_0 k_B T}} \tag{2.18}$$

The Debye-Hückel length $x_D$ is defined as the thickness of the layer of ions that screens the surface potential. Equation (2.18) shows that $x_D$ depends on the ionic strength $I$ of the bulk medium, which is given by the following:

$$I = \frac{1}{2}\sum_i z_i^2 c_i^0 \tag{2.19}$$

For example, the Debye-Hückel length of a 0.1 M aqueous NaCl solution at 25 °C is 0.96. In water, the Debye-Hückel length cannot be longer than 680 nm. Due to the dissociation of water, the ion concentration cannot be less than 2 x $10^{-7}$ M[42].

Combining equations (2.17) and (2.18) yields the following:

$$\frac{d^2\Psi}{dx^2} = \Psi\kappa^2 \tag{2.20}$$

Considering the boundary conditions to be $\Psi \rightarrow \Psi_0$ as x $\rightarrow$ 0 and $\Psi \rightarrow$ 0 as $x \rightarrow \infty$, equation (2.20) can be converted to obtain $\Psi$ as a function of the distance and the reciprocal Debye-Hückel length[42, 62]:

$$\Psi(x) = \Psi_0 e^{-\kappa x} \tag{2.21}$$

$\Psi_0$ is the particle surface potential when the potential drop in the Stern layer is neglected. However, the calculation is only valid for the diffuse layer. Considering the Stern layer, $\Psi_0$ is an approximation of the zeta potential $\Psi_\zeta$[64]. The potential around colloidal particles is calculated as follows[47]:

$$\Psi(x) = \Psi_0 (R_S/r) e^{-\kappa(r-R_S)} \tag{2.22}$$

where $R_S$ is the radius of the spherical particle and $r$ is the radial distance at any point in the double layer from the center of the particle, such that $x = r - R_S$. The applied boundary conditions are $\Psi \rightarrow \Psi_0$ as $r \rightarrow R_S$ and $\Psi \rightarrow 0$ as $r \rightarrow \infty$. The total electric charge density in the diffuse layer equals the surface charge density $\sigma_0 = -\int_0^\infty \rho_e$ (see Chapter 2.2.1), yielding the following[61, 63, 65]:

$$\Psi_0 = \frac{\sigma_0}{\varepsilon_r \varepsilon_0 \kappa \left(1 + \frac{1}{\kappa R_S}\right)} \tag{2.23}$$

Because equation (2.23) was derived from the linearized Poisson-Boltzmann equation (2.17), it is only valid for surface potentials of ≤ 25 mV. For higher potentials, the more complex non-linearized Poisson-Boltzmann equation is required[63]. Additional considerations for the Poisson-Boltzmann equation can be found in the references[42, 47, 49, 50, 63, 64].

Figure 2.5 illustrates the dependencies of the introduced terms. Figure 2.5a depicts the Debye-Hückel length as a function of the ion concentration in the bulk medium. Figure 2.5b illustrates the decrease in electrostatic potential with increasing distance from the particle surface as a function of the ion concentration. Figure 2.5c depicts the surface potential as a function of the surface charge density at a constant ionic strength. As the ionic strength increases, the thickness of the double layer and consequently the electric potential decrease. The larger the surface charge density, the larger the surface potential at a constant ionic strength.

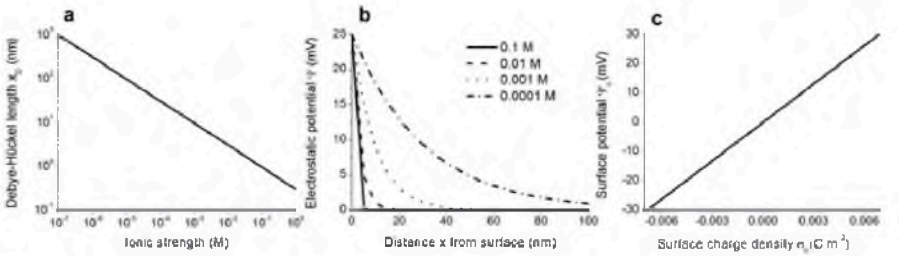


Figure 2.5 (a) Debye-Hückel length as a function of the ion concentration (calculated using equation (2.18)). (b) Decrease in the electrostatic potential with increasing distance from the particle surface as a function of the ion concentration in bulk medium for a surface potential of $\Psi_0$= 25 mV (calculated using equation (2.21)). (c) The surface potential as a function of the surface charge density at a constant ionic strength of 0.01 M (calculated using equation (2.23)). All calculations were performed using a particle diameter of 161 nm at 25 °C.

### 2.2.4 The electrostatic interaction energy between two spheres

For two spheres with different radii, $R_1$ and $R_2$, and different surface potentials, $\Psi_1$ and $\Psi_2$, the interaction energy can be calculated as follows[63]:

$$W_{DL}(H) = \pi\varepsilon_r\varepsilon_0 \frac{R_1 R_2}{(R_1 + R_2)} \{(\Psi_1 + \Psi_2)^2 ln(1 + e^{-\kappa H}) + (\Psi_1 - \Psi_2)^2 ln(1 - e^{-\kappa H})\} \quad (2.24)$$

This equation is analytically derived from the linearized Poisson-Boltzmann equation and is consequently only valid for surface potentials ≤ 25 mV[63]. Figure 2.6 presents the interparticle interaction potential of two 161-nm spheres as a function of the distance between the spheres, which was calculated using equation (2.24) for different ionic strengths (Figure 2.6a) and surface potentials (Figure 2.6b and c). The interparticle energy decreases at higher ionic strengths and lower surface potentials. The magnitude of the surface potential determines the attraction between two oppositely charged spheres.

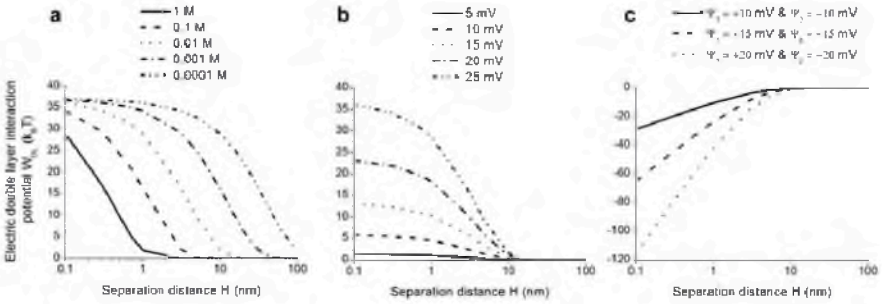


Figure 2.6 (a) Interparticle interaction potential of two spheres as a function of the spheres' separation distance calculated for different ionic strengths. $\Psi_1$ = $\Psi_2$ = 25 mV was used for the calculations. (b) Interparticle interaction potential of two spheres at a constant ionic strength of 0.01 M for different surface potentials. (c) Interparticle interaction potential of two spheres with opposing surface potentials at a constant ionic strength of 0.01 M. All calculations employed a particle diameter of 161 nm at 25 °C and equation (2.24).

Furthermore, the mechanism of repulsion is not only a result of the surface charge. When two charged particles approach each other, their double layers overlap. The particles are attracted to each other if they have opposite surface charges, and the surface charge of the first particle contributes to the charge compensation of the second particle. Conversely, if the particles are similarly charged, the double layers repulse due to the osmotic pressure resulting from the ions between the particles[49].

A homogenous charge distribution on the particles was assumed in these calculations. By contrast, a heterogeneous surface charge distribution is generally assumed when the distance between the surface charges on the particle surfaces is larger than the Debye length[42, 47]. Heterogeneous charge distributions can result in interactions between net-neutral or similarly charged surfaces. Whether the interactions are attractive or repulsive depends on the orientation of the charged regions[42, 47].

## 2.3 The DLVO theory

Derjaguin, Landau, Verwey, and Overbeek described how a combination of van der Waals forces and electrostatic forces influences interparticle interaction. In their honor, this theory is called the DLVO theory[49]. The DLVO theory defines interparticle interaction as a function of the particles' separation distance via the simple summation of electrostatic double layer forces and van der Waals forces:

$$W_{DLVO}(H) = W_{vdW}(H) + W_{DL}(H) \tag{2.25}$$

The theory is a simple method to estimate the stability of colloidal particle suspensions and to understand adsorption processes. Despite the assumptions made during the calculations of the individual forces, values calculated according to the DLVO theory correlate well with experimental data[42, 47, 49]. Figure 2.7 illustrates how different parameters influence the interparticle interaction potential $W_{DLVO}$. Figure 2.7a illustrates the influence of the Hamaker constant on the interparticle interaction potential between two 161-nm-diameter spheres. Calculations were performed for a

1:1 electrolyte solution with a constant ionic strength of 0.001 M and a surface potential of $\Psi_1 = \Psi_2 = 25$ mV. Figure 2.7b depicts the influence of the surface potentials of particles with constant Hamaker constants at a constant ionic strength of 0.001 M. Figure 2.7c demonstrates the influence of different ionic strengths on the interparticle potential of particles with constant Hamaker constants and constant surface potentials of 25 mV.

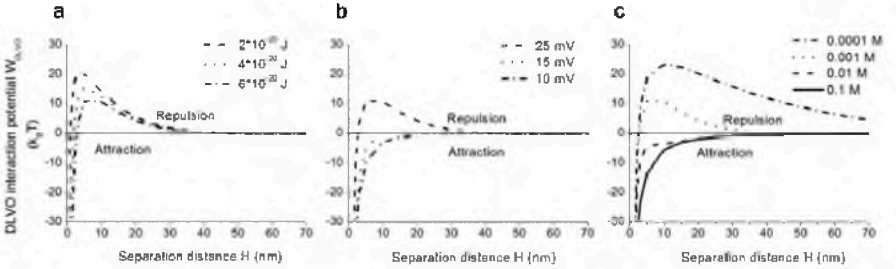


Figure 2.7 (a) The influence of different Hamaker constants on the interparticle interaction potential between two 161-nm-diameter spheres with a surface potential of $\Psi_1 = \Psi_2 =$ 25 mV and a constant ionic strength of 0.001 M in a 1:1 electrolyte solution. (b) The influence of different surface potentials of particles at a constant ionic strength of 0.001 M and with a constant Hamaker constant of $6*10^{-20}$ J. (c) Influence of different ionic strengths on the interparticle potential of particles with a constant Hamaker constant of $6*10^{-20}$ J and a constant surface potential of $\Psi_1 = \Psi_2 = 25$ mV. All calculations employed a particle diameter of 161 nm at 25 °C and equation (2.25).

Negative values indicate attraction, whereas positive values indicate repulsive forces. Consequently, as the maximum of the curve increases, the tendency of a suspension to aggregate decreases because of stronger repulsive forces. A higher Hamaker constant leads to stronger attractive forces. A larger particle surface potential causes larger repulsion between the spheres, and a higher ionic strength diminishes the repulsive forces.

Thus, the DLVO theory enables an approximation of the interaction potentials between metal oxide particles and proteins. Figure 2.8 depicts the interaction potentials of α-chymotrypsin interacting with $Al_2O_3$, $SiO_2$ and $TiO_2$ particles. For the $Al_2O_3$, $SiO_2$ and $TiO_2$ particles, a positive surface potential of 25 mV and particle diameters of 159, 180 and 161 nm, respectively, were assumed. For α-chymotrypsin, a diameter of 4.7 nm and surface potentials of -7 mV or 7 mV were assumed. A stronger attraction is predicted between α-chymotrypsin and $TiO_2$ or $Al_2O_3$ particles,

whereas the attraction between α-chymotrypsin and $SiO_2$ occurs at smaller distances (see Figure 2.8a).

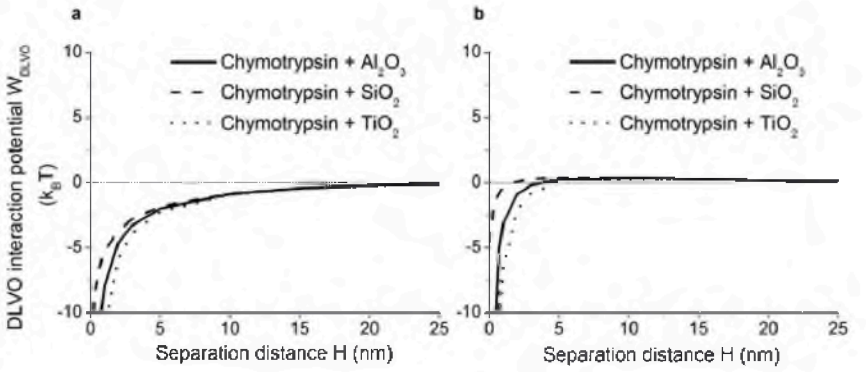


Figure 2.8 Interparticle interaction potentials for α-chymotrypsin interacting with $Al_2O_3$, $SiO_2$ and $TiO_2$ (rutile) particles. For $Al_2O_3$, $SiO_2$ and $TiO_2$ particles, diameters of 159, 180, and 161 nm, respectively, and a surface potential of 25 mV were assumed. For α-chymotrypsin, a diameter of 4.7 nm and α-chymotrypsin surface potentials of -7 mV (a) and 7 mV (b) were assumed. The Hamaker constants stated in Table 2.1 were applied for the calculation using equation (2.25). The assumed conditions were an ionic strength of 0.001 M in a 1:1 electrolyte solution at 25 °C.

## 2.4 Non-DLVO forces

Forces other than the van der Waals and electric double-layer forces also influence interparticle interactions. The following forces are also relevant for aqueous systems and are "far from being understood"[42]: repulsive steric forces, hydration, and hydrophobic forces[42, 43, 47, 49]. Repulsive steric forces are caused by exposed molecules that project from the surface of colloidal particles[42, 47, 61]. The protruded molecules can sterically interfere with the approach of two particle surfaces because of entropic or osmotic repulsive forces. However, depending on the type of molecule on the particle surface, steric forces can also build a bridge between particles, implying attraction[49].

Hydration and hydrophobic forces depend on the interaction of the particle surface with water molecules. These forces are essential for many biological interactions, such as the formation of protein structures and for protein-material interactions. The hydrogen-bonding free energy of

cohesion of the water molecules that surround colloidal particles controls the interactions[42, 43, 47]. Forces that induce repulsion due to the water layers on hydrophilic surfaces are referred to as 'hydration forces'. Because of these hydration forces, the removal of water layers on hydrophilic surfaces requires more energy than on hydrophobic surfaces. However, this process is necessary for particle-particle attraction. Conversely, the water layer has a high free energy and is simple to replace on hydrophobic particle surfaces. When hydrophobic particles interact with each other, the free energy decreases due to a decrease in the surface area exposed to water[43, 49]. Hydration forces have a range of approximately 1 nm, and hydrophobic attraction forces have a range of 1-2 nm and are consequently stronger than van der Waals forces[42, 47]. However, the origin and the effects of hydration and hydrophobic interactions are not completely understood and require further investigation[42, 43, 47]. The effects of steric forces, hydration, and hydrophobic interaction forces must be included in the DLVO theory to generate the extended DLVO theory[42, 43, 47].

Hydrogen bonds are another type of intermolecular force that affects the interactions between colloidal particles and between proteins and particles. These forces occur between electronegative atoms and hydrogen atoms that are covalently bound to similar electronegative atoms with a free pair of electrons. Hydrogen bonding generates a bridge between such molecules by 'sharing' the hydrogen atom[49]. Hydrogen bonds are short-range forces and only exist when the molecules are in almost direct contact. Hydrogen bonding forces are weaker than covalent or ionic bonds but stronger than van der Waals forces[49]. The forces described above are not the only forces that influence the interactions between molecules and particles in aqueous media. In 2006, van Oss detailed 17 non-covalent forces published in the literature[43]. However, van der Waals, electrostatic, hydrophobic, and hydration forces as well as hydrogen bonding are the major forces and are of higher priority. Other forces are mainly derived from one or several of these main forces[43].

# 3 Proteins

*ABSTRACT: Chapter 3 introduces the molecular structures and amino acid compositions of proteins. In addition, the definition and classification of enzymes will be explained, and the selected enzyme, α-chymotrypsin, will be introduced. The mechanism of covalently catalyzed hydrolysis of peptide bonds by α-chymotrypsin will be presented in detail.*

## 3.1 The amino acid composition of proteins

All proteins are various polymers of the 20 common amino acids. Some proteins also contain derived amino acids, which are generally formed via enzymatic modification of a common amino acid after it has been integrated into a protein. The common amino acids feature a central α-carbon atom to which a carboxylic acid group, an amino group, and a hydrogen atom are covalently bonded. Additionally, the central α-carbon atom is bound to a specific chemical group, referred to as the R side chain. This side chain uniquely defines each of the 20 common amino acids[66]. The general structure of a common amino acid is depicted in Figure 3.1.

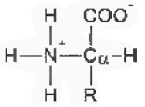


Figure 3.1 General structure of a common amino acid in ionized form.

The polymerization of the 20 common amino acids into polypeptide chains occurs via a dehydration reaction. The α-carboxyl group of one amino acid forms a covalent peptide bond with the α-amino group of another amino acid via the elimination of a molecule of water. Repetition of this process generates a polypeptide or protein with a specific amino acid sequence[66-69].

## 3.2 Protein structure

The specific amino acid sequence of a protein is the primary structure of the protein. The unique primary structure allows a polypeptide chain to fold into a specific three-dimensional structure that confers the protein's physiological and chemical properties. The location of disulfide bonds is also dictated by the primary structure of a protein. The native conformation of a protein is the conformation with the lowest total Gibbs free energy kinetically accessible to the polypeptide under the specific conditions of folding, such as ionic strength, pH, and temperature. Higher levels of protein organization are termed secondary, tertiary, and quaternary structure and refer to non-covalently generated conformations of the polypeptide chain[66-69].

The secondary structure implies local folding of the polypeptide backbone into helical, pleated sheet, or random conformations. The bond between the nitrogen and $\alpha$–carbon is called the $\Phi$ bond, and the bond between the $\alpha$–carbon and the carbonyl carbon is called the $\psi$ bond. The third bond formed by each amino acid is the peptide bond. The partial double-bond nature of bonds between carbon and nitrogen is a barrier to the free rotation of the peptide bond. The $\alpha$-helix and $\beta$-strand conformations of polypeptides are the most thermodynamically stable of the regular secondary structures and are illustrated for $\alpha$-chymotrypsin in Figure 3.2. Such structures occur in the segments of a polypeptide chain in which all $\Phi$ bond angles are equal and all $\psi$ bond angles are equal. Some sequences can possess an unordered or random secondary structure in which both the $\Phi$ bond angles and the $\psi$ bond angles vary. In addition, the amino acid proline interrupts an $\alpha$-helical conformation due to its pyrrolidine side chain and prevents the formation of an $\alpha$-helical structure. A polypeptide chain adopting a $\beta$-structure hydrogen bonds to another similar polypeptide region oriented in a parallel or an antiparallel direction. Hydrogen-bonded $\beta$-strands resemble a pleated sheet with the side chains aligned above and below the pleated sheet-like structure[66-69].

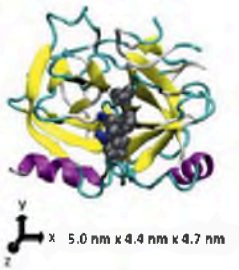


Figure 3.2 Secondary structural elements of chymotrypsin, with the α-helix in purple and the β-sheet in yellow. The active site is shown in black and includes a trio of amino acids: serine (Ser 195), histidine (His 57) and aspartic acid (Asp 102). The secondary structure was visualized using Visual Molecular Dynamics (VMD) software[70]. The protein structure was taken from the protein database PDB-ID 4CHA (RCSB Protein Data Bank, http://www.rcsb.org).

Tertiary structure refers to the three-dimensional structure of a polypeptide. This includes the geometric relationships between distant regions of the polypeptide and the spatial relationships of the side chains. A long polypeptide chain typically folds into multiple compact semi-independent domains, each exhibiting a characteristic compact geometry with a polar surface and hydrophobic core. Domains in a multidomain protein can be connected by a region that lacks a regular secondary structure and may perform a different task. Quaternary structure refers to the non-covalent association of discrete polypeptide subunits into a multi-subunit protein. Not all proteins have a quaternary structure. *α*-Chymotrypsin, for example, contains three polypeptides that are covalently joined by interchain disulfide bonds into a single covalent unit and does not have a quaternary structure[66-69].

## 3.3 Enzymes

Enzymes are proteins that catalyze biological reactions. A catalyst increases the rate of a chemical reaction. Enzymes are outstandingly efficient catalysts that not only increase the rate of conversion of substrate to product but also recognize a specific structure in the presence

of similar structures to form a unique product[66]. An enzyme accelerates the rate of product formation by lowering the energy of activation, i.e., the height of the barrier to the formation of product from substrate[66, 67]. The energy of activation is altered when the enzyme interacts with the substrate to stabilize the substrate in a state that will ensure product formation, i.e., the transition state. The less stable the transition state, the more energy is required for the conversion of a substrate to a product, and the slower the reaction will be[66].

There are six major classes of enzymes, with each class catalyzing a different chemical reaction: oxidoreductases, transferases, hydrolases, lyases, isomerases, and ligases. The enzyme selected in this study, called α-chymotrypsin, belongs to the class of hydrolases and will be further described below. An enzyme is usually much larger than its substrate, and the part of the enzyme where the substrate binds is referred to as the substrate-binding site or the active site (see Figure 3.2). Some enzymes are very specific and will bind only one unique structure, whereas others can bind many different substrates. The velocity at which an enzyme converts substrate to product can be described by the Michaelis-Menten equation, which will be introduced in Chapter 6.1[66-69].

### 3.3.1 *α*-Chymotrypsin

The enzyme *α*-chymotrypsin belongs to the class of hydrolases. Hydrolases catalyze hydrolysis reactions, in which water is added to a chemical bond. Moreover, *α*-chymotrypsin belongs to the class of serine proteases, which are so named due to their reactive serine residue. In the natural environment, *α*-chymotrypsin hydrolyzes the peptide bonds of dietary proteins as a digestive enzyme in the pancreas. *α*-Chymotrypsin also cleaves the ester bonds of artificial substrates[71]. Figure 3.3 depicts the reaction mechanism for *α*-chymotrypsin based on numerous chemical and structural data[72].

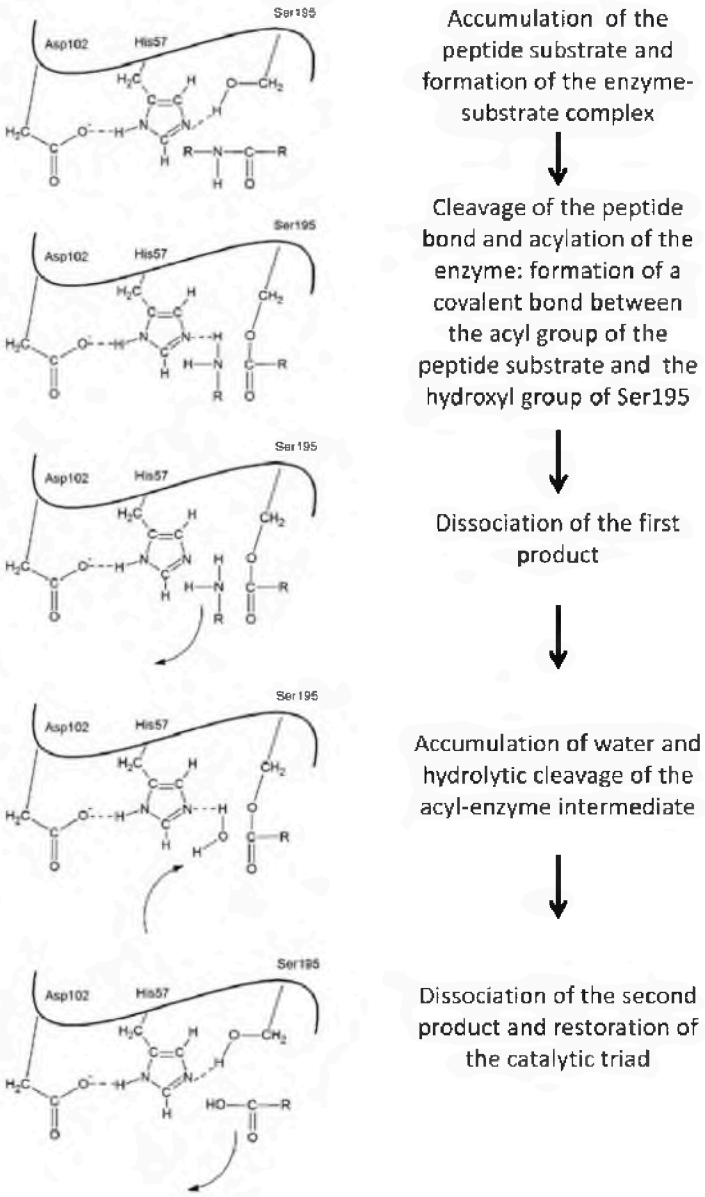


Figure 3.3 Covalently catalyzed hydrolysis of peptide bonds by *α*-chymotrypsin (adapted from a reference[72]).

# 4 Colloidal particles, their surface functionalization and covalent enzyme immobilization

*ABSTRACT: Chapter 4 introduces selected colloidal particles and discusses their structures and relevant properties. The method used for the surface functionalization of colloidal particles will be introduced. Selected methods of covalent enzyme immobilization will be explained in detail.*

## 4.1 Alumina colloidal particles

The thermodynamically stable phase of aluminum oxide is α-$Al_2O_3$, which is also called corundum and is the fifth-hardest substance after diamond. Large quantities of α-$Al_2O_3$ are produced industrially via the wet processing of bauxite, an aluminum ore, followed by calcination of $Al(OH)_3$[73].

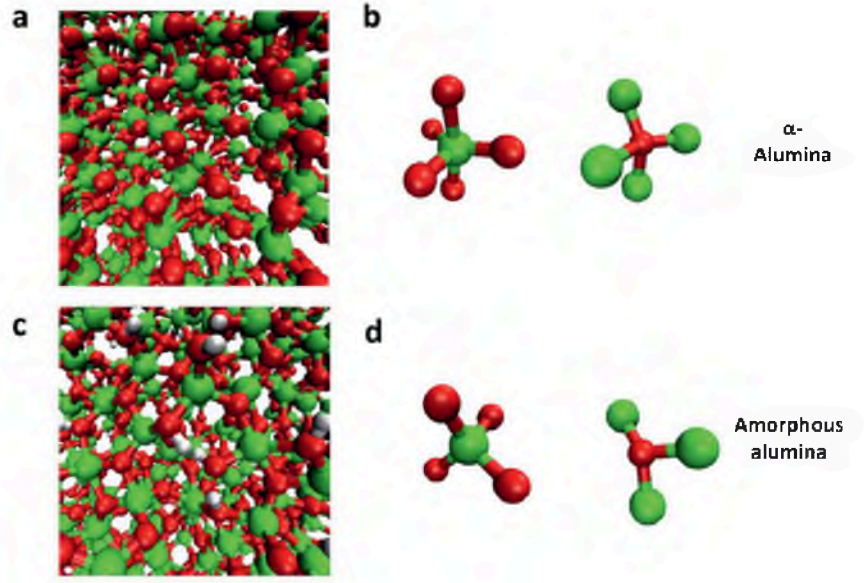


Figure 4.1 Crystal structures of α-$Al_2O_3$ and amorphous $Al_2O_3$ visualized using VMD[70]. An overview of the structures of α-$Al_2O_3$ (a) and amorphous $Al_2O_3$ (c). Detailed arrangement of aluminum atoms and oxygen atoms in α-$Al_2O_3$ (b) and amorphous $Al_2O_3$ (d). The atoms are

represented as follows: aluminum as green spheres, oxygen as red spheres and hydrogen as white spheres. The corresponding PDB-ID was kindly provided by the Hybrid Materials Interfaces Group (University of Bremen, Germany).

The atomic surface compositions of an α-$Al_2O_3$ particle and a flat surface are presented in Figure 4.1a-b. The oxygen atoms are arranged in approximately hexagonal close-packed layers[74]. In contact with aqueous environments, the surface atoms can be hydrolyzed to form hydroxyl groups. These hydroxyl groups can be protonated or deprotonated depending on pH as described in Chapter 2.2.1 in Figure 2.2[42, 47, 74]. The solubility of $Al_2O_3$ is low, $10^{-6}$-$10^{-7}$ M, resulting in good stability of $Al_2O_3$ at pH values of > 4 and < 10. The solubility increases beyond this pH range and with increasing temperature[74, 75]. In addition, $Al_2O_3$ particles are normally not single crystals but polycrystalline particles with different crystal planes. Furthermore, amorphous hydroxide structures can be formed on the surface of $Al_2O_3$ particles, as shown in Figure 4.1c-d[76]. These factors result in a particle surface with several types of outer Al-OH groups, and thus the coordination between aluminum ions and hydroxyl groups can vary, particularly when additional surface defects are present. These variations in coordination lead to different dissociation constants and, consequently, different reactivities of the Al-OH groups[74, 77]. However, α-$Al_2O_3$ is usually basic because the PZC of α-$Al_2O_3$ is 7.2-9.5[42].

## 4.2 Silica colloidal particles

Crystalline silicon dioxide is rather inert and has numerous structures, of which quartz is probably the best known[73]. However, the selected colloidal particles in this study are amorphous, as illustrated in Figure 4.2. $SiO_2$ that is freshly prepared, amorphous, and hydrated is usually reactive and dissolves in alkaline solutions. After a storage period and drying or at high temperatures, it ages and becomes less soluble in alkaline solutions[73]. This phenomenon can be explained by the chemical reactions that occur at the silica surface. Silanol groups, Si-OH, which are present in freshly synthesized silica, condense during aging to siloxane groups, Si-O-Si, which exhibit higher chemical stability[73]. The PZC of $SiO_2$ is 1.8-3.4[42]. The variation of the surface charge with pH is the result of the following processes[42]:

$$SiOH_2^+ \leftrightarrow SiOH + H^+ \quad (4.1)$$

$$SiOH \leftrightarrow SiO^- + H^+ \quad (4.2)$$

Due to these processes, the surface charge becomes more negative with increasing pH[42]. For additional information, the reader is referred to the references[73, 78].

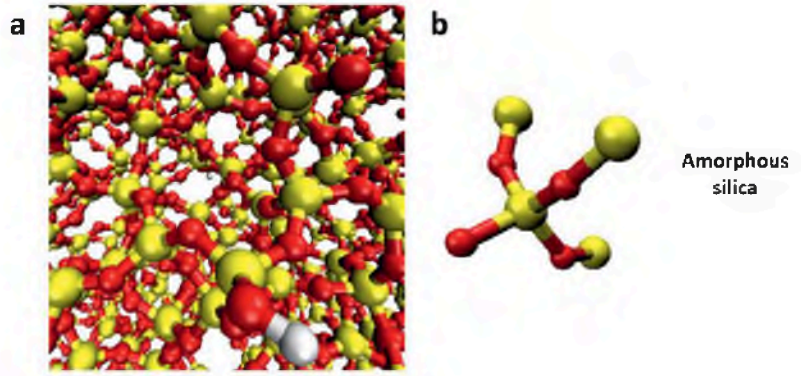


Figure 4.2 The surface of amorphous $SiO_2$ was visualized using VMD[70]. An overview of the structure (a) and the detailed arrangement (b) of silicon atoms and oxygen atoms are shown. The atoms are visualized as follows: silicon as yellow spheres, oxygen as red spheres and hydrogen as white spheres. The corresponding PDB-ID was kindly provided by the Hybrid Materials Interfaces Group (University of Bremen, Germany).

## 4.3 Titania colloidal particles

Titanium dioxide, also known as titanium(IV) dioxide and titania, mainly occurs in three forms: i) a tetragonal crystal system in rutile, ii) a tetragonal crystal system in anatase, and iii) an orthorhombic crystal system in brookite[73, 79]. The two types of $TiO_2$ colloidal particles selected were rutile and a mixture of rutile and anatase (78 wt%/ 22 wt%). Both structures are presented in Figure 4.3. $TiO_2$ has an amphoteric nature, i.e., both acidic and basic properties. However, its basic nature is stronger

and its acidic nature is weaker compared to $SiO_2$. The PZC of $TiO_2$ is usually 2.9-6.4[42].

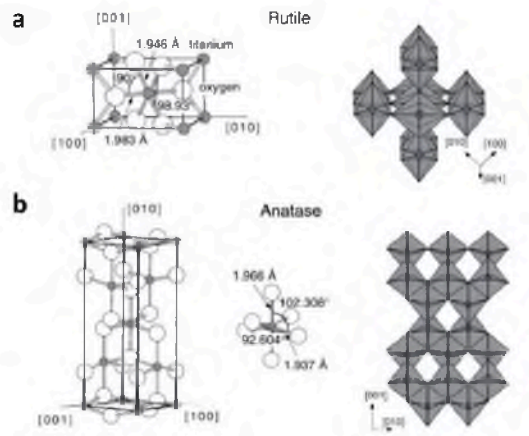


Figure 4.3 Bulk structures of rutile (a) and anatase (b). The tetragonal bulk unit cell of rutile has the dimensions $a = b = 4.587$ Å, $c = 2.953$ Å, and the dimensions of anatase are $a = b = 3.782$ Å, $c = 9.502$ Å. In both structures, slightly distorted octahedrons are the basic building units. The bond lengths and angles of the octahedrally coordinated titanium atoms are indicated, and the stacking of the octahedra in both structures is shown on the right side. This figure is reprinted from a reference[79] with kind permission from Elsevier (License number: 3618320341726).

## 4.4 Surface functionalization of colloidal particles

In contact with an aqueous environment, the surface atoms of metal oxides can hydrolyze to form hydroxyl groups, providing a foundation for the surface functionalization of colloidal particles. Silane coupling agents are often used to incorporate the desired functional group on the inorganic particle surface[80]. Common functional groups on particles that enable protein coupling include carboxylate, aldehyde, amine, hydrazide, thiol, epoxide, and amide groups. In this work, 3-aminopropyltriethoxysilane was used to create primary amine groups as shown in Figure 4.4. 3-Aminopropyltriethoxysilane contains a short organic 3-amino propyl group that terminates in a primary amine. This compound is less reactive than 3-aminopropyltrimethoxysilane and requires prior hydrolysis in an aqueous environment to form silanols. This hydrolysis is usually

performed in 5wt% water in ethanol at pH 4.5-5.5 and leads to a layer with a thickness of approximately 3–8 organosilanes. Consequently, the underlying inorganic material is masked, and the aminopropyl functional groups on the surface can be used for subsequent functionalization or directly for covalent enzyme immobilization[80-82].

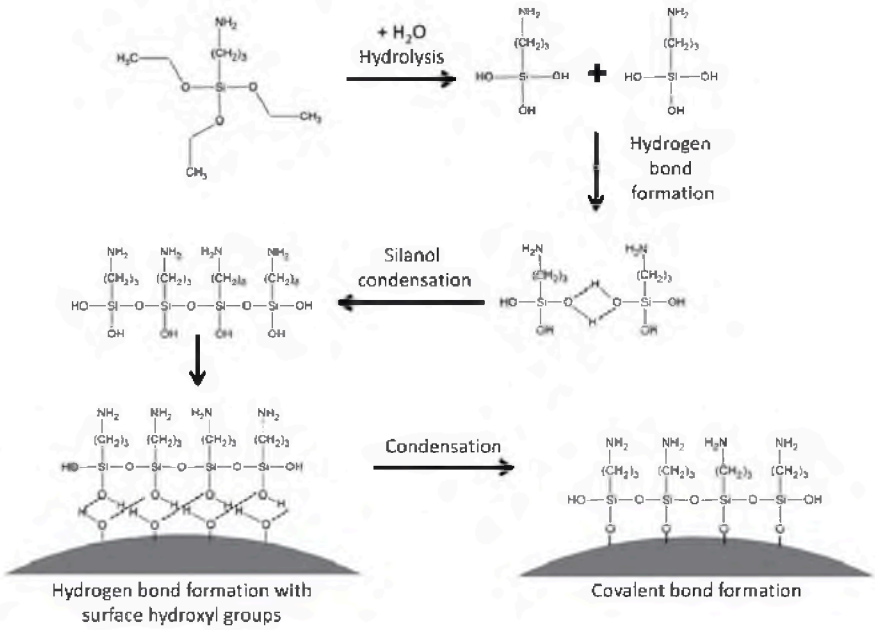


Figure 4.4 Chemical structure of 3-aminopropyltriethoxysilane and its reaction on the surface of colloidal particles (this figure was adapted from a reference[80]).

## 4.5 Covalent enzyme immobilization

In addition to particle functionalization, there are numerous protocols for covalent enzyme immobilization. Equally numerous are the possible linkers, crosslinkers, spacers and other reactive substances that can be applied for the synthesis of covalently bound enzymes. In addition, every functional group of an enzyme can be used for immobilization. Consequently, the number of possible synthesis routes is enormous. The interested reader is referred to the references for additional and extensive details[7, 11, 13, 15-19, 26, 80-83]. The immobilization route via the carboxyl

groups of the enzyme selected in this study is presented in Figure 4.5. The immobilization requires two popular crosslinking agents: 1-ethyl-3-(3-dimethylaminopropyl)carbodiimide hydrochloride and N-hydroxy-succinimide[81, 82, 84].

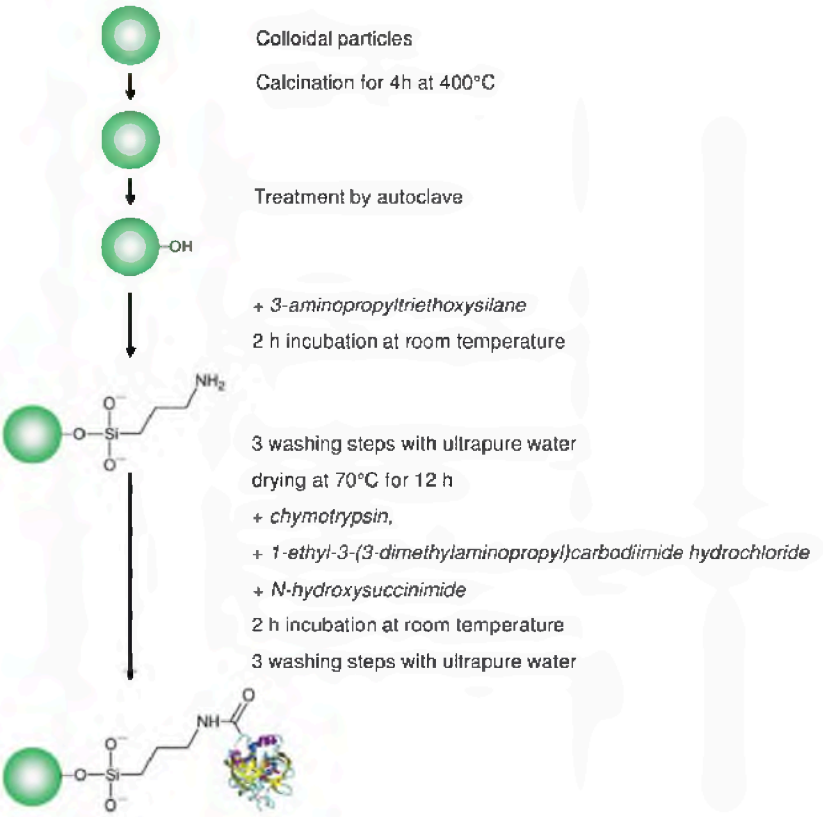


Figure 4.5 Simplified synthesis route involving the stepwise modification of colloidal particles using 3-aminopropyltriethoxysilane, followed by immobilization of α-chymotrypsin during activation with 1-ethyl-3-(3-dimethylaminopropyl)carbodiimide hydrochloride and N-hydroxysuccinimide.

1-Ethyl-3-(3-dimethylaminopropyl)carbodiimide hydrochloride is a well-known carbodiimide used for conjugating biological substances containing amines and carboxylates. 1-Ethyl-3-(3-dimethyl-aminopropyl)carbo-diimide hydrochloride is water soluble and thus can be directly added to a reaction without prior dissolution in organic solvent[81, 82, 84]. Because both 1-ethyl-3-(3-dimethyl-aminopropyl)carbodiimide hydrochloride and the

isourea formed as a by-product of the crosslinking reaction are water soluble, they can be easily removed by dialysis or gel filtration[84-86]. However, 1-ethyl-3-(3-dimethylaminopropyl)carbodiimide hydrochloride is labile in the presence of water, which should be considered when establishing storage conditions and preparing stock solutions.

After activation with 1-ethyl-3-(3-dimethylaminopropyl)carbodiimide hydrochloride and formation of the intermediate ester, the ester is directly reacted with the amino groups of the functionalized colloidal particles. The addition of N-hydroxysuccinimide leads to the formation of another intermediate, the N-hydroxysuccinimide ester. The N-hydroxysuccinimide ester is a more stable intermediate in aqueous solution than the one formed with 1-ethyl-3-(3-dimethylaminopropyl)carbodiimide hydrochloride, thus increasing the reaction yield of the second ester. Formation of the secondary N-hydroxysuccinimide ester is also advantageous because excess 1-ethyl-3-(3-dimethylaminopropyl)carbodiimide can be removed from the particles before adding protein, thus preventing carbodiimide-mediated protein polymerization due to the presence of both amines and carboxylates on the proteins[84, 87, 88].

Side reactions can occur when EDC is used with proteins. 1-Ethyl-3-(3-dimethylaminopropyl)carbodiimide itself may form a stable complex with exposed sulfhydryl groups[89]. Tyrosine residues react with 1-ethyl-3-(3-dimethylaminopropyl)carbodiimide through the ionized phenolate form of its side chain[90]. 1-Ethyl-3-(3-dimethylaminopropyl)carbodiimide can also cause unwanted polymerization via amide bond formation due to the presence of both amines and carboxylates on protein molecules[84].

# 5 Protein adsorption

*ABSTRACT: Chapter 5 describes the factors that influence protein adsorption on colloidal particles. The corresponding forces are discussed in Chapter 2. This chapter focuses on protein, colloidal particles, and media properties that govern the interactions and processes on the particle surface, such as conformational changes in proteins and exchange processes between proteins. Thermodynamic considerations for protein adsorption are also introduced. Typical models for protein adsorption isotherms and kinetics, such as the Langmuir model, are presented.*

## 5.1 Influences on protein-particle interactions

Different parameters and their interplay influence the interactions between colloidal particles and proteins. Chapter 2 described how electrostatic, hydrophobic, van der Waals, and hydrogen-bonding interaction forces influence proteins and particles in an aqueous solution[27, 29, 91].

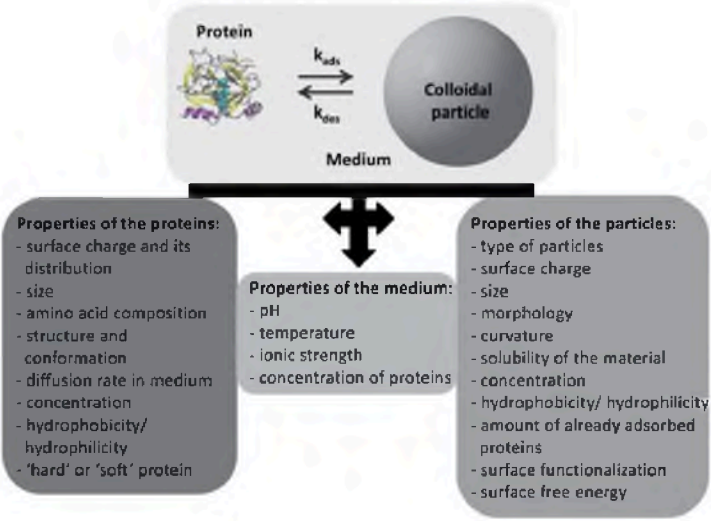


Figure 5.1 Properties of proteins, the surrounding media, and colloidal particles that govern protein adsorption. The data present a summarized overview from the references[9, 22, 24, 25, 27, 29, 35, 91-93].

Surface chemistry, hydrophobicity/ hydrophilicity of proteins and particles, surface charge, protein structure and the properties of the media affect these forces and are therefore the key factors for protein-particle adsorption as summarized in Figure 5.1[9, 22, 24, 27, 29, 35, 91, 92].

Figure 5.2 provides an overview of the processes on the particle surface that critically influence protein-particle interactions. The orientation of the protein on the particle surface is essentially a determining factor. Non-globular, asymmetric proteins may adsorb via their short end ('end-on') or via their long side ('side-on') on the particle surface[29, 94]. Some proteins bind only via a specific amino acid segment that is referred to as a binding epitope[92]. Because the protein orientation specifies the area that the protein occupies on the particle surface, it determines the density of the protein monolayer, bilayer or multilayer. Depending on orientation and shape, adsorbed proteins in the first layer may sterically hinder the adsorption of additional proteins. Proteins may also undergo conformational changes due to their interactions with the particle surface. These changes can have a strong effect on protein function, with positive or negative changes in enzymatic activity[13, 22, 95, 96]. Furthermore, lateral interactions between neighboring adsorbed proteins can have stabilizing or destabilizing effects on the adsorbed protein layer and can modify protein function[29], and adsorption can be reversible. Desorption can be initiated by changes in the media conditions or additional proteins with a higher affinity for the particle surface that replace the first protein. The time-dependent exchange of proteins on particle surfaces is referred to as the 'Vroman effect'[25, 93]: proteins with greater mobility adsorb on the surface more rapidly but over time will be replaced by proteins with lower mobility but higher affinity for the surface[25, 93]. Numerous influencing factors and reactions on the particle surface lead to a complex interplay whose correlative processes are incompletely understood[24, 97].

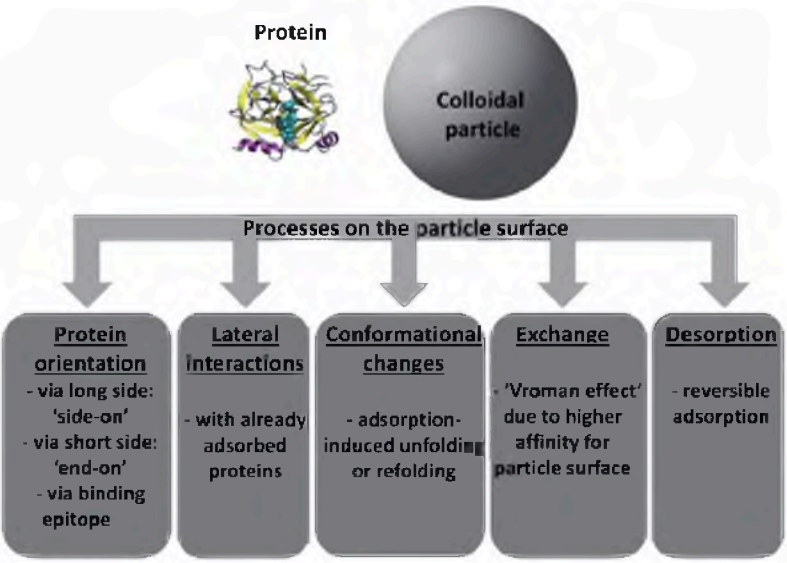


Figure 5.2 Processes on the particle surface that influence protein-particle interactions. The data are summarized from the references[9, 22, 24, 25, 27, 29, 35, 91-93].

## 5.2 Thermodynamic approach

Protein-particle adsorption occurs spontaneously, if the Gibbs energy *G* of the system decreases during adsorption[28]:

$$\Delta_{ads} G = (\Delta_{\mathrm{ads}} \mathrm{H} - \mathrm{T}\Delta_{\mathrm{ads}} \mathrm{S}) < 0 \qquad (5.1)$$

Here, *H* is enthalpy, *S* is entropy, *T* is the temperature of the system, and $\Delta_{ads}$ represents the variation resulting from the protein adsorption process at a constant pressure and temperature[28]. To determine the energy for the overall protein adsorption, the energy terms of all sub-processes contributing to overall protein-particle adsorption must be calculated[28, 32, 98]. These sub-processes include the contributions of electrostatic interactions (subscript *el*), conformational changes in the protein caused by adsorption (subscript *conf*) and hydrophobic interactions (subscript *phobic*). Additional factors influencing the energetic and entropic

processes directing protein adsorption are described in the references[28, 43, 99, 100].

$$\Delta_{ads} G = (\Delta_{ads} G)_{el} + (\Delta_{ads} G)_{conf} + (\Delta_{ads} G)_{phobic} + \ldots \quad (5.2)$$

## 5.3 Protein adsorption models

Different adsorption models have been proposed to illustrate and predict the time and concentration dependence of protein adsorption on the particle surface. The adsorption of a protein on a colloidal particle to form a protein-particle complex is analogous to a chemical reaction[98, 101]. The rate constants for adsorption, $k_{ads}$, and desorption, $k_{des}$, which are illustrated in Figure 5.1, can be calculated as follows[98, 101]:

$$K = \frac{[protein][colloidal\ particle]}{[\text{protein} - \text{particle complex}]} = \frac{k_{des}}{k_{ads}} \quad (5.3)$$

The subsequent subchapters will introduce the conventional models that describe the kinetics of protein adsorption and adsorption rates.

### 5.3.1 The Langmuir adsorption model

In 1918, Langmuir introduced an adsorption model to describe the adsorption of gases[102]. This model has since been widely used to describe protein adsorption processes because of its simple mathematical solution[102].
The Langmuir adsorption model is based on the following assumptions[42, 47, 48, 101, 103]:

- Adsorption is reversible.
- The adsorbent surface has a certain number of identical binding sites $S_B$. Free adsorption sites $S_0$ can be calculated as $S_B - S_{ads}$,

where $S_{ads}$ is the number of adsorption sites that are already occupied with proteins or the concentration of the adsorbed proteins.

- Adsorption is assumed to lead only to a monolayer of proteins and assumes that all $S_B$ can be occupied. Multilayer formation is not considered.
- Adsorbed proteins do not influence the protein adsorption of other proteins.
- Lateral interactions between the adsorbed molecules are excluded.

Based on these assumptions, the adsorption and desorption rates can be calculated as follows, where $c$ is the protein concentration in solution[42]:

$$k_{des} S_{ads} = k_{ads} c S_0 = k_{ads} c(S_B - S_{ads}) \tag{5.4}$$

Considering $S_{ads}/S_B$ as the coverage $\theta$ of the surface with proteins and using the Langmuir constant $K_L = k_{ads}/k_{des}$ and equations (5.3) and (5.4), the Langmuir equation is defined as follows[102]:

$$\theta = \frac{K_L c}{1 + K_L c} \tag{5.5}$$

This formula requires the equilibrium conditions. The rate at which the adsorption equilibrium is reached is given by the following[102]:

$$\frac{d\theta}{dt} = k_{ads} S_B - S_B(k_{ads} + k_{ads})\theta \tag{5.6}$$

Considering protein adsorption as a chemical equilibrium reaction with equilibrium constant $K$, the standard Gibbs energy of adsorption $\Delta_{ads}G^0$ can be calculated using the Langmuir adsorption model[42]:

$$\Delta_{ads} G^0 = -RT \ln \frac{1}{K} \quad (5.7)$$

$K$ is the reciprocal of the Langmuir constant $K_L$[42]. Calculation of the Gibbs energy for protein adsorption from the Langmuir constant must be performed with some reservation, as many assumptions are made in the model that do not completely apply to protein adsorption. Protein adsorption is often irreversible, and bilayers or multilayers can be formed[9, 28, 35, 91].

### 5.3.2 Other adsorption models

To resolve the limitations of the Langmuir model, more complex adsorption models have been introduced. One of the most popular is the 'random sequential adsorption' (RSA) model[104]. This model assumes that proteins adsorb irreversibly and sequentially at random positions on a surface and do not overlap with already adsorbed proteins; thus, the adsorption density on the surface can maximally reach 54.7%[104]. Other alternative models, such as the 'surface clusters' and the 'spreading particle' models, consider factors such as the diffusion of proteins on adsorbents and conformational and orientation changes. A detailed overview of current kinetic adsorption models can be found in the references[43, 48, 91, 100].

## 5.4 Methods for studying protein-particle adsorption

The methods for analyzing protein adsorption on colloidal particles are usually divided into two groups. The first group consists of methods to study the free proteins that remain in the supernatant after the incubation of proteins and particles. These methods enable the indirect measurement of adsorbed proteins using conventional analysis methods. The particles with the adsorbed proteins must be separated from free proteins before such measurements, such as by centrifugation. The free proteins are then analyzed by UV spectroscopy, mass spectroscopy, or sodium dodecyl-sulfate-polyacrylamide gel electrophoresis (SDS-PAGE)[24, 34, 36, 105, 106].

The second group comprises methods that directly analyze the adsorbed proteins on the particle surface or the changes in surface properties caused by protein adsorption. Atomic force microscopy (AFM) can be used to determine the morphology before and after protein adsorption. The surface charges and charge distribution on particles can also be analyzed[107-110]. Surface plasmon resonance (SPR) can be used to investigate protein adsorption kinetics and adsorption and desorption from particle surfaces[21, 111, 112]. Electroacoustic spectroscopy can be applied to analyze the changes in zeta potential and possible IEP shifts after protein adsorption[32, 33, 113]. Further studies can be performed via isothermal titration calorimetry (ITC), which allows the measurement of the affinity and enthalpy of protein binding[20, 31, 114]. Circular dichroism studies of proteins before and after adsorption can also be performed to detect possible structural changes due to the adsorption process[36, 106, 115]. Additional analysis methods include the detection of fluorescent or radioactive signals of proteins that are labeled with fluorescent markers or radioactive isotopes[30, 37, 38, 100]. However, a disadvantage of labeling is that it may influence and change the properties of the protein.

The limiting factor of the techniques in the second group compared with the first group is that the particles can interfere with the analysis method. All possible effects must be considered. The introduced techniques provide a brief overview of convenient methods for the characterization of protein adsorption on a particle surface but are not comprehensive. The main techniques that were applied for this work are described in detail in Chapter 7. For further information on methods for studying protein-particle adsorption, the reader is referred to the references[9, 10, 22-24, 116].

# 6 Enzymatic activity

*ABSTRACT: Chapter 6 provides a detailed introduction to Michaelis-Menten kinetics to provide a foundation for an explicit explanation of the correlation between the Michaelis-Menten constant $K_M$ and substrate efficiency. A central assay for the analysis of the enzymatic activity of α-chymotrypsin is introduced, and an overview of the general frameworks of the most convenient methods is presented. Furthermore, the preliminary analyses that must be performed to establish each assay are presented in detail. Convenient linearization plots to determine $K_M$ and $V_{max}$ are also introduced.*

## 6.1 Michaelis-Menten kinetics

A simple enzyme-catalyzed reaction with one substrate is analogous to a second-order reaction. This reaction can be written as follows[66, 72, 117]:

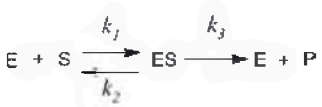


(6.1)

As the concentration of the substrate increases, the rate of reaction also increases. The velocity decreases during the ongoing reaction because the concentration of the substrate decreases or product begins to accumulate. The velocity will reach equilibrium, assuming that the reaction is reversible[66, 72, 117].

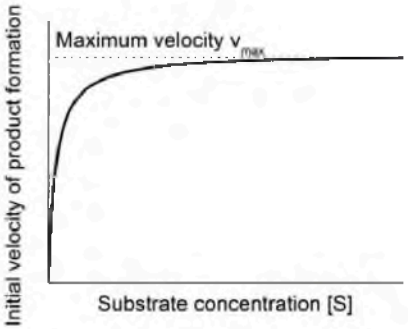


Figure 6.1 Initial velocity $v_0$ plotted versus substrate concentration for an enzyme-catalyzed reaction.

The curve shown in Figure 6.1 can be obtained by calculating the initial velocity of the reaction $v_0$ at different substrate concentrations. Due to the high concentration of substrate, the velocity becomes zero order. The enzyme and substrate form a complex, and the rate of product formation is proportional to the concentration of the complex. Thus, the velocity no longer increases with increasing [S]. The rate of formation of product is given by the following[66, 72, 117]:

$$\mathrm{dP/dt} = k_3[ES] \tag{6.2}$$

To derive the Michaelis-Menten equation, it is necessary to determine the concentration of *ES*. The rate of formation of *ES* is given by $k_1\,[E_{free}]\,[S]$, where $[E_{free}]$ is the concentration of free enzyme. Two reactions are important in this case: *ES* returning to the starting material, given by $k_2\,[ES]$, and *ES* going to products, $k_3\,[ES]$. The combination of these terms leads to the following equation[66, 72, 117]:

$$\frac{d[ES]}{dt} = k_1[E_{free}][S] - k_2[ES] - k_3[ES] \tag{6.3}$$

The concentration of *ES* is assumed to be constant except for the first few milliseconds after contact between the substrate and enzyme, thus giving

*d[ES]/dt = 0*. This is referred to as the "steady-state assumption", which can be proven mathematically. Substitution of $[E_{free}]$ with $[E_{total}] - [ES]$, where $[E_{total}]$ is the total enzyme concentration, leads to the following[66, 72, 117]:

$$k_1([E_{total}] - [ES])[S] = (k_2 + k_3)[ES] \tag{6.4}$$

After rearranging, we obtain[66, 72, 117]

$$[ES] = \frac{k_1[E_{total}][S]}{((k_2 + k_3) + k_1[S])} \tag{6.5}$$

Multiplying the above equation by $k_3$ because the rate $v$ of the reaction is $k_3\,[ES]$ leads to[66, 72, 117]

$$v = \frac{k_3 k_1[E_{total}][S]}{((k_2 + k_3) + k_1[S])} \tag{6.6}$$

To convert this equation to the usual format of the Michaelis-Menten equation, the denominator and numerator must be divided by $k_1$[66, 72, 117].

$$v = \frac{k_3[E_{total}]\,[S]}{\frac{k_2 + k_3}{k_1} + [S]} = \frac{V_{max}\,[S]}{K_M + [S]} \tag{6.7}$$

$V_{max}$ is the maximum velocity of the reaction (see Figure 6.1) when the entire enzyme is in the ES form, and therefore $k_3$ is $k_{cat}$ (see also equation (6.8)). The units of $V_{max}$ are moles of product per unit time. $k_{cat}$ has units of time$^{-1}$ and is referred to as the turnover number of the enzyme. The turnover number indicates the number of molecules of substrate converted to product per unit time per molecule of enzyme. The larger the value of $k_{cat}$ for an enzyme, the faster the reaction[66-68, 71].

The constants in the denominator of equation (6.7) comprise the Michaelis-Menten constant $K_M$. $K_M$ is not a simple dissociation constant. If

$k_3$ is very small compared to $k_2$, the resulting ratio is $k_2/k_1$, which is the dissociation constant $K_d$. The value of $K_M$ indicates how well a substrate interacts with an enzyme. A smaller value of $K_M$ indicates a tighter interaction between the substrate and enzyme. Furthermore, $K_M$ is the concentration of substrate at which the velocity of the reaction $v$ is one-half the maximum velocity $V_{max}$. When $v$ is equal to 0.5 $V_{max}$, one-half of the total enzyme is in complex with the substrate and one-half is free. When $[S] >> K_M$, 100% of the enzyme is in the *ES* complex, and the reaction reaches $V_{max}$. In practice, one usually assumes that $V_{max}$ is approached when $[S]$ is greater than 10 times $K_M$[66-68, 71].

The equation (6.7) has the form of a general hyperbolic equation. When the value of $[S]$ is much larger than the value of $K_M$, the value of the denominator approaches the value of $[S]$, and the equation is approximated by[66]

$$v = \frac{k_{cat}[E][S]}{[S]} = k_{cat}[E] \tag{6.8}$$

The velocity becomes independent of the concentration of *S*, and the reaction becomes zero order with respect to *S*. When $[S]$ is very small compared to $K_M$, equation (6.7) can be written as[66]

$$v = \frac{k_{cat}[E_{total}][S]}{K_M} = \frac{V_{max}[S]}{K_M} \tag{6.9}$$

When $[S] << K_M$, a plot of $v$ versus $[S]$ is linear. The term $k_{cat}/K_M$ can be considered a second-order rate constant because there are two concentration terms in the rate equation, $[E_{total}]$ and $[S]$. In general, a rate constant cannot be faster than the rate at which two molecules diffuse in solution. The rate constant for a second-order diffusion reaction is approximately $10^9$ mole$^{-1}$ s$^{-1}$. Thus, if $k_{cat}$ is very large, $K_M$ cannot be very small or it would exceed the diffusion rate. At a fixed concentration of substrate, the overall velocity is faster when $K_M$ is high. Such conditions

force $k_{cat}$ to be larger to satisfy the $k_{cat}/K_M$ ratio. To evaluate different substrates for an enzyme, the substrates with the highest $k_{cat}/K_M$ values and not those with the lowest $K_M$ should be considered the better substrates for the enzyme [66].

## 6.2 Determination of $K_M$ and $V_{max}$ from linearization plots

$K_M$ can be approximated from plots of $v$ versus substrate concentration $[S]$. One of the most common graphical presentations is the Lineweaver-Burk plot, which is based on the reciprocal of the Michaelis-Menten equation (6.7)[66, 117].

$$\frac{1}{v} = \frac{1}{V_{max}} + \frac{K_M}{V_{max}} \cdot \frac{1}{[S]} \tag{6.10}$$

A plot of $1/v$ versus $1/[S]$ is a straight line with slope $K_M/V_{max}$. The intercept on the x-axis is $-1/K_M$, and the intercept on the y-axis is $1/V_{max}$[66, 117].

Hanes and Eadie-Hofstee plots are also often used to determine $K_M$ and $V_{max}$[117]. Table 6.1 provides an overview of linearization plots. All plots exhibit a manipulated error distribution due to linearization and provide only an approximation of the kinetic constants[117].

Table 6.1 Linearization plots for the determination of $K_M$ and $V_{max}$ (adapted from the references[66, 117])

| Plot | Graphical presentation | | Intercept on the | | Slope |
|---|---|---|---|---|---|
| | x-axis | y-axis | x-axis | y-axis | |
| **Lineweaver-Burk** | 1/[S] | $1/v$ | $-1/K_M$ | $1/V_{max}$ | $K_M/V_{max}$ |
| **Hanes** | [S] | $[S]/v$ | $-K_M$ | $K_M/V_{max}$ | $1/V_{max}$ |
| **Eadie-Hofstee** | $v$/[S] | $v$ | $V_{max}/K_M$ | $V_{max}$ | $-K_M$ |

## 6.3 Activity assays: principles

External conditions such as pH, temperature, and salt concentration affect enzyme activity and should be considered when developing enzymatic assays[66, 117]. Plots of velocity versus temperature for most mammalian enzymes yield a bell-shaped curve with an optimum between 40 °C and 45 °C. Heat denaturation of the enzyme occurs above this temperature. Many enzymes exhibit a two-fold increase in activity for every 10 °C increase in temperature between 0 °C and 40 °C[66].

Plots of velocity versus pH also yield bell-shaped curves for most enzymes. Nevertheless, the pH optimum varies greatly for different enzymes. The shape of the curve and the position of the maximum on the x-axis are dependent on the ionized state of the substrate, which is in turn dependent on the ionization of specific amino acid residues that constitute the active site. Amino acid residues that are involved in catalyzing the reaction must be in the appropriate charge state to be functional[66].

Studies of the kinetics of enzymes before and after immobilization on colloidal particles require a highly reproducible enzyme assay. A good assay is based on temperature and pH control, as well as control of the concentrations of substrates and other relevant factors such as co-substrates, cofactors, and inhibitors[117]. Thus, the $K_M$, enzyme concentration dependence and substrate concentration dependence of the selected enzyme must be determined. Usually, assays must be performed under $V_{max}$ conditions. It is essential to measure the concentration of a product formed or the substrate remaining as a function of time. For products or substrates that absorb light, the change in light absorption can be detected as a function of time. More details regarding specific enzymatic assays can be found in the literature[66-69, 71, 72, 117].

# 7 Experimental methods and principles

*ABSTRACT: Chapter 7 presents the fundamentals of key measurement techniques used in this thesis. Additional details can be found in the methods sections of Chapters 8-11.*

## 7.1 Electroacoustic spectroscopy: zeta potential

The zeta potentials of particles before and after protein adsorption can be measured via electroacoustic spectroscopy using a DT1200 (Dispersion Technology Inc., USA). In this method, a zeta potential probe emits an acoustic wave at a frequency between 2 and 10 MHz into a stirred particle suspension. The acoustic wave induces motion of the particles relative to the medium if the density of the particles is different than the density of the medium[118]. This particle motion leads to a rearrangement of the double layer around the particle and causes a dipole moment and an electric field as shown in Figure 7.1. An electric current called the colloidal vibration current (CVI) is generated via the interference of the electric fields for all particles in the suspension. The CVI can be measured by a receiving transducer in the zeta potential probe[63, 119, 120]. The relationship between the CVI and the dynamic electrophoretic mobility of the particles $\mu_D$ was described by O'Brien[121]:

$$CVI = A(\omega)F(Z_T,Z_S)\varphi\frac{\rho_p - \rho_m}{\rho_m}\mu_D \qquad (7.1)$$

$A(\omega)$ is an acoustic wave frequency that is dependent on the constants of the device determined by calibration. $F(Z_T, Z_S)$ is a function of the acoustic impedances of the transducer ($Z_T$) and the suspension ($Z_S$), $\varphi$ is the particle volume fraction, and $\rho_m$ and $\rho_p$ are the densities of the medium and the particles, respectively[121]. The zeta potential can also be calculated using an equation for electrophoretic mobility based on the Smoluchowski equation[121]:

$$\mu_D = \frac{2\varepsilon_0\varepsilon_r\zeta}{3\eta} M\left(\frac{\omega r^2}{\nu}\right)\left(1 + f(\lambda,\omega')\right) \tag{7.2}$$

η is the viscosity, $\varepsilon_0$ is the permittivity of free space, $\varepsilon_r$ is the relative permittivity of the medium, and ζ is the zeta potential. $M$ is a function of the frequency of the acoustic wave $\omega$, the particle radius $r$ and the kinematic viscosity given by $\nu = \eta/\rho_m$. $f$ is a function of λ and $\omega'$. $\lambda$ can be calculated using the equation $\lambda = K_S/(K^\infty r)$, where $K_S$ is the surface conductivity of the double layer, $K^\infty$ is the electrical conductivity of the medium, and $\omega' = \frac{\omega\varepsilon_r\ell_0}{K^\infty}$. However, O'Brien's theory is not universal and is only valid for dilute suspensions of less than 2 vol%[118, 121]. Duhkin and Oshima established extensions of this theory for higher-concentration suspensions up to 60 vol%[63, 121, 122]. Thus, the zeta potential can be obtained from the CVI if the particle size, particle concentration, and density of the medium are known. Beneficially, molecules such as free proteins in an aqueous medium or other dissolved chemical compounds do not interfere with the zeta potential measurement of the particles or protein-particle complexes when their density does not differ significantly from that of the medium. Because most devices have an integrated titration unit, the zeta potential can be automatically measured as a function of pH. These measurements can be used to calculate the IEP (see also Chapter 2.2.2).

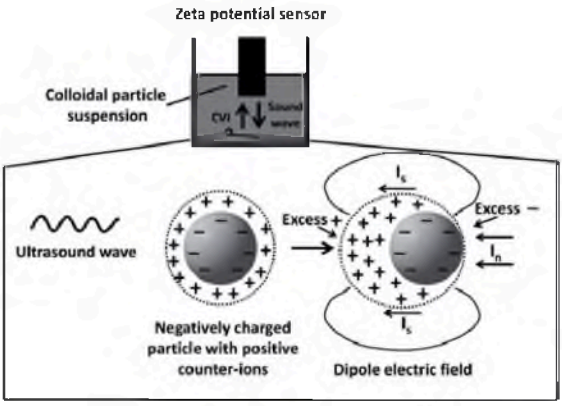


Figure 7.1 Schematic structure of a zeta potential measurement. The particle's electric double layer is polarized by an acoustic wave, resulting in an electric field and CVI. The surface current $I_s$ reduces the number of positive ions near the right particle pole. By

contrast, the double layer receives extra ions near the left pole. Thus, the equilibrium of the double layer shifts. The induced dipole moment affects ions in the bulk medium and induces an electric current $I_n$. $I_n$ compensates for $I_s$ (adapted from the references[63, 118]).

## 7.2 Gas adsorption isotherms: specific surface area $SSA_{BET}$, hydrophobicity/ hydrophilicity

Volumetric measurements of gas adsorption isotherms were performed using a BELSORP-mini device and a BELSORP 18-3 device (both from Bel Inc., Japan). Nitrogen adsorption isotherms were used to assess the specific surface area *($SSA_{BET}$)* of the particles. Water vapor and n-heptane adsorption isotherms were used to determine the hydrophilic/ hydrophobic properties of the particle surface. The same general principle underlies both measurements and will be explained below.

To measure the adsorption isotherm, the gas is gradually transported to the sample cell with the particles. Accordingly, the gas pressure $p$ is increased from $\sim 10^{-3}$ kPa to the saturation vapor pressure $p_0$ at a given temperature. This temperature is 77 K for nitrogen adsorption and 297 K for water and n-heptane adsorption. At each addition step, the adsorbed amount is assessed as the difference between the gas added to the sample cell and the amount of non-adsorbed gas. The pressure of the added gas is gradually decreased to determine the desorption isotherm. The shapes of the adsorption and desorption isotherms and the amounts of adsorbed gases provide information regarding the porosity of the particles and the affinity of the gas for the particle surface[42, 48, 123]. A comparison of the adsorption data for polar water molecules with the adsorption of non-polar n-heptane is essential for the assessment of the hydrophilic/ hydrophobic properties of the particles[124].

To calculate the $SSA_{BET}$ of the particles, the volume of nitrogen molecules required to build a monolayer on the particle surface ($V_m$) is obtained by fitting the adsorption isotherm with the BET adsorption model. The BET adsorption model was developed by Brunauer, Emmet, and Teller in 1938 and is an extension of the Langmuir model introduced in Chapter 5.3.1[125]. The specific surface area $SSA_{BET}$ is then given as follows:[42, 48, 123]

$$SSA_{BET} = \frac{V_m N a \rho}{M} \quad (7.3)$$

$N$ is Avogadro's number, $a$ is the cross-sectional area of a nitrogen molecule, which is approximately 0.162 $nm^2$, $\rho$ is the density, and $M$ is the molecular weight of the nitrogen molecules.

## 7.3 UV-Vis spectroscopy: protein quantification

Ultraviolet-visible (UV-Vis) spectroscopy is used for both protein quantification via a Pierce™ bicinchoninic acid protein assay[126] (BCA assay) and activity assays using p-NPA as a chymotrypsin substrate[39, 41, 127]. Activity assays for free and adsorbed α-chymotrypsin are described in Chapter 7.4. Thus, the general basis for UV-Vis measurements will be explained using the BCA assay as an example. After the incubation of a particle suspension with enzyme, the particles and the free enzymes were separated by centrifugation. The resulting supernatant was particle-free and contained only free enzymes.

Protein concentrations in the supernatants and in reference protein solutions incubated without colloidal particles were measured with the BCA assay according to the manufacturer´s instructions (Thermo Fisher Scientific GmbH, Germany). Briefly, 25 µL of each supernatant was mixed with 200 µL of the working solution (freshly prepared by mixing two solutions in the kit) in a well of a 96-well microtiter plate (Nunc™, Denmark). The plate was thoroughly mixed on a horizontal plate shaker for 30 seconds, covered, incubated at 37 °C for 30 minutes, and cooled to room temperature. The absorbance was measured at 562 nm using a photometer plate reader (Chameleon II, Hidex, Finland and Sunrise, Tecan, Austria). This assay combines the well-known reduction of $Cu^{2+}$ to $Cu^{+}$ by a protein in an alkaline medium (the so-called biuret reaction)[128] with the highly sensitive and selective colorimetric detection of the cuprous cation $Cu^{+}$ using a reagent containing BCA[126, 129]. The purple-colored reaction product of this assay is formed by the chelation of one cuprous ion by two molecules of BCA. This water-soluble complex features a strong absorbance at 562 nm that is nearly linear with increasing protein concentration over a broad working range of 20-2000 µg $mL^{-1}$. The

working range can be further enhanced to 5-250 µg $mL^{-1}$ by increasing the incubation temperature to 60 °C[129].

Quantification is generally based on the correlation of the amount of absorbed light with the protein concentration in the sample. Light with a wavelength of 562 nm and an intensity $I_0$ is passed across the protein sample in a microtiter plate or in a cuvette with a thickness *d* given in cm. The Lambert-Beer law describes the relationship between the absorption, the intensity of the transmitted light $I$, and the protein concentration *c* (given in units of mol $L^{-1}$) [66, 71, 130]:

$$A = log_{10}(I_0/I) = \varepsilon cd \qquad (7.4)$$

Here, $\varepsilon$ is the extinction coefficient given in units of L $mol^{-1}$ $cm^{-1}$. The extinction coefficient is a matter constant and depends on the wavelength of the light and on the medium conditions[117]. Figure 7.2 presents a measured standard curve for chymotrypsin using the BCA assay. For all experiments, protein quantification was performed in the linear range of the standard curve. This approach enables the highest sensitivity and precision.

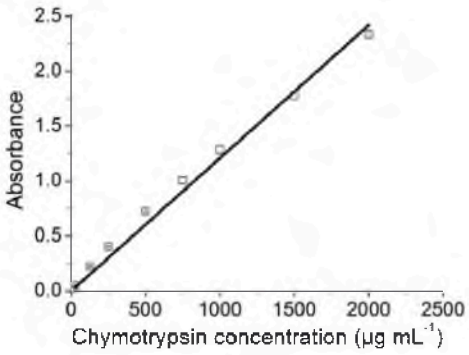


Figure 7.2 Absorbance of visible light at 562 nm by α-chymotrypsin samples as a function of enzyme concentration.

## 7.4 Activity assessment of free and adsorbed α-chymotrypsin

The enzymatic activity of free chymotrypsin in supernatants was determined as described in the references[40, 131, 132] and depicted in Figure 7.3a. Briefly, 20 µL of each supernatant was mixed with 140 µL of 100 mM potassium phosphate buffer at pH 8.5 in a 96-well microtiter plate (Nunc™, Denmark). A 160-µL aliquot of 0.2 mM p-NPA was added, and the increase in absorbance due to the formation of p-nitrophenolate (p-NP) ions was measured at 405 nm using a microtiter plate reader (Sunrise, Tecan, Austria). The non-enzymatically catalyzed hydrolysis of p-NPA[133], referred to as spontaneous hydrolysis, was determined by mixing 20 µL of $ddH_2O$ with 140 µL of 100 mM potassium phosphate buffer for use as a blank measurement.
One of the key challenges for the analysis of the enzymatic activity of adsorbed enzymes is that assays based on UV/Vis spectrometry are not directly applicable due to the light scattering caused by colloidal particles. Therefore, a detailed optimization of the photometric assay based on p-NPA as a chymotrypsin substrate was performed as part of this thesis. The optimization included proof of reliable stability of enzyme adsorption, adjustment of the amount of enzyme adsorbed on the colloidal particles, selection of suitable experimental conditions such as pH and ionic strength during physisorption, concentration of the enzyme substrate, and adequate incubation times. Adjustments of all of these parameters were required to obtain sufficient extinction signals in a linear measurement range.

Consequently, the enzymatic activity of adsorbed chymotrypsin was determined using the enzymatic assay presented in Figure 7.3b. In detail, after a specified incubation time, the colloidal particles were briefly rinsed and mixed with 280 µL of 100 mM potassium phosphate buffer at pH 8.5 in 1.5-mL polypropylene tubes. Then, 320 µL of p-NPA at concentrations ranging from 0.01 to 0.4 mM was added. After a specified incubation time, e.g., 20, 30 or 40 min, the samples were centrifuged, and the supernatants were collected. A 320-µL aliquot of the supernatant was used to measure the increase in absorbance due to the formation of p-NP at 405 nm at each of the three time points. The selected time points can vary and were adjusted based on the dependence of the extinction signals on the amount of adsorbed enzymes and their activity as well as the

selected substrate concentration (see also the experimental sections in Chapters 8 and 9).

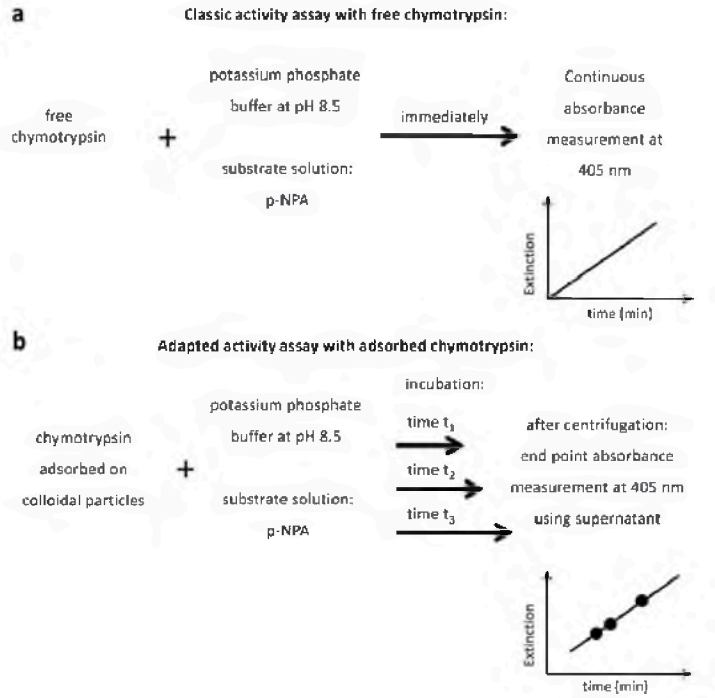


Figure 7.3 Schematic view of the experimental set-up for a classic activity assay with free chymotrypsin (a) and an adapted activity assay with chymotrypsin adsorbed on colloidal particles (b) (adapted with permission from Figure 8.2 from a reference[134]).

The main requirements were that the measurements must be performed in linear mode and the absorbance must be less than 1. The spontaneous hydrolysis of p-NPA was measured using a colloidal suspension that was not incubated with chymotrypsin according to a reference[133]. Using the extinction data for all three measured time points, a straight line was formed. Similar to the enzymatic assay for free chymotrypsin, the slope of the line was $\Delta E\ min^{-1}$. Further calculations were based on the Lambert-Beer law and are explained in Chapter 7.3. Furthermore, the specific enzymatic activity of chymotrypsin was determined as a function of the chymotrypsin concentration as follows:

$$Specific\ activity\ in\ nmol\ p-NPA\ min^{-1}mg^{-1} = \frac{Absolute\ activity\ in\ nmol\ p-NPA\ min^{-1}ml^{-1}}{Enzyme\ concentration\ in\ mg\ ml^{-1}} \quad (7.5)$$

## 7.5 Matrix-assisted laser desorption ionization time-of-flight mass spectroscopy

Mass spectrometry (MS) is an analytical method that is used to determine the composition of chemical substances by measuring accurate molecular masses. The basic process in an MS analysis is as follows. The molecules of interest are vaporized and ionized, and the mass-to-charge (m/z) ratios of the molecular ions are determined. Based on the gas-phase ions, which are broken down into characteristic fragments, the measurement of the masses of the fragments provides information regarding the molecular structure of the original ion. The ability to vaporize and ionize larger biopolymers such as proteins was once a limiting factor in this technique. Breakthrough studies in soft ionization methods, acknowledged by the Nobel Prize to Koichi Tanaka and John B. Fenn in 2002, greatly advanced the application of MS to protein analysis[135]. MS has developed into a highly sensitive and accurate method for the rapid qualitative and semi-quantitative characterization of peptides and proteins and can even be used in biological fluids[135]. The matrix-assisted laser desorption ionization (MALDI) MS technique is now widely applied for the mass spectrometric analysis of large, nonvolatile molecules, particularly peptides, proteins, oligonucleotides, oligosaccharides, fullerenes, dendrimers, and synthetic polymers of high molecular weight[136].

MS analysis consists of two basic steps: i) the vaporization and ionization of substances of interest from a sample, followed by ii) determination of the masses of the resulting ions. MALDI is one of the most effective soft ionization methods for proteins. The ionization of biomolecules by MALDI results in limited fragmentation, and thus larger molecules can be analyzed. In MALDI, a liquid or solid biological substance is usually co-crystallized with a large excess of UV-absorbing matrix. The illumination of the matrix-analyte crystals by a UV laser leads to a microexplosion that results in primarily singly charged gaseous analyte ions[135]. In this work, the MALDI ionization approach was combined with a time-of-flight (ToF) mass analyzer. In ToF analyzers, the ions are formed in the ionization

source and accelerated by an applied potential such that all ions have the same kinetic energy before entering the field-free region of the mass analyzer. Hence, ions move at different velocities depending on the kinetic energy of the ion. The flight time of each ion in the field-free region is transformed to an m/z value. Thus, the ToF instrument is a mass analyzer with the ability to measure ions over a wide mass range[135]. For more detailed information about MALDI-ToF-MS, please refer to the Methods section in Chapter 11 and to the extended supplementing literature[135, 136].

## 7.6 Circular dichroism spectroscopy: changes in protein structure

Circular dichroism (CD) spectroscopy is a form of adsorption spectroscopy in the UV/ Vis range and is used to measure the differential adsorption of right- and left-handed circularly polarized light by an optically active molecule such as a peptide or protein. Aromatic amino acids in a protein and a polypeptide chain cause an optical rotation and generate a CD spectrum across a range of wavelengths. Because the spectra of α-helical, β-sheet, and random structures differ, CD spectroscopy provides a sensitive method to determine the type and amount of secondary structure[66, 115, 117]. Figure 7.4 presents typical CD spectra for polypeptide chains with different conformations.

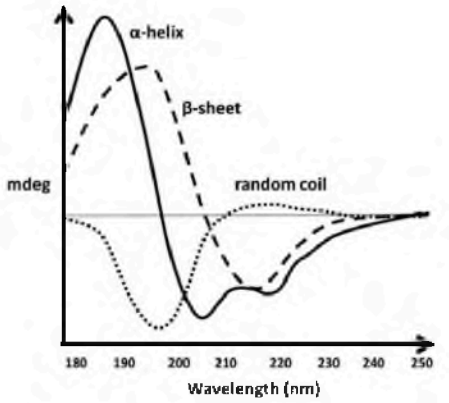


Figure 7.4 CD spectra for polypeptide chains in α-helical, β-sheet, and random conformations (adapted from a reference[66]).

The ellipticity $\Theta$ indicates the extent to which linear polarized light is transformed into elliptically polarized light by an optically active sample. The ellipticity $\Theta$ can be converted to the specific ellipticity $[\Psi]$[117]:

$$[\Psi] = \frac{\Theta}{100\, c' l} \tag{7.6}$$

Here, $c'$ is the concentration of the optically active substance in g $mL^{-1}$ and $l$ is the path length in cm. The ellipticity $\Theta$ should be given in mdeg. It is customary to present CD results as molar ellipticity $[\Theta]$, which can be calculated as follows[117]:

$$[\Theta] = \frac{\Theta}{10\, c\, l} \tag{7.7}$$

In this equation, $c$ is also the concentration of the optically active substance but is given in mol $L^{-1}$. It is convenient for proteins to present the results as mean molar ellipticity, which is normalized to the mean residue weight (MRW)[117]:

$$[\Theta]_{MRW} = \frac{M_{MRW}\Theta}{10 c' l} \tag{7.8}$$

The analysis of secondary structure often requires a database of proteins with known secondary structures. For more detailed information about analyses using complex algorithms, please refer to the extended supplementing literature[115, 117, 137]. Table 7.1 presents data for the secondary structures of selected proteins.

Table 7.1 Secondary structure elements for selected proteins given as %. Data are taken from a reference[117].

| Protein | α-helix | β-sheet antiparallel | β-sheet parallel | turn | rest |
|---|---|---|---|---|---|
| **α-Chymotrypsin** | 10 | 34 | 0 | 20 | 36 |
| **Trypsin** | 8 | 32 | 0 | 30 | 30 |
| **Lysozyme** | 36 | 9 | 0 | 32 | 23 |
| **Hemoglobin** | 75 | 0 | 0 | 14 | 11 |

## 7.7 Visual molecular dynamics: modeling of proteins

Visual Molecular Dynamics (VMD, Version 1.8.7 and 1.9.1) is protein visualization software and not an actual measurement method[70]. An example is presented in Figure 3.2. Protein size, secondary structure, the distribution of hydrophilic/ hydrophobic amino acids, and surface potential distribution are modeled from protein structure files, which are available from the PDB database at http://www.pdb.org/. The atomic coordinates of all atoms in the proteins given in the structure files are usually assessed by X-ray diffraction or NMR analysis. Based on this information, the protein's secondary structure and amino acid composition can be illustrated and analyzed in VMD. The surface potential in VMD can be displayed as an isosurface, which is a surface with a constant potential value at the distance from the protein surface at which this potential occurs. The potential distribution can also be shown on the water-accessible protein surface. To determine the surface potential distribution and its dependence on pH and ionic strength, numerical solutions of the Poisson-Boltzmann equation can be calculated (see Chapter 2). The Adaptive Poisson-Boltzmann Solver (APBS) plug-in of VMD finds the solution for the non-linearized Poisson-Boltzmann equation[138], and the program PDB2PQR allows the addition of protonation states and atomic

charges to the protein structure files as a function of pH[139]. Further details can be found in the method sections of Chapters 8-11.

# 8 Physisorption of enzymatically active chymotrypsin on titania colloidal particles

*ABSTRACT: In this study we use a straightforward experimental method to probe the presence and activity of the proteolytic enzyme α-chymotrypsin adsorbed on $TiO_2$ colloidal particles. We show that the adsorption of α-chymotrypsin on the particles is irreversible and pH-dependent. At pH 8 the amount of adsorbed chymotrypsin is threefold higher compared to the adsorption at pH 5. However, we observe that the adsorption is accompanied by a substantial loss of enzymatic activity, and only approximately 6-9 % of the initial enzyme activity is retained. A Michaelis-Menten kinetics analysis of both unbound and $TiO_2$-bound chymotrypsin shows that the $K_M$ value is increased from ~10 μM for free chymotrypsin to ~40 μM for the particle bound enzyme. Such activity decrease could be related by the hindered accessibility of substrate to the active site of adsorbed chymotrypsin, or by adsorption-induced structural changes. Our simple experimental method does not require any complex technical equipment, can be applied to a broad range of hydrolytic enzymes and to various types of colloidal materials. Our approach allows an easy, fast and reliable determination of particle surface-bound enzyme activity and has high potential for development of future enzyme-based biotechnological and industrial processes.*

## 8.1 Introduction

Immobilization of enzymes onto water-insoluble carriers is of increasing importance for a wide range of applications including bioanalysis, biosensoring, biotechnology, medical therapy, diagnostic, pharmaceutics and proteomics[6-8, 140]. Enzyme immobilization offers several advantages including more convenient handling of the enzyme, facile separation from the enzymatic products, efficient recovery and reuse of costly enzymes. In the past decades, different immobilization approaches have been designed to limit activity loss, decrease the response rate to selected substrates or

avoid possible irreversible damage to the enzyme during the immobilization steps. One of the major challenges is still the need of an easy and straightforward method that makes it possible to determine the activity of adsorbed or surface-bound enzymes. The activity of surface-bound enzymes may be altered by several factors, including denaturation, orientation on the surface, and steric hindrance[7, 13, 15-17, 19, 141-144]. Conventional assays for direct measurement of the activity of free enzymes are often based on UV/ Vis spectrometry. These assays are not reliable if enzymes are immobilized on particles, because the particles increase light scattering and consequently can lead to false results. This problem can be circumvented if a so-called end-point-mode assay is used, which consists of removing the particles from suspensions before measuring the product generated by the particle-bound enzymes[36, 106, 145, 146].

Here we investigate the adsorption of the serine protease α-chymotrypsin on colloidal $TiO_2$ particles. $TiO_2$ colloidal particles are frequently used as a carrier because of their lack of toxicity, their stability and easy availability, as well as their relevance for several applications including bio-inorganic hybrids[147-149], catalysis[150], bioanalytical devices[151] and proteomics[152]. Chymotrypsin represents a good model for studying the modulation of activity after immobilization due to its well-defined structure, well-characterized enzymatic properties[153-155], and its practical applications[146, 156].

In this study chymotrypsin was immobilized by physisorption to $TiO_2$ particles to avoid interference by additional chemicals or coupling reagents with the activity assay[36, 157]. A well-known enzymatic assay based on the hydrolysis of the artificial substrate p-NPA[40, 131, 132] was then optimized to determine chymotrypsin activity before and after adsorption of the enzyme on $TiO_2$ particles. Our data demonstrate that chymotrypsin adsorbs efficiently to $TiO_2$ colloidal particles in a pH-dependent and concentration-dependent manner, but only little enzymatic activity is retained after binding on the particle surface.

## 8.2 Experimental section

### 8.2.1 Materials

$TiO_2$ particles (DuPont™ Ti-Pure® R-101, 97 wt% rutile, Lot. No. 811969T.07) were obtained from DuPont de Nemours GmbH (Germany). Lyophilized α-chymotrypsin type II from bovine pancreas (molar weight 25300 g $mol^{-1}$, purity 94.1 wt%, Lot. No. 60M7007V, 65.622 units $mg^{-1}$ protein, whereby one unit will hydrolyze 1 micromole of N-benzoyl-L-tyrosine ethyl ester per minute at pH 7.8 at 25 °C), p-nitrophenyl acetate (p-NPA; CAS No. 830-03-5, Lot. No. 0001422901), potassium dihydrogen phosphate (≥ 99 wt%, CAS No. 7778-77-0) and 1,4-dioxane (>99.8 wt%, CAS No. 123-91-1, Lot. No. STBB3939) were purchased from Sigma-Aldrich (Germany) and used without any modifications. Pierce™ bicinchoninic acid protein assay kit (BCA assay) was obtained from Thermo Fisher Scientific GmbH (Germany). All other chemicals were purchased from Fluka (Switzerland) or Merck (Germany) at analytical grade. For all aqueous solutions double deionized water ($ddH_2O$) with a conductivity of 0.04 µS $cm^{-1}$ was used as the solvent (Millipore Synergy®, Millipore Corporation, Germany).

### 8.2.2 Characterization of $TiO_2$ colloidal particles

Prior to the investigations, the $TiO_2$ colloidal particles were calcinated at 400 °C for 4 h with a heating and cooling rate of 3 °C $min^{-1}$ (oven L3/11/S27, Nabertherm, Germany) to remove any possible organic contaminants. The particle size was determined by dynamic light scattering (DLS, Malvern Zetasizer Nano SP, Malvern Instruments Ltd, UK) using 0.003 vol % $TiO_2$ suspension at pH 8. Before each DLS measurement, the suspensions' conductivity and pH were adjusted to avoid or to minimize particle agglomeration. The pH was adjusted to pH 5 and pH 8 with 1 M KOH or 1 M HCl using a pH-meter (Five Easy™ FE20, Mettler-Toledo GmbH, Switzerland). The conductivity was set at 500 µS $cm^{-1}$ using 3 M KCl, which corresponds to an ionic strength of 3 mM.

The particles' specific surface area ($SSA_{BET}$) was obtained by volumetric nitrogen adsorption measurements using a BELsorp-mini II device (Bel

Japan Inc, Japan) and assuming a cross-sectional area of the nitrogen molecule of 0.162 $nm^2$[36]. Adsorption isotherms were recorded at −196 °C. All samples were out-gassed at 100 °C under flowing argon for 24 h before measurement.

Zeta potential (ζ-potential) measurements were carried out using an electroacoustic spectrometer DT1200 (Dispersion Technology Inc., USA), as previously reported[118]. ζ-potential measurements were carried out using 1 vol. % $TiO_2$ suspensions with an initial conductivity of 500 µS $cm^{-1}$ and the pH was varied with the integrated titration unit using 1 M HCl and 1 M KOH. The quantity of hydroxyl groups present on the surface of $TiO_2$ particles was determined by potentiometric titrations (TitraLab® TIM 840 Titration Workstation, Hach Lange GmbH, Germany) according to Hidber[158, 159]. The $TiO_2$ particle density was measured by a helium pycnometer (Pycnomatic ATC, Porotec GmbH, Germany).

Transmission electron microscopy (TEM) imaging was performed using a FEI Titan 80/300 kV (FEI, The Netherlands) equipped with a Cs-corrector for spherical aberration of the objective lens at 300 kV and a vacuum of $1.3 \times 10^{-7}$ mbar. $TiO_2$ particles were deposited on graphene-coated copper grids (Graphene Supermarket, New York, USA). The particle morphology was analyzed by scanning electron microscopy (SEM; field-emission SEM SUPRA 40, Zeiss, Germany) operating at 2.00 kV mounted on carbon tape.

The hydrophilic/ hydrophobic surface properties were investigated by volumetric water and n-heptane adsorption measurements using a BELsorp 18-3 device (Bel Japan Inc, Japan) according to[124, 160]. Amounts of adsorbed water and n-heptane are reported as a ratio $p/p_0$ of 0.95, to most accurately simulate atmospheric conditions. Prior to the adsorption measurements, all samples were out-gassed at 100 °C under flowing argon for 24 h. The average and standard deviations of three single measurements are given.

### 8.2.3 Hydrophobic/ hydrophilic properties of chymotrypsin

Chymotrypsin representation of secondary structure, spatial surface potential distribution and surface hydrophilic/ hydrophobic regions were

visualized using the software Visual Molecular Dynamics (VMD, Version 1.9.1)[70]. The atomic coordinates of the proteins were taken from the Brookhaven Protein Database (PDB-ID: 4CHA). After a 1 ns Molecular Dynamics simulation in explicit solvent, the projection of the hydrophobic and hydrophilic amino acids on the "solvent accessible surface area" were calculated using the corresponding function included in VMD with a probe radius of 0.14 nm.

### 8.2.4 Time-dependent and pH-dependent adsorption/ desorption of chymotrypsin

Adsorption of proteins and enzymes depends on environmental factors such as ionic strength and pH[7, 36]. Based on previous research on protein adsorption[158] we set the conductivity of the suspension to 500 µS $cm^{-1}$ which corresponds to the ionic strength of 3 mM to ensure a stable adsorption conditions.$TiO_2$ aqueous suspensions were prepared by mixing 2.07 g of $TiO_2$ with 49.5 ml of $ddH_2O$ (corresponding to 1 vol % suspension). The pH was adjusted to pH 5 and 8 and the suspension conductivity was set at 500 µS $cm^{-1}$ as mentioned above. The Hamaker constant of rutile is rather high (60 x $10^{-21}$ J)[52]. Thus, the $TiO_2$ particles tend to build agglomerates and were deagglomerated, prior to incubation with chymotrypsin, using an ultrasound sonotrode at output 150 W and pulse rate 0.5 s (Sonifier® 450, Branson, USA) for 10 min. Chymotrypsin stock solutions (concentration of 20 mg $ml^{-1}$) were freshly prepared by dissolving lyophilized chymotrypsin in $ddH_2O$ and adjusting the pH to 5 and 8 with 1 M HCl and 1 M KOH, respectively. The initial concentration of chymotrypsin was measured by means of a BCA assay.

A schematic description of the experimental set up for adsorption and desorption studies is shown in Figure 8.1. First, 900 µl of $TiO_2$ suspension were mixed with 100 µl chymotrypsin (Incubation I) in 1.5-ml polypropylene tubes (Eppendorf, Germany). The conductivity at the start of the incubation was determined to be approximately 550 µS $cm^{-1}$. Tubes were constantly overhead shaken (Stuart rotator STR4, Bibby Scientific Ltd., UK) at room temperature at a speed of 30 rpm to prevent agglomeration.

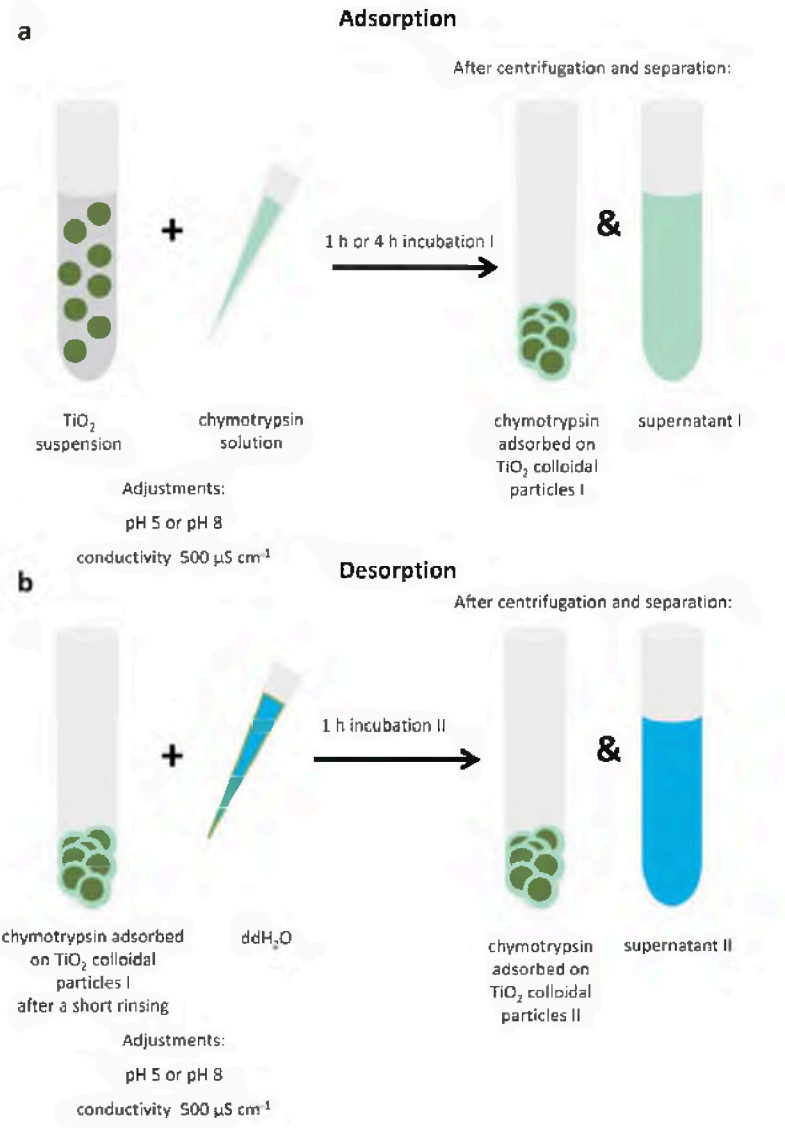


Figure 8.1 Schematic description of the experimental set-up for adsorption (a) and desorption (b) studies.

After 1 or 4 h the suspensions were centrifuged for 10 min at 21,100 g (Heraeus Fresco 21 centrifuge, Fisher Scientific, Germany). 950 µl of supernatant (supernatant I containing the free chymotrypsin) were collected and $TiO_2$ particles with adsorbed chymotrypsin were shortly

rinsed with 950 µl $ddH_2O$. Afterwards, 950 µl $ddH_2O$ with a pH 5 or 8 and a conductivity of 500 µS $cm^{-1}$ were added (incubation II). Identical incubation pH values were used in incubation I and incubation II. The concentration of chymotrypsin in the supernatants I and II was measured using the BCA assay.

### 8.2.5 Concentration-dependent adsorption of chymotrypsin on $TiO_2$

$TiO_2$ suspensions were prepared as described above and the pH and conductivity of the suspension were adjusted to pH 8 and to 500 µS $cm^{-1}$, respectively. Chymotrypsin stock solutions of different concentrations (2.5, 5, 7.5, and 20 mg $ml^{-1}$) were freshly prepared by dissolving lyophilized chymotrypsin in $ddH_2O$. The pH of these stock solutions was adjusted to 8. 900 µl of 1 vol % $TiO_2$ suspension were mixed with 100 µl of chymotrypsin stock solutions. Samples were overhead shaken at a speed of 30 rpm at room temperature for 1 h, and then centrifuged at 21,100 g for 10 min. 950 µl of supernatants were collected and chymotrypsin concentration measured by BCA assay.

### 8.2.6 Determination of the enzymatic activity of chymotrypsin

The enzymatic activity of free chymotrypsin remaining in the supernatants of colloidal particles was determined according to references[40, 131, 132]. Briefly, 20 µL of the supernatant were mixed with 140 µL 100 mM potassium phosphate buffer at pH 8.5 in wells of a 96-well microtiter plate (Nunc™, Denmark). 160 µL 0.2 mM p-NPA were added and the increase in absorbance due to the formation of p-nitrophenolate (p-NP) ion was continuously measured at 405 nm using a microtiter plate reader (Sunrise, Tecan, Austria) (Figure 8.2a). The same conditions were used to determine the $K_M$ and $V_{max}$ of free chymotrypsin, whereby the applied substrate concentrations were 0.01, 0.03, 0.05, 0.07, 0.1, 0.15 mM.

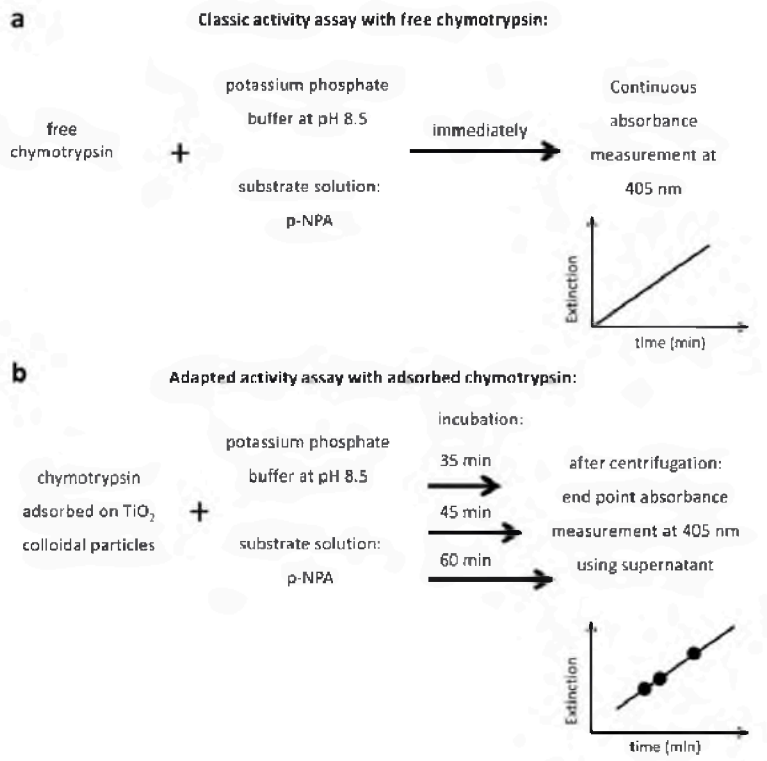


Figure 8.2 Schematic description of the experimental set-up for classic activity assay with free chymotrypsin (a) and optimized activity assay with chymotrypsin adsorbed on $TiO_2$ colloidal particles (b).

The enzymatic activity of adsorbed chymotrypsin was determined by using an end-point measurement (Figure 8.2b). After adsorption of chymotrypsin under the conditions given in the legends of each figure, the suspensions were centrifuged for 10 min at 21,100 g and the supernatant was collected to determine the loss in chymotrypsin content due to particle adsorption. The particles were shortly rinsed with 950 µl $ddH_2O$ and mixed with 280 µl 100 mM potassium phosphate buffer at pH 8.5 in a 1.5 mL polypropylene tubes. 320 µl 0.25 mM (if not stated otherwise) p-NPA were added and after 45 min the reaction mixtures were again centrifuged, the supernatant collected, and 320 µl of each supernatant were used to measure the absorbance at 405 nm. Preliminary experiments using incubation periods of 35, 45 and 60 min revealed that the absorbance at 405 nm due to the formation of p-NP increased almost

proportional to time. Therefore, incubation periods of 45 min were chosen to determine the enzyme-dependent hydrolysis of p-NPA by particle-bound chymotrypsin. Analogically, the described conditions were used to determine the $K_M$ and $V_{max}$ of adsorbed chymotrypsin, whereby the applied substrate concentrations were 0.01, 0.03, 0.05, 0.07, 0.1, 0.15 mM.

Control experiments revealed that, under the experimental conditions used, some hydrolysis of p-NPA occurred in the absence of chymotrypsin. Therefore, for all experimental conditions applied, also the enzyme-independent hydrolysis of p-NPA was recorded. For kinetic analysis of the concentration-dependency, the values obtained for the spontaneous enzyme-independent hydrolysis of p-NPA were subtracted from the values for the respective enzyme-containing reactions. The Hanes plot was used to linearize the data for the enzyme-dependent hydrolysis in order to calculate the values for the Michaelis-Menten constant $K_M$ and the maximal reaction rate $V_{max}$. The specific enzymatic activity of chymotrypsin was determined by normalizing the absolute chymotrypsin activity with respect to the protein content of the corresponding chymotrypsin solution. Additionally, controls of spontaneous hydrolysis using pure water and particles suspensions (without enzyme) were carried out showing that adsorption of hydrolysis products does not take place on colloidal particles.

### 8.2.7 Statistical analysis

All experiments were performed at least three times. The data given in the figures and the tables are mean values ± standard deviations (SD). Statistical analyses were performed by a paired or unpaired t-test using the GraphPad InStat 3 software (GraphPad Software Inc, USA.). $p > 0.05$ was considered as not significant.

## 8.3 Results

### 8.3.1 Characterization of $TiO_2$ colloidal particles

The properties of the $TiO_2$ particles used in this study are summarized in Table 8.1.

Table 8.1 Properties of $TiO_2$ colloidal particles. [a] The data were obtained by manufacturer. All measured data represent means ± SD of values that were obtained in 3 independent experiments.

| Property | $TiO_2$ colloidal particles | |
|---|---|---|
| | values | method |
| **Purity[a] (wt%)** | ≥ 97 | - |
| **Size (nm)** | $d_{50}$: 161 ± 7 | dynamic light scattering |
| **$SSA_{BET}$ ($m^2\ g^{-1}$)** | 5.9 ± 0.1 | volumetric nitrogen adsorption |
| **Exchange capacity (OH $nm^{-2}$)** | 5.1 ± 0.1 | titrations according to Hidber[158, 159] |
| **Isoelectric point (IEP)** | 8.3 ± 0.3 | electroacoustic colloidal vibration current technique |
| **Density (g $cm^{-3}$)** | 4.13 ± 0.01 | pycnometer |
| **Hamaker constant ( x $10^{-21}$ J)** | 60[52] | full spectral method |
| **Crystal structure** | rutile | X-ray diffraction and electron diffraction with HR-TEM |

$TiO_2$ particles are non-spherical (Figure 8.3) and feature a narrow size distribution based on DLS measurements (Table 8.1). TEM analysis confirmed that particles mainly consist of 97 % rutile. The $SSA_{BET}$ of the particles is 5.9 $m^2 g^{-1}$ and the exchange capacity 5.1 OH-groups per $nm^2$.

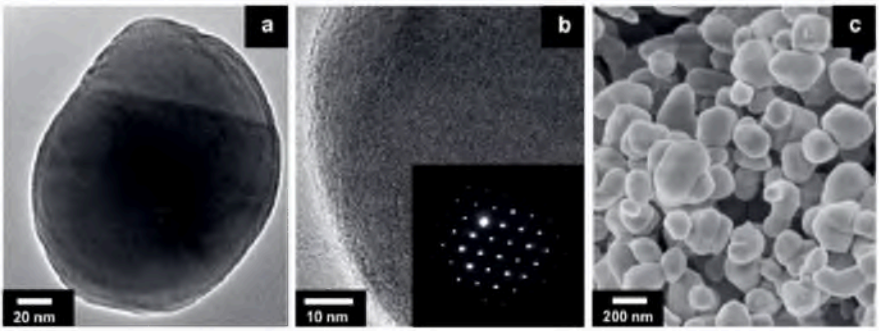


Figure 8.3 HR-TEM images of $TiO_2$ before incubation with different magnification (a and b). Inlet picture in b shows diffraction pattern of rutile. Scanning electron micrographs of $TiO_2$ before (c) incubation with chymotrypsin.

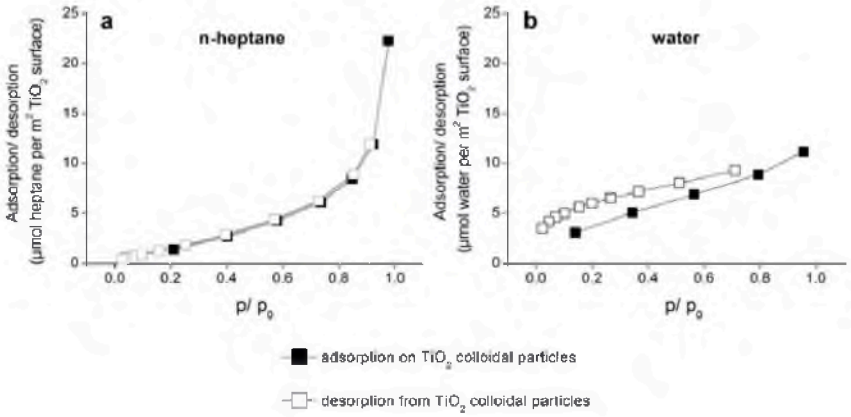


Figure 8.4 Hydrophilic/ hydrophobic properties of $TiO_2$ colloidal particles. $SSA_{BET}$ was taken into account for normalized calculations and adsorption/ desorption is shown for n-heptane (a) and water (b) on/ from $TiO_2$ surface.

The water and n-heptane adsorption capacities (Figure 8.4) were normalized to the $SSA_{BET}$ of the particles (Table 8.1). A higher affinity for n-heptane (~ 23 µmol $m^{-2}$) than for water (~ 12 µmol $m^{-2}$) was determined.

### 8.3.2 Time-dependent and pH-dependent adsorption/ desorption of chymotrypsin

The dependence of the adsorption of chymotrypsin to the surface of $TiO_2$ particles on time and pH was investigated as depicted in Figure 8.1a by determining the chymotrypsin content in the supernatant. Of the initially applied 1.64 mg chymotrypsin, 15 % and 58 % were found adsorbed after 1 h incubation at pH 5 and pH 8, respectively (Figure 8.5a). Increasing the incubation time to 4 h, 18 % and 64 % of the initially applied chymotrypsin was adsorbed at pH 5 and pH 8, respectively. The adsorption of chymotrypsin under these conditions was practically irreversible. Namely, at pH 8 only a few percent of the previously adsorbed chymotrypsin desorbed within 1 h of incubation in the pure solvent at adjusted pH (Figure 8.5b).

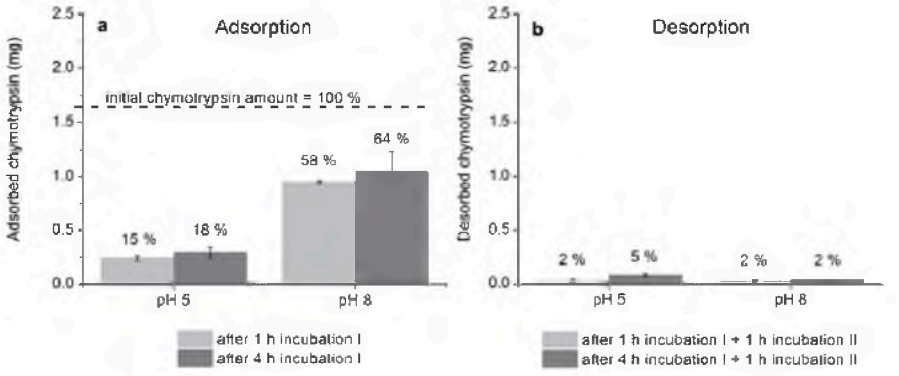


Figure 8.5 Time- and pH-dependent adsorption/ desorption behavior of chymotrypsin on $TiO_2$ colloidal particles. Chymotrypsin at a concentration of 1.64 mg $ml^{-1}$ was incubated with 0.9 vol % $TiO_2$ suspension at the indicated pH values for 1 h and 4 h (incubation I). After centrifugation, the supernatant was used to determine the chymotrypsin concentration. The

absolute values of adsorbed chymotrypsin (a) were calculated by subtracting the concentration of free chymotrypsin in the supernatant from the initial chymotrypsin concentration. Desorption studies were performed after a given adsorption condition (incubation I) by incubating chymotrypsin-adsorbed $TiO_2$ colloidal particles for 1 h at the indicated pH values. Absolute amount of desorbed chymotrypsin (b) was measured in the supernatant after incubation II. The percental amounts of average adsorbed/ desorbed chymotrypsin are given as percent of the initially applied chymotrypsin concentrations. The data shown represent means ± SD of values obtained in 3 independent experiments.

### 8.3.3 Concentration-dependent adsorption of chymotrypsin on $TiO_2$

The amount of adsorbed chymotrypsin on $TiO_2$ increased gradually with the increase of the applied enzyme concentration (Figure 8.6). For chymotrypsin concentrations of 0.21, 0.34, 0.53 and 1.64 mg $ml^{-1}$, approximately 50, 60, 63 and 58 % of the initially applied protein content (Figure 8.6a) and 34, 80, 72 and 63 % of the initially measured enzyme activity (Figure 8.6b), respectively, had disappeared from the supernatant after 1 h incubation with $TiO_2$ colloidal particles. The specific activity of the remaining chymotrypsin in the supernatant was found to be rather constant at approximately 10 nmol p-NPA hydrolysis $min^{-1}$ $mg^{-1}$. This is not substantially different from the specific activity of chymotrypsin incubated in the absence of particles (Figure 8.6c).

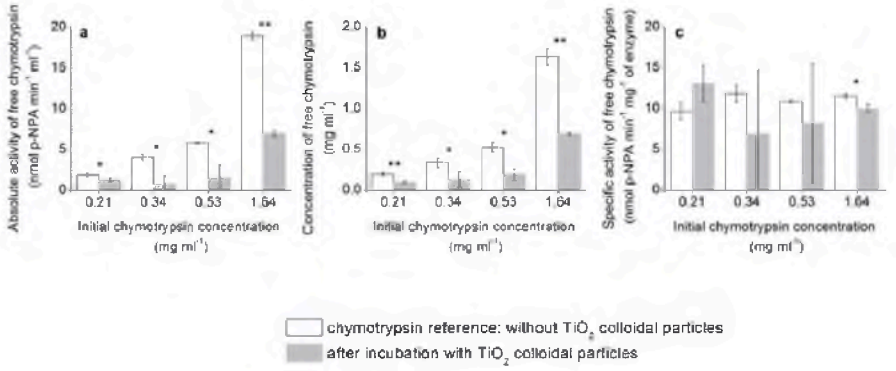


Figure 8.6 Concentration-dependent adsorption of chymotrypsin on $TiO_2$ colloidal particles. Chymotrypsin in the concentrations indicated was incubated without or with 0.9 vol % $TiO_2$ colloidal particle suspension at pH 8 for 1 h. After centrifugation, the supernatant was used to determine the absolute enzymatic activity (a) and the concentration (b) of free chymotrypsin in the supernatant. These data were combined to calculate the specific activity (c) of free chymotrypsin in the supernatant. The data shown represent means ± SD of values obtained

in 3 independent experiments. Asterisks indicate the significance of differences between the controls (before incubation with $TiO_2$ colloidal particles) and after the incubation with $TiO_2$ with *p < 0.05 and **p < 0.01 calculated in an unpaired t-test.

To determine the concentration-dependent amount of active chymotrypsin adsorbed on $TiO_2$ colloidal particles, the particles were exposed to chymotrypsin in concentrations of up to 0.53 mg $mL^{-1}$ (Table 8.2). After an adsorption period of 1 h, the non-bound chymotrypsin was removed and the activity of the bound chymotrypsin was determined by measuring the hydrolysis of p-NPA during an incubation period of 45 min. The hydrolytic activity of particle-bound chymotrypsin increased almost proportionally to the initial chymotrypsin concentration, at least up to a chymotrypsin concentration of 0.53 mg $mL^{-1}$. Higher concentrations of chymotrypsin were not used, as particles exposed to 0.53 mg $mL^{-1}$ chymotrypsin were already able to hydrolyze p-NPA in an amount corresponding to an absorbance of 1 (Figure 8.7).

Table 8.2 Concentration-dependent adsorption of chymotrypsin on $TiO_2$ colloidal particles and its influence on enzymatic activity

| **Initial chymotrypsin applied** | | **Adsorbed chymotrypsin (difference in supernatant)** | | **Activity of bound chymotrypsin** | | |
|---|---|---|---|---|---|---|
| *mg $mL^{-1}$* | *nmol $min^{-1}$* | *mg $mL^{-1}$* | *nmol $min^{-1}$* | *nmol $min^{-1}$* | *% of adsorbed* | *% of initial* |
| 0.21 | 2.00 ± 0.21 | 0.10 ±0.01 | 0.67 ± 0.23 | 0.18 ± 0.05 | 27 ± 8 | 9 ± 3 |
| 0.34 | 4.08 ± 0.37 | 0.21 ± 0.10 | 3.27 ± 0.99 | 0.26 ± 0.08 | 8 ± 3 | 6± 2 |
| 0.53 | 5.82 ± 0.10 | 0.33 ± 0.08 | 4.17 ± 1.46 | 0.44 ± 0.13 | 11 ± 3 | 8 ± 2 |

As a negative control, the same assay was run on incubations of chymotrypsin-free particles. In this case we found an absorbance of 0.48, which derives from the spontaneous (enzyme-independent) hydrolysis of p-NPA (Figure 8.7).

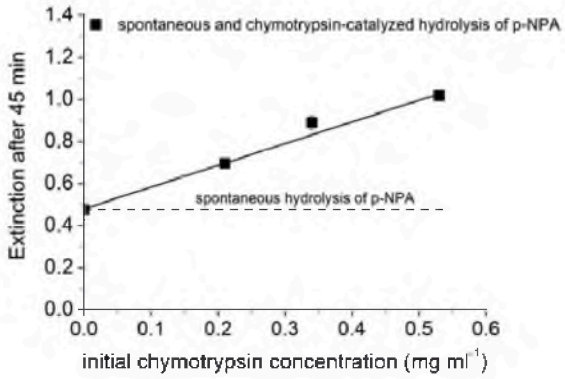


Figure 8.7 Hydrolytic activity of $TiO_2$-bound chymotrypsin. Chymotrypsin in the indicated initial concentrations was incubated with 0.9 vol % $TiO_2$ colloidal particle suspension at pH 8 for 1 h. After centrifugation, the chymotrypsin adsorbed on $TiO_2$ colloidal particles was incubated with buffer and 0.25 mM p-NPA for 45 min and the absorbance of the formed p-NP in the supernatant was determined at 405 nm. The spontaneous non-enzymatically catalyzed hydrolysis of p-NPA is indicated by the dashed line. The data shown represent means ± SD of values obtained in 3 independent experiments.

### 8.3.4 Substrate concentration-dependency for free and adsorbed chymotrypsin

In order to perform a Michaelis-Menten kinetic analysis of chymotrypsin activity, we investigated the dependency of the hydrolyzing activity of both particle-bound and free chymotrypsin on the concentration of the p-NPA substrate. For both conditions, the spontaneous, enzyme-independent hydrolysis increased almost proportional to the concentration of applied p-NPA (Figure 8.8a-b).

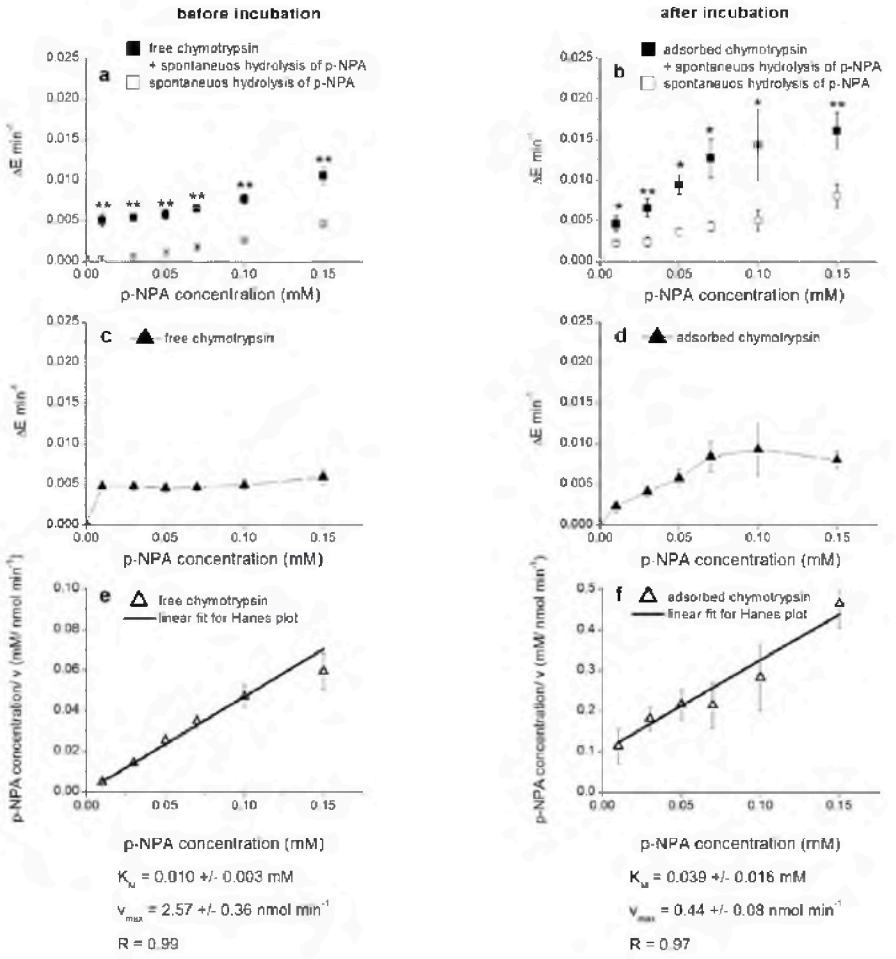


Figure 8.8 Substrate concentration-dependency for free chymotrypsin and adsorbed chymotrypsin on $TiO_2$ colloidal particles. As a non-enzymatically catalyzed hydrolysis of substrate, p-NPA takes place, the samples of spontaneous hydrolysis are also shown for free (a) (using pure water at adjusted pH 8 as blank measurement) and for adsorbed chymotrypsin (b) (using pure titania suspension at adjusted pH 8 as blank measurement). Subtraction results show Michaelis-Menten kinetics for free (c) and for adsorbed chymotrypsin (d). A Hanes plot was used to linearize the data for free (e) and adsorbed chymotrypsin (f) and to calculate the $K_M$ and $V_{max}$ values. The data shown represent means ± SD of values obtained in 3 independent experiments. Asterisks in a and b indicate the significance of differences between the controls (spontaneous hydrolysis) and the chymotrypsin-containing conditions with *$p < 0.05$ and **$p < 0.01$ calculated in a paired t-test.

Statistical analysis for $K_M$ and $v_{max}$ values was performed by the unpaired t-test and p is $< 0.05$.

Similarly, the rate of p-NP generation in the presence of free chymotrypsin (Figure 8.8a) or of particle-bound chymotrypsin (Figure 8.8b) (which represents the sum of enzyme-dependent and enzyme-independent hydrolysis) increased with the concentration of p-NPA. Subtraction of the spontaneous hydrolysis from the respective values recorded for chymotrypsin-containing reactions revealed a Michaelis-Menten-like kinetics behavior for the enzyme-dependent reactions (Figure 8.8c-d). Linearization of the data by Hanes plot gave a good linear correlations and allowed to calculate the Michaelis-Menten constant $K_M$ and maximal reaction rate $V_{max}$ (Figure 8.8e-f), as previously described[69]. For the free chymotrypsin, $K_M$ and $V_{max}$ values of $10 \pm 3$ µM and $2.57 \pm 0.36$ nmol $min^{-1}$ were determined, respectively. These values changed for chymotrypsin adsorbed to $TiO_2$ colloidal particles to $39 \pm 16$ µM ($K_M$) and $0.44 \pm 0.08$ nmol $min^{-1}$ ($V_{max}$) (Figure 8.8).

## 8.4 Discussion

In this study we have investigated the adsorption of chymotrypsin on $TiO_2$ colloidal particles. In addition to simply measure the amount of enzyme adsorption, we have also determined its hydrolytic activity both in the particle-bound fraction and in the supernatant fraction. For supernatant samples the enzymatic hydrolysis of p-NPA was directly measured by on-line monitoring of the appearance of p-NP in the reaction mixture by a well-known activity assay[40, 131, 132], which had been miniaturized to microtiter plate format. In contrast, an end-point measuring system had to be applied to determine the activity of the particle-bound enzyme (Figure 8.1 and Figure 8.2).

For all conditions used here, the enzyme-independent hydrolysis of p-NPA was observed to increase almost linearly with the applied substrate concentration, as expected. Since the enzyme-independent hydrolysis of p-NPA did not differ for reactions without or with $TiO_2$ colloidal particles, a stimulated p-NPA hydrolysis by $TiO_2$ can be excluded for the conditions

used in this work. Nevertheless, we performed for all incubation conditions appropriate enzyme-free control incubations to determine the enzyme-independent hydrolysis of p-NPA. These values for spontaneous hydrolysis were subtracted from the respective data observed for the enzyme-containing reactions to obtain the data for the enzyme-dependent hydrolysis.

The amount of adsorbed chymotrypsin on $TiO_2$ colloidal particles was found to be much higher after incubation at pH 8 than at pH 5 (see Figure 8.5a). As the IEP of chymotrypsin is approximately 8.5-8.8[40, 161-163], chymotrypsin is positively charged at pH 5 but almost neutral at pH 8. Similarly, $TiO_2$ colloidal particles have an IEP of 8.3 (Table 8.1) and are also positively charged at pH 5 and almost neutral at pH 8. Thus, repulsion between chymotrypsin and $TiO_2$ is much stronger at pH 5 than at pH 8, which is consistent with the observed low adsorption at pH 5. It is interesting to note that strong adsorption takes place at conditions of electrostatic neutrality (pH 8). However, we stress that net charges are present in equal amount on both the surface (due to the amphoteric character of $TiO_2$) and the protein, so that local ionic interactions at the protein/ surface interface cannot be excluded. In general, protein adhesion to oxide surfaces is governed by water-mediated favorable match between surface sites of different nature (charged, polar and non-polar) with the equally diverse amino acid distribution of the protein[164-166]. In particular, mutually interacting hydrophobic/ hydrophilic patterns often lead to stable, in our case practically irreversible, protein adsorption. This is consistent with previous results of adsorption of chymotrypsin on hexamethyldisiloxane films with a wide range of wettabilities[167] and for colloids of polystyrene, styrene/ 2-hydroxyethyl methacrylate, and silica[168]. Indeed, the employed $TiO_2$ particles present a partially hydrophobic surface (Figure 8.4) and approximately 30 % of the chymotrypsin surface was calculated to be hydrophobic (Figure 8.9).

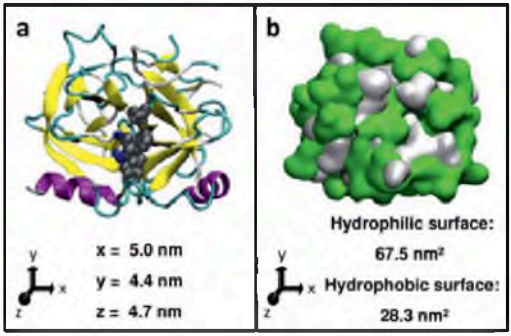


Figure 8.9 Secondary structure of chymotrypsin (a) with the active site in dark grey. The active site includes triad of amino acids Ser 195, His 57, Asp 102. Hydrophilic (green) and hydrophobic (white) areas of chymotrypsin are shown in b.

For the analysis of the behavior of particle-bound chymotrypsin it was an essential prerequisite, that the enzyme was not desorbed by incubation at high pH, as also the activity measurements were performed at high pH. The hydrolytic activity of chymotrypsin in the supernatant of $TiO_2$ particles decreased after the incubation. The reason for this decrease is adsorption of the protein to the particles, as also the protein content of the respective sample decreases accordingly. In fact, as the specific activity of the hydrolytic activity in the supernatant remained almost constant, it can be excluded that unbound chymotrypsin was inactivated by the presence of rutile $TiO_2$ particles. This contrasts literature data for $TiO_2$ with anatase crystal structure, which has been found to inactivate chymotrypsin by oxidative damages at least after exposure to ultraviolet light[169, 170]. In addition, autolysis of chymotrypsin, which has been reported to take place during incubations at around pH 8[171-173], appears not to be involved in the observed loss of chymotrypsin activity from the supernatant, consistent with recently published data under similar conditions[105].

The adsorbed amount of chymotrypsin on $TiO_2$ colloidal particles was proportional to the initial concentrations of applied chymotrypsin, as demonstrated by the almost linear concentration-dependent disappearance of chymotrypsin and decrease of activity from the supernatant of $TiO_2$-containing reactions and the almost linear increase in particle-bound hydrolytic activity.

The activity of particle-bound chymotrypsin depended on the concentration of the substrate p-NPA. After subtraction of the respective spontaneous enzyme-independent hydrolysis, the particle-bound chymotrypsin showed apparent Michaelis-Menten-like kinetic behavior (Figure 8.8c-d). Linearization of the data in a Hanes plot[69] was used to calculate the kinetic parameters $K_M$ and $V_{max}$ for the adsorbed chymotrypsin. The apparent $K_M$ value calculated for adsorbed chymotrypsin was higher and the $V_{max}$ value was much lower than the respective values determined for free chymotrypsin, suggesting that enzyme-substrate interactions are strongly altered by the binding of chymotrypsin to $TiO_2$. We observe that the adsorption is matched by a substantial loss of enzymatic activity, so that only approximately 6-9 % of the initial enzyme activity is preserved (Table 8.2).

Possible reasons of the increase in $K_M$ value and for the decline in maximal hydrolytic activity could be conformational changes or blockage of the active site caused by adsorption of the enzyme on the $TiO_2$ surface. The observed increase in the $K_M$ value of $TiO_2$-bound chymotrypsin for its substrate is consistent with literature data for chymotrypsin that had been immobilized on synthetic polyurethane grafted with acrylic acid[132] or on porous glass[174]. An almost complete loss of the enzymatic activity was reported for chymotrypsin adsorbed on the hydrophobic surfaces of polystyrene and Teflon, which was connected with severe structural perturbations[36]. Impairment of catalytic properties of protease have also been reported for the serine-protease trypsin after contact with nano-sized $TiO_2$ films, where both geometrical constraints of $TiO_2$ nanopores and the cluster-wise adsorption of trypsin were suggested as the main factors underpinning the steric hindrance of the immobilized enzyme[34]. Similarly, a decline of specific activity of trypsin occurred after encapsulation of trypsin in sol-gel matrices[175].

Furthermore, the geometrical arrangement and interfacial behavior of chymotrypsin were considered as the surface density of adsorbed enzymes can directly influence enzyme conformation and, subsequently, its activity. At the applied concentrations (Table 8.2) 0.011, 0.023 and 0.036 chymotrypsin molecules had adsorbed per $nm^2$. These densities are below the theoretical end-on and side-one regular monolayers calculated using the molecular dimensions of chymotrypsin (5.0 nm x 4.4 nm x 4.7 nm) and according to[94]. The theoretical end-on and side-one regular monolayers correspond to 0.052 and 0.040 chymotrypsin molecules per

$nm^2$, respectively. Due to these low coverage densities, the formation of multilayers is negligible and lateral interactions between adsorbed enzymes are rather weak. Saha et al.[176] showed that the activity of trypsin on CuS nanoparticles depends on surface density. When trypsin molecules form a complete monolayer the 98% of the native enzyme activity was almost retained. At higher trypsin surface densities partial activity loss was observed, and possibly influenced by alteration in the tertiary enzyme conformation. This can be the consequence of either the decrease in the absolute number of active enzyme molecules on the particle surface or the reduced kinetics. Nevertheless, even low density of adsorbed enzymes could cause adsorption-induced structural changes. Wei et al.[177] investigated the relationship between the conformation and activity of adsorbed lysozyme on fumed silica at different conditions. A 60% loss of activity was found when lysozyme formed approximately a monolayer. Reduction of enzymatic activity is considered to be directly proportional to the degree of adsorption-induced changes of the protein's structure. A less direct role seems to be played by protein-protein interactions which tend to stabilize the structure of adsorbed lysozyme as suggested by structural studies.

Concerning potential technical applications of chymotrypsin that is immobilized by physisorption to titania particles it is important to investigate in future studies the stability and reusability of the particle-bound enzyme. For alumina and silica colloidal particles we have recently reported such data[105] and have demonstrated reusability of the immobilized enzymes by determining the proteolytic activity of the particle-bound enzyme in three consecutive 24 h lysozyme digestion steps. In addition, even after 7 weeks storage at room temperature, the immobilized chymotrypsin was still active to digest lysozyme as a substrate. These data suggest that also for other types of colloidal particles, the hydrolytic activity of adsorbed chymotrypsin is maintained and that these particles can be reused for multiple proteolytic cycles.

## 8.5 Conclusions

In this study we have demonstrated that the proteolytic enzyme chymotrypsin adsorbs efficiently on $TiO_2$ colloidal particles in a concentration-dependent and pH-dependent process. pH 8 was found to be the preferred condition for strong chymotrypsin adsorption. However,

adsorption on $TiO_2$ colloidal particles negatively influenced the enzymatic activity of particle-bound chymotrypsin as a substantial loss in enzymatic activity and an increase in the $K_M$ value for the artificial substrate p-NPA were observed. Further studies are needed to prove whether structural alteration of chymotrypsin or other factors are responsible for the observed change of activity. Our experimental settings and the simple and fast methods developed in this study do not require any complex technical equipment and could be useful to study also the interactions of other hydrolytic enzymes with various types of colloidal materials.

## 8.6 Acknowledgments

We thank Felix Bulcke (Center for Biomolecular Interactions Bremen, University of Bremen, Germany) for supporting the statistical analysis of the data.

## 8.7 Source

This chapter was adapted from:

Derr L., Dringen R., Treccani L., Hildebrand N., Colombi Ciacchi L., and Rezwan K.; Physisorption of enzymatically active chymotrypsin on titania colloidal particles. Journal of Colloid and Interface Science. 2015; 455, 236-244, License number: 3651491140032.

The article is mainly based on the work of the first author and author of this thesis Ludmilla Derr. The precise contributions of each single author are listed below. All the used literature references are summarized in Chapter 14.

| Author | Contribution |
|---|---|
| ***Ludmilla Derr*** | Conceptualization of work, planned and performed all adsorption and enzymatic activity experiments, performed characterization analysis on all samples, optimized and evaluated activity assay for adsorbed chymotrypsin, interpreted and discussed data, wrote manuscript |
| Ralf Dringen | Gave conceptual advices, discussed data, edited manuscript |
| Laura Treccani | Gave conceptual advices, discussed data, edited manuscript |
| Nils Hildebrand | Performed the calculation of hydrophilic/ hydrophobic surface of chymotrypsin in Figure 8.9 |
| Lucio Colombi Ciacchi | Contributed to interpret the experimental results and proof-read the manuscript |
| Kurosch Rezwan | Gave conceptual advices, discussed data, edited manuscript |

# 9 Effects of silica and alumina colloidal particles on the enzymatic activity of α-chymotrypsin after adsorption

*ABSTRACT: A proteolytic enzyme, α-chymotrypsin, was adsorbed from aqueous solution on $SiO_2$ and $Al_2O_3$ colloidal particles using the physisorption method. The main focus of this study was to compare the influence of adsorption on $SiO_2$ or $Al_2O_3$ colloidal particles on the enzymatic activity of the adsorbed enzyme. Therefore, a known photometric assay based on p-NPA as a chymotrypsin substrate was optimized to enable the assessment of enzymatic activity for adsorbed chymotrypsin. The affinity of adsorption was higher for $Al_2O_3$ colloidal particles than for $SiO_2$ due to the greater hydrophobicity of the $Al_2O_3$ surface. Consequently, chymotrypsin does not reach the theoretical regular monolayer side-on on the $SiO_2$ surface under either acidic (pH 5) or basic conditions (pH 8). By contrast, the theoretical regular monolayer side-on was attained on the $Al_2O_3$ surface under both acidic and basic conditions. For both materials, chymotrypsin exhibited a strong decrease in specific activity after adsorption under both pH conditions. Compared to $SiO_2$, a significantly stronger decrease in specific activity occurred after adsorption on $Al_2O_3$ at pH 8, likely due to the higher packing density of $Al_2O_3$. The optimized assay is a rapid and straightforward method that can be easily applied to other colloidal systems to determine the enzymatic activities of adsorbed enzymes.*

## 9.1 Introduction

Ceramic colloidal particles, specifically those composed of silica ($SiO_2$) and alumina ($Al_2O_3$), are widely used as insoluble support materials for enzyme immobilization[7, 9, 13, 19, 178-180]. Due to their numerous practical applications, proteolytic enzymes are also often employed for immobilization studies[146, 152, 179, 181-183]. A large number of studies have investigated enzymatic activity before and after immobilization[14-17]. Studies using different analysis methods to assess the activity of immobilized enzymes are necessary to compare the suitability of support materials.

Based on these considerations, we analyzed the enzymatic activity of a proteolytic enzyme, α-chymotrypsin, before and after immobilization on $SiO_2$ and $Al_2O_3$ colloidal particles. For this purpose, a known enzymatic assay[40, 131, 132] typically used for enzymes in solution was specifically adapted for immobilized chymotrypsin. To avoid any additional influence of chemicals such as linkers and other coupling substances on enzymatic activity, we chose physisorption as the most straightforward immobilization method.

The main challenge in the analysis of the enzymatic activity of adsorbed enzymes is that assays based on UV/ Vis spectrometry cannot be directly used due to the light scattering caused by the colloidal particles. Consequently, the detailed optimization of the photometric assay based on p-nitrophenyl acetate (p-NPA) as a chymotrypsin substrate included a demonstration of the reliable stability of enzyme adsorption and confirmation of the choice of the amount of enzyme adsorbed on the colloidal particles; the experimental conditions during physisorption, such as pH and ionic strength; the concentration of p-NPA; and suitable incubation times. These variables are essential to obtain reasonable extinction signals in a linear measurement range.

The applied method is simple, fast and does not require specialized complex facilities. Furthermore, the experiments for assay optimization represent a good basis for studies using other colloidal particles and can be applied in flexible and versatile ways.

## 9.2 Experimental section

### 9.2.1 Materials

$SiO_2$ colloidal particles (> 99.9% wt, $SiO_2$P015-01, lot. no. 100618-02V) were obtained from Fiber Optic Center (New Bedford, USA). $Al_2O_3$ colloidal particles (>99.99% wt, Taimei, TM-DAR, lot. no. 8086) were purchased from Krahn Chemie (Germany). Lyophilized α-chymotrypsin type II from bovine pancreas (molar mass 25300 g $mol^{-1}$, purity 94.1% wt, lot. no. 60M7007V), p-nitrophenyl acetate (p-NPA, lot. no. 0001422901), potassium dihydrogen phosphate (≥99% wt) and 1,4-dioxane (> 99.8% wt, lot. no. STBB3939) were obtained from Sigma-Aldrich (Germany) and used without any modifications. A Pierce™ bicinchoninic acid protein assay kit (BCA assay) was obtained from Thermo Fisher

Scientific GmbH (Germany). All other chemicals were of analytical grade and were purchased from Fluka (Switzerland) or Merck (Germany). For all aqueous solutions, double-deionized water ($ddH_2O$) with a conductivity of 0.04 µS $cm^{-1}$ was used as the solvent (Millipore Synergy®, Millipore Corporation, Germany).

### 9.2.2 Characterization of $SiO_2$ and $Al_2O_3$

To remove potential organic residues, the $SiO_2$ and $Al_2O_3$ powders were calcinated at 400 °C for 4 h at a heating and cooling rate of 3 °C $min^{-1}$ (oven L3/11/S27, Nabertherm, Germany). The particle size was determined by dynamic light scattering (DLS, Beckman-Coulter DelsaNanoC, Beckman Coulter GmbH, Germany) using 0.003 vol % $SiO_2$ and $Al_2O_3$ suspensions at pH 5. Prior to each DLS measurement, the conductivity and pH of the suspensions were adjusted to avoid or minimize particle agglomeration. The conductivity was set at 500 µS $cm^{-1}$ using 3 M KCl, and the pH was adjusted with 1 M KOH or 1 M HCl using a pH meter (Five Easy™ FE20, Mettler-Toledo GmbH, Switzerland). The conductivity was set at 500 µS $cm^{-1}$, which corresponds to an ionic strength of 3 mM.

The specific surface area ($SSA_{BET}$) was obtained by volumetric nitrogen adsorption measurements using a BELsorp-mini II device (Bel Japan Inc., Japan) and assuming a cross-sectional area of the nitrogen molecule of 0.162 $nm^2$[236]. Adsorption isotherms were recorded at −196 °C. All samples were out-gassed at 100 °C under flowing argon for 24 h before measurement.

Zeta potential (ζ-potential) measurements were performed using an electroacoustic spectrometer DT1200 (Dispersion Technology Inc., USA) as previously reported[118]. ζ-potential/ pH titrations of 1 vol % $SiO_2$ and $Al_2O_3$ suspensions with an initial conductivity of 500 µS $cm^{-1}$ were performed with the integrated titration unit using 1 M HCl and 1 M KOH, respectively. The number of hydroxyl groups present on the surfaces of the $SiO_2$ and $Al_2O_3$ particles was determined by potentiometric titrations (TitraLab® TIM 840 Titration Workstation, Hach Lange GmbH, Germany) according to Hidber[158, 159]. $SiO_2$ and $Al_2O_3$ particle densities were

measured with a helium pycnometer (Pycnomatic ATC, Porotec GmbH, Germany).

Transmission electron microscopy (TEM) imaging was performed using a FEI Titan 80/300 kV (FEI, The Netherlands) equipped with a Cs-corrector for spherical aberration of the objective lens at 300 kV and a vacuum of $1.3 \times 10^{-7}$ mbar. Colloidal particles were deposited on chemical vapor deposition (CVD) graphene film-coated copper grids (Graphene Supermarket, New York, USA). The particle morphology was analyzed by scanning electron microscopy (SEM; field-emission SEM SUPRA 40, Zeiss, Germany) operating at 2.00 kV mounted on carbon tape.

The hydrophilic/ hydrophobic surface properties were investigated via volumetric water and n-heptane adsorption measurements using a BELsorp 18-3 device (Bel Japan Inc., Japan) as described previously[124, 160]. The amounts of adsorbed water and n-heptane are reported as a ratio $p/p_0$ of 0.95 to most accurately simulate atmospheric conditions. Prior to the adsorption measurements, all samples were out-gassed at 100 °C under flowing argon for 24 h. $SSA_{BET}$ and the molar masses of n-heptane and water were taken into account for normalized calculations, and adsorption/ desorption was calculated in µmol $m^{-2}$ for the $SiO_2$ and $Al_2O_3$ surfaces. The average and standard deviations of three single measurements are reported.

### 9.2.3 Size determination and hydrophobic/ hydrophilic properties of chymotrypsin

Hydrophilic/ hydrophobic surface regions were visualized using the software Visual Molecular Dynamics (VMD) (Version 1.9.1)[70]. The atomic coordinates of the proteins were taken from the Brookhaven Protein Database (PDB-ID: 4CHA). Molecular dynamic simulation with an explicit solvent was applied for 1 ns, and projections of the hydrophobic and hydrophilic amino acids on the 'solvent accessible surface area' were calculated using the 'measure solvent accessible surface area' function included in VMD with a probe radius of 0.14 nm.

### 9.2.4 Adsorption and desorption studies of chymotrypsin

$SiO_2$ and $Al_2O_3$ aqueous suspensions were prepared by mixing 1.30 g of $SiO_2$ or 1.99 g of $Al_2O_3$ with 49.5 mL of $ddH_2O$ (corresponding to 1 vol % suspension). The pH was adjusted to pH 5 or 8, and the suspension conductivity was set at 500 µS $cm^{-1}$ as previously described. Prior to incubation with chymotrypsin, the particle suspensions were deagglomerated for 10 min using an ultrasound sonotrode at output 150 W, pulse rate 0.5 s (Sonifier® 450, Branson, USA). A chymotrypsin stock solution (concentration of 20 mg $mL^{-1}$) was freshly prepared by dissolving lyophilized chymotrypsin in $ddH_2O$ and adjusting the pH to 5 or 8 with 1 M KOH or 1 M HCl. The initial concentration of chymotrypsin was measured using the BCA assay.

A schematic description of the experimental set up for the adsorption and desorption studies is presented in Figure 9.1. First, 900 µL of either $SiO_2$ or $Al_2O_3$ suspension was mixed with 100 µL of chymotrypsin (Incubation I) in 1.5-mL polypropylene tubes (Eppendorf AG, Germany), and the resulting conductivity was ~ 550 µS $cm^{-1}$. The tubes were shaken continuously (Stuart rotator STR4, Bibby Scientific Ltd., UK) at a speed of 30 rpm to prevent agglomeration and were maintained at room temperature. After 2 h, the suspensions were centrifuged for 10 min at 21,100 g (Heraeus Fresco 21 centrifuge, Fisher Scientific, Germany). A 950-µL aliquot of the supernatant (supernatant I containing the free chymotrypsin) was collected, and $SiO_2$ and $Al_2O_3$ particles with adsorbed chymotrypsin were briefly rinsed with 950 µL of $ddH_2O$ at pH 5 or 8 and a conductivity of approximately 500 µS $cm^{-1}$ (incubation II). A 950-µL aliquot of supernatant (supernatant II containing the desorbed chymotrypsin) was collected. Then, 950 µL of $ddH_2O$ at pH 5 or 8 and a conductivity of 500 µS $cm^{-1}$ was added (incubation III). After 1 or 18 h, the suspensions were centrifuged for 10 min at 21,100 g. A 950-µL aliquot of the supernatant (supernatant III containing the desorbed chymotrypsin) was collected. The same pH was used for incubation I, incubation II and incubation III. The chymotrypsin concentrations in supernatants I, II and III were measured using the BCA assay.

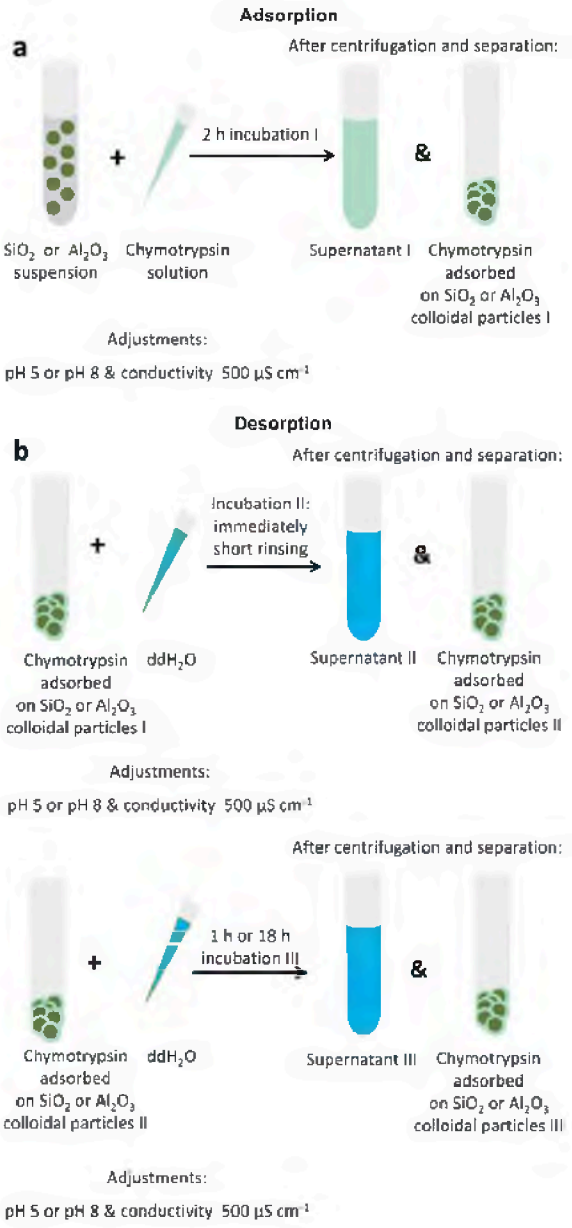


Figure 9.1 Schematic description of the experimental set-up for the adsorption (a) and desorption (b) studies.

### 9.2.5 Quantitative determination of adsorbed chymotrypsin

After the incubations, the free chymotrypsin concentration in the collected supernatants and in the control chymotrypsin solutions without colloidal particles was measured using a sufficiently sensitive BCA assay according to the instructions for the Pierce™ BCA Protein Assay Kit. The amount of adsorbed chymotrypsin was calculated by subtracting the measured free chymotrypsin in the supernatant from the initial chymotrypsin concentration in the control samples.

### 9.2.6 Enzymatic activity measurements of free chymotrypsin

The enzymatic activity of free chymotrypsin in the supernatants was determined according to references[40, 131, 132]. Briefly, 20 µL of the supernatant was mixed with 140 µL of 100 mM potassium phosphate buffer in a 96-well microtiter plate (Nunc™, Denmark). A 160-µL aliquot of 0.2 mM p-NPA was added, and the increase in absorbance due to the formation of p-nitrophenolate (p-NP) ions was measured at 405 nm using a microtiter plate reader (Sunrise, Tecan, Austria). The non-enzymatically catalyzed hydrolysis of p-NPA[133], called spontaneous hydrolysis, was determined by mixing 20 µL of $ddH_2O$ with 140 µL of 100 mM potassium phosphate buffer as a blank.

### 9.2.7 Enzymatic activity measurements of adsorbed chymotrypsin

The enzymatic activity of adsorbed chymotrypsin was determined using the enzymatic assay presented in Figure 9.2. In detail, after the 2 h incubation, the $SiO_2$ and $Al_2O_3$ particles were briefly rinsed and mixed with 280 µL of 100 mM potassium phosphate buffer in 1.5-mL polypropylene tubes. A total of 320 µL of 0.4 mM p-NPA was added, and after 20, 30 and 40 min, the samples were centrifuged, and the supernatants were collected. Then, 320 µL of supernatant was used to measure the increase in absorbance due to the formation of p-NP at 405 nm after all three time points. The spontaneous hydrolysis of p-NPA was measured using $SiO_2$ and $Al_2O_3$ suspensions that were not incubated with chymotrypsin

according to a reference[133]. A straight line was constructed from the extinction data for the three time points. Similar to the enzymatic assay for free chymotrypsin, the slope of the line was $\Delta E\ min^{-1}$. Further calculations were based on the Lambert-Beer law; the fundamentals of this calculation can be found in numerous books and publications[69] (see Chapters 6 and 7.4). The specific enzymatic activity of chymotrypsin was determined as a function of the chymotrypsin concentration.

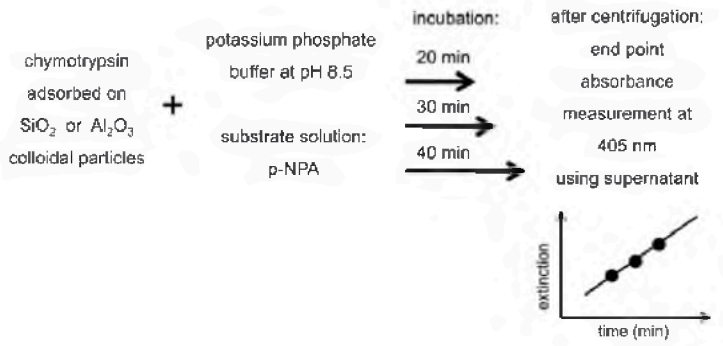


Figure 9.2 Schematic description of the experimental set-up for the optimized activity assay for chymotrypsin adsorbed on $SiO_2$ or $Al_2O_3$ colloidal particles.

### 9.2.8 Statistical analysis

All experiments were performed at least three times. The data in the figures and tables represent mean values ± standard deviation (SD). Statistical analysis was performed with unpaired t-tests using the software GraphPad InStat 3 (GraphPad Software Inc., USA.). Values of $p > 0.05$ were considered not significant.

## 9.3 Results

### 9.3.1 Characterization of $SiO_2$ and $Al_2O_3$

The properties of the highly pure $SiO_2$ and $Al_2O_3$ colloidal particles used in this study are summarized in Table 9.1, and SEM and HR-TEM images are presented in Figure 9.3. The $SiO_2$ colloidal particles were amorphous, and the $Al_2O_3$ colloidal particles were in α-phase. $SiO_2$ was spherical, and $Al_2O_3$ was non-spherical, but both exhibited a narrow size distribution based on DLS measurements (Table 9.1).

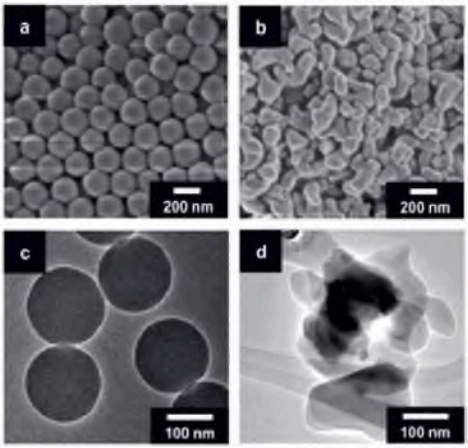


Figure 9.3 Scanning electron micrographs of $SiO_2$ (a) and $Al_2O_3$ (b). Representative HR-TEM images of $SiO_2$ (c) and $Al_2O_3$ (d).

The $SSA_{BET}$ values determined by nitrogen adsorption were 34.0 $m^2\ g^{-1}$ and 12.8 $m^2\ g^{-1}$ for $SiO_2$ and $Al_2O_3$, respectively. The $SSA_{BET}$ values and the amounts of colloidal particles in the analyzed suspensions were considered in the calculation of adsorbed chymotrypsin; the values of both materials were compared in units of ng $cm^{-2}$. The values of the exchange capacities were 4.9 OH-groups $nm^{-2}$ and 2.8 OH-groups $nm^{-2}$ for $SiO_2$ and $Al_2O_3$, respectively.

Table 9.1 Properties of $SiO_2$ and $Al_2O_3$ colloidal particles

| Property | $SiO_2$ | $Al_2O_3$ | Method |
|---|---|---|---|
| **Purity[a] (wt%)** | ≥ 99.99 | ≥ 99.99 | - |
| **Size (nm)** | $d_{50}$: 180 ± 3 | $d_{50}$: 159 ± 7 | dynamic light scattering |
| **Specific surface area ($SSA_{BET}$) ($m^2\ g^{-1}$)** | 34.0 ± 0.3 | 12.8 ± 0.1 | volumetric nitrogen adsorption |
| **Exchange capacity ($OH\ nm^{-2}$)** | 4.9 ± 0.2 | 2.8 ± 0.2 | titrations according to Hidber[158, 159] |
| **Isoelectric point (IEP)** | 2.7 ± 0.1 | 9.9 ± 0.1 | electroacoustic colloidal vibration current technique |
| **Hamaker constant[52] ($x\ 10^{-21}$ J)** | 1.6 | 27.5 | full spectral method |
| **Density ($g\ cm^{-3}$)** | 2.6 ± 0.1 | 4.0 ± 0.1 | pycnometer |
| **Crystal structure** | amorphous | α-phase | X-ray diffraction and electron diffraction with high-resolution transmission electron microscopy |

[a] The data were obtained from the manufacturer. All measured data represent the means ± standard deviations of values obtained in 3 independent experiments.

The water and n-heptane adsorption capacities (Figure 9.4) were normalized to the $SSA_{BET}$ of the particles (Table 9.1). $Al_2O_3$ exhibited higher affinity for n-heptane (~ 25 µmol $m^{-2}$) than for water (~ 20 µmol $m^{-2}$). By contrast, $SiO_2$ exhibited lower affinity for n-heptane (~ 17 µmol $m^{-2}$) than for water (~ 85 µmol $m^{-2}$). The Hamaker constant of $SiO_2$ was significantly lower than that of $Al_2O_3$[52] (Table 9.1). $Al_2O_3$ colloidal particles tended to form more agglomerates than $SiO_2$. However, both materials exhibited suitable suspension stability under the indicated experimental conditions.

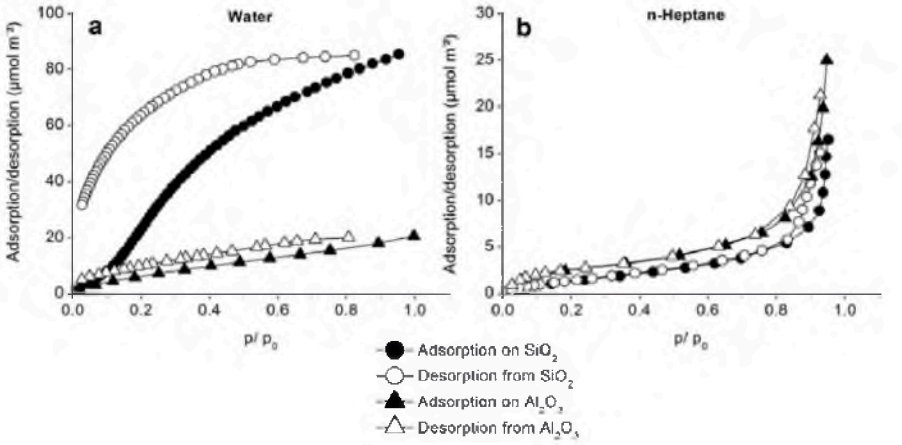


Figure 9.4 Hydrophilic/ hydrophobic properties of $SiO_2$ and $Al_2O_3$ colloidal particles. The $SSA_{BET}$ and molar masses of n-heptane and water were considered for normalized calculations, and adsorption/ desorption is shown for water (a) and n-heptane (b) on $SiO_2$ and $Al_2O_3$ surfaces.

### 9.3.2 Size determination and hydrophobic/ hydrophilic properties of chymotrypsin

The size of chymotrypsin was determined using VMD[70] and PDB-ID 4CHA: 4.4 nm x 4.7 nm x 5.0 nm for x, y and z. The hydrophobic surface area was 28.3 nm², and the hydrophilic surface area was 67.5 nm². The pI value of chymotrypsin is approximately 8.5-8.8[40, 161-163].

### 9.3.3 Adsorption of chymotrypsin on $SiO_2$ and $Al_2O_3$ colloidal particles

The adsorption data were analyzed considering the different values of $SSA_{BET}$ (Figure 9.5). At pH 5, ~ 32 ng $cm^{-2}$ adsorbed on $SiO_2$, and approximately 160 ng $cm^{-2}$ adsorbed on $Al_2O_3$ (Figure 9.5a). Significantly more chymotrypsin was adsorbed at pH 8 on $SiO_2$, ~ 110 ng $cm^{-2}$. Approximately 176 ng $cm^{-2}$ adsorbed on $Al_2O_3$ colloidal particles at pH 8. A second normalization was performed to compare the adsorption data with the calculated theoretical regular monolayer according to Adamczyk[94]. Chymotrypsin was assumed to occupy a circular area on the particle surface with the diameter of the enzyme's largest side as the side-on adsorption area and the enzyme's smallest side as the end-on adsorption area. The maximal surface packing density corresponded to 78.5 %, assuming quadratic packing of circles for a regular monolayer. A regular end-on monolayer consisted of 0.052 chymotrypsin molecules $nm^{-2}$, and a regular side-on monolayer consisted of 0.040 chymotrypsin molecules $nm^{-2}$ for the given enzyme dimensions. The enzyme amount close to the theoretical regular side-on monolayer adsorbed on $Al_2O_3$ colloidal particles under both pH conditions, whereas monolayer coverage was not attained on the $SiO_2$ surface (Figure 9.5b). Approximately 17 % and 61 % of the theoretical regular side-on monolayer were reached at pH 5 and pH 8, respectively.

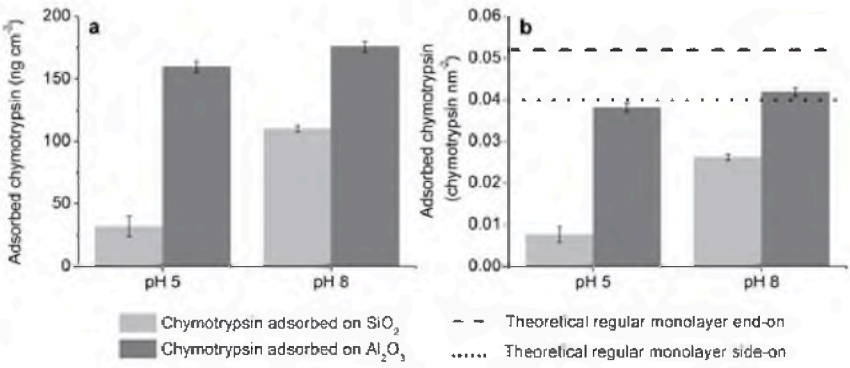


Figure 9.5 Adsorption of chymotrypsin on $SiO_2$ and $Al_2O_3$ colloidal particles at pH 5 and pH 8. The chymotrypsin solution was incubated with 1 vol % colloidal particle suspensions with an ionic strength of 3 mM at pH 5 and pH 8 for 2 h. The data show the amount of chymotrypsin obtained after the subtraction of free chymotrypsin in the supernatant from the initial chymotrypsin concentration. Normalized values of adsorbed chymotrypsin on $SiO_2$ and $Al_2O_3$

are shown in ng $cm^{-2}$ in a and in chymotrypsin molecules $nm^{-2}$ in b. $SSA_{BET}$ was taken into account for both normalized calculations. The theoretically calculated values for the regular monolayer in end-on and side-on adsorption orientations are marked as black dashed lines. The standard deviations were obtained in 3 independent experiments.

### 9.3.4 Adsorption/ desorption studies of chymotrypsin

The initial chymotrypsin concentrations after pH adjustment were ~ 1.86 mg $mL^{-1}$ and ~ 1.57 mg $mL^{-1}$ at pH 5 and pH 8, respectively. At pH 5, adsorption on $SiO_2$ was less pronounced than on $Al_2O_3$ (Figure 9.6a). We measured ~ 1.7 mg $mL^{-1}$ free chymotrypsin in the supernatant after 2 h of incubation I with the $SiO_2$ suspension. After incubation I with the $Al_2O_3$ suspension at pH 5, ~ 0.9 mg $mL^{-1}$ was not adsorbed. At pH 8, we measured 0.6 and 0.5 mg $mL^{-1}$ free chymotrypsin after incubation I with $SiO_2$ and $Al_2O_3$, respectively. Very low concentrations of desorbed chymotrypsin were measured in all experimental steps. In particular, less than 0.04 mg $mL^{-1}$ chymotrypsin for the $SiO_2$ suspension and less than 0.1 mg $mL^{-1}$ for the $Al_2O_3$ suspension were measured under both pH conditions.

The second assay measuring the absolute activity of free chymotrypsin in the supernatant gave similar results (Figure 9.6b). The initial absolute activities were ~ 22.10 nmol p-NPA $min^{-1}$ $mL^{-1}$ and ~ 19.98 nmol p-NPA $min^{-1}$ $mL^{-1}$ at pH 5 and pH 8, respectively (Figure 9.6). The absolute activity of free chymotrypsin in the supernatant was ~ 20.85 nmol p-NPA $min^{-1}$ $mL^{-1}$ after 2 h of incubation I with the $SiO_2$ suspension at pH 5. After incubation I with the $Al_2O_3$ suspension at pH 5, ~ 9.40 nmol p-NPA $min^{-1}$ $mL^{-1}$ remained. At pH 8, 5.69 and 3.51 nmol p-NPA $min^{-1}$ $mL^{-1}$ were measured after incubation I with $SiO_2$ and $Al_2O_3$, respectively. Very low absolute activities were measured for desorbed chymotrypsin in all experimental steps. In particular, less than 1.65 nmol p-NPA $min^{-1}$ $mL^{-1}$ at pH 5 and less than 1.35 nmol p-NPA $min^{-1}$ $mL^{-1}$ at pH 8 were measured for both materials.

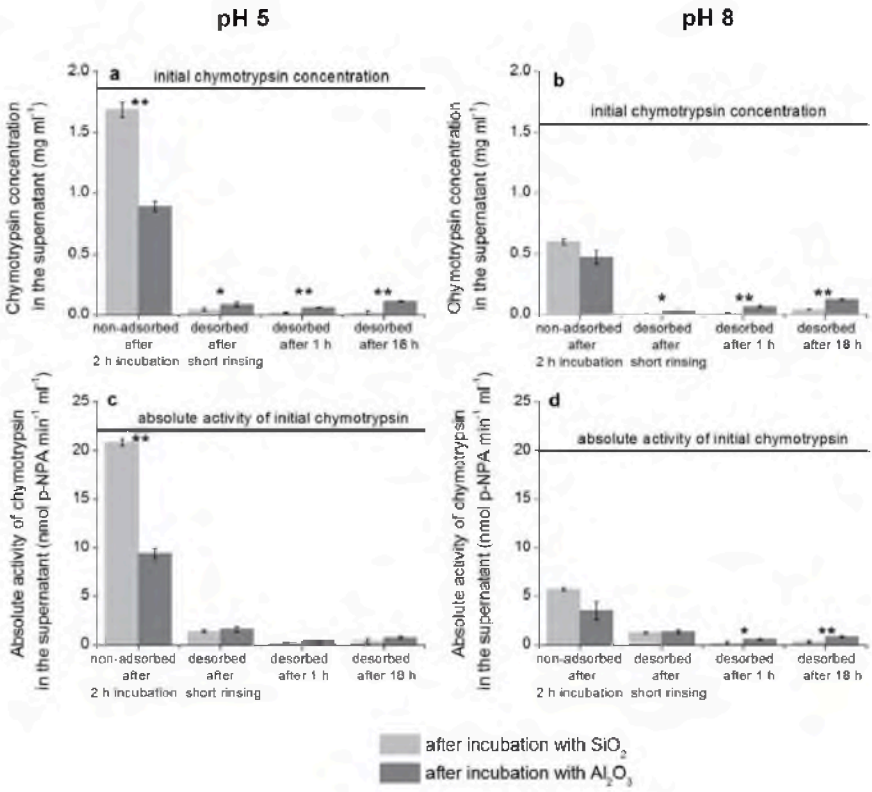


Figure 9.6 Adsorption and desorption studies of chymotrypsin with $SiO_2$ and $Al_2O_3$ colloidal particles at pH 5 and pH 8. Chymotrypsin at the indicated concentration was incubated with 1 vol % suspensions with an ionic strength of 3 mM at pH 5 and pH 8 for 2 h. The supernatant was removed to measure the concentration of non-adsorbed chymotrypsin and its absolute activity. Pure water with pH adjusted accordingly was then added to the chymotrypsin adsorbed on $SiO_2$ or $Al_2O_3$ colloidal particles to investigate whether chymotrypsin can desorb after brief rinsing. The amount of desorbed chymotrypsin after brief rinsing and the absolute activity were determined. Pure water with pH adjusted accordingly was then added again to chymotrypsin adsorbed on $SiO_2$ or $Al_2O_3$ colloidal particles, and the mixture was incubated for 1 h and 18 h. After incubation, the supernatants were collected and assayed to quantify the desorbed chymotrypsin and its absolute activity. Graphs a and b show the concentrations of chymotrypsin in the supernatant at pH 5 (a) and pH 8 (b) for all experimental steps shown in Figure 9.1. Graphs c and d show the absolute activity of chymotrypsin in the supernatant in nmol p-NPA $min^{-1}$ $mL^{-1}$ at pH 5 (c) and pH 8 (d). Additionally, control samples using chymotrypsin solution without colloidal particles were measured in all steps of the experiment (solid line). The standard deviation values were obtained in 3 independent experiments. Asterisks indicate significant differences between incubation with $SiO_2$ and with $Al_2O_3$, with *$p < 0.05$ and **$p < 0.01$ calculated in an unpaired t-test.

### 9.3.5 Enzymatic activity of adsorbed chymotrypsin

The absolute amount of adsorbed chymotrypsin is shown in Figure 9.7a. At pH 5, ~ 0.26 mg and ~ 0.73 mg of chymotrypsin adsorbed on $SiO_2$ and $Al_2O_3$, respectively. At pH 8, ~ 0.88 mg of chymotrypsin adsorbed on $SiO_2$, and ~ 0.80 mg of chymotrypsin adsorbed on $Al_2O_3$. The absolute activity was calculated (Figure 9.7b) using the data obtained in the optimized assay (Figure 9.2). The absolute activities of adsorbed chymotrypsin on $SiO_2$ were 1.77 nmol p-NPA $min^{-1}$ and 2.24 nmol p-NPA $min^{-1}$ at pH 5 and 8, respectively. Chymotrypsin adsorbed on $Al_2O_3$ particles exhibited absolute activities of 1.04 and 1.36 nmol p-NPA $min^{-1}$ at pH 5 and 8, respectively.

To compare the specific activity values after adsorption with that of the initial chymotrypsin solution that was not incubated with colloidal particles, a solid line marks the initial specific activity of ~ 14.69 nmol p-NPA $min^{-1}$ $mg^{-1}$ (Figure 9.7c). The specific activity of chymotrypsin adsorbed on $SiO_2$ colloidal particles drastically changed at pH 5 to 1.77 nmol p-NPA $min^{-1}$ $mg^{-1}$. At pH 8, a value of 2.24 nmol p-NPA $min^{-1}$ $mg^{-1}$ was attained. The specific activity for chymotrypsin adsorbed on $Al_2O_3$ colloidal particles at pH 5 decreased by ~ 93% to 1.04 nmol p-NPA $min^{-1}$ $mg^{-1}$. At pH 8, a decrease of ~ 91% to 1.36 nmol p-NPA $min^{-1}$ $mg^{-1}$ was observed for chymotrypsin adsorbed on $Al_2O_3$ colloidal particles.

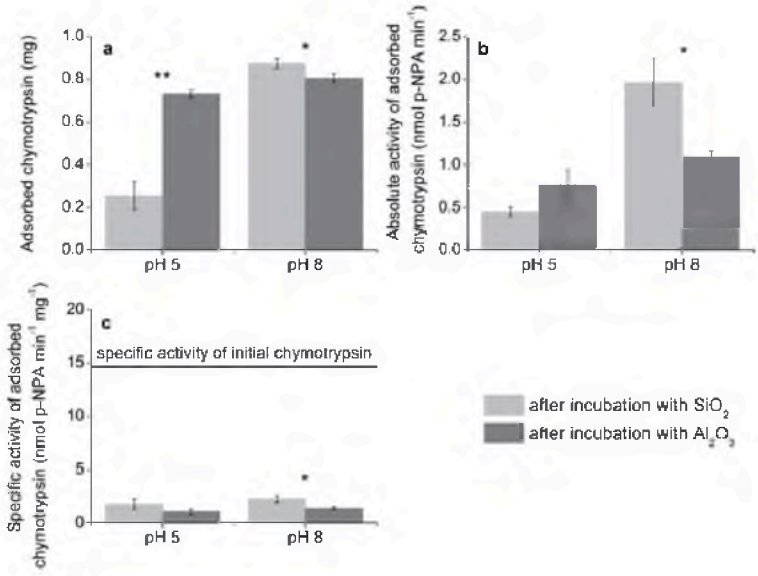


Figure 9.7 Specific activity of adsorbed chymotrypsin on $SiO_2$ and $Al_2O_3$ colloidal particles at pH 5 and pH 8. The chymotrypsin solution was incubated with 1 vol % suspensions for 2 h as previously described. The supernatant was used to measure the activity of free chymotrypsin. The data in the graph indicate the amount of adsorbed chymotrypsin obtained after the subtraction of free chymotrypsin in the supernatant from the initial chymotrypsin concentration. The chymotrypsin substrate p-NPA and buffer were directly added to the chymotrypsin adsorbed on $SiO_2$ or $Al_2O_3$ colloidal particles and incubated for 20, 30 and 40 min as shown in Figure 9.2. After incubation, the supernatants were collected, and the absorbance due to the formation of p-NP was measured at 405 nm. Graph b shows the absolute activity of adsorbed chymotrypsin in nmol p-NPA per min. Specific activity (shown in graph c) was calculated by combining the data in graphs a and b and is given in nmol p-NP per min per mg enzyme. Due to the spontaneous hydrolysis of p-NPA, control samples using colloidal suspensions without chymotrypsin were also measured at all steps of the experiment. The standard deviation values were obtained in 3 independent experiments. Asterisks indicate the significance of the differences between incubation with $SiO_2$ and with $Al_2O_3$; *$p < 0.05$ and **$p < 0.01$ were calculated in an unpaired t-test.

## 9.4 Discussion

Highly pure $SiO_2$ and $Al_2O_3$ colloidal particles were selected as the carrier material due to their non-toxicity, stability, easy availability and well-characterized properties (Table 9.1), as well as their relevance for several systems, including bio-inorganic hybrids[6-8]. The pH values for the adsorption/ desorption studies were selected based on the IEP values of both materials to facilitate implementation for pH-dependent adsorption/ desorption studies. Additionally, the Hamaker constant of $Al_2O_3$ is higher than that of $SiO_2$[52] (Table 9.1), increasing the affinity of the former for agglomeration and destabilization of the suspensions. Consequently, deagglomeration of the suspensions was carefully performed prior to each incubation using an ultrasound sonotrode. In addition to pH adjustments, adsorption was controlled by adjusting the ionic strength. Based on the findings of our previous study for general protein adsorption, the ionic strength was set to 3 mM to ensure stable adsorption[158].

Using two analysis methods, we determined that chymotrypsin adsorbed on both $SiO_2$ and $Al_2O_3$ colloidal particles (Figure 9.5 and Figure 9.6). The adsorption was pH dependent, although adsorption on $Al_2O_3$ was favored. At pH 5 and pH 8, adsorption on $Al_2O_3$ was 5 and 1.6 times higher, respectively, than that on $SiO_2$. Whereas the theoretical regular monolayer side-on adsorption was reached on the $Al_2O_3$ surface under both acidic and basic pH conditions, the amount of chymotrypsin adsorbed on $SiO_2$ was far less than the theoretical monolayer formation.

Because the pI of chymotrypsin is approximately 8.5-8.8[40, 161-163] and the IEP values are 2.7 for $SiO_2$ and 9.9 for $Al_2O_3$ (Table 9.1), electrostatic interactions do not appear to be the driving force for adsorption. At pH 5, $Al_2O_3$ is positively charged, and $SiO_2$ is negatively charged. Thus, the adsorption of chymotrypsin on $SiO_2$ should be preferred, considering the positive charge of chymotrypsin at this pH. However, adsorption on $Al_2O_3$ was favored for both pH conditions. Rabe *et al.* previously discovered that at pH conditions close to the pI, proteins can exhibit more dense surface coverage because they are nearly neutrally charged[184, 185]. Indeed, the highest adsorption on both materials was observed at pH 8, at which chymotrypsin is nearly neutral. However, due to the net charges on both the particle surface and the protein, local ionic interactions can still be present on the protein/ particle interface. Although the $Al_2O_3$ surface is

slightly positively charged at pH 8 based on an IEP of 9.9, this material exhibited the highest adsorption. In fact, for some large proteins, such as bovine serum albumin and ovalbumin, the maximum adsorption occurred close to their pIs, irrespective of the type of particle[168].

Generally, protein adhesion to oxide particles is controlled by a water-mediated favorable match between charged, polar and non-polar surface sites with diverse amino acid distributions within the protein[164-166]. Thus, in addition to electrostatic interactions, the hydrophobic/ hydrophilic properties of the surface also influence adsorption[167]. A higher affinity for the adsorption of n-heptane than water was measured for $Al_2O_3$. By contrast, notably higher water adsorption was observed on $SiO_2$ colloidal particles (Figure 9.4). These results indicate that the $SiO_2$ colloidal particles have a more hydrophilic surface, whereas the $Al_2O_3$ colloidal particles have a more hydrophobic surface. Furthermore, approximately 30% of the chymotrypsin surface is theoretically calculated to be hydrophobic (Figure 8.9). These differences in the hydrophilic/ hydrophobic properties of both materials underlie the favorability of chymotrypsin adsorption on the $Al_2O_3$ surface. This result is consistent with previous results for the adsorption of chymotrypsin on hexamethyldisiloxane films with a wide range of wettabilities[167] and for colloids of polystyrene, styrene/ 2-hydroxyethyl methacrylate, and $SiO_2$[168]. Moreover, the pH dependence of chymotrypsin adsorption at pH 5 and 8 can be explained by the strong pH dependence of the isosurfaces of chymotrypsin (see Figure 10.1). The substantial role of hydrophobic interactions in the binding between both particles and chymotrypsin is also consistent with the limited desorption of adsorbed chymotrypsin from the particles after the removal of free chymotrypsin, in contrast to the binding of small biomolecules to colloidal ceramic particles, which is predominantly mediated by electrostatic interactions[113, 186, 187].

We successfully investigated the enzymatic activity of adsorbed chymotrypsin on $SiO_2$ and $Al_2O_3$ colloidal particles. One of the main challenges was to modify and optimize a classic enzymatic activity assay[40, 131, 132] based on p-NPA as a chymotrypsin substrate to enable its specific application to adsorbed chymotrypsin on $SiO_2$ and $Al_2O_3$ colloidal particles. Establishing this assay first required the identification of appropriate pH conditions to enable sufficient and stable adsorption. The selected values of pH 5 and 8 were both appropriate pH conditions for this study because sufficient chymotrypsin was adsorbed on both materials with limited

desorption (Figure 9.6). This result was confirmed using a protein quantification assay and, in parallel, an enzymatic activity assay. We did not calculate specific activity at this point because the values for desorbed chymotrypsin were low in both the quantification and activity assays, which would lead to misinterpretation of the data.

A second important condition is the selection of a suitable incubation time during the activity assay to obtain a linear increase in absorbance during the measured time. This step also includes the selection of an appropriate substrate concentration and tests to demonstrate sufficient intensity of the extinction signal, which should preferably be approximately 1. Numerous preliminary measurements confirmed the linear increase in extinction (Figure 9.2) during the tested timescale as well as the intensity of the signal under the given conditions.

Specific activity is a conventional parameter for comparing the influence of adsorption on different materials on the enzymatic activity of enzymes[188]. Because different amounts of chymotrypsin adsorbed on the surfaces of both materials, the specific activity, which was normalized to the amount of enzyme on the material of interest, was an appropriate benchmark (Figure 9.7c). At this point, calculating the specific activity was reasonable because both the amount of chymotrypsin adsorbed on both materials and the signal were sufficient. A strong decrease in specific activity was detected for chymotrypsin after adsorption on $SiO_2$ and on $Al_2O_3$. Specifically, chymotrypsin retained ~ 12 % and ~ 7 % of its initial specific activity on $SiO_2$ and on $Al_2O_3$, respectively, after adsorption at pH 5; this difference was not significant. However, statistically significant differences between both materials were observed at pH 8. Adsorbed chymotrypsin retained ~ 15 % and ~ 9 % of its initial specific activity on $SiO_2$ and on $Al_2O_3$, respectively.

A possible explanation for the pronounced decrease in the specific activity of chymotrypsin adsorbed on $SiO_2$ and $Al_2O_3$ particles under both pH conditions is the dense enzyme coverage, which may prevent access to the active site after adsorption. The more pronounced decrease in specific activity of chymotrypsin adsorbed on the $Al_2O_3$ surface at pH 5 and particularly at pH 8 could be explained as follows. A high adsorption density close to theoretical monolayer formation occurred under both pH conditions. In particular, at pH 8, where chymotrypsin is almost neutral, a higher packing density was observed[184, 185]. This could lead to steric

hindrance of the active site caused by neighboring chymotrypsin molecules[189]. Due to the high amount of adsorbed chymotrypsin, enzyme clusters may also form on the surface and potentially render the active site inaccessible. A previous study performed by Gailite et al. demonstrated that trypsin, which has a structure similar to that of chymotrypsin, adsorbed on hydrophobic titania films, forming enzyme clusters rather than a well-structured monolayer[34]. Moreover, the $Al_2O_3$ surface was more hydrophobic than the $SiO_2$ surface. In general, enzymes undergo greater conformational changes on hydrophobic surfaces than on hydrophilic surfaces[36]. Finally, active sites can orient toward the immobilization surface, resulting in reduced activity[157]. Indeed, because proteins immobilized via physisorption are randomly oriented on the surface, some fraction of the binding sites within a population of immobilized proteins are likely not accessible[157]. Orientation may be a primary factor because similar results were observed for the $SiO_2$ surface. However, the observed decrease in specific activity reflects the interplay of all of these factors.

The approach utilized in this research study clearly demonstrates a method for determining the enzymatic activity of adsorbed enzymes. We selected physisorption as the most straightforward immobilization method. There were no general limitations, and the optimized assay can also be applied in studies employing other enzyme immobilization methods. The presented framework of the experiments provides a good basis for use with other colloidal particles and demonstrates how to adjust a known assay to a specific system. Moreover, this method is simple, rapid and requires only conventional technical equipment such as a UV/ Vis spectrometer.

## 9.5 Conclusions

The main focus of this study was to compare the influence of adsorption on $SiO_2$ and $Al_2O_3$ colloidal particles on the enzymatic activity of the proteolytic enzyme α-chymotrypsin. A known photometric assay based on p-NPA as a chymotrypsin substrate was optimized to enable the assessment of the enzymatic activity of the adsorbed chymotrypsin. Chymotrypsin's affinity toward adsorption via physisorption was higher for $Al_2O_3$ colloidal particles than for $SiO_2$ due to the greater hydrophobicity of

the $Al_2O_3$ surface. Theoretical regular monolayer side-on adsorption was achieved on the $Al_2O_3$ surface under both acidic (pH 5) and basic conditions (pH 8). However, theoretical regular monolayer side-on adsorption of chymotrypsin on the $SiO_2$ surface was not achieved under acidic or basic conditions. Chymotrypsin exhibited a strong decrease in its initial specific activity after adsorption on both colloidal materials, although the decrease was slightly more pronounced after adsorption on $Al_2O_3$ (by 91-93 %) compared to adsorption on $SiO_2$ (by 85-88 %). This decrease may be due to steric hindrance based on the packing density on $Al_2O_3$ as well as its hydrophobic surface, which induces a higher degree of structural changes in the adsorbed enzymes. By utilizing two different colloidal materials, we demonstrated that the optimized assay is a rapid and simple method that enables the determination of the enzymatic activity of adsorbed enzymes using conventional photometric devices and can easily be applied to numerous other colloidal systems.

## 9.6 Acknowledgments

We thank Nils Hildebrand (Hybrid Materials Interfaces Group, Bremen Center for Computational Materials Science, University of Bremen, Germany) for calculating the hydrophobic/ hydrophilic surface areas of chymotrypsin.

# 10 Physisorption of α-chymotrypsin on $SiO_2$ and $TiO_2$: a comparative study via experiments and molecular dynamics simulations

*ABSTRACT: In order to understand fundamental interactions at the interface between immobilized enzymes and ceramic supports, we compare the adsorption features of chymotrypsin on $SiO_2$ and $TiO_2$ colloidal particles by means of a combination of adsorption experiments and molecular dynamics simulations. While the dependency of the adsorption amount on pH is consistent with the trend predicted by DLVO theory, other effects can only be rationalized if the atomic-scale details of the water-mediated protein-surface interactions are considered. On both surfaces, a clear driving force for the formation of a double monolayer at the saturation coverage is found. Although nearly equal free energies of adsorption are estimated on the two materials via a Langmuir adsorption analysis, about 50 % more proteins per unit of surface can be accommodated on $TiO_2$ than on $SiO_2$. This is probably due to the lower surface diffusion mobility of the adsorbed protein in the latter case. Surface anchoring is realized by a combination of direct ionic interactions between charged proteins and surface sites (more pronounced for $SiO_2$) and distinct structuring of the surface hydration layers in which the contact residues are embedded (more pronounced for $TiO_2$). Finally, normalization of the data with respect to particle surface areas accessible to the proteins, rather than determined by BET nitrogen adsorption, is crucial for a correct interpretation of the results.*

## 10.1 Introduction

Enzymes are widely exploited for industrial and technological applications as catalysts in complex chemical processes operating under mild environmental conditions. Since free and soluble enzymes pose several handling problems, they are often immobilized onto solid insoluble supports[15, 17, 18]. Immobilization confers enzymes higher stability towards temperature variations and solvents[6-8], permits enzyme reusability in continuous processes[12-14], facilitates their recovery after the reaction without any significant loss to its biochemical properties[6, 8] and allows an easier separation from other dissolved compounds[3-6, 140]. Immobilization

of enzymes on solid supports via covalent binding, entrapment or adsorption via e.g. hydrophobic and ionic interactions may provide stability to the immobilized enzyme structure, ultimately resulting in an improved enzyme activity and stability[6, 8]. Covalent binding permits a stable enzyme fixation to the carrier material and suppresses enzyme leaching. However, it often requires several synthesis steps including surface conditioning with hazardous chemicals[190]. On the contrary, immobilization by physical adsorption is considered to be a more straightforward and therefore economically attractive and environment-friendly approach[6, 8, 146]. It does not require any additional chemicals and can be carried out at mild conditions[191].

Numerous studies have focused on the application of ceramics such as silica ($SiO_2$) and titania ($TiO_2$) as solid supports or carrier materials in biotechnological applications[2, 180, 192-195]. These include bioreactors, water purification devices[196-199], chromatography applications systems[200], biomedical implants and drug delivery systems[2, 180, 192, 193, 201-203]. It is well known that adsorption on hydrophobic materials may induce strong conformational changes of the adsorbed proteins, which could inactivate them[36, 106, 204]. On hydrophilic surfaces, adsorption is generally found to better conserve the native protein structure[36, 106, 204], which makes ceramic particles suitable for technical use as enzyme carrier material. $SiO_2$ and $TiO_2$, considered in this work, have different isoelectric points (IEPs) and different surface charge distributions. They are therefore representative candidates to carry out a fundamental study of non-covalent interaction mechanisms between their surfaces and adsorbed enzymes in aqueous solutions[33]. For our study we have selected the well-characterized and technically relevant enzyme α-chymotrypsin. Chymotrypsin is a mammalian digestive enzyme involved in the proteolytic activity of pancreatic juice, and in the hydrolysis of ester bonds[36]. It hydrolyzes specifically peptide bonds in which the carbonyl group belongs to phenylalanine, tyrosine or tryptophan amino acids[172]. Chymotrypsin is widely used both diagnostically and therapeutically for the treatment of pancreatic disease, and is involved in cancer metastases[205-207].

Protein adsorption onto carrier materials is driven by a complex combination of Derjaguin- Landau- Verwey- Overbeek (DLVO) interactions[47], solvent-mediated effects, hydrogen bonds, ionic bonds and metal ion bridges[7, 33, 158, 208]. Furthermore, the reported activity and

amount of adsorbed enzymes vary widely depending on the specific carrier material/ enzyme pair[36, 106, 209]. Previous circular dichroism (CD) studies of chymotrypsin adsorbed on hydrophobic Teflon or on hydrophilic fumed $SiO_2$ performed by Zoungrana et al.[106] and Norde et al.[36] showed that chymotrypsin tends to build tightly-packed adsorbed layers. On $SiO_2$, a clear loss of the helical content of the molecule due to the interaction with $SiO_2$ was reported [106]. Nevertheless, the measured activity was observed to diminish only slightly after adsorptions, suggesting an overall conservation of the tertiary protein structure in proximity of the enzymatically active site. This is consistent with the idea that globular proteins adsorb on solid particles forming a rather compact layer with thickness comparable to the dimension of the native molecule[210], even though structural rearrangements could take place at the protein/ surface interface region.

Regarding the strength of the protein/ surface interactions, it has been shown that the binding affinity of proteins to particle surfaces do not correlate with their net charges, but rather depends on the mutual distribution of charged sites on either side of the interface[211, 212]. For the case of chymotrypsin on $SiO_2$, Zoungrana et al.[106] and Welzel[213] were not able to desorb previously adsorbed molecules neither in phosphate buffer at pH 7.1 nor in 0.01 M sodium chloride solutions[106], and interpreted the results in terms of a non-reversible adsorption.

Although several studies on enzyme physisorption on ceramic materials have been reported, the precise effects of different surfaces on the adsorption behavior of enzymes are still poorly understood. In this study, we perform a systematic comparison of the adsorption of chymotrypsin on $SiO_2$ and $TiO_2$ particles, taking into account environmental parameters such as pH, ionic strength, enzyme concentration and incubation time. The obtained experimental results are rationalized by means of comprehensive Molecular Dynamics (MD) simulations that give insights into the adsorption orientation, surface diffusion mobility and atomistic details of the protein-surface contact points. The combined experimental and simulation analyses elucidate the adsorption behavior of chymotrypsin from single molecules up to a dense protein layer at a saturation coverage corresponding to at least a double monolayer. In our analysis, we highlight the crucial role played by correct quantification of the particle surface area accessible to proteins, which we suggest to differ considerably from the one measured by conventional BET nitrogen

adsorption. This is especially the case for microporous materials, such as some types of $SiO_2$ particles.

## 10.2 Materials and methods

### 10.2.1 Materials

Silica colloidal particles ($SiO_2$; $SiO_2$P015-01, > 99.9 % wt, Lot. No. 100618-02V) were obtained from Fibre Optic Center (USA). Titania colloidal particles ($TiO_2$; PT401L, 78 % wt rutile and 22 % wt anatase, Lot. No. 0108) were purchased from Ishihara Sangyo Kaisha Ltd (Japan). Lyophilized α-chymotrypsin type II from bovine pancreas (molar weight 25300 g $mol^{-1}$, purity 94.1 % wt, Lot. No. 60M7007V), p-nitrophenol acetate (CAS No. 830-03-5, Lot. No. 0001422901), potassium dihydrogen phosphate (≥99 % wt, CAS No. 7778-77-0), sinapic acid (Lot. No 1392702 32008266) and 1,4-dioxan (> 99.8 % wt, CAS No. 123-91-1, Lot. No. STBB3939) were obtained from Sigma-Aldrich (Germany) and used without any modifications. Pierce™ bicinchoninic acid protein assay kit (BCA assay) was obtained from Thermo Fisher Scientific GmbH (Germany). All other chemicals were purchased from Fluka (Switzerland) or Merck (Germany) at analytical grade. For all aqueous solutions double deionized water ($ddH_2O$) with a conductivity of 0.04 µS $cm^{-1}$ was used as the solvent (Millipore Synergy®, Millipore Corporation, Germany).

### 10.2.2 Characterization of $SiO_2$ and $TiO_2$

Prior to the investigation, $SiO_2$ and $TiO_2$ particles were calcinated at 400°C for 4 h with a heating and cooling rate of 3°C $min^{-1}$ (oven L3/11/S27, Nabertherm, Germany) to remove any organic contaminants. The particle size was determined by dynamic light scattering (DLS, Beckman-Coulter DelsaNanoC, Beckman Coulter GmbH, Germany) using 0.003 vol % $SiO_2$-suspension at pH 5 or 0.003 vol % $TiO_2$-suspension at pH 3. Prior to each DLS measurement, the suspensions' conductivity and pH were adjusted to avoid or to minimize particle agglomeration and the particle suspensions were deagglomerated for 10 min using an ultrasound sonotrode Sonifier®

450 (output 150 W, pulse rate 0.5 s, Branson, USA). Deagglomeration did not change any surface-specific property such as IEP. The suspension conductivity was set at 500 µS $cm^{-1}$ using 3 M KCl and pH was adjusted with 1 M KOH or 1 M HCl. The BET specific surface area ($SSA_{BET}$) was obtained by volumetric nitrogen adsorption measurements using a BELsorp-mini II device (BEL Japan, Japan) and assuming a cross-sectional area of the nitrogen molecule of 0.162 $nm^2$ [36]. The ζ-potential measurements were performed in 1 vol % aqueous suspensions of $SiO_2$ and $TiO_2$ using the electroacoustic colloidal vibration current technique (Acoustic & Electroacoustic Spectrometer DT-1200, Dispersion Technology, USA) as described in[118]. $SiO_2$ and $TiO_2$ suspensions with an initial conductivity of 500 µS $cm^{-1}$ were titrated using 1 M KOH or 1 M HCl to measure the ζ-potential as a function of pH and to determine the isoelectric point (IEP). The quantity of hydroxyl groups present on the surface of the colloidal particles was determined by titrations according to Hidber[158, 159].

The particle morphology was analyzed by scanning electron microscopy (SEM; field-emission SEM SUPRA 40, Zeiss, Germany) operating at 2.00 kV mounted on carbon tape. Transmission electron microscopy (TEM) imaging was performed using a FEI Titan 80/300 kV (FEI, The Netherlands) equipped with a Cs-corrector for spherical aberration of the objective lens at 300 kV and a vacuum at 1.3 x $10^{-7}$ mbar. $SiO_2$ and $TiO_2$ particles were deposited on chemical vapor deposition (CVD) graphene film coated copper grids (Graphene Supermarket, New York, USA). The hydrophilic/ hydrophobic surface properties were investigated by volumetric water vapor and n-heptane adsorption measurements using a BELsorp 18-3 device (Bel Japan Inc, Japan).

### 10.2.3 MALDI-ToF-MS

MALDI-ToF-MS was used to investigate the presence of self-digestion-derived peptides in the supernatants collected after chymotrypsin incubation for 20 h at pH 8. We used a MALDI-ToF-MS Voyager DE-Pro (Applied Biosystems, Foster City, USA) controlled by the Voyager Control Panel Software. Measurements were carried out on polished steel targets, using a sinapic acid solution in a acetonitrile/ $ddH_2O$ mixture as the matrix. Spectra were recorded in linear mode at the mass ranges of 5-30

kDa and 10-100 kDa to see the typical patterns associated with the chymotrypsin monomer and the possible presence of the chymotrypsin dimer. In order to achieve statistically relevant results, 100 shots per position were taken. Furthermore, measurements were repeated at three different positions within the spotted sample and accumulated. To investigate the time-dependent autolysis of chymotrypsin reference without colloidal particles, MALDI-ToF-MS measurements were performed in the low measuring range of 800-5000 Da at incubation start, after 1 h, 4 h, and 20 h of incubation. Prior to the measurements, an external calibration was carried out using the calibration mixtures CalMixI and CalMixII, according to the manufacturer's instructions.

### 10.2.4 Time- and pH-dependent adsorption of chymotrypsin to $SiO_2$ and $TiO_2$

Aqueous suspensions (1 vol %) of $SiO_2$ and $TiO_2$ particles were prepared by mixing 1.3 g of $SiO_2$ or 2.12 g of $TiO_2$ with 49.5 ml of $ddH_2O$. The values of density used for the calculation are given in Table 10.1. The pH was adjusted using 1 M HCl or 1 M KOH solutions to pH 3, 5, 7.4 or 8 and the suspension conductivity was set to 500 µS $cm^{-1}$, which corresponds to an ionic strength of 3 mM, using 3 M KCl. Prior to incubation with chymotrypsin, the particle suspensions were de-agglomerated for 10 min using an ultrasound sonotrode Sonifier® 450 (output 150 W, pulse rate 0.5 s, Branson, USA). Chymotrypsin stock solution (concentration of 20 mg $ml^{-1}$) was freshly prepared by dissolving chymotrypsin in $ddH_2O$ and the pH was adjusted as described before.

Incubation was carried out by mixing 900 µl of particle suspension with 100 µl chymotrypsin stock solution in 1.5 ml polypropylene tubes (Eppendorf AG, Germany). Precipitation was prevented by permanent overhead shaking (Stuart rotator STR4, Bibby Scientific Ltd., UK) at a speed of 30 rpm at room temperature for 1, 4 or 20 h. The suspensions were centrifuged for 10 min at 21100 g (Heraeus Fresco 21 centrifuge, Fisher Scientific, Germany). Chymotrypsin concentrations in the supernatants and in chymotrypsin reference solutions without colloidal particles were measured with the BCA assay [126, 129, 214, 215] with the lowest detection limit of 5 µg $ml^{-1}$ according to manufacturer's instructions. The enzymatic activity of chymotrypsin was determined according to[40, 131, 132].

Briefly, 20 µL of the supernatant were mixed with 140 µL 100 mM potassium phosphate buffer in a well of a 96-microtiter plate (Nunc™, Denmark). The reaction was started by the addition of chymotrypsin substrate, 160 µL 0.2 mM p-nitrophenol acetate. The increase in absorbance due to the formation of p-nitrophenolate ion was measured at 405 nm using a microtiter plate reader (Sunrise, Tecan, Austria).

### 10.2.5 Concentration-dependent adsorption of chymotrypsin to $SiO_2$ and $TiO_2$

The incubation was performed by mixing 900 µl of particle suspensions with 100 µl chymotrypsin stock solution reaching the start chymotrypsin concentrations of 0.22, 0.55, 0.69, 2.37, 4.95 and 6.85 mg $ml^{-1}$. After an incubation time of 20 h, the chymotrypsin concentration and the enzymatic activity in the supernatant were measured as previously described[134]. The experimental data were fitted using the Langmuir isotherm:[113, 216]

$$\Gamma = \frac{\Gamma_{max} \cdot c}{K_L^{-1} + c} \tag{10.1}$$

Here, $\Gamma$ and $\Gamma_{max}$ are the adsorbed and maximal adsorbed quantities, respectively, c is the chymotrypsin concentration in solution, and $K_L$ is the Langmuir constant. The Gibbs energy of adsorption $\Delta G^0_{ads}$ can be estimated from the Langmuir constant[113, 216] as

$$\Delta G^0_{ads} = -RT \cdot ln\left(\frac{c_{solv}}{K_L^{-1}}\right) \tag{10.2}$$

where R is the gas constant, T is the temperature, and $c_{solv}$ is the molar concentration of pure water (55.5 $molL^{-1}$). The non-linear least squares fit was performed by a Levenberg-Marquardt algorithm using SciPy[217]. The correlation of the non-linear fit with the experimental data was quantified with a Pearson's correlation coefficient calculated by the scipy.stats.pearsonr function included in SciPy[217].

### 10.2.6 Desorption studies

To test whether adsorption was reversible or irreversible, desorption studies with several washing steps were performed. Therefore, supernatant and colloidal particles were separated and $ddH_2O$ was added to the particles at the same pH as during the previous incubation. After short rinsing, the supernatant was collected. This procedure was repeated three times. All the supernatants were used to measure the amount of adsorbed protein.

### 10.2.7 Moiecuiar Dynamics simulations

The protein structure for the performed simulations was taken from the Brookhaven Protein Database (PDB-ID: 4CHA). Missing residues and atoms were added to the protein monomer with the LEaP program (Link, Edit and Parm, which is included in the AmberTools simulation package at http://ambermd.org)[218]. The size of the enzyme was approximated as a rectangular cuboid with edge lengths of 4.4, 4.7 and 5.0 nm in x, y and z directions. The secondary structure of chymotrypsin comprises for the major part beta sheets, but presents two alpha helix motifs located on one side of the protein (Figure 10.1a). The enzymatically active site includes a triad of amino acids (serine 195 , histidine 57 and aspartic acid 102)[219] which is highlighted in cyan in Figure 10.1a.

The 'constant-pH' feature of the AMBER package[218] was used to adjust the protonation state of all titratable amino acids of the protein to the pH 3, 5, 7.4 and 8. The isoelectric point of chymotrypsin ranges between 8.5 and 8.8[40, 161-163]. At our experimental conditions at $3 < pH < 8$, chymotrypsin has an overall positive charge. The distribution of the electrostatic potential around the protein was calculated by a numerical solution of the Poisson-Boltzmann equation using the 'pbsa' program included in the AMBER package[218]. Consistently with the experiments, the salinity was set to 3 mM including monovalent ions only, and the temperature to 300 K. The electrostatic potential around chymotrypsin at pH 3, 5, 7.4 and 8 are represented in Figure 10.1b-d by negative (red) and positive (blue) isovalue surfaces at ± 30 mV. At pH 3 chymotrypsin has a positive net charge of +7 e, giving rise to a predominantly positive potential surface, especially on one protein side. The net charge decreases to +4 e at pH 5 and +3 e at pH 7.4 and 8, resulting in the formation of separated positive (bottom) and negative (top) protein regions. Accordingly, a strong dipole moment of 529 D ($1.76\ 10^{-27}$ Cm) is oriented towards the positive end,

directly facing the alpha helix region and is shown as an orange arrow in Figure 10.1a.

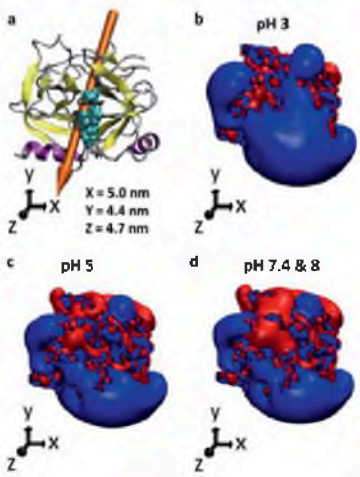


Figure 10.1 (a) Schematic view of chymotrypsin. The catalytic triad is displayed in cyan spheres, the α-helices in purple and the β-sheets in yellow. The molecular dipole is shown as an orange arrow. (b-d) Isosurfaces representing the calculated electrostatic potential around the protein at the values of -1kBT/e (-25.85 mV) (red) and +1kBT/e (+25.85 mV) (blue) at pH 3.0 (b), 5.0 (c) and 7.4 or 8.0 (d).

The protein is equilibrated for ~ 1 ns in explicit solvent using the TIP3P water model[220]. The charge of the simulation cell is balanced including an appropriate number of chlorine ions. The final bare protein structure is taken for further simulations. The parameters for the simulation of the protein, ions and the TIP3P water model are taken from the AMBER_99SB force field[218]. The amorphous structure of the $SiO_2$ slab is taken from Cole et al[221]. To adjust the surface charge according to the pH, the protonation state of the surface terminal groups is changed as described by Butenuth et al.[222]. The surface charges used in this work are average values of the results of potentiometric titration experiments[223-226]. This results in a final surface charge density of 0.0, -0.005, -0.05 and -0.07 C $m^{-2}$ at pH 3.0, 5.0, 7.4 and 8.0, respectively.

A model for an amorphous $TiO_2$ surface was created by cutting a single rutile crystal in an arbitrary direction, relaxing the surface atoms and annealing at 500 K for 200 ps to heal surface defects. The surface was

then immersed in water. Water molecules next to under-coordinated Ti atoms with a coordination number smaller than five were dissociated by adding an OH-group to the Ti atom and binding the remaining proton to a neighbor bridging oxygen as described in[227] for the creation of $TiO_2$ particles. Terminal OH groups on Ti atoms and protonated bridging O atoms were considered as potential protonation/ deprotonation sites, as described by a modified multi site complexation (MUSIC) model[228] by Köppen et al.[229] (Figure 10.2), resulting in a surface charge density of 0.113, 0.037, -0.055 and -0.078 C $m^{-2}$ at pH 3.0, 5.0, 7.4 and 8.0, respectively.

The intramolecular interactions among the $TiO_2$ crystal atoms were described by the force field developed in[230], while the intermolecular interactions of the $TiO_2$ atoms with water and biomolecules were described by the force field developed in[231].

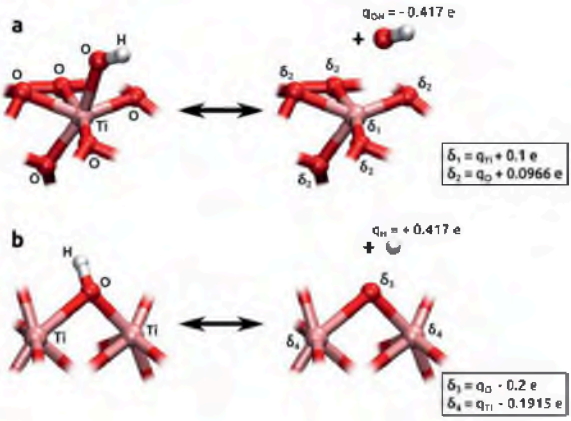


Figure 10.2 Equilibrium of charged surface groups on $TiO_2$. Partial charges $q_i$ are computed as described in[230, 231]. Local changes of the charges $\delta_i$ after protonation/ deprotonation are indicated on the right. (a) De-hydroxylation of a terminal Ti-OH group, resulting in a total surface charge change of -1 e. (b) De-protonation of a bridging OH group resulting in a total surface charge change of +1 e.

The complete simulated systems consisted of one or multiple proteins above each of the two surfaces. The static calculations were performed in implicit solvent according to the Onufriev-Bashford-Case Generalized Born model[232]. The height of the protein over the surface was defined as the

distance between the closest two atoms of surface and protein in the normal direction of the surface. No periodic boundary conditions were used. Therefore, the surface dimensions (18.1 x 18.1 $nm^2$ for the $SiO_2$ surface and 16.2 x 19.1 $nm^2$ for the $TiO_2$ surface) were set large enough to avoid spurious edge effects. The distance cutoff of the non-bonded interactions was set to 100 nm. Force-distance profiles were evaluated for 36 different orientations of the protein from surface contact up to 5 nm above the surface in steps of 0.2 Å.

The molecular dynamics simulations were performed in explicit TIP3P water molecules under periodic boundary conditions using the GROMACS version 4.5.5 simulation package[233]. A dense protein layer formation with a total surface density of 0.077 proteins $nm^{-2}$ over $TiO_2$ and 0.073 proteins $nm^{-2}$ over $SiO_2$ was placed as the initial structure over the respective surfaces. The orientations of the individual proteins were randomized. The charge was neutralized by an appropriate number of sodium ions. The water density was adjusted to the TIP3P water density at 300 K, namely 0.983 g $cm^{-3}$. All surface atoms were constrained. In order to use a time step of 2 fs, the hydrogen atoms in the system were constrained by the 'linear constraint solver' (LINCS) algorithm[234]. The temperature in the dynamic simulation was adjusted with a modified Berendsen thermostat with an additional stochastic term that enables a correct canonical ensemble[235]. The coupling constant is set to 1 ps and the non-bonded interaction cutoff to 1.2 nm. Visualization analyses were performed with VMD[70]. The amount of secondary structure elements of the dissolved and adsorbed proteins was quantified using the Define Secondary Structure of Proteins (DSSP) method of Kabsch and Sander[236].

## 10.3 Results

### 10.3.1 Characterization of $SiO_2$ and $TiO_2$ colloidal particles

We begin our study with a detailed characterization of the used $SiO_2$ and $TiO_2$ colloidal particles, which is essential to interpret correctly the later presented protein adsorption experiments. The particle properties are summarized in Table 10.1 and SEM and HR-TEM images are reported in Figure 10.3.

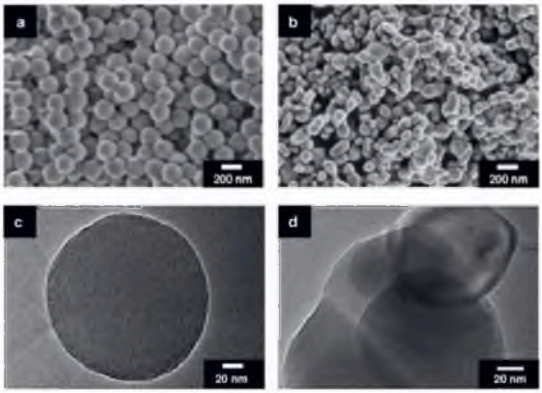


Figure 10.3 Typical SEM (a,b) and HR-TEM (c,d) images of the employed $SiO_2$ (a,c) and $TiO_2$ (b,d) colloidal particles.

These reveal almost perfectly spherical $SiO_2$ particles with an average diameter of 150 nm and agglomerates of more irregular $TiO_2$ primary particles with an average diameter of 130 nm, obtained approximating the irregular particles with spheres. On the other hand, dynamic light scattering measurements offer diameters for $TiO_2$ particles twice as large as those of $SiO_2$ particles (384 vs 180 nm, respectively). This could be due to the formation of $TiO_2$ agglomerates, which are probable according to the significant higher Hamaker constant (Table 10.1). To ensure particle suspension, all probes are threatened with ultrasound. Despite the similar primary particle sizes visible in the SEM and HR-TEM images, the specific surface area ($SSA_{BET}$) determined by nitrogen adsorption is three times higher for $SiO_2$ (34.0 $m^2g^{-1}$) than for $TiO_2$ (12.4 $m^2g^{-1}$) (Table 10.1). Instead, if spherical particle shapes are assumed in both cases, less dissimilar values or 12.1 and 8.6 $m^2\ g^{-1}$ are obtained for $SiO_2$ and $TiO_2$, respectively. We believe the lager $SiO_2$ BET surface area to be a consequence of the microporous structure of the Stöber silica material[237, 238]. This would also explain the dramatically higher adsorption capacity and the hysteresis visible in the water adsorption isotherm of $SiO_2$ compared to $TiO_2$ (Figure 10.4).

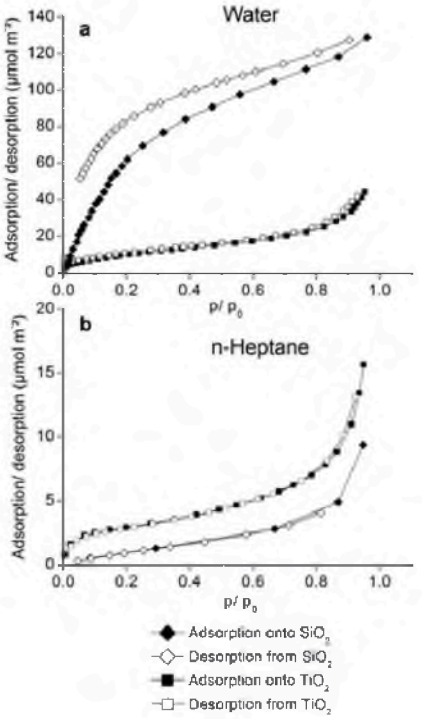


Figure 10.4 Adsorption isotherms of (a) water and (b) n-heptane on $SiO_2$ and $TiO_2$ colloidal particles, normalized to their $SSA_{BET}$ surfaces.

Also the values of proton exchange capacity (given in OH-groups per nm²) are by a factor of 8 higher for $SiO_2$ than for $TiO_2$ (see Table 10.1). Both surfaces, however, are predominantly hydrophilic, as revealed by the significantly smaller affinity to n-heptane than to water for both particle species. Concerning the adsorption of larger biomolecules such as chymotrypsin, we define here a Protein Accessible Area based on the geometrical analysis of the SEM images ($PAA_{SEM}$, see Table 10.1), assuming that the proteins cannot diffuse into the smaller micropores accessible instead to $N_2$ and $H_2O$ molecules. This distinction between $SSA_{BET}$ and $PAA_{SEM}$ will be important to interpret correctly the formation of dense protein layers on the particle surfaces, as described in the next section.

Table 10.1 Properties of $SiO_2$ and $TiO_2$ colloidal particles. All measured data represent means ± standard deviation of values that were obtained in 3 independent experiments. Theoretically calculated values are calculated as average of 20 values and reported with their standard deviation. [a] The data were given by the manufacturer.

| Property | $SiO_2$ | $TiO_2$ | Method |
|---|---|---|---|
| **Purity[a] (wt%)** | ≥ 99.9 | ≥ 99.9 | - |
| **DLS Size (nm)** | $d_{50}$: 180 ± 3 | $d_{50}$: 384 ± 3 | dynamic light scattering |
| **SEM Size (nm)** | 142 ± 7 | 130 ± 15 | SEM images |
| **Specific surface area ($SSA_{BET}$) ($m^2\ g^{-1}$)** | 34.0 ± 0.3 | 12.4 ± 0.5 | volumetric nitrogen adsorption |
| **Theoretical protein accessible surface area ($PAA_{SEM}$) ($m^2\ g^{-1}$)** | 12.8 ± 0.8 | 8.6 ± 1.0 | geometrical analysis of the SEM images |
| **Exchange capacity (OH $nm^{-2}$)** | 4.9 ± 0.2 | 0.6 ± 0.1 | titrations according to Hidber[158, 159] |
| **Isoelectric point (IEP)** | 2.7 ± 0.1 | 6.6 ± 0.1 | electroacoustic colloidal vibration current technique |
| **Hamaker constant[52, 53] ( x $10^{-21}$ J)** | 1.6 | rutile: 60<br>anatase: 37 | full spectral method |
| **Density (g $cm^{-3}$)** | 2.6 ± 0.1 | 4.2 ± 0.1 | pycnometer |
| **Crystal structure** | amorphous | rutile: 78 wt%<br>anatase: 22 wt% | X-ray diffraction and electron diffraction with HR-TEM |

### 10.3.2 Dependence of the protein adsorption on incubation time and pH

The amount of chymotrypsin adsorbed on the $SiO_2$ and $TiO_2$ particles was measured as a function of the incubation time (1 h, 4 h and 20 h) and solution pH (3, 5, 7.4 and 8) via two methods. Namely, both the concentration of protein remaining in solution after prolonged incubation and its enzymatic activity are determined and reported in Figure 10.5. Immediately evident is the decrease of solution concentration of the enzyme at increasing pH values for both particles. This is consistent with previous studies[134] and indicates preferred adsorption of chymotrypsin on negatively charged surfaces. Concerning the incubation time, statistically insignificant variations were observed between 1 and 4 h, but a significant reduction in concentration was observed after 20 h for the case of $SiO_2$ at the higher pH values. This is in line with previous reports showing that an equilibrium adsorption coverage on hydrophilic $SiO_2$ is reached after about 16 h[106, 239, 240].

The quantification of enzymatic activity in the supernatant follows a very similar trend. The used initial concentration of about 2 mg $ml^{-1}$ results in a reference absolute activity of about 20 nmol p-nitrophenol $min^{-1}$ $ml^{-1}$ (Figure 10.5d). During incubation with the particles, the activity diminishes with increasing pH and incubation time. Here it must be mentioned that the activity of the chymotrypsin reference solution itself is reduced by up to 30 % after 20 h of incubation at higher pH, so that the dramatic supernatant activity reduction in the presence of particles is also due to aging effects and not solely due to surface adsorption.

These combined measurements suggest a strong binding affinity of chymotrypsin to both $SiO_2$ and $TiO_2$ particles at neutral or basic pH. The affinity seems to be stronger for the case of $TiO_2$, for which the enzymatic activity of the supernatant was not measurable anymore after 20 h of incubation. Binding to $SiO_2$ seems to proceed via a slower kinetics, given the differences observed between 4 and 20 h of incubation. Repeated washing of the particles after chymotrypsin adsorption was not sufficient to remove a protein amount measurable with BCA assays (data not shown), suggesting an irreversible adsorption behavior on the time scale of the performed experiments. Finally, aging of the protein solution leads to a reduced enzyme activity also in the absence of particles. Whether this

is caused by autolysis or by other effects is investigated in the next section by means of MALDI-ToF-MS.

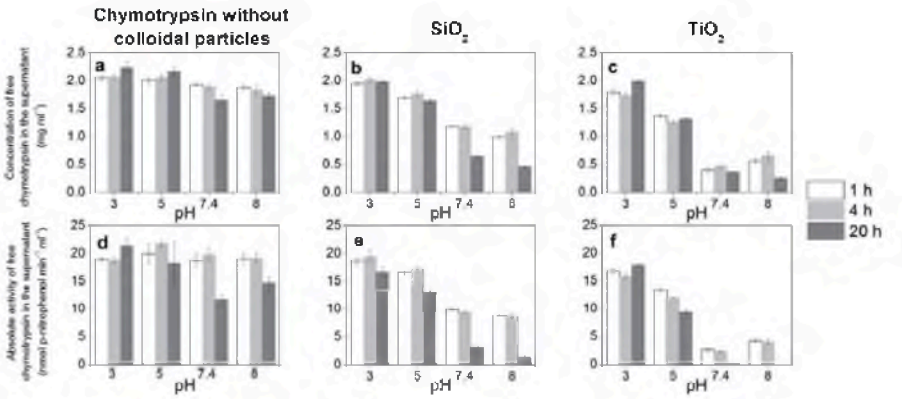


Figure 10.5 Time and pH dependence of the concentration in the supernatant (a-c) and the absolute enzymatic activity in the supernatant (d-f) of chymotrypsin reference solutions (a,d) and after incubation with $SiO_2$ (b,e) and $TiO_2$ (c,f) colloidal particles. The data shown represent means ± SD of values obtained in 3 independent experiments with a starting chymotrypsin concentration of 2.0 mg $ml^{-1}$ prior to pH adjustment (see panel (a)).

### 10.3.3 MALDI-ToF-MS analysis of possible autolysis

The possible autolysis of chymotrypsin in solution and in the supernatant of $TiO_2$ and $SiO_2$ particle suspension was analyzed by means of MALDI-ToF-MS measurements at pH 8, where autolysis is most favorable[171-173]. The collected spectra are reported in Figure 10.6 in the m/z ranges from 5 to 30 kDa and 10 to 100 kDa, and in Figure 10.7 in the m/z range of 800-5000 Da.

In the spectra the typical peaks arising from chymotrypsin monomers (around 25.2 kDa) and dimers (50.5 kDa) are well visible. Moreover, peaks of multiply charged proteins occur at around 12.6 and 6.3 kDa/ charge unit. Notably, no peaks attributable to peptide fragments derived from autolysis could be observed, irrespective of the incubation time and the absence or presence or particles (Figure 10.7), consistently with a previous study[105]. In summary, this investigation confirms that the protein remains complete within the time scale of our experiments, and

that the chymotrypsin monomer is by far the predominant species present in the used solutions.

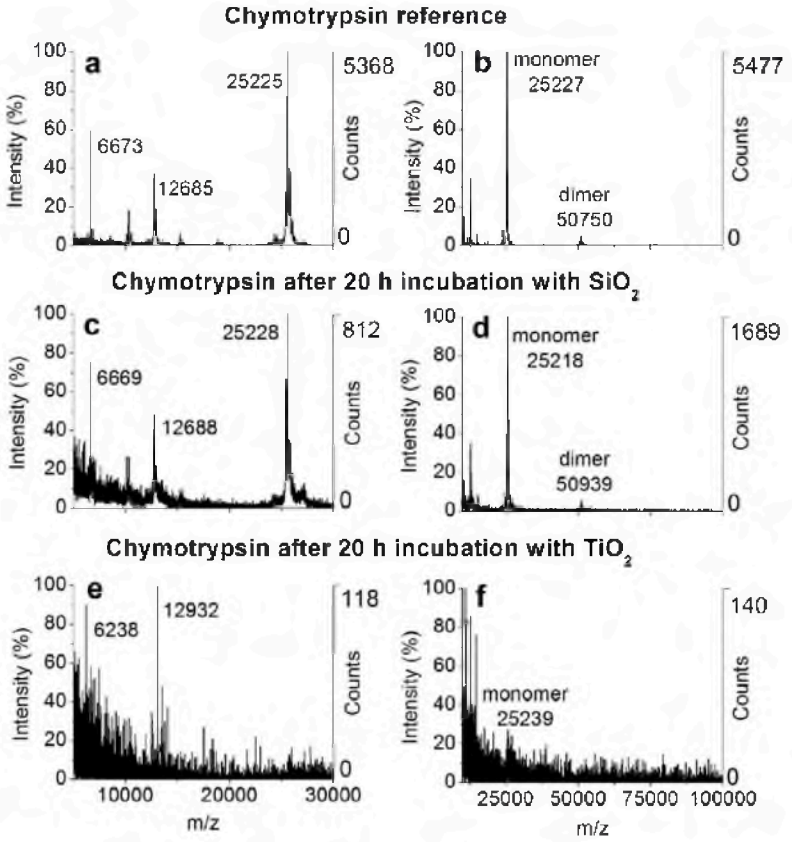


Figure 10.6 MALDI-ToF-MS spectra of (a,b) the chymotrypsin reference, and of chymotrypsin after 20 h incubation at pH 8 with $SiO_2$ (c,d) or $TiO_2$ (e, f). The spectra are shown for the m/z ranges from 5 to 30 kDa/e (a,c,e), and from 10 to 100 kDa/e (b,d,f).

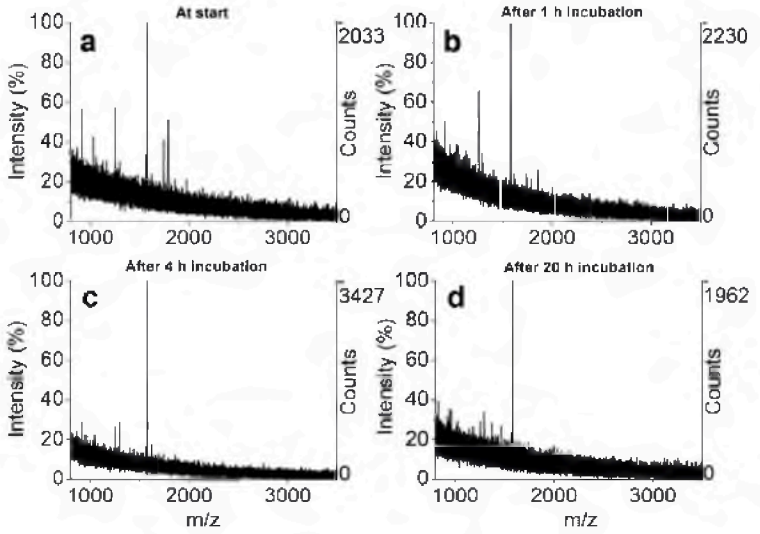


Figure 10.7 MALDI-ToF-MS spectra of chymotrypsin reference solutions without colloidal particles immediately after the start of the incubation (a), after 1 h (b), after 4 h (c), and after 20 h of incubation (d) at pH 8. The spectra show the low measured range of 800-3500 Da/e.

### 10.3.4 Analysis of the adsorption layers

The amount of adsorbed chymotrypsin monomers was computed from the data shown in Figure 10.5, subtracting the measured concentration in the supernatant from the initial concentration prior to incubation (Figure 10.8a-d). Normalization of the adsorbed protein amount to the particle surface was performed considering both the $SSA_{BET}$ and the $PAA_{SEM}$ surfaces (see Table 10.1), as anticipated above. As references for a side-on or an end-on monolayer we consider rectangular surface units along the two main directions of the protein's envelope, corresponding to 25.0 and 19.4 $nm^2$ occupied by a single protein, respectively (see scheme in Figure 10.8e). The amount of adsorbed protein (given both as protein number per $nm^2$ and as protein mass per $cm^2$) is reported as a function of the pH and incubation time.

Using $SSA_{BET}$ to normalize to the particle surface, the amount of chymotrypsin adsorbed onto $TiO_2$ appears to be almost twice as high as onto $SiO_2$ (Figure 10.8a,b). Namely, the data obtained after 20 h of incubation increased from 25 ng $cm^{-2}$ at pH 3 to 160 ng $cm^{-2}$ at pH 8 on

$SiO_2$ (Figure 10.8a), while on $TiO_2$ the adsorbed concentration varied from a minimum of 50 ng $cm^{-2}$ at pH 3 to 310 ng $cm^{-2}$ at pH 7.4 and 8 (Figure 10.8b). These values would correspond to a double layer of side-on adsorbed proteins on $TiO_2$ and to a single side-on layer on $SiO_2$. Simple arguments cannot explain this difference, especially given the considerably larger surface charge and water affinity of $SiO_2$ with respect to $TiO_2$, two properties that often correlate with the protein adsorption affinity. However, considering the $PAA_{SEM}$ as the normalizing particle's surface, the situation changes. In this case, the maximum amount of adsorbed chymotrypsin is only slightly larger for $TiO_2$ (460 ng $cm^{-2}$ at pH 7.4 after 20 h of incubation) than for $SiO_2$ (440 ng $cm^{-2}$ at pH 8 after 20 h of incubation) (Figure 10.8c,d). As an important difference between the two materials, we note the continuous increase of adsorbed protein amount with pH on $SiO_2$, while the adsorption maximum was reached already at pH 7.4 for $TiO_2$. Other subtle differences such the variations of the adsorbed amount on $TiO_2$ between pH 7.4 and 8.0, being of the same order as the error bars, are probably insignificant and shall not be discussed in further detail.

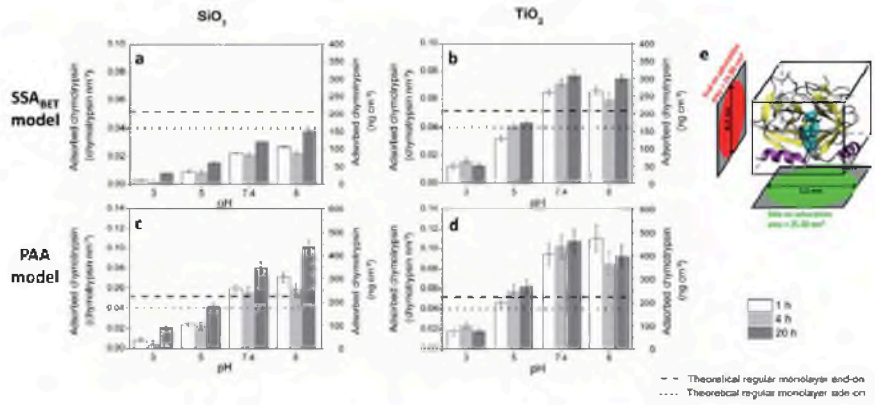


Figure 10.8 Amount of chymotrypsin adsorbed on $SiO_2$ (a,c) and $TiO_2$ (b,d) as a function of time and pH. The data are expressed both in terms of ng $cm^{-2}$ and of number of molecules per $nm^2$ (right and left vertical axes in each panel, respectively). The concentration data are normalized to the $SSA_{BET}$ (a,b) or the $PAA_{SEM}$ (c,d) surface areas (see Table 10.1 and text). Theoretically calculated values for regular end-on and side-on monolayers are marked as black dashed and dotted lines, according to the scheme in (e). The experiments are performed with a starting protein concentration of 2.0 mg $ml^{-1}$ prior to pH adjustment.

### 10.3.5 Dependence of the adsorbed amount on the protein concentration

To investigate the dependence of the amount of adsorbed chymotrypsin on the initial concentration in solution, chymotrypsin was incubated with $SiO_2$ and $TiO_2$ at pH 8 in concentrations ranging from 0.22 to 6.85 mg $ml^{-1}$ for 20 h. After incubation, the concentration in the supernatant was measured and, by subtraction, the adsorbed concentration was determined.

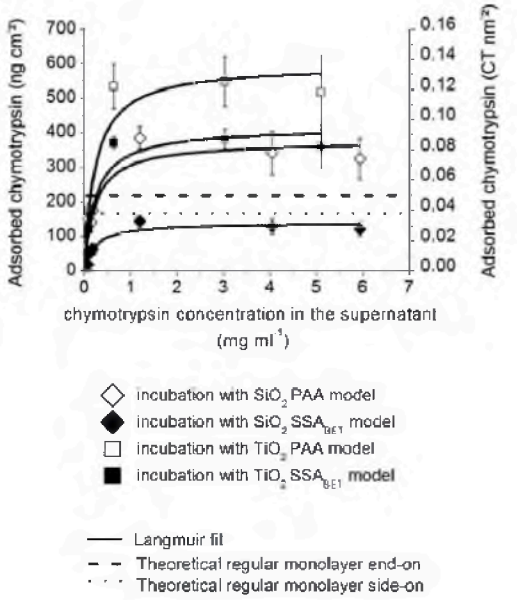


Figure 10.9 Concentration-dependent adsorption of chymotrypsin on $SiO_2$ and $TiO_2$ colloidal particles at pH 8 after 20 h of incubation. The data are normalized with respect to the $SSA_{BET}$ and $PAA_{SEM}$ surface areas. Theoretically calculated values for regular monolayer in adsorption orientation end-on and side-on are marked as black dashed lines. The data shown represent means with standard deviations of values obtained in 3 independent experiments, and were fitted with a Langmuir isotherm model (black lines).

The results are reported in Figure 10.9 considering both the $SSA_{BET}$ and $PAA_{SEM}$ surfaces for normalization, and were fitted with Langmuir isotherms to estimate the saturation adsorption amounts $\Gamma_{max}$ and the free energies of adsorption $\Delta G^0_{ads}$. For both particles types, saturation was

reached in correspondence of supernatant concentrations of about 2 mg $ml^{-1}$. Consistently with the analyses in the previous section, more protein was found adsorbed on $TiO_2$ than on $SiO_2$. Namely, considering the $SSA_{BET}$ the values differed by a factor of three ($\Gamma_{max}$ = 488 ± 65 ng $cm^{-2}$ for $TiO_2$ and $\Gamma_{max}$ = 155 ± 18 ng $cm^{-2}$ for $SiO_2$), whereas the difference was less dramatic if normalization is performed with the $PAA_{SEM}$ surface ($\Gamma_{max}$ = 700 ± 103 ng $cm^{-2}$ for $TiO_2$ and $\Gamma_{max}$ = 436 ± 58 ng $cm^{-2}$ for $SiO_2$). These values again correspond to adsorption well beyond a monolayer, and indicate important differences in the adsorption modes of chymotrypsin on the two different surfaces. Interestingly, $\Delta G^0_{ads}$ (which is independent on the surface normalization) is almost the same for both materials, amounting to -34.3 ± 1.0 kJ $mol^{-1}$ for $TiO_2$ and -35.6 ± 1.0 kJ $mol^{-1}$ for $SiO_2$. Possible reasons leading to these effects were investigated by means of all atom Molecular Dynamics simulations in the next sections.

### 10.3.6 Long-range interaction force of chymotrypsin over $SiO_2$ and $TiO_2$

From the experiments described above, the amount of adsorbed protein on $TiO_2$ is either three times as high ($SSA_{BET}$) or about 50 % larger ($PAA_{SEM}$) than on $SiO_2$, depending on the used normalization surface. This motivates an in-depth theoretical analysis of the adsorption modes at the atomistic level. In this section static calculations were used to evaluate the force-distance profiles and predict the most favorable adsorption orientation of single protein molecules onto models of amorphous $SiO_2$ and $TiO_2$ surfaces at different pH values, according to Hildebrand et al[166].

For this aim, 36 different protein orientations are considered, giving rise to a broad interaction profile and revealing the most attractive orientation for each surface and pH (Figure 10.10). For both surfaces, the protein/ surface force profiles are largely defined by the interaction between the strong protein dipole moment and the charge distribution at the surface. For the case of $SiO_2$, an average attraction interaction (negative forces) is observed at all pH values, with an increased attraction and clearer dipole orientation while the pH increases and the surface become more and more negative.

On $TiO_2$, on the other hand, repulsion is predicted at pH values lower than the surface IEP (6.0), whereas attraction takes place only at pH 7.4 and 8.0. Note also the inversion of the dipole moment in the most attractive (or least repulsive) protein orientation in passing from pH 5.0 to pH 7.4 (Figure 10.10, left). At pH 8, in the most attractive orientation the protein faces the surface with its two $\alpha$-helix motifs, and the enzymatically active site points sideways with respect to the surface normal.

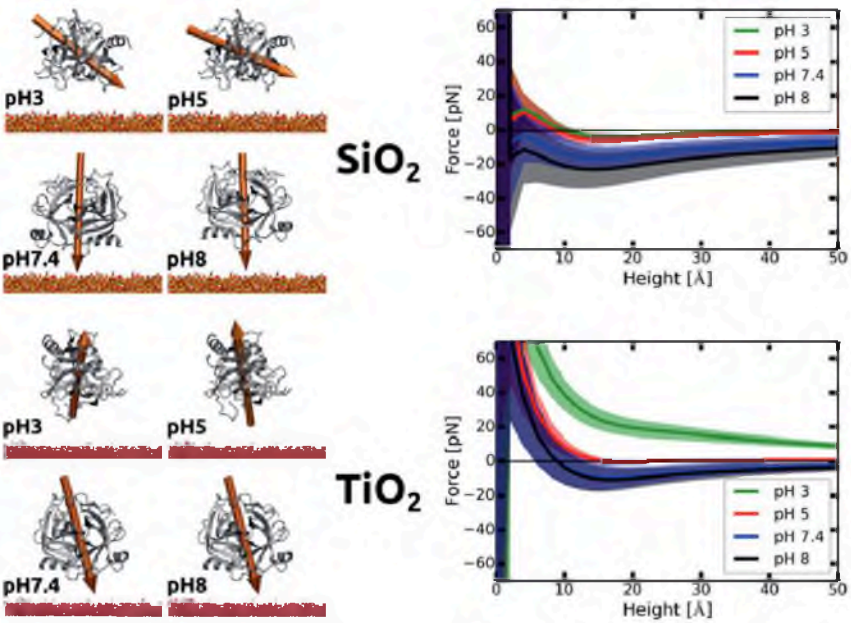


Figure 10.10 (*left*) Predicted most attractive orientations of chymotrypsin over $SiO_2$ and $TiO_2$ at different pH values. The molecular dipole moment is shown as an orange arrow. (*right*) Force-height profiles calculated in implicit solvent for 36 different orientations at each pH value. The averages over all orientations are drawn with the bold colored lines and the standard deviations are represented with semitransparent colored regions. Negative values define attractive forces. The height is defined as the distance in the surface normal direction between the highest surface atom and the lowest protein atom.

The maximum attractive forces are experienced by the protein at pH 8 at a height of about 1.5 nm over either surface. It has to be stressed that these calculations only take into account the DLVO interactions in a continuum-solvent approximation, and that further protein approach to

the surface below 1.0 nm is strongly mediated by the structuring of the water molecules in surface proximity[166, 221, 241]. At this stage it can be only concluded that long-range DLVO attraction is clearly evident at the larger pH values, which agrees with the measured trend of the adsorbed protein amount (Figure 10.8), and that stronger attraction is experienced over $SiO_2$, which instead does not correlate with the experimental observation. The interaction profiles over $TiO_2$ are less deep and more narrow compared to $SiO_2$. One can thus expect an easier reorientation of chymotrypsin over $TiO_2$ because of a less distinct force dependence of the orientation.

This was indeed confirmed by analyzing the relative energy changes upon rotation of the proteins around two independent axes at the constant height of 1.0 nm (Figure 10.11). Here, at all considered pH values a belt-like feature in the diagram can be observed, which corresponds to an orientation of the molecular dipole normal to the surface (in either direction), as discussed in detail in Hildebrand et al.[166]. This interaction pattern is less distinct for smaller pH values. In the energy diagram, the attraction or repulsion forces are shown with the small black arrows. The differences in the relative energy upon molecular reorientation are about 24 kcal $mol^{-1}$ over $SiO_2$ and 12 kcal $mol^{-1}$ over $TiO_2$.

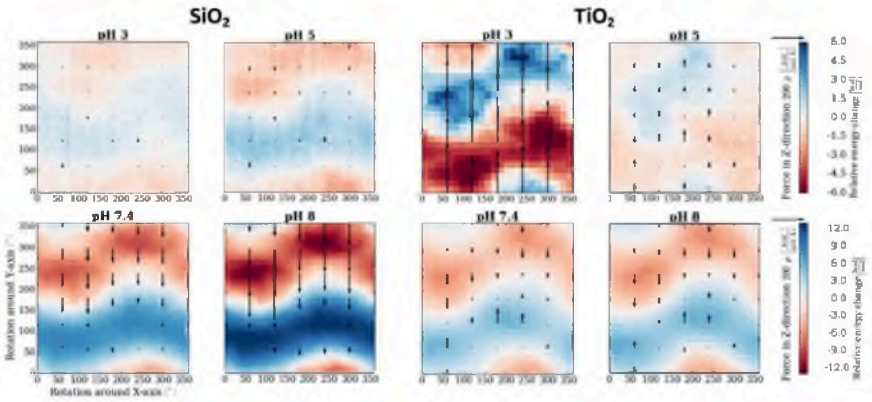


Figure 10.11 Calculated relative energy changes associated with rotation of chymotrypsin at a height of 10 Å over the surfaces for (left) $SiO_2$ and (right) $TiO_2$, for four different pH values. The superimposed arrows represent the force values (downward for attractive, upward for repulsive forces).

### 10.3.7 Interaction forces for chymotrypsin multi-layers

While the previous section has dealt with the case of a single protein approaching the surfaces, we consider here the presence of a pre-adsorbed protein monolayer, thus explicitly taking into account protein-protein interactions (Figure 10.12). A first calculation was performed evaluating the relative energy changes associated with the reorientation of one protein within a pre-adsorbed protein monolayer (Figure 10.12a) with a density of 0.034 molecule $nm^{-2}$ (corresponding to a theoretical end-on monolayer, see Figure 10.8). Here, the protein height is fixed at 0.3 nm, and the map of energy changes obtained upon rotation around two axes is reported in Figure 10.12b for the representative case of $SiO_2$. A visually almost identical map was obtained for $TiO_2$. Starting from the most attractive adsorption orientation predicted for single proteins (at x = y = 0), rotation in any direction is associated with an energy increase, and an energy maximum is obtained for the molecular dipole pointing in the opposite direction (x = 180 y= 0; or x = 0, y = 180). The maximum is 30 kcal $mol^{-1}$ higher than the minimum for the case of $SiO_2$ and 20 kcal $mol^{-1}$ higher than the minimum for the case of $TiO_2$. This suggests that, in spite of the parallel arrangement of the molecular dipoles, in the most favorable configuration within a monolayer all proteins are oriented in the same way, with their $\alpha$-helices pointing towards the surface.

A second calculation was then performed to evaluate the force-distance profile associated with the approach of a single chymotrypsin molecule towards an already present protein monolayer either adsorbed on the two surfaces (Figure 10.12c), or suspended in solution, as a reference. The resulting profiles averaged over 36 different protein orientations (Figure 10.12d) revealed that *repulsion* is predicted in the absence of an underlying surface, thus suggesting no favorable driving force for spontaneous formation of protein agglomerates in solution. However, *attraction* is predicted for a monolayer on either $SiO_2$ or $TiO_2$, as a consequence of the strong interaction exerted by the surface, which is not completely shielded by the presence of an adsorbed monolayer. Also in this case, attraction is slightly stronger for the case of $SiO_2$ and the most attractive protein orientation is as in the pre-formed monolayer.

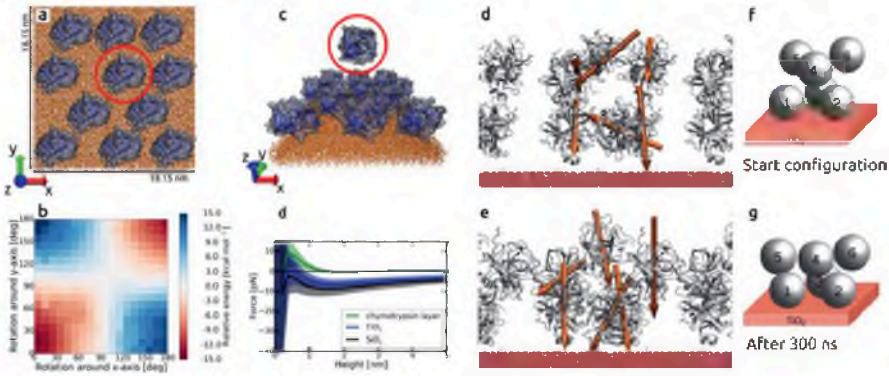


Figure 10.12 Driving force for the formation of protein multilayers on $SiO_2$ and $TiO_2$. (a) Atomistic representation of an end-on monolayer at the density of 0.034 ± 0.001 molecules per $nm^2$. The red circle marks a protein which is rotated along two axis (x and y), giving rise to the energy map in (b). The force profiles calculated for an additional protein (c) interacting with the monolayer in the absence (green curve) or in the presence of surfaces (blue and grey curves) are shown in (d). Here, a height of zero is defined when the highest monolayer atom and the lowest atom of the additional protein are at the same height in the direction of the surface normal. (d) and (e) show the initial and final configurations of a protein double layer (0.077 protein molecules $nm^{-2}$) on $TiO_2$ in an explicit-solvent MD simulation lasting 300 ns. (f) and (g) are schemes showing the protein positions in the double layers corresponding to (d) and (e).

To confirm that the attractive interactions may in fact lead to adsorption beyond one monolayer, a Molecular Dynamics simulation in explicit water solvent was performed starting from a double-layer configuration with randomly oriented proteins (Figure 10.12d,f). After 300 ns of simulation, we observe two mayor trends: first, on both surfaces the proteins collectively move closer to the surface and form a more compact layer. Second, the individual proteins rotate towards the most-attractive orientation presented in Figure 10.10 (*left*). In some cases, rotation is hindered by close protein-protein contacts which remain stable for the whole simulation time (Figure 10.12e,g).

### 10.3.8 Explicit-solvent MD simulations of chymotrypsin adsorption on $TiO_2$ and $SiO_2$

To analyze the atomistic details of the protein approach and adsorption on the two surfaces, we have performed MD simulations in explicit solvent at pH 8 following Hildebrand et al.[166]. In the input structures, the protein is placed at a height of 10 Å in arbitrary orientations (Figure 10.13). During the simulations, the protein spontaneously adsorb on the surface after about 5 ns and find a stable adsorption configuration, undergoing a rotation towards the most favorable orientation predicted by the implicit-solvent calculations (cf. Figure 10.13a,b with Figure 10.10). The simulations are stopped after 50 ns.

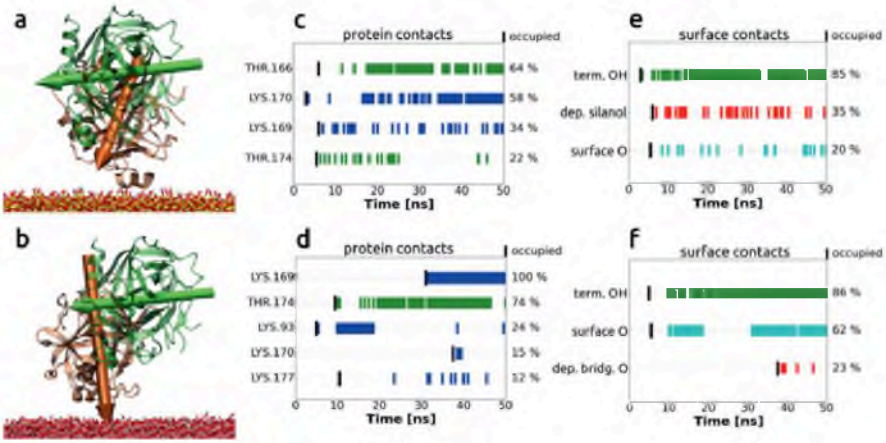


Figure 10.13 (a,b) Initial (green arrow) and final (orange arrow) chymotrypsin orientations upon adsorption on (a) $SiO_2$ and (b) $TiO_2$ obtained in MD simulations in explicit water solvent. (c-d) Contact analysis of the protein residues for $SiO_2$ (c) and $TiO_2$ (d). The color code represents positively charged amino acids (blue) and polar amino acids (green). (e,f) Contact analysis for the surface residues of (e) $SiO_2$ and (f) $TiO_2$. The percentages reported at the right side of each subfigure indicate the occupancies over time after the first contact (marked with a bold black bar). Groups forming contacts for less than 10 % of the time are not shown.

The evolution of the protein-surface contacts during the simulation is shown in Figure 10.13c-f. Here, a protein-surface contact is defined if the distance between one atom of the surface and one atom of the protein becomes less that 2.4 Å. For both surfaces, the most frequent binding motifs of the protein are the positively charged amino acid lysine as well

as the polar amino acid threonine (Figure 10.13c-d). The most common surface sites involved in the contacts are terminal OH groups both on $SiO_2$ and $TiO_2$. Deprotonated silanol groups play a very important role on $SiO_2$, whereas deprotonated O sites on $TiO_2$ are much less frequently involved. Neutral O sites are also present in the analysis, in larger proportion on $TiO_2$ than on $SiO_2$ (Figure 10.13e-f). These differences could have their origin in the larger density of negatively charged surface groups present on silica, and are likely to influence the protein adsorption modes.

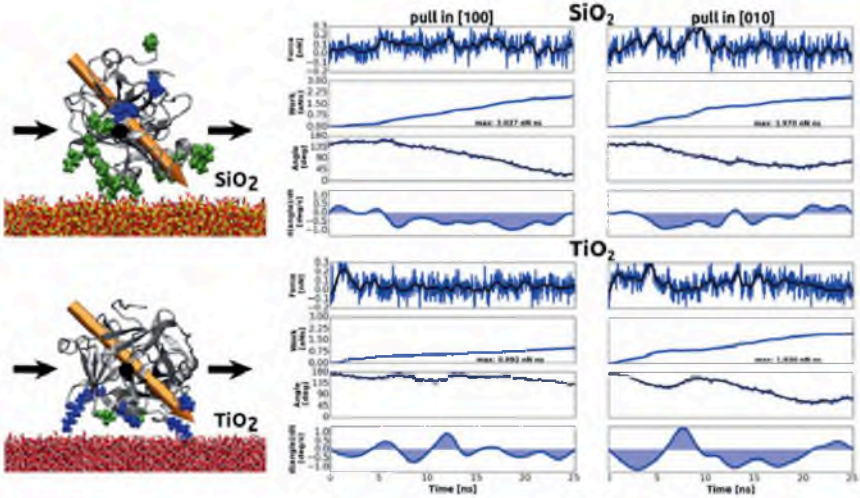


Figure 10.14 (*Left*) Initial configurations of steered MD simulations of chymotrypsin pulled over the $SiO_2$ and $TiO_2$ surfaces. (*Right*) Time evolutions along the corresponding trajectories of the constrained force, the cumulative work, the angle of the dipole moment to the surface normal and its time derivative (from top to bottom in each panel) for $SiO_2$ (top) and $TiO_2$ (bottom). The protein is pulled in each case along the <100> and <010> directions of the simulation box.

Differences in the adsorption behavior of the two proteins may also be related to their mobility after adsorption. To investigate this issue, we performed steered MD simulations in explicit solvent, in which the previously adsorbed protein is pulled parallel to the surfaces by means of a harmonic constraint applied to its center of mass (Figure 10.14). The pulling velocity is 0.5 m/s and the constraint force-constant is 1000 kJ $mol^{-1}$ $nm^{-2}$. Two perpendicular pulling directions were chosen to alleviate direction-dependent effects, namely the <100> and <010> directions of

the simulation box, We stress that in these simulations the proteins are free to roll and/ or slide over the surface, and even to desorb, since no constraint over the position, but only the velocity, of their centers of mass is applied.

The protein/ surface contacts formed during these simulations (see Figure 10.15) correspond to a large extent to those reported in Figure 10.13, with the exception that on $SiO_2$ more amino acid types (including hydrophobic ones) are involved in surface binding. More interesting, however, is the analysis of the rolling/ sliding behavior of the protein over the two surfaces, as reported in Figure 10.14.

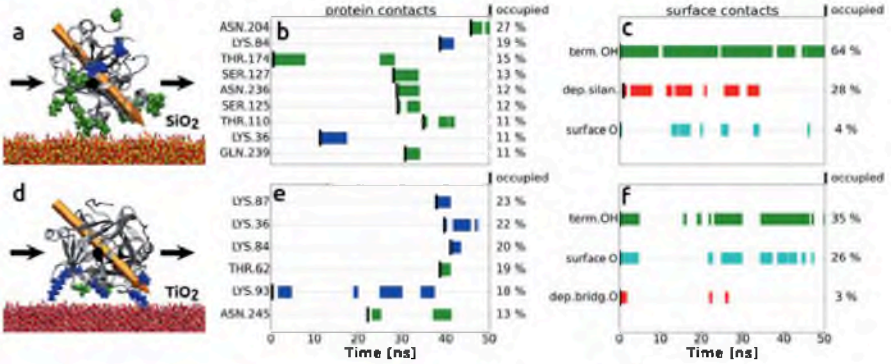


Figure 10.15 *(left)* Initial position of chymotrypsin pulled with its center of mass along the <100> and <010> directions of the simulation box over the silica (a) and the titania (b) surfaces. *(middle)* contact analysis of the protein residues for (b) $SiO_2$ and (e) $TiO_2$. *(right)* contact analysis for the surface residues of $SiO_2$ (e) and $TiO_2$ (f); The percentages reported at the right edge of each subfigure indicate the occupancy over the time after the first contact is formed. This is marked with a bold black bar. All groups forming a contact for less than 3 % of the time after the first contact are not shown.

The force required to pulling the whole protein over the surface and the associated cumulative work are slightly larger for the $SiO_2$ surface. Especially in one simulation (pulling along <100> on $TiO_2$), the smaller force and work result from temporary desorption of the protein between 5 and 15 ns. A striking difference lies in the fact that the protein tends to roll over $SiO_2$, while it tends to slide over $TiO_2$. This is visible from the evolution of the angle between the molecular dipole moment and the

direction normal to the surface and especially from its time derivative, as shown in Figure 10.14. For $SiO_2$, the angle varies more continuously towards smaller and smaller values, and the angle derivative is most of the time negative, indicating progressive rolling. This is noteworthy if one takes into account that rotation of the dipole is associated with a considerable amount increase of potential energy (see Figure 10.12a-b). For $TiO_2$ the derivative of the angle tends to oscillate around zero, indicative of predominant sliding.

Further differences in the adsorption mode of chymotrypsin on the $SiO_2$ and $TiO_2$ surfaces are highlighted through the calculation of the radial distribution function (RDF) between selected pairs of all atoms of the surface, the water solvent and the protein (Figure 10.16). Water molecules are known to form shell-like structures around hydrophilic surface terminal groups[166]. The RDF of water around all surface atoms shows a less distinct structuring on $SiO_2$ (Figure 10.16 *top left*) compared to the very evident structuring in two hydration layers on $TiO_2$ (Figure 10.16 *top right*).

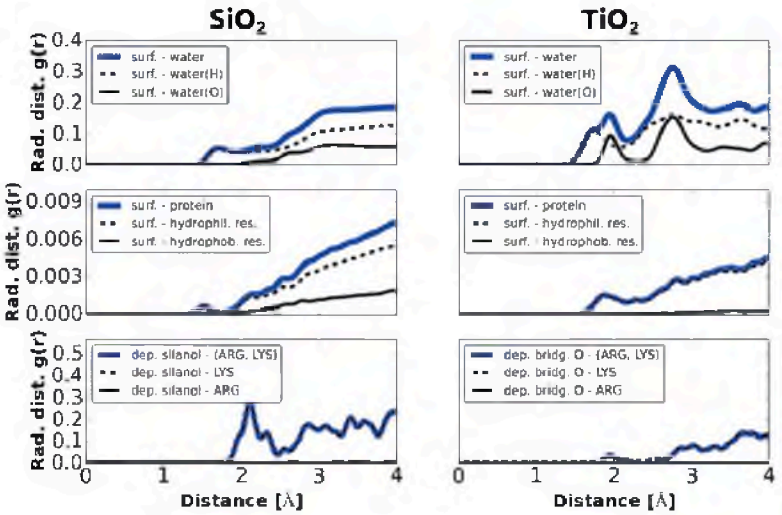


Figure 10.16 Radial distribution function (RDF) of selected pairs of atoms for chymotrypsin adsorbed and pulled over SiO2 *(left)* and TiO2 (*right*). (*Top*) surface-water RDF. (*Middle*) surface-protein RDF, separating the contributions of hydrophilic and hydrophobic residues. (*bottom*) RDF between positively charged amino acids with negatively charged surface sites.

As far as the protein is concerned, the RDF shows that hydrophobic residues are in close contact (within the first 4 Å) to the surface in the case of silica, whereas only hydrophilic residues are in direct contact with titania. Interesting is the small peak of the $SiO_2$ protein-surface RDF at about 1.5 Å, i.e. before the first peak of the water-surface RDF (at 1.8 Å), indicating that some protein residues are able to deeply penetrate the first hydration layer and very tightly bind to surface sites. As already shown by the temporary evolution of the contacts (Figure 10.13), the positively charged lysine and arginine residues are abundantly present close to deprotonated silanol groups on $SiO_2$, and present only to a minor extent around deprotonated bridging oxygen on $TiO_2$.

## 10.4 Discussion and conclusions

Motivated by the need to optimize the conditions leading to maximum adsorption of chymotrypsin on colloidal ceramic supports, we have performed a comparative study of the adsorption features of the protein on highly pure $SiO_2$ and $TiO_2$ colloidal particles combining adsorption experiments with all-atom MD simulations. The analysis has revealed some common features, such as the same preferred adsorption orientation on the two materials at neutral and basic pH driven by interaction of the negatively charged surfaces with the strong protein dipole moment (Figure 10.10). Moreover, a nearly equal free energy of adsorption in the low-concentration limits (about -35 kJ/mol) was estimated by the Langmuir adsorption isotherm analysis (Figure 10.9). However, a number of differences have been also identified, which we believe to be responsible for the experimentally observed larger amount of adsorbed proteins found on $TiO_2$ than on $SiO_2$ (Figure 10.8 and Figure 10.9).

Anchoring to the $SiO_2$ surface (IEP ~ 2.7) takes place mostly via positively charged amino acids that interact with both neutral and deprotonated silanol groups. However, also other neutral polar and even hydrophobic residues contribute to frequent and tight surface-protein contacts (see Figure 10.13 and Figure 10.16, and [166]). Anchoring to the $TiO_2$ surface (IEP ~ 6.6), which presents a smaller density of deprotonated sites at the pH values relevant to adsorption (7.4 and 8.0), is rather dominated by neutral terminal OH and bridging O sites, although involving almost

exclusively positively charged amino acids. We believe that the distinct structuring of the surface hydration layers in which the amino acids are embedded (see Figure 10.16) effectively compensates for the absence of direct ionic interactions between protein and surface, so that, overall, the free energy of binding to either surface is nearly the same. Different, however, is the ability of the protein to diffuse over the surface once tightly adsorbed. Our steered MD simulations (Figure 10.14) reveal that chymotrypsin can easily slide over the $TiO_2$ surface, and even temporarily desorb and adsorb again at a farther site. On the contrary, no temporary desorption is observed from the $SiO_2$ surface, also consistently with the larger attraction forces predicted by our static calculations (Figure 10.10). In this case, rupture of the tight surface-protein contacts only takes place if new contacts are concomitantly formed, resulting in a predominant rolling behavior. A change of the dipole orientation due to rolling, in turn, is associated with a considerable energy loss (see Figure 10.11 and Figure 10.12a-b), so that diffusion over the $SiO_2$ surface is expected to be more hindered than diffusion over the $TiO_2$ surface.

Considering these arguments, it is possible to rationalize both why a larger maximum adsorption amount is reached on $TiO_2$ (Figure 10.8 and Figure 10.9) and why reaching the maximum adsorption amount is slower on $SiO_2$ (Figure 10.8), so that adsorption equilibrium is obtained only after 20 h of incubation. While our simulations clearly show that at least a double monolayer is energetically stable on either surface (Figure 10.11), its actual formation relies on diffusion of pre-adsorbed proteins to accommodate new ones from the solution. This process is probably easier on $TiO_2$ because of the observed more favorable diffusion mobility.

A crucial point to consider in the analysis of the protein adsorption amount is the normalization with respect to the available surface area of the particles. Traditionally, the particle surface area is measured by means of $N_2$ adsorption at low temperature and fitting of the data with the BET adsorption isotherm[33, 36, 106, 242]. The so-obtained $SAA_{BET}$ therefore represents an $N_2$-accessible surface, which includes the cavity walls of micropores (with diameters of the order of 2 nm or smaller) possibly present on the particle surfaces. Such pores are not accessible by chymotrypsin, which has a diameter of about 5 nm (Figure 10.1). Notably, reports about the presence of microporosity in Stöber silica are not uncommon[237, 238]. Because of this reason we have also normalized the experimental data with respect to a here-defined Protein Accessible Area,

estimated from a geometrical analysis of the particles imaged by SEM ($PAA_{SEM}$). In doing this, the difference in the maximum protein amount adsorbed on $TiO_2$ and $SiO_2$ is reduced from a factor of 3 to a factor of 1.5. This is more consistent with the rather subtle differences in the adsorption behavior observed in the MD simulations. Moreover, only after $PAA_{SEM}$ normalization do the data suggest formation of a double protein monolayer also on $SiO_2$. Instead, the $SSA_{BET}$ normalization would predict formation of barely a single monolayer (Figure 10.8), in striking contrast with the driving force for double monolayer formation emerging from all simulations.

The presence of micropores in the employed $SiO_2$ particles would easily explain the much larger amount of adsorbed water with respect to $TiO_2$ (Figure 10.4), and also the hysteresis observed in the water adsorption/ desorption curves, which could be caused by trapping of water molecules within the micropores due to steric and capillary effects. Notably, the adsorption isotherm of heptane (a larger molecule that probably does not enter into the smaller micropores) reveals slightly reduced adsorption on $SiO_2$ with respect to $TiO_2$ and no appreciable hysteresis.

We finally note that a precise determination of the surface area accessible to protein adsorption is also complicated by the tendency of the particles to form agglomerates, especially in the case of $TiO_2$, which is less charged at neutral pH and presents a larger Hamaker constant than $SiO_2$. Agglomeration also prevents the use of DLS radii to estimate the actual size (and thus the surface area) of the particles. Therefore, a careful pretreatment with ultrasound is absolutely necessary prior to each incubation and adsorption study, and the possibility of re-agglomeration needs to be taken into account when performing experiments with long incubation times.

Future studies shall focus on the conformational changes that the protein may undergo after adsorption, and may severely influence its enzymatic activity[105, 134]. Also in this case, a combination of experimental studies (e.g. by means of circular dichroism spectroscopy) and molecular dynamics simulations would be desirable in order to achieve a comprehensive description of the protein's behavior at the atomic scale.

## 10.5 Acknowledgments

We thank Katharina Richter and Klaus Rischka (Fraunhofer Institute for Manufacturing Technology and Advanced Materials (IFAM) in Bremen) for technical support with the MALDI-ToF-MS experiments. This work was funded by the Deutsche Forschungsgemeinschaft under grants KO3811|3-1, CI144/2 (Emmy Noether Program), and by APF program „Keramische Grenzflächentechnologie". Computational resources were provided by the North-German Supercomputing-Alliance system (HLRN).

## 10.6 Appendix: Circular dichroism studies

Possible structural changes of free chymotrypsin after contact with colloidal particles via CD spectroscopy measurements were monitored. Incubations with chymotrypsin solutions (start concentrations of chymotrypsin incubation: 0.13, 0.39 and 0.44 mg $mL^{-1}$) were carried out as described in Chapter 10.2.5. After 20 h at pH 8, the collected supernatants and chymotrypsin reference solutions without colloidal particles were used for CD measurements using Chirascan™ Spectrometer (Applied Photophysics Ltd, UK) equipped with a temperature control to determine possible structural changes. Quartz cuvettes with path length of 0.01, 0.5 and 0.1 cm were used (Hellma® Analytics, Germany). $ddH_2O$ blanks with adjusted pH and conductivity as previously described were used to set the baseline. Far-UV spectra were collected between 185 and 240 nm in 0.5 nm intervals, using a 1 nm bandwidth and 0.5 s time per point. All measurements were performed at room temperature at 25 °C. The raw CD signal, $\theta$, was converted to mean residue ellipticity using the equation $\theta_{MRW} = \theta / (10 C_r l)$, where $C_r$ represents concentration (units = M * residue number) and $l$ is the cuvette path length[243]. The same supernatants were also used to obtain the chymotrypsin concentration and the enzymatic activity as previously described.

Several studies discuss surface induced structural changes of protein molecules being adsorbed on particles and solid surfaces[106, 184, 185, 244-248]. The effect on the activity due to structural changes cannot be addressed here, but the stability of chymotrypsin under experimental conditions work out in this study should be examined. In experiments, circular dichroism spectra can offer possible structural perturbation caused by colloidal

particles. The CD experiments are carried out using the same experimental conditions as for the concentration-dependent activity experiments. Chymotrypsin concentrations of 0.13, 0.39 and 0.44 mg $mL^{-1}$ have been used to measure the CD spectra.

In the interest of showing the largest possible difference or not, measurements are performed after 20 h incubation at pH 8 at the three protein concentrations. For the analysis of CD experiments the changes of mean residue ellipticity are investigated[137]. The differences between the chymotrypsin reference without colloidal particles at start and after 20 h are negligible for all initial concentrations (Figure 10.17) and it could be assumed that no structural changes occurs during 20 h incubation at pH 8 without any colloidal particles. Two negative bands approximately 202 nm and 228 nm, and a positive band approximately 190 nm are observed, which indicates the α-helix and the β-sheet content and confirms a well-known structure of native folded chymotrypsin[115]. The low helix content of chymotrypsin is also determined from studies in the crystal[249]. Additionally, a histidine residue may also contribute to the band approximately 228 nm[250].

After incubation with the particles, several changes in the mean residue ellipticity are measured for chymotrypsin on both particle species. The positive band completely disappears for the samples with $SiO_2$ and $TiO_2$ for all protein concentrations. For the range between 215 and 240 nm the curve approximates the zero line for both materials at all investigated chymotrypsin start concentrations. Normally, there is also a very low ellipticity above 210 nm, which is not the case here. The curve shape is typical for disordered proteins with a negative band near 195 nm[115]. However, the complete absence of the two negative bands approximately 202 and 228 nm, and the positive band approximately 190 nm, as shown for the reference samples, are distinct evidences for significant structural changes and indeed further careful analysis addressing conformational changes and their effect on the activity of adsorbed chymotrypsin are necessary in future works.

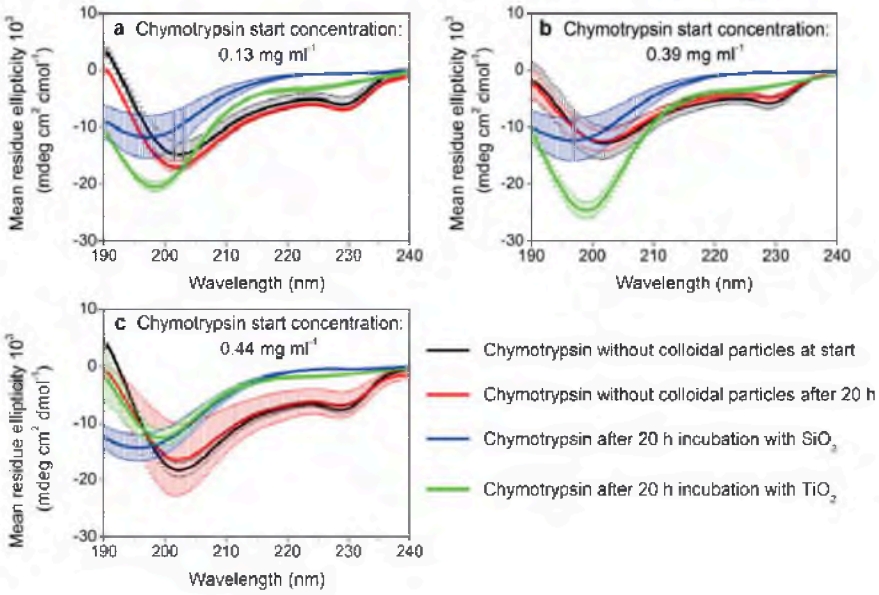


Figure 10.17 Mean residue ellipticity of chymotrypsin at chymotrypsin start concentration of 0.13 mg $mL^{-1}$ (a), 0.39 mg $mL^{-1}$ (b), and 0.44 mg $mL^{-1}$ (c). Chymotrypsin solutions at indicated start concentrations were incubated without or with 0.9 vol % of $SiO_2$ and $TiO_2$ particle suspensions at pH 8 for 20 h. After centrifugation, the supernatant was used to determine the concentration of chymotrypsin and to measure a row CD spectroscopy signal. Using these data the mean residue ellipticity of chymotrypsin was calculated. The data shown represent means ± SD of values obtained in 3 independent experiments.

For the technical use of biofunctionalized particles as carrier systems for biological devices, not only the highest possible amount but the presence of active enzymes is the ultimate goal. In this chapter, no analysis of the activity of the adsorbed enzyme is presented but the structural stability of the protein under the suggested optimal experimental conditions was investigated by CD measurements. Unfortunately, significant changes in the CD spectra indicate changes in the activity of chymotrypsin. In the preferred orientation of the protein, identified by simulations, the two helix motifs in chymotrypsin were always facing the surfaces. The loss of the band in the range between 215 and 240 nm in the measurements performed in this work matches very well with the observing from Zoungrana et al.[106] found a loss of the band at 222 nm and could indicate the loss of the helical structures. These changes in the secondary

structure were marked for only slightly changes in the enzymes activity[106] and would not exclude the system from professional use. In addition, the shift to negative values at 195 nm indicates a loss of the defined secondary structure motifs at all. The CD measurements have been performed at protein concentrations of up to 0.44 mg $ml^{-1}$ being four times smaller than the evaluated saturation concentration of 2 mg $mL^{-1}$. Zoungrana et al.[106] and Norde et al.[36] stated a conformational stability to be higher with higher surface coverage. Further elaborating CD and activity measurements at saturation concentration conditions would be necessary to really satisfy this question. Nevertheless, smaller sized particles are needed to directly measure the possible structural changes of adsorbed enzymes via CD measurements as no sedimentation processes are allowed during the CD measurements.

## 10.7 Source

This chapter was adapted from:

Derr L., Hildebrand N., Köppen S., Kunze S., Treccani L., Dringen R., Rezwan K., and Colombi Ciacchi L.,; Physisorption of α-chymotrypsin on $SiO_2$ and $TiO_2$: a comparative study via experiments and molecular dynamics simulations. A Journal of Biomaterials and Biological Interfaces, Biointerphases 11, 011007, 2016 ; License numbers: 3841321115371 & 3841321387875.

The article is mainly based on the work of the first author and author of this thesis Ludmilla Derr. The precise contributions of each single author are listed below. All the used literature references are summarized in Chapter 14.

| Author | Contribution |
|---|---|
| ***Ludmilla Derr*** | Conceptualization of work, planned and performed adsorption and enzymatic activity experiments, carried out the preliminary investigations via circular dichroism measurements, performed characterization analysis on all samples, interpreted and discussed data, wrote manuscript |
| Nils Hildebrand | Performed and supervised the simulations and analysis of simulations, and helped in manuscript evaluation |
| Susan Köppen | Gave conceptual advices, discussed data, edited manuscript |
| Simon Kunze | Performed simulations (bachelor thesis, HMI Group, University of Bremen, Germany) |
| Laura Treccani | Gave conceptual advices, discussed data, edited manuscript |
| Ralf Dringen | Gave conceptual advices, discussed data, edited manuscript |
| Kurosch Rezwan | Gave conceptual advices, discussed data, edited manuscript |
| Lucio Colombi Ciacchi | Coordinated the work, contributed to plan the simulations and interpret all results, co-wrote the manuscript |

# 11 Assessment of the proteolytic activity of α-chymotrypsin immobilized on colloidal particles by matrix-assisted laser desorption ionization time-of-flight mass spectroscopy

*ABSTRACT: The immobilization of enzymes onto solid materials is a promising strategy in biotechnological applications and proteomics. It can improve the enzymes' stability, and enables a more convenient handling, easy separation from the reaction solution and cyclic reuse of the enzymes. In order to investigate the proteolytic properties of a particle-bound protease, chymotrypsin was covalently immobilized onto $SiO_2$ and $Al_2O_3$ colloidal particles. The enzymatic activity of the bound chymotrypsin at different times, in consecutive proteolytic cycles and after storage up to several weeks was investigated by MALDI-ToF MS. In this way, the proteolysis products could be identified without using artificial protease substrates or intermediate chemicals. Lysozyme was used as model protein to perform enzymatic digestion using immobilized chymotrypsin and the peptides generated from the proteolytic digestion were determined. Compared to the activity of chymotrypsin applied for the immobilization reactions, more active chymotrypsin was bound to $Al_2O_3$ (between 1 and 10 % of the initial concentration) than to $SiO_2$ (below 1 %) colloidal particles. Compared to an excess of unbound chymotrypsin, the digestion of lysozyme was slower with chymotrypsin immobilized on colloidal particles and only 60 % of the maximal amounts of lysozyme peptides were detected. The proteolytic activity of chymotrypsin immobilized on colloidal particles was maintained during storage at room temperature for up to at least seven weeks, while it was lowered during consecutive digestions.*

## 11.1 Introduction

Due to their catalytic properties and high selectivity enzymes have been used since many years in numerous biotechnological applications and for a variety of chemical reactions, especially requiring mild processing conditions[251-254]. As the employment of free enzymes is often hampered by difficult recovery, lack of long-term stability and cyclic reusability, enzyme immobilization onto solid supports is considered a promising

strategy to overcome these main drawbacks[17]. Immobilization of the enzyme onto inorganic supports such as polymers, magnetic nanoparticles or metal oxides[180] enables a more convenient handling of the enzyme, facile product separation, prevention from autolysis or auto-digestion and may be beneficial to maintain or increase enzyme stability under both operation and storage conditions[255]. All these aspects have made enzyme immobilization particularly attractive for downstream processes or proteomic analysis[256, 257]. In several studies, three main factors influencing the performance of immobilized enzymes have been identified: 1) the properties of the enzyme, 2) the immobilization method employed and 3) the properties of the support material[7, 16-18].

For example, phosphorylated pepsin immobilized on alumina nanoparticles showed high thermal stability and retained a very high enzymatic activity, also because of the diffusion of the substrate to the active site was not limited as a consequence of the immobilization process[178]. Limited substrate diffusion was instead observed for pepsin immobilized inside the pores of microsized porous alumina, causing decreased accessibility for the substrate hemoglobin[178]. In addition, multipoint covalent attachment of chymotrypsin by linking its amino groups to agarose-aldehyde gels caused a 60,000-fold increase in enzyme availability, associated with a loss in enzymatic activity of only 35 %[181]. A strong reduction of the autolytic cleavage of chymotrypsin has been recently observed when the enzyme was immobilized onto magnetic bead cellulose[182].

Despite the significant attention paid to the development of enzyme immobilization strategies on various supports, a major challenge in this field is the scarce availability of reliable methods enabling a direct characterization of enzyme activity and overall enzymatic performance at different operation and storage conditions[258-261].

In this study we investigate at a semi-quantitative level the enzymatic catalytic activity of chymotrypsin covalently immobilized on alumina and silica colloidal particles. Apart from being affordable and highly available, these materials feature high chemical and thermal stability and are of particular relevance for many medical and biotechnological applications[2], motivating their use as model substrates. Chymotrypsin is covalently immobilized by amine coupling via reactive esters. This straightforward technique is suitable for covalently linking biomolecules at mild reaction conditions to hydrophilic solid surfaces[2]. The immobilization efficiency, the

enzymatic activity and stability and the potential reusability of immobilized chymotrypsin are investigated at different operation and storage conditions by matrix-assisted laser desorption/ ionization time-of-flight mass spectrometry (MALDI-ToF-MS) after lysozyme digestion. Our approach does not follow specific enzymatic activity protocols[262] and is thus of great advantage as a relatively rapid and feasible tool for proteomic studies and diverse biotechnological applications, at the expenses perhaps of a more precise quantification, which is not in the main focus of the present work.

## 11.2 Materials and methods

### 11.2.1 Materials

The α-alumina colloidal particles (> 99.99 % wt, Taimei, TM-DAR, lot. no. 8086) were purchased from Krahn Chemie GmbH (Germany). Silica colloidal particles (> 99.9 % wt, lot. no. 100618-02) were obtained from Fiber Optic Center (New Bedford, USA). Lyophilized a-chymotrypsin type II from bovine pancreas (94.1 % wt, 65.622 units $mg^{-1}$ protein, lot. no. 60M7007V), lysozyme (> 90 % wt, > 40000 units $mg^{-1}$ protein, lot. no. SLBG8654V), (3-aminopropyl)triethoxysilane (98 % wt, lot. no. BCBH2173V), N-hydroxysuccinimide (97 %, lot. no. BCBB3130), and a-cyano-4-hydroxycinnamic acid (98%, lot. no. 81K3720) were obtained from Sigma-Aldrich (Germany). The 1-Ethyl-3-(3-dimetylaminopropyl)-carbodiimide (lot. no. ML164683) was purchased from Thermo Fisher Scientific Inc. (Germany). Ammonium bicarbonate buffer (lot. no. 171166396) was obtained from Carl Roth (Germany). Dithiothreitol (lot. no. L1610611) and iodoacetamide (lot. no. 398265A) were purchased from Bio-Rad (Germany) and GE Healthcare (Germany), respectively. All other chemicals were obtained from Fluka (Switzerland) or Merck (Germany) at analytical grade. For all solutions, double deionized water ($ddH_2O$) with a conductivity of 0.04 μS $cm^{-1}$ produced by a Synergy system (Synergy, Millipore GmbH, Germany) was used.

### 11.2.2 Characterization of alumina and silica colloidal particles

In order to remove any organic residues, alumina and silica colloidal particles were calcinated at 400 °C for 4 h with a heating and cooling rate of 3 °C $min^{-1}$ (oven L3/11/S27, Nabertherm GmbH, Germany). The particle size was determined by dynamic light scattering (DLS, Microtrac UPA150, Grimm Labortechnik, Germany) and the specific surface area was measured by nitrogen volumetric adsorption using a BELsorp-mini II device (BEL Japan, Japan). The ζ-potential measurements were performed in 1 vol % aqueous suspensions of alumina or silica colloidal particles using the electroacoustic colloidal vibration current technique (Acoustic & Electroacoustic Spectrometer DT-1200, Dispersion Technology, USA) as described previously[118]. Alumina or silica colloidal particles suspensions were titrated using 1 M KOH or 1 M HCl to measure the ζ-potential as a function of pH and to determine the IEP. The quantity of hydroxyl groups present on the surface of the colloidal particles was determined by titrations according to Hidber using a titrator (TIM840, HACH LANGE GmbH, Germany)[158, 159]. Particle size, specific surface area, isoelectric point and charge exchange capacity of alumina and silica colloidal particles before immobilization are given in Table 11.1. Comprehensive particle characterization using SEM and TEM techniques has been performed in previous work from our group[158, 263].

Table 11.1 Properties of alumina and silica colloidal particles[a]

| Property | Silica colloidal particles | | | Alumina colloidal particles | | | n |
|---|---|---|---|---|---|---|---|
| Particle size (nm) | 160 | ± | 1 | 159 | ± | 7 | 3 |
| Specific surface area ($m^2/g$) | 34.0 | ± | 0.3 | 12.8 | ± | 0.1 | 3 |
| Isoelectric point (IEP) | 2.74 | ± | 0.14 | 9.87 | ± | 0.05 | 5 |
| Exchange capacity ($OH/nm^2$) | 4.9 | ± | 0.2 | 2.8 | ± | 0.2 | 3 |

[a] The data represent means ± SD of values that were obtained in n experiments.

### 11.2.3 Chymotrypsin immobilization on alumina and silica colloidal particles

Aqueous suspensions of alumina and silica colloidal particles were prepared by mixing 15 g of particles with 50 ml of $ddH_2O$, sterilized by autoclaving for 15 min at 121 °C and 2.05 bar (Systec 2540ELV, Systec, Germany) and afterward ultrasonicated for 10 min using an ultrasound sonotrode Sonifier® 450 (output 150 W, pulse rate 0.5 s, Branson, USA) to break down particle agglomerates prior to precursor addition. Precursor solutions were prepared by mixing (3-aminopropyl)triethoxysilane with 50 ml of $ddH_2O$ to a final concentration of 0.1 M (corresponding to a surface coverage of 26 µmol $m^{-2}$ silane molecules normalized to the specific surface area of the unmodified alumina colloidal particles which is 12.8 $m^2$ $g^{-1}$ from our measurements. At this precursor concentration, a maximal shift of the particle IEP and formation of 3.4 amino groups per $nm^2$ for alumina colloidal particles is obtained as shown in our previous publication[158].

Taking into account the specific surface area of silica colloidal particles (Table 11.1), (3-aminopropyl)triethoxysilane was added to a final amount of 0.3 M to generate an equal amount of amino groups on the silica surface. The precursor solutions were then added to the particle suspensions and stirred for 2 h at room temperature. Afterward, alumina and silica colloidal particles were centrifuged for 30 min at 1500 g (Heraeus Megafuge 16, Fisher Scientific, Germany). The supernatant was discarded and the particles resuspended in 100 mL of $ddH_2O$. This washing procedure was repeated three times to remove any excess of precursors. The particles were subsequently dried at 70 °C for 24 h by using a compartment dryer (UT6120, Heraeus Instruments, Germany).

For chymotrypsin immobilization (see Figure 11.1), suspensions of functionalized alumina and silica colloidal particles were prepared considering the different values of specific surface area at the concentrations of 80.40 mg $mL^{-1}$ for alumina and 30.27 mg $mL^{-1}$ for silica, which correspond to 2 vol% and 1.2 vol%, respectively and sonicated prior to chymotrypsin addition. 310 µL chymotrypsin solution (2.68 mg $mL^{-1}$) were mixed with 200 µL freshly prepared 1-ethyl-3-(3-dimetylaminopropyl)carbodiimide solution using $ddH_2O$ (10 mg $mL^{-1}$). 500 µl of α-alumina or silica suspension were added to this mixture and mixed.

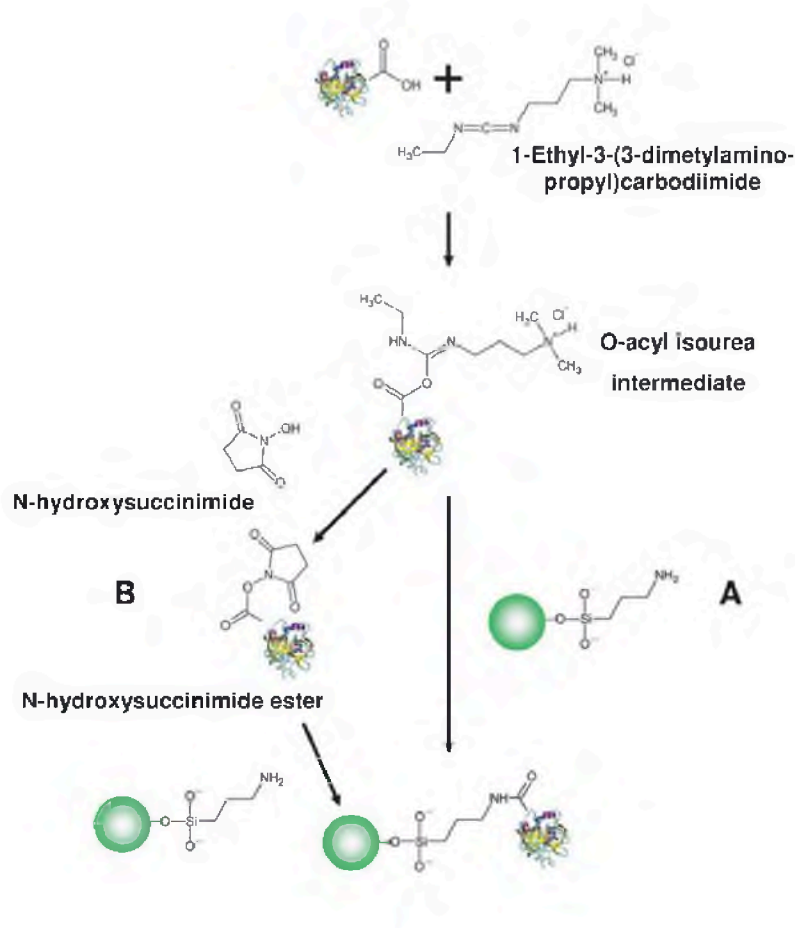


Figure 11.1 Detailed mechanism of colloidal particle functionalization with chymotrypsin via linking with 1-ethyl-3-(3-dimetylaminopropyl)carbodiimide and N-hydroxysuccinimide. The activation of 1-ethyl-3-(3-dimetylaminopropyl)carbodiimide results in an O-acyl-isourea intermediate, which can bind to the previously amino-functionalized particles (route A), but is prone to hydrolysis. The addition of N-hydroxysuccinimide leads to the fast formation of a N-hydroxysuccinimide ester and subsequent stable reaction with amino-functionalized colloidal particles (route B).

Afterward, 100 µl N-hydroxysuccinimide solution in $ddH_2O$ (3 mg $mL^{-1}$) were added to the colloidal particles suspensions, stirred for 2 h at room temperature. Colloidal particles with immobilized chymotrypsin were centrifuged for 20 min at 21100 g (Heraeus Fresco 21 centrifuge, Fisher

Scientific, Germany). The supernatant was discarded and the particles were resuspended in 1 mL of $ddH_2O$. This washing procedure was repeated three times to remove any possible by-products.

### 11.2.4 Proteolysis test by MALDI-ToF-MS measurements

Lysozyme was used as a substrate and digested by immobilized chymotrypsin over night at 37 °C in 400 mM ammonium bicarbonate buffer (pH 8), at a theoretical chymotrypsin/ lysozyme (wt/ wt) ratio of 1/13 using 10 µL of chymotrypsin immobilized on colloidal particles assuming that 100 % of used chymotrypsin had been immobilized. During incubation, all samples were shaken at 1400 rpm at a shaker (Thermomixer Comfort, Eppendorf GmbH, Germany) to avoid sedimentation of the colloidal particles and to assure continuous mixing of substrate and enzyme. Before digestion, lysozyme was reduced with 45 mM dithiothreitol at 50 °C for 15 min and then alkylated with 100 mM iodoacetamide at room temperature for 15 min to improve accessibility of the lysozyme cleavage sites[264]. The digestion was stopped by freezing the solution with liquid nitrogen for 30 seconds. As positive controls for chymotrypsin immobilized on colloidal particles, in-solution-digests of lysozyme with unbound chymotrypsin were performed, while unmodified colloidal particles and lysozyme were used as negative controls.

Samples from the digestion were taken at different times (5 minutes, 1 h, 2 h, 3.5 h, 5 h, 22 h, 23 h, 24 h, 25.5 h and 27 h) to probe the time dependency of the proteolytic process. To test the reusability of chymotrypsin immobilized on colloidal particles, samples for MALDI analysis were taken after 24 h, 48 h and 72 h. After each 24 h time interval, the digests were centrifuged for 5 min at 21,000 g, the supernatant was removed, and the pellets were washed three times with ammonium bicarbonate buffer to remove any weakly bound peptides. The pellets were finally dispersed in a freshly prepared lysozyme solution for the next digestion period of 24 h. As a control, fresh samples with chymotrypsin immobilized on colloidal particles were stored at room temperature for 24 h, 48 h and 72 h before starting the digestion assay. For long-term stability experiments, samples with chymotrypsin immobilized on colloidal particles were stored for 7 weeks at room temperature and subsequently used for digestion as described above.

In order to obtain the activity equivalence of chymotrypsin immobilized on colloidal particles, a 0.75 mg $mL^{-1}$ chymotrypsin stock solution was prepared and diluted to be used in concentrations of 100 %, 10 %, 1 %, 0.8 %, 0.4 %, 0.2 %, 0.1 %, 0.01 %, 0.001 % and 0.0001 % for digests of lysozyme.

The MALDI-ToF-MS analysis of peptides derived from proteolytic cleavage by chymotrypsin was performed on a Voyager-DETM PRO Biospectrometry Workstation from Applied Biosystems controlled by the Voyager Control Panel Software (USA). Before all MALDI-ToF-MS measurements an external calibration was performed using the calibration mix II from the peptide mass standard kit (AB SCIEX). The preparation of the calibration samples was performed as described in the manufacturer's protocol. All measurements were carried out on polished steel targets coated with a α-cyano-4-hydroxycinnamic acid thin-film matrix. The latter was freshly prepared with a saturated α-cyano-4-hydroxycinnamic acid solution in 100 % acetone, which was allowed to dry before starting the MALDI experiments.

### 11.2.5 Data analysis

The MALDI spectra were analyzed concerning the peak positions (m/z values) and the peak areas of individual peptides after the digestion of lysozyme. Measurements were repeated five times to achieve statistically relevant results. The standard deviations are reported as error bars in the figures. The peptides were identified by comparing the experimental peak data with in-silico-digests data using the FindPept tool from ExPASy Bioinformatics Resource Portal (Swiss Institute of Bioinformatics) with a tolerance of 0.8 Da. The lysozyme sequence from *Gallus gallus* was used as the input for the in-silico-digest analysis (Accession code AAA48943, NCBI, 147 amino acids). The experimental peak areas were analyzed with the Data Explorer 4.0 software from Applied Biosystems after performing an automated baseline correction of the spectra.

The kinetic data were fitted using the PRISM software (v. 5.01, GraphPad Software Inc., USA) with the equation (11.1)

$$Y = Y_0 + (Y_{max} - Y_0) * (1 - e^{-K*t}) \quad (11.1)$$

where Y is the MALDI peak area of a selected peptide and t is the time. $Y_0$ is the Y value when time is zero and $Y_{max}$ are the fitted values of peak area plateaus for t = ∞. K represents a rate constant considering the velocity of enzyme-substrate interaction. The faster the reaction the higher is the constant determined by the software.

## 11.3 Results

Due to their use in many biotechnological applications, alumina and silica colloidal particles with a comparable size were selected as support materials for chymotrypsin immobilization. Since alumina and silica colloidal particles have comparable particle sizes but different exchange capacities and specific surface areas (Table 11.1), different precursor concentrations were used in order to create the same amino group density on both materials and therefore the same amount of immobilized chymotrypsin molecules. The amount of (3-aminopropyl)triethoxysilane required for obtaining 3.4 amino groups per $nm^2$ was calculated by taking into account the different specific surface area as previously reported[158].

The immobilization of chymotrypsin on the colloidal particles was achieved by amine coupling via reactive esters using the 1-ethyl-3-(3-dimetylaminopropyl)carbodiimide/ N-hydroxysuccinimide method[190], as 1-ethyl-3-(3-dimetylaminopropyl)carbodiimide is water-soluble and it can be directly added to chymotrypsin solutions and colloidal particles aqueous suspensions without using organic solvents (see Figure 11.1). To directly compare the immobilization efficiency for both materials, an identical concentration of chymotrypsin was used for the immobilization to alumina and silica. Successful immobilization was confirmed qualitatively by checking that characteristic peaks relative to amide bonds and alkyl groups were present in FTIR spectra collected for the functionalized colloidal particles (see Figure 11.9 in Chapter 11.7). Nevertheless, it was not possible to determine the amount of the immobilized protein. Due to the presence of 1-ethyl-3-(3-dimetylaminopropyl)carbodiimide, N-hydroxysuccinimide and their by-products, neither conventional protein

quantification[126, 129, 214, 215] nor enzymatic activity assays[40, 132] could be employed to quantify the chymotrypsin remaining in solution after the immobilization step, as these assays were strongly disturbed by the presence of the reactants (data not shown). Therefore, the chymotrypsin activity was directly analyzed by MALDI-ToF-MS by monitoring the generation of proteolytic peptides formed by the digestion of lysozyme by immobilized chymotrypsin.

Proteolytic digests were performed by incubation of chymotrypsin immobilized on colloidal particles with lysozyme and subsequently the supernatant of the solution was investigated for lysozyme-derived peptides with MALDI-ToF-MS (Figure 11.2). When lysozyme was exposed to either chymotrypsin immobilized on alumina or silica colloidal particles, distinct peptide pattern were observed in the MALDI spectra (Figure 11.2a-b). On the contrary, peptide peaks in the same spectral region were not found after incubation of lysozyme with non-functionalized colloidal particles (Figure 11.2c-d). Peptide sequence analysis with the FindPept tool (in-silico-digest) revealed that the peptides identified (Figure 11.2a-b) covered 44 % of the lysozyme sequence. For comparison, a digest of lysozyme with unbound chymotrypsin was performed and an almost identical peptide pattern with a sequence coverage of 40 % was observed (Figure 11.2a, b and e).

Similar protein sequence coverages were recently reported by Xiao *et al.*[265]. Furthermore, Xu *et al.* and Lin et al. reported coverage values ranging from 40-90 % for the used proteins[260, 261]. For further analysis of digestion studies, the lysozyme derived peptides methionylarginyl-serinylleucine (MRSL, 506 Da) and glycylarginylcysteinylglutamylleucine (GRCEL, 634 Da), marked with asterisks in Figure 11.2, were selected as these two peptides were present in all obtained spectra and showed consistently high intensities.

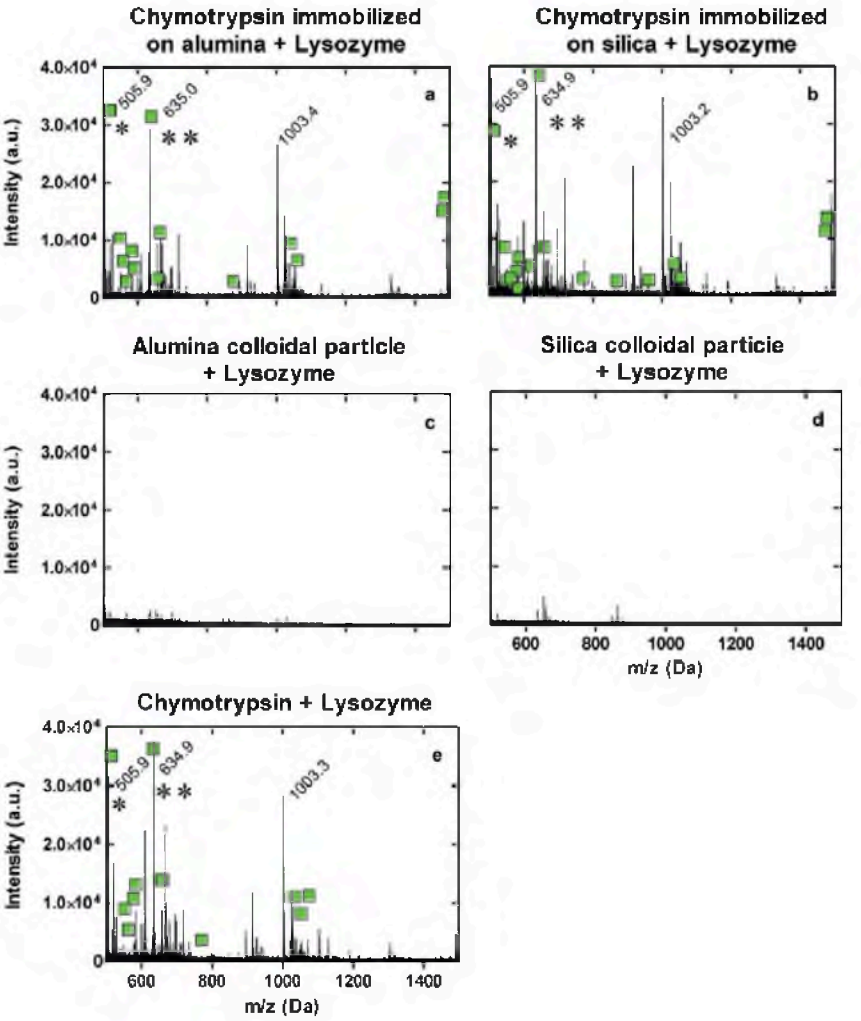


Figure 11.2 a, b: MALDI-ToF-MS spectra of lysozyme digested using chymotrypsin immobilized to alumina and silica colloidal particles. c, d: Spectra collected after the incubation of lysozyme with amino groups-functionalized alumina and silica colloidal particles as negative controls. e: *In-solution-digest* of lysozyme using free chymotrypsin as a positive control. The incubation time for all experiments was 24 h. Green squares indicate peaks which can be identified by database search as lysozyme fragments. The asterisks indicate the peaks associated with the peptides MRSL (505.9 Da) and GRCEL (634.9 Da), used for further analysis. For a better orientation, some of the most intense peaks were labeled with corresponding m/z values.

In order to compare the enzymatic activity of the immobilized chymotrypsin with the activity of the unbound chymotrypsin, a series of in-solution-digests were performed with constant concentration of lysozyme and stepwise decreasing the concentrations of unbound chymotrypsin (Figure 11.3). The 100 % value represents the activity determined for the concentration of chymotrypsin that was initially used for the immobilization procedure, which corresponds to 0.75 µg $mL^{-1}$. Under the assumption that the MALDI peak areas of the lysozyme derived peptides MRSL and GRCEL are proportional to the concentrations of these peptides after digest[265] we used those as a semi-quantitative estimate of the enzymatic activities of the chymotrypsin present in the digest. Indeed, both the MRSL (Figure 11.3a) and GRCEL (Figure 11.3b) peak areas measured after 24 h in-solution digests were lowered with decreasing concentration of unbound chymotrypsin. Comparison of the peak areas determined for the samples with chymotrypsin immobilized on colloidal particles (Figure 11.3, black and white bars for alumina and silica colloidal particles, respectively) with those of in-solution-digests containing different concentrations of chymotrypsin (Figure 11.3, grey bars) revealed that more active chymotrypsin (corresponding to 1 % - 10 % of the initial chymotrypsin concentration used for immobilization) was present on alumina samples than on silica samples (less than 1 %).

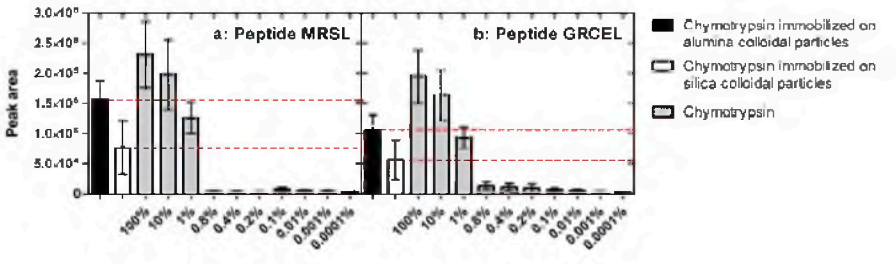


Figure 11.3 MALDI-ToF-MS peak areas of the MRSL and GRCEL peptides obtained after 24 h digestion with immobilized chymotrypsin (black bars for alumina, white bars for silica colloidal particles supports) and with free chymotrypsin in solution (grey bars) at different relative concentration with respect to the initial chymotrypsin concentration used in the immobilization protocol (75 µg $mL^{-1}$).

MALDI-ToF-MS was used further to compare the time-dependence of the lysozyme digestion by unbound and immobilized chymotrypsin. The average peak areas of the peptides GRCEL and MRSL in the spectra of the digests were determined and plotted as a function of the incubation time (Figure 11.4). Comparison of the appearance of the two peptide peaks in the digests containing chymotrypsin immobilized on silica (Figure 11.4a and c), chymotrypsin immobilized on alumina (Figure 11.4b and d) or unbound chymotrypsin (Figure 11.4e) revealed that the peptides were generated more rapidly in the presence of an excess of unbound chymotrypsin. The fast increase in the peak areas in the digests with unbound chymotrypsin reached a plateau within 2.5 h (Figure 11.4e), while the generation of peptides was slower in the digests containing chymotrypsin immobilized on colloidal particles and maximal peptide levels were observed after more than 5 h (Figure 11.4a-d). The data were fitted with an exponential function (see Materials and Methods, equation (11.1)) where the peak areas at t = 0 were constraining to 0 ($Y_0$ value in eq. (11.1)). The fitted values of the maximum peak area $Y_{max}$ and of the characteristic rate constant K are shown in Table 11.2. Interestingly, the maximum peak area of the two peptides generated in digests with unbound chymotrypsin was remarkably smaller than of that determined for digests containing chymotrypsin immobilized on colloidal particles (Table 11.2). The addition of extra chymotrypsin after 23 h caused a further increase of the peak areas for the case of chymotrypsin immobilized on colloidal particles (Figure 11.4a, b) whereas additional lysozyme produced no variation (Figure 11.4c and d). Notably, the addition of lysozyme to unbound chymotrypsin also revealed no changes in the measured peak areas (Figure 11.4e).

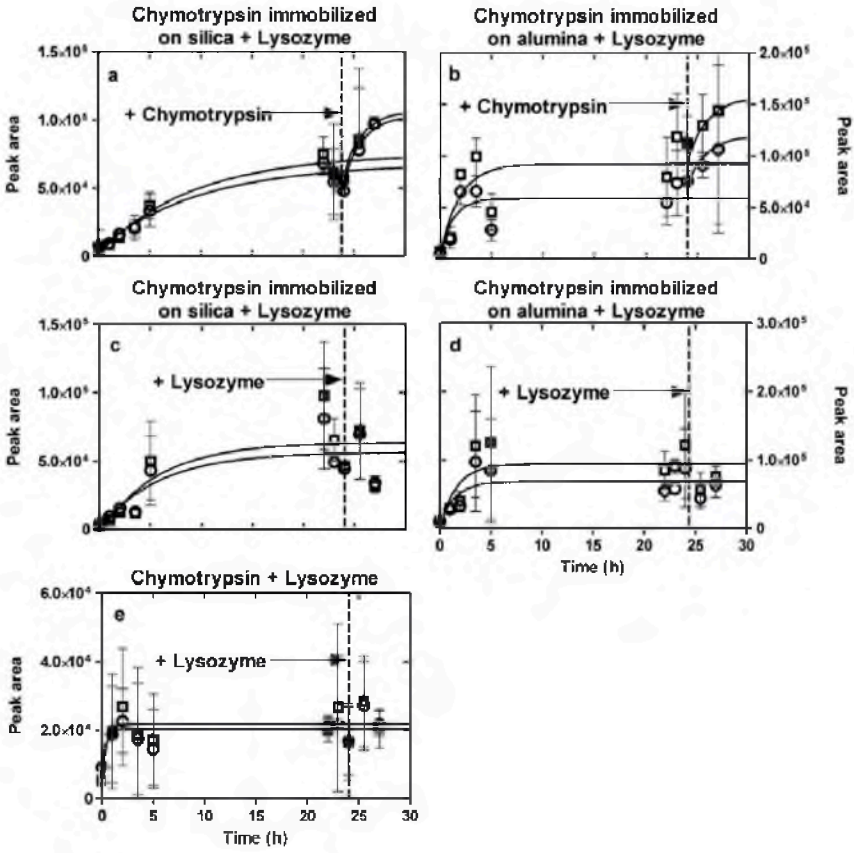


Figure 11.4 Temporal evolution of the MALDI-ToF-MS peak areas of the MRSL (○) and GRCEL (□) peptides obtained during the digestion of lysozyme with: (a, c) chymotrypsin immobilized on silica colloidal particles; (b, d) chymotrypsin immobilized on alumina colloidal particles; and (e) free chymotrypsin in solution. The solid lines are fits to the exponential function defined in equation (11.1), leading to characteristic kinetic parameters reported in Table 11.2. After 23 hours of incubation, lysozyme and chymotrypsin were added to investigate potential influences of fresh substrate and enzyme, respectively, on the proteolytic performance.

Table 11.2 Characteristic kinetic parameters obtained by fitting equation (11.1) (see Methods) to the temporal evolution of the peak areas of the GRCEL and MRSL peptides during digestion of lysozyme with immobilized and free chymotrypsin.

| Colloidal particles | Chymotrypsin immobilized on silica (+chymotrypsin) | | Chymotrypsin immobilized on silica (+lysozyme) | | Chymotrypsin immobilized on alumina (+chymotrypsin) | | Chymotrypsin immobilized on alumina (+lysozyme) | | Control | |
|---|---|---|---|---|---|---|---|---|---|---|
| **Peptide** | **GRCEL** | **MRSL** | **GRCEL** | **MRSL** | **GRCEL** | **MRSL** | **GRCEL** | **MRSL** | **GRCEL** | **MRSL** |
| **K** ($hours^{-1}$) | 0.11 | 0.10 | 0.18 | 0.17 | 0.54 | 0.85 | 0.62 | 0.68 | 2.45 | 2.27 |
| $Y_{max}$ ($10^4$ intensity units) | 7.3 | 6.3 | 6.7 | 5.6 | 8.9 | 5.6 | 9.4 | 6.3 | 1.7 | 1.1 |

*Note:* In the fitting procedure, performed with the PRISM software, $Y_0$ was constrained to zero. To each sample (chymotrypsin immobilized on silica and alumina colloidal particles, respectively) chymotrypsin (+ chymotrypsin) or lysozyme (+ lysozyme) were added after 23 h to reveal influences of fresh enzyme or substrate to the proteolytic performance. The control consists of free chymotrypsin in solution with lysozyme as substrate without any colloidal particles (*in-solution-digest*).

To probe the reusability of the immobilized enzymes we tested the proteolytic activity of the chymotrypsin immobilized on colloidal particles in three consecutive lysozyme digestion steps. During these 24 h steps, the samples with chymotrypsin immobilized on colloidal particles were allowed to digest lysozyme as a substrate. After each step, the samples were rinsed, MALDI-ToF-MS spectra of the supernatant solutions were collected, and new 24 h digestions were started. The resulting peptide peaks in the MALDI spectra were used to assess the enzymatic activity at a semi-quantitative level, as in the previous experiments (Figure 11.5).

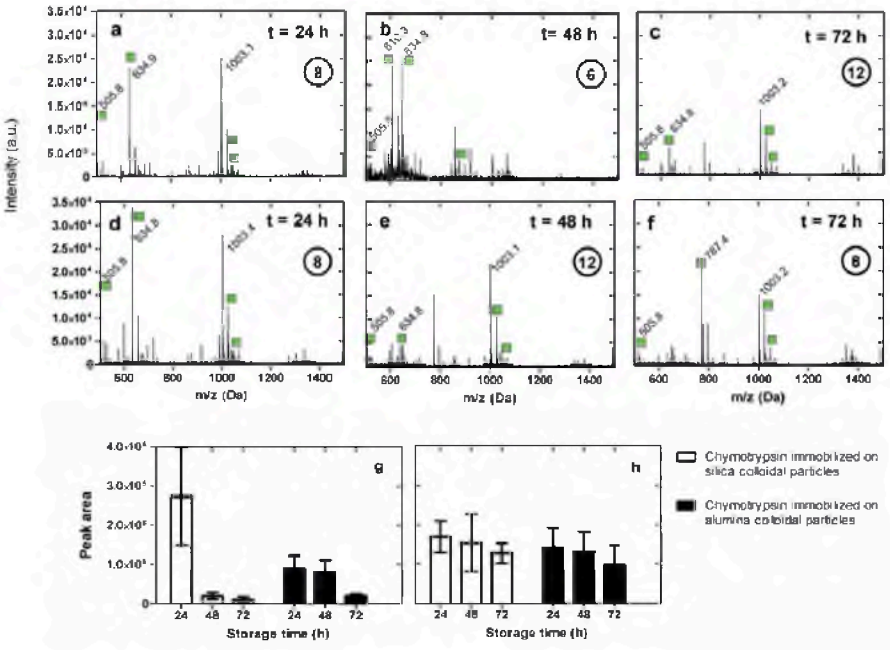


Figure 11.5 MALDI-ToF-MS spectra of fresh lysozyme solutions digested with chymotrypsin immobilized on alumina (a–c) or silica (d–f) collected in three consecutive digestion steps, each lasting 24 h. The number of identified lysozyme peptide sequences is shown in circles in the panels (a–f). Panel (g) shows the sum of peak areas of both peptides (MRSL and GRCEL) in the consecutive digestion step (black and white bars for alumina and silica colloidal particles, respectively). Panel (h) shows the summarized peak areas of the same peptides after one digestion step started following storage of fresh chymotrypsin immobilized on colloidal particles suspensions for 24, 48, and 72 h. The most indicative peaks belonging to the lysozyme sequence were marked by green squares. For a better orientation, some of the most intense peaks were labeled with corresponding m/z values.

Both chymotrypsin immobilized on alumina and chymotrypsin immobilized on silica were able to digest lysozyme within each of the three consecutive steps as demonstrated by the generation of a high number of peptides clearly identified as part of the lysozyme sequence (Figure 11.5). However, the averaged peak areas of the MRSL and GRCEL peptides strongly decreased after the first 24 h digest period, especially in the case of chymotrypsin immobilized on silica, while a less pronounced effect was observed for chymotrypsin immobilized on alumina (Figure 11.5g).

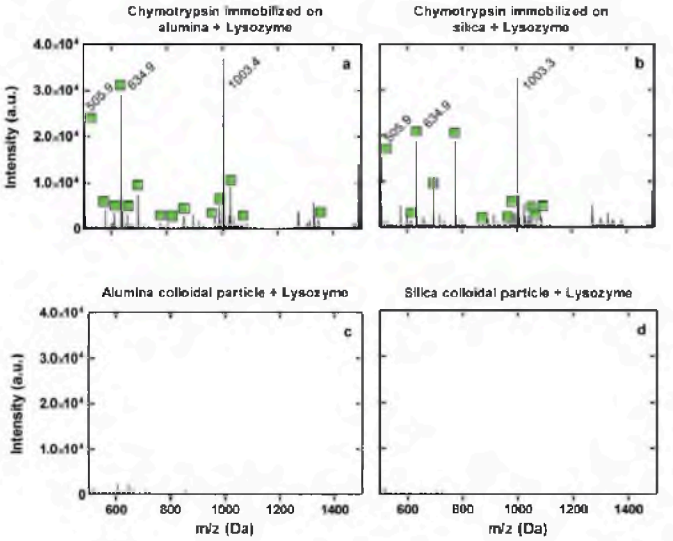


Figure 11.6 a, b: Enzymatic activity of chymotrypsin immobilized to alumina and silica functionalized with amino groups measured by MALDI-ToF-MS using lysozyme as substrate. c, d: Amino group functionalized alumina and silica with lysozyme as negative controls. Green markers indicate peaks that can be identified by database as corresponding to lysozyme. Measurements were performed after 7 weeks of storage at room temperature.

Storage of chymotrypsin immobilized on colloidal particles for 24 h, 48 h and 72 h at room temperature before incubation with lysozyme revealed substantial peptide formation after all storage periods and only a slight decrease of the peak areas for both colloidal materials (Figure 11.5h). In addition, fresh samples of chymotrypsin immobilized on colloidal particles that had been stored at room temperature for 7 weeks generated characteristic lysozyme peptide peaks in a 24 h digest although the overall peak intensity was rather low (Figure 11.6).

## 11.4 Discussion

In our study the popular and simple immobilization approach based on amine coupling with 1-ethyl-3-(3-dimetylaminopropyl)carbodiimide and N-hydroxysuccinimide was found to be suitable to covalently bound

chymotrypsin to the amine-functionalized alumina and silica colloidal particles and preserve the activity of chymotrypsin, as already demonstrated by Hong *et al.*[266], who immobilized chymotrypsin on superparamagnetic nanogels. In our work, the preservation of chymotrypsin activity has been demonstrated by the MALDI-ToF-MS observation of multiple lysozyme-derived peptides after proteolytic digestion (Figure 11.2), similarly as obtained after chymotrypsin in-solution-digests. The formation of lysozyme-derived peptides is clearly induced by the presence of chymotrypsin on the particles' surface as no lysozyme digestion peaks were observed using amino-functionalized colloidal particles suspensions. The number of identified peptides after the digestion experiments is comparable to previous results obtained using trypsin and chymotrypsin[261, 265, 267, 268]. Also in these previous works, the efficiency of digestion by immobilized enzymes was evaluated by analyzing the sequence coverage.

Although no direct information about the total amount of immobilized chymotrypsin could be obtained, the MALDI-ToF-MS analysis of the peak areas of the peptides MRSL and GRCEL, resulting from the digestion of lysozyme, allowed us to compare the enzymatic activities of the immobilized chymotrypsin with that of chymotrypsin free in solution. This comparison was performed assuming that the amount of non-immobilized chymotrypsin in solution after several washing steps is insignificant. The results presented in Figure 11.3 show that, for the peptides MRSL and GRCEL, smaller peak values could be detected from digested lysozyme using chymotrypsin immobilized to silica colloidal particles than to alumina colloidal particles, possibly due to a different amount of immobilized chymotrypsin. Moreover, it is conceivable that the immobilized enzymes present a reduced intrinsic activity. This may be due to several and in part concomitant factors[16, 269] such as: (i) the hindered accessibility of the substrate to the active site of chymotrypsin, (ii) conformational changes of immobilized chymotrypsin; (iii) the formation of chymotrypsin agglomerates by cross-linking induced by the linking protocol; and (iv) an increased (material-dependent) tendency for chymotrypsin oxidation, as described in earlier studies[269].

The factors above are also expected to be responsible for the slower digestion kinetics of immobilized chymotrypsin with respect to free chymotrypsin in solution. For a better comparison, kinetic experiments were conducted by adjusting the concentration of unbound chymotrypsin

to 10 % (Figure 11.3). The kinetic analysis over 27 h showed a plateau that was reached within 2.5 h for unbound chymotrypsin and more than 5 h for chymotrypsin immobilized onto both materials. This plateau is probably due to an occlusion of the active site by the proteolysis products, since the addition of extra substrate (+lysozyme) leads to no obvious changes in the kinetic curves. In contrast, after addition of extra enzymes (+chymotrypsin), an increase of the reaction products (in this case, the peptides MRSL and GRCEL) was observed. A reduction of enzymatic activity and slower digestion kinetics after immobilization to solid supports has been already observed for other enzymes such as glucose oxidase[270] or trypsin[271].

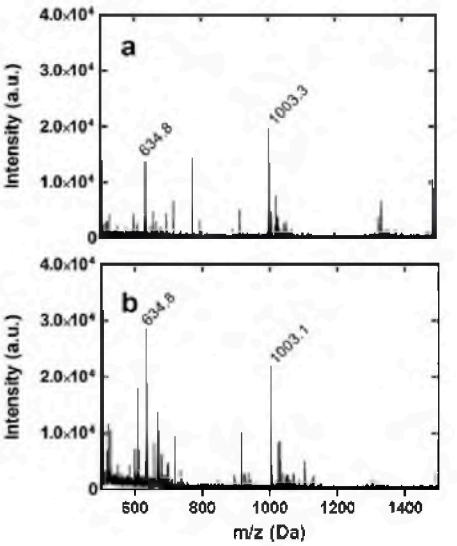


Figure 11.7 Influence of chymotrypsin autolysis on protease activity. Spectra comparison between lysozyme in-solution-digest using (a) chymotrypsin that was incubated for 24 h before starting digest (to provoke chymotrypsin autolysis) and (b) *in-solution-digest* without pre-incubation of chymotrypsin.

The kinetic analysis shows that both unbound as well as colloidal particles-bound chymotrypsin became inactive after 23 h of incubation, as the addition of fresh lysozyme did not lead to an additional increase in the amounts of proteolytic peptides. However, compared to unbound

chymotrypsin, the maximal amount of peptides determined after 23 h was twice as much. This may suggest that colloidal particles-bound chymotrypsin remained longer active than unbound chymotrypsin. As mentioned above, an inactivation of the enzyme due to autolysis is quite unlikely under our reaction conditions. In fact, a pre-incubation of unbound chymotrypsin (that could provoke chymotrypsin autolysis) followed by lysozyme in-solution-digest revealed negligible changes in the observed peak pattern compared to digest using fresh chymotrypsin (Figure 11.7). However, a very small amount of autolysis cannot be excluded for the chymotrypsin immobilized on colloidal particles, for which low intensity autolysis peaks were detectable (Figure 11.8). Nevertheless, using the PeptFind tool from Expasy.org, it was found that only 2.9 % and 4.4 % (after 24 h and 48 h, respectively) of all mass peaks can be assigned to chymotrypsin autolysis fragments. Other peaks might be impurities or other unspecific cleavage products (as it is indicated by the PeptFind tool).

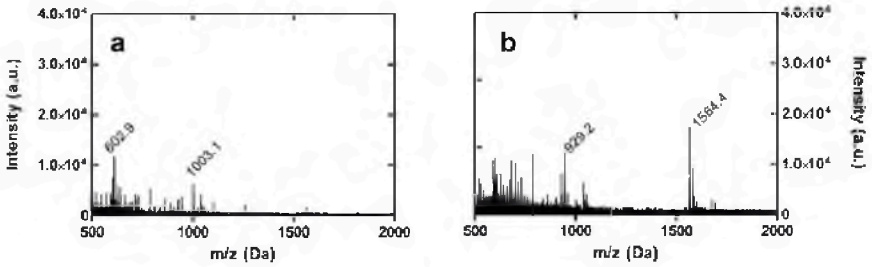


Figure 11.8 Check for autolysis peaks from non-immobilized chymotrypsin after 24 h (a) and 48 h (b) incubation in 400 mM ammonium bicarbonate buffer.

For technical applications, an important parameter to assess the efficacy of enzyme-functionalized materials is their cyclic reusability. Our cyclic reusability experiments (see Figure 11.5) showed that after each digestion roughly the same number of lysozyme peptide sequences could be identified, as a consequence of the active lysozyme cleavage by chymotrypsin. These results are in agreement with previous investigations with chymotrypsin immobilized on an epoxy-modified silica monolithic

support[267, 268]. However, we found that the MALDI peak areas associated to the cleaved peptides MRSL and GRCEL decreased, indicating a progressive loss of enzymatic activity. This loss appears to be more pronounced for silica than for alumina, suggesting that the type of support material has an influence on the reusability efficacy. Interestingly, a very limited loss of enzymatic activity was observed when the immobilized enzymes were stored at room temperature and freshly used after 24 h, 48 h and 72 h (Figure 11.5 h). In fact, the materials were found to be active toward lysozyme digestion even after 7 weeks of storage at room temperature, comparable to studies with chymotrypsin immobilized onto chitosan grafted with polymethyl methacrylate[272]. Therefore, the activity loss in the reusability tests is not expected to originate from slow conformational changes of the enzyme in the immobilized state, which would also take place during long-term storage, but rather connected with the digestion reaction. For instance, occlusion of the active site by reaction intermediates that remain trapped due to steric hindrances caused by the tethering to the ceramic particles, or that remain adsorbed to the particle surfaces, could lead to a progressive "poisoning" of the immobilized enzyme. Future studies shall be devoted to optimizing the immobilization procedure in order to maximize the efficiency and improve the reusability of immobilized enzyme on the colloidal ceramic particles.

## 11.5 Conclusions

This study investigated the coupling efficiency, enzymatic activity and enzyme kinetics of chymotrypsin immobilized onto silica and alumina colloidal particles with amino groups using MALDI-ToF-MS. Although this analysis does not allow an exact quantification of the amount of chymotrypsin immobilized onto colloidal particles, it delivered a semi-quantitative information on the activity of the immobilized enzymes by comparing the data from in-solution-digests with different protease concentrations. Application of MALDI-ToF-MS allowed us to measure the actual proteolysis products without the using of artificial protease substrates or intermediate chemicals that are required in other methods[40, 132, 273, 274]. The spectra offer a visual overview on the amount of enzymatic products as well as detailed information about many single peptides in a single experiment. Beside this, the detection limit of MALDI-ToF-MS in the femtomole range[275] is substantially lower than that of many other

colorimetric or fluorescence techniques used for enzyme activity measurements[276, 277]. Adaptation of this method should also be possible for other studies which aim at comparing the immobilization efficiency of several proteases. The results of this study will help to advance the knowledge about immobilization of proteins to inorganic substrates. In proteomic research, particularly in the field of bioengineering (e.g., in batch processes, bioreactors etc.) it is of prime importance to control enzymatic processes or, if needed, to isolate enzymes from reactions fast and easy by the usage of colloidal particles bound enzymes.

## 11.6 Acknowledgments

We thank Dr. Katharina Richter from the Fraunhofer Institute for Manufacturing Technology and Advanced Materials (IFAM) in Bremen for supporting the MALDI-ToF-MS experiments. Sascha Steckbeck and Lucio Colombi Ciacchi acknowledge funding from the Deutsche Forschungsgemeinschaft (DFG) under the Emmy Noether grant CI 144/2 and from the European Commission via the FP7-NMP grant 229205 "ADGLASS".

## 11.7 Appendix: Characterization of colloidal particles after surface functionalization and enzyme immobilization using Fourier transform infrared (FTIR) spectroscopy

Additional FTIR spectroscopy measurements were performed using a Nicolet 320 FT-IR spectrometer (Thermo Scientific, Germany). Spectra were obtained from KBr (Merck, Germany) pellets containing approximately 1 wt% particles and measured between 4000 and 400 $cm^{-1}$ after 100 accumulations at 1 $cm^{-1}$ resolution. FTIR measurements were carried out using $Al_2O_3$ (Figure 11.9a) and $SiO_2$ particles (Figure 11.9b). Data analysis was performed using the Omnic software (version 4.1).

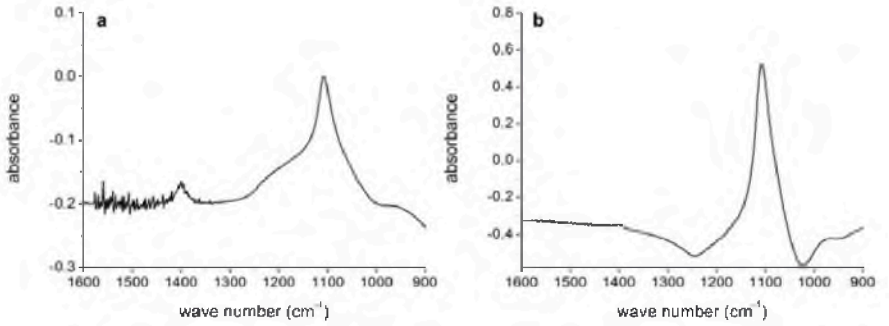


Figure 11.9 Chymotrypsin immobilized on $Al_2O_3$ (a) and $SiO_2$ (b) with amino groups minus the reference (colloidal particles functionalized with amino groups).

To characterize colloidal particles before and after chemical surface modification and enzyme immobilization, for each particle type the following samples were analyzed:

- pure colloidal particles (untreated)
- colloidal particles functionalized with amino groups
- colloidal particles functionalized with amino groups after a treatment with 1-ethyl-3-(3-dimetylaminopropyl)carbodiimide and N-hydroxy-succinimide
- chymotrypsin immobilized on colloidal particles after functionalization with amino groups using 1-ethyl-3-(3-dimetylaminopropyl)carbodiimide and N-hydroxysuccinimide

To compare the spectra and to interpret the results, the reference spectra of colloidal particles functionalized with amino groups was subtracted from the graph of chymotrypsin immobilized on colloidal particles after functionalization with amino groups using 1-ethyl-3-(3-dimetylaminopropyl)carbodiimide and N-hydroxysuccinimide. Additionally, a baseline correction was carried out. As show in Figure 11.9a and Figure 11.9b, a peak approximately 1100 $cm^{-1}$ was observed for both particle types. The presence of this peak, which is characteristic for amide bonds, indicates the presence of immobilized chymotrypsin on colloidal particles functionalized with amino groups[278]. Additionally, a vibration at approximately 1400 $cm^{-1}$ suggests a presence of alkyl groups which are also traced back to chymotrypsin immobilization on both particle types[278].

## 11.8 Source

This chapter was adapted from:

Derr L., Steckbeck S., Dringen R., Colombi Ciacchi L., Treccani L., and Rezwan K.; Assessment of the proteolytic activity of α-chymotrypsin immobilized on colloidal particles by matrix-assisted laser desorption ionization time-of-flight mass spectrometry. Analytical Letters. 2014; 48[3]: 424-441, License number: P062415-02.

Ludmilla Derr and Sascha Steckbeck (Hybrid Materials Interfaces Group, University of Bremen, Germany) have shared first authorship for this publication. The precise contributions of each single author are listed below. All the used literature references are summarized in Chapter 14.

| Author | Contribution |
|---|---|
| ***Ludmilla Derr*** | Conceptualization of work, planned and performed covalent immobilization experiments, characterization of the colloidal particles before and after covalent immobilization, performed characterization analysis on all samples, interpreted and discussed data, wrote manuscript |
| Sascha Steckbeck | Conceptualization of work, planned and performed MALDI-ToF-MS experiments and their analysis, interpreted data, wrote manuscript |
| Ralf Dringen | Gave conceptual advices, discussed data, edited manuscript |
| Lucio Colombi Ciacchi | Contributed to conceive the work and interpret the results, co-wrote the manuscript |
| Laura Treccani | Gave conceptual advices, discussed data, edited manuscript |
| Kurosch Rezwan | Gave conceptual advices, discussed data, edited manuscript |

# 12 Conclusions

*ABSTRACT: This Chapter summarizes all key findings of this study.*

The main goal of this thesis was to analyze the effects of colloidal ceramic particles on the enzymatic activities of adsorbed or covalently immobilized enzymes. Because the interplay of interactions between enzymes and colloidal particles is very complex, a simple model system using a serine protease, α-chymotrypsin, was chosen. α-Chymotrypsin is not only well characterized but also has a wide range of potential applications. Two main immobilization strategies, physisorption and covalent immobilization, were employed in this study. Depending on the experimental requirements, four types of colloidal materials were used as carrier materials: $Al_2O_3$, $SiO_2$ and two types of $TiO_2$.

As the most straightforward and mild method, physisorption was selected to examine the effects of colloidal ceramic particles on the enzymatic activity of adsorbed chymotrypsin. Because no additional reagents were required, activity changes caused by linkers and additional chemical substances could be excluded. Desorption processes were examined and prevented by controlling the pH and ionic strength.

Experimental conditions that enabled the stable adsorption of chymotrypsin on $Al_2O_3$, $SiO_2$, and $TiO_2$ with rutile and rutile/ anatase crystal structures were identified. The following trends were determined for enzyme adsorption in all chosen colloidal systems:

- Chymotrypsin adsorbed efficiently on all tested colloidal particles in a concentration-dependent manner.
- Adsorption was pH dependent and increased with increasing pH.
- Among the tested experimental conditions, pH 8 was optimal for strong chymotrypsin adsorption.
- Adsorption increased as the hydrophobicity of the particles increased.
- Both types of $TiO_2$ exhibited the highest adsorption affinity, followed by $Al_2O_3$ and, finally, $SiO_2$.
- Normalization of the experimental data with respect to the Protein Accessible Area ($PAA_{SEM}$), as defined in this study, seemed to be

more suitable than normalization using the traditionally obtained $SSA_{BET}$ based on the $N_2$ accessible surface.

The experimental results were considered in terms of the results of the simulations, which were performed under the same conditions as in the experiments examining chymotrypsin adsorption on $SiO_2$ and $TiO_2$. The simulations were possible thanks to a collaborative project involving the Advanced Ceramics Group (Faculty of Production Engineering, University of Bremen, Germany), the Center for Biomolecular Interactions Bremen (Faculty of Biology/ Chemistry, University of Bremen, Germany), and the Hybrid Materials Interfaces Group (Faculty of Production Engineering and Bremen Center for Computational Materials Science, University of Bremen, Germany).

A combination of experimental studies and molecular dynamics simulations using $SiO_2$ and $TiO_2$ (rutile/ anatase) colloidal particles helped to obtain the following findings:

- The same preferred adsorption orientation of chymotrypsin was found on both materials at both neutral and basic pH values, driven by interaction of the negatively charged surfaces with the strong protein dipole moment.
- A nearly equal free energy of adsorption in the low-concentration limits (approximately -35 kJ/mol) was estimated by Langmuir adsorption isotherm analysis.
- A larger amount of adsorbed chymotrypsin was found in the experiments on $TiO_2$ than in those on $SiO_2$.
- Anchoring to the $SiO_2$ surface occurred mostly via positively charged amino acids that interacted with both neutral and deprotonated silanol groups, although neutral polar and even hydrophobic residues contributed to frequent and tight surface-protein contacts.
- Anchoring to the $TiO_2$ surface was dominated by neutral terminal OH and bridging O sites but, involved positively charged amino acids nearly exclusively.
- Steered MD simulations showed that chymotrypsin can easily slide over the $TiO_2$ surface and can even temporarily desorb and adsorb again at a farther site.
- No temporary desorption from the $SiO_2$ surface was observed, so rupture of the tight surface-protein contacts only occurred if new

contacts were concomitantly formed, resulting in a predominant rolling behavior for chymotrypsin.

- A change in the dipole orientation due to rolling was associated with considerable energy loss, so diffusion over the $SiO_2$ surface is expected to be more hindered than diffusion over the $TiO_2$ surface is.

The main focus of this thesis was the assessment of the enzymatic activities of immobilized enzymes, which is a complex challenge because conventional assays usually cannot be applied to colloidal particles. To circumvent this obstacle, a known method for measuring the activities of free enzymes using p-NPA as an enzyme substrate was adapted and optimized to allow its use with adsorbed enzymes. After establishing the assay, different colloidal particles were used as the carrier material for adsorbed chymotrypsin to measure the effects of adsorption on catalytic activity, demonstrating the simple application and versatility of the optimized assay. The simple and rapid method developed in this study does not require any complex technical equipment and will also be useful for studying the interactions of other hydrolytic enzymes with various types of colloidal materials.

For all colloidal particles, adsorption negatively influenced the enzymatic activity of adsorbed chymotrypsin, as indicated by substantial losses in enzymatic activity. Approximately 12-15 %, 7-9 %, and 6-9 % of the initial enzyme activity was preserved after adsorption on $SiO_2$, $Al_2O_3$ and $TiO_2$ (rutile), respectively. The dependence on substrate concentration was determined for adsorbed chymotrypsin on $TiO_2$ (rutile), and an increase in the $K_M$ value for the artificial substrate p-NPA was observed. The increase in the $K_M$ value and the decrease in maximal hydrolytic activity may have been due to blockage of the active site or conformational changes caused by the adsorption of chymotrypsin on the particle surface. Lateral enzyme-enzyme interactions did not appear to play an important role because the enzymatic activity was similar for all colloidal particles and was largely independent of the surface density of the adsorbed enzymes.

Because the covalently immobilized enzymes exhibited limited desorption, this immobilization method was also applied using amine-functionalized $Al_2O_3$ and $SiO_2$ colloidal particles. The popular immobilization method

based on amine coupling with 1-ethyl-3-(3-dimetylaminopropyl)-carbodiimide and N-hydroxysuccinimide was performed. However, the coupling substances used for covalent immobilization interfered with the optimized assay. Therefore, the enzymatic activity of covalently immobilized chymotrypsin was estimated by MALDI-ToF-MS using lysozyme as the enzyme substrate and analyzing multiple lysozyme-derived peptides after proteolytic digestion.

The findings can be summarized as follows.

- The formation of lysozyme-derived peptides was obviously induced by the presence of chymotrypsin on the particle surface.
- Colloidal particle-bound chymotrypsin remained active for a longer period of time than unbound chymotrypsin in kinetic studies.
- Cyclic reusability experiments demonstrated that after each digestion, roughly the same number of lysozyme peptide sequences could be identified, indicating active lysozyme cleavage by chymotrypsin.
- A reduction in enzymatic activity and slower digestion kinetics after immobilization were observed for both particle types.
- The loss of enzymatic activity was more pronounced for silica than for alumina in cyclic reusability studies.
- Both materials retained lysozyme digestion activity, even after 7 weeks of storage at room temperature.
- The activity loss in the reusability experiments was likely due to the digestion reaction and possible steric hindrance and not to slow conformational changes of the enzyme in the immobilized state because such changes would also occur during long-term storage.

# 13 Outlook

*ABSTRACT: This Chapter presents some potential projects for continuation.*

The two immobilization methods applied in this study, physisorption and covalent immobilization, should be considered separately.

The study of adsorption interactions between enzymes and ceramic colloidal particles can be extended in two ways. First, enzyme engineering methods could be applied to modify enzyme properties such as surface charge and surface functional groups and to measure their influence on adsorption and the catalytic activity of the adsorbed enzymes. Second, it is also feasible to investigate the influence of surface functionalization of the ceramic colloidal particles on the enzymatic activities of adsorbed enzymes. Of particular interest are the effects of surfaces with different wettabilities, porosities and roughness on adsorption behavior. Based on current knowledge, the second approach might be easier to accomplish because the methods and the optimized enzymatic assay described in this study can be applied immediately. A combination of the results and findings of this thesis and the knowledge recently shared by Fabian Meder from our research group regarding surface functionalization[158, 279] might be particularly fruitful. Furthermore, the applied assay is also suitable for examining other enzymes such as trypsin. Extension of the model would highlight and confirm once again the simple application of the utilized methods.

The size and weight of the colloidal particles allowed the use of essential procedures, such as centrifugation, to separate free enzymes from enzymes that were adsorbed or covalently immobilized on the particles. However, the size and weight of the colloidal particles were not suitable for direct analysis of the possible structural changes in the immobilized enzymes via CD measurements. Additional analyses should utilize a model with smaller particles suitable for the applied enzymatic assay and for direct CD measurements. A combination of experimental studies and molecular dynamics simulations would also be desirable to obtain a broader picture of the enzyme's behavior at the atomic scale.

Because reusability is a very important factor for the application of enzymes, extended reusability studies could be performed for both

covalently immobilized chymotrypsin and chymotrypsin adsorbed via physisorption, as well as for other enzymes. Analysis of covalently immobilized chymotrypsin in the performed reusability study indicated that the immobilized chymotrypsin retained lysozyme digestion activity, even after 7 weeks of storage at room temperature. It might therefore be interesting to focus on the pH and temperature stability of the immobilized enzyme, particularly with the aim of practical applications in the fields of proteomic research and bioengineering.

# List of students projects

This thesis could not have been carried out without having motivated and intelligent undergraduate students helping. The following list acknowledges all undergraduate's work (student assistants, internships, semester projects, diploma thesis) in alphabetical order:

| | |
|---|---|
| Regina Bektev | "Modellbildung zur Ladungsverteilung auf Proteinoberflächen", Semester Project, 2011 |
| Sebastian Bitzenhofer | "Enzyme immobilization", Student Assistant, 2012 |
| Cagla Cengel | "Modellbildung zur Ladungsverteilung auf Proteinoberflächen", Semester Project, 2011 |
| Sonia Jahn | "Enzyme immobilization", Student Assistant, 2012-2013 |
| Supreet Kaur | "Enzyme adsorption", Student Assistant, 2013 |
| Ertugrul Kuzu | „Untersuchungen der Wechselwirkungen zwischen Nanopartikeln und Biomolekülen", Internship, 2010-2011 |
| Sandra Projahn | "Modellbildung zur Ladungsverteilung auf Proteinoberflächen ", Semester Project, 2011 |
| Sonia Tambou | „Charakterisierung biofunktionalisierter Nanopartikel für biotechnologische Anwendungen", Diploma thesis, 2011 |
| Murat Yöyen | "Modellbildung zur Ladungsverteilung auf Proteinoberflächen ", Semester Project, 2011 |

# List of publications

**During the time as PhD student at the University of Bremen:**

1. **Derr, L.**; Hildebrand, N.; Köppen, S.; Kunze, S.; Treccani, L.; Dringen, R.; Rezwan, K.; Colombi Ciacchi, L.; Effect of α-chymotrypsin on SiO2 and TiO2: a comparative study via experiments and molecular dynamics simulations. Biointerphases 2016, 11, (1), 011007.

2. **Derr, L.**; Dringen, R.; Treccani, L.; Colombi Ciacchi, L.; Rezwan, K.; Physisorption of enzymatically active chymotrypsin on titania colloidal particles. J Colloid Interf Sci 2015, 455, 236-244.

3. **Derr, L.**; Steckbeck, S.; Dringen, R.; Colombi Ciacchi, L.; Treccani, L.; Rezwan, K.; Assessment of the proteolytic activity of α-chymotrypsin immobilized on colloidal particles by matrix-assisted laser desorption ionization time-of-flight mass spectrometry. Analytical Letters 2014, 48 (3), 424-441.

4. Hildebrand, N.; Köppen, S.; **Derr, L.**; Li, K.; Koleini, M.; Rezwan, K.; Colombi Ciacchi, L. Adsorption orientation and binding motifs of lysozyme and chymotrypsin on amorphous silica. J. Phys. Chem. C 2015, 119 (13), 7295-7307.

5. Schmidt, M. M.; Köhler, Y.; **Derr, L.**; Treccani, L.; Rezwan, K.; Dringen, R.; Interaction of the physiological tripeptide glutathione with colloidal alumina particles. J. Phys. Chem. C 2012, 116, 23136-23142.

6. Dringen, R.; Koehler, Y.; **Derr, L.**; Tomba, G.; Schmidt, M. M.; Treccani, L.; Colombi Ciacchi, L.; Rezwan, K.; Adsorption and reduction of glutathione disulfide on alpha-$Al_2O_3$ nanoparticles: experiments and modeling. Langmuir 2011, 27, (15), 9449-9457.

**During the time at Fraunhofer Institute for Wood Research Wilhelm-Klauditz Institute:**

7. Deppe, B.; Kruse, D.; Pfafenrot, H.; Lepadatu, A.; **Derr, L.**; Haß, S.; Verbesserung der Witterungsstabilität von Brandschutzbeschichtungen. Internationaler Verein für technische Holzfragen 2008, Summary Report Nr.23/08, Braunschweig/ Germany.

8. Deppe, B.; Pfafenrot, H.; Kruse,D.; **Derr, L.**; Fire retardant coatings under climatic stress. Conference proceedings for Fire Retardant Coatings Conference 2008, Berlin/ Germany.

9. Kruse, D.; Simon, S.; **Derr, L.**; Gatzke, A.; High Performance Fire Protection Coatings - Development, Qualification, Application. Conference proceedings for 5th International Woodcoatings Congress "Enhancing Service Life" 2006, Prag/ Czech Republic.

10. Kruse, D.; Simon, S.; **Derr, L.**; Brandschutz eines karbonfaserverstärkten Kunststoffbauteils. Internationaler Verein für technische Holzfragen 2005, Summary Report Nr.10/05, Braunschweig/ Germany.

## Selected oral and poster presentations

**Derr, L.;** Dringen, R.; Schmidt, M. M.; Köhler, Y.; Treccani, L.; Tomba, G.; Colombi Ciacchi, L.; Rezwan, K.; Peptide and enzyme adsorption onto oxide nanoparticles *(poster).* 8th NanoBio Europe Conference, Varese/ Italy, 2012.

**Derr, L.;** Dringen, R.; Schmidt, M. M.; Köhler, Y.; Treccani, L.; Tomba, G.; Colombi Ciacchi, L.; Rezwan, K.; Peptide and enzyme adsorption onto oxide nanoparticles *(poster).* Gordon Research Conference on Biointerface Science, Les Diablerets/ Switzerland, 2012.

**Derr, L.;** Schmidt, M. M.; Köhler, Y.; Treccani, L.; Tomba, G.; Colombi Ciacchi, L.; Dringen, R.; Rezwan, K.; Biomolecule adsorption to oxide nanoparticles *(oral).* 12th International Conference and Exhibition of the European Ceramic Society, Stockholm/ Sweden, 2011.

**Derr, L.;** Schmidt, M. M.; Köhler, Y.; Treccani, L.; Tomba, G.; Colombi Ciacchi, L.; Dringen, R.; Rezwan, K.; Peptide adsorption to oxide nanoparticles *(oral).* European Symposium on Biomaterials and Related Areas, Jena/ Germany, 2011.

# 14 References


1. Parveen, S.; Misra, R.; Sahoo, S. K., Nanoparticles: a boon to drug delivery, therapeutics, diagnostics and imaging. *Nanomedicine-Uk* **2012,** 8, (2), 147-66.

2. Treccani, L.; Klein, T. Y.; Meder, F.; Pardun, K.; Rezwan, K., Functionalized ceramics for biomedical, biotechnological and environmental applications. *Acta Biomater* **2013,** 9, (7), 7115-7150.

3. Andreescu, S.; Njagi, J.; Ispas, C., Chapter 7 - Nanostructured materials for enzyme immobilization and biosensors. In *The New Frontiers of Organic and Composite Nanotechnology*, Erokhin, V.; Ram, M. K.; Yavuz, O., Eds. Elsevier: Amsterdam, 2008; pp 355-394.

4. Bhakta, S. A.; Evans, E.; Benavidez, T. E.; Garcia, C. D., Protein adsorption onto nanomaterials for the development of biosensors and analytical devices: A review. *Anal Chim Acta* **2015,** 872, (0), 7-25.

5. Monzo, A.; Sperling, E.; Guttman, A., Proteolytic enzyme-immobilization techniques for MS-based protein analysis. *TrAC Trends in Analytical Chemistry* **2009,** 28, (7), 854-864.

6. Brady, D.; Jordaan, J., Advances in enzyme immobilisation. *Biotechnol Lett* **2009,** 31, (11), 1639-1650.

7. Hanefeld, U.; Cao, L. Q.; Magner, E., Enzyme immobilisation: fundamentals and application. *Chem Soc Rev* **2013,** 42, (15), 6211-6212.

8. Mateo, C.; Palomo, J. M.; Fernandez-Lorente, G.; Guisan, J. M.; Fernandez-Lafuente, R., Improvement of enzyme activity, stability and selectivity via immobilization techniques. *Enzyme Microb Tech* **2007,** 40, (6), 1451-1463.

9. Nel, A. E.; Madler, L.; Velegol, D.; Xia, T.; Hoek, E. M. V.; Somasundaran, P.; Klaessig, F.; Castranova, V.; Thompson, M., Understanding biophysicochemical interactions at the nano-bio interface. *Nat Mater* **2009,** 8, (7), 543-557.

10. Wang, K.; Zhou, C.; Hong, Y.; Zhang, X., A review of protein adsorption on bioceramics. *Interface focus* **2012,** 2, (3), 259-77.

11. Bommarius, A. S.; Paye, M. F., Stabilizing biocatalysts. *Chem Soc Rev* **2013,** 42, (15), 6534-6565.

12. Franssen, M. C. R.; Steunenberg, P.; Scott, E. L.; Zuilhof, H.; Sanders, J. P. M., Immobilised enzymes in biorenewables production. *Chem Soc Rev* **2013,** 42, (15), 6491-6533.

13. Hartmann, M.; Kostrov, X., Immobilization of enzymes on porous silicas - benefits and challenges. *Chem Soc Rev* **2013,** 42, (15), 6277-6289.

14. Liese, A.; Hilterhaus, L., Evaluation of immobilized enzymes for industrial applications. *Chem Soc Rev* **2013,** 42, (15), 6236-6249.

15. Rodrigues, R. C.; Ortiz, C.; Berenguer-Murcia, A.; Torres, R.; Fernandez-Lafuente, R., Modifying enzyme activity and selectivity by immobilization. *Chem Soc Rev* **2013,** 42, (15), 6290-6307.

16. Secundo, F., Conformational changes of enzymes upon immobilisation. *Chem Soc Rev* **2013,** 42, (15), 6250-6261.

17. Sheldon, R. A.; van Pelt, S., Enzyme immobilisation in biocatalysis: why, what and how. *Chem Soc Rev* **2013,** 42, (15), 6223-6235.

18. Singh, R. K.; Tiwari, M. K.; Singh, R.; Lee, J. K., From protein engineering to immobilization: Promising strategies for the upgrade of industrial enzymes. *Int J Mol Sci* **2013,** 14, (1), 1232-1277.

19. Magner, E., Immobilisation of enzymes on mesoporous silicate materials. *Chem Soc Rev* **2013,** 42, (15), 6213-6222.

20. Cedervall, T.; Lynch, I.; Lindman, S.; Berggard, T.; Thulin, E.; Nilsson, H.; Dawson, K. A.; Linse, S., Understanding the nanoparticle-protein corona using methods to quantify exchange rates and affinities of proteins for nanoparticles. *P Natl Acad Sci USA* **2007,** 104, (7), 2050-2055.

21. Diaconu, G.; Schafer, T., Study of the interactions of proteins with a solid surface using complementary acoustic and optical techniques. *Biointerphases* **2014,** 9, (2), 029015.

22. Fenoglio, I.; Fubini, B.; Ghibaudi, E. M.; Turci, F., Multiple aspects of the interaction of biomacromolecules with inorganic surfaces. *Adv Drug Deliv Rev* **2011,** 63, (13), 1186-209.

23. Lee, W. H.; Loo, C. Y.; Rohanizadeh, R., A review of chemical surface modification of bioceramics: effects on protein adsorption and cellular response. *Colloids Surf B Biointerfaces* **2014,** 122, 823-34.

24. Mahmoudi, M.; Lynch, I.; Ejtehadi, M. R.; Monopoli, M. P.; Bombelli, F. B.; Laurent, S., Protein-nanoparticle interactions: opportunities and challenges. *Chem Rev* **2011,** 111, (9), 5610-37.

25. Vroman, L.; Adams, A. L., Findings with the recording ellipsometer suggesting rapid exchange of specific plasma proteins at liquid/solid interfaces. *Surf Sci* **1969,** 16, (0), 438-446.

26. Cantone, S.; Ferrario, V.; Corici, L.; Ebert, C.; Fattor, D.; Spizzo, P.; Gardossi, L., Efficient immobilisation of industrial biocatalysts: criteria and constraints for the selection of organic polymeric carriers and immobilisation methods. *Chem Soc Rev* **2013,** 42, (15), 6262-6276.

27. Norde, W., Driving forces for protein adsorption at solid surfaces. *Macromol Symp* **1996,** 103, (1), 5-18.

28. Norde, W., Protein adsorption at solid surfaces: A thermodynamic approach. *Pure Appl Chem* **2009,** 66, (3), 491-496.

29. Shemetov, A. A.; Nabiev, I.; Sukhanova, A., Molecular interaction of proteins and peptides with nanoparticles. *Acs Nano* **2012,** 6, (6), 4585-4602.

30. Ethève, J.; Déjardin, P., Adsorption kinetics of lysozyme on silica at pH 7.4: Correlation between streaming potential and adsorbed amount. *Langmuir* **2002,** 18, (5), 1777-1785.

31. Huang, R.; Carney, R. P.; Ikuma, K.; Stellacci, F.; Lau, B. L., Effects of surface compositional and structural heterogeneity on nanoparticle-protein interactions: different protein configurations. *Acs Nano* **2014,** 8, (6), 5402-12.

32. Rezwan, K. Protein treated aqueous colloidal oxide particle suspensions: driving forces for protein adsorption and conformational changes. [Dissertation], 2005.

33. Rezwan, K.; Meier, L. P.; Gauckler, L. J., Lysozyme and bovine serum albumin adsorption on uncoated silica and AlOOH-coated silica particles: the influence of positively and negatively charged oxide surface coatings. *Biomaterials* **2005,** 26, (21), 4351-4357.

34. Gailite, L.; Scopelliti, P. E.; Sharma, V. K.; Indrieri, M.; Podesta, A.; Tedeschi, G.; Milani, P., Nanoscale roughness affects the activity of enzymes adsorbed on cluster-assembled titania films. *Langmuir* **2014,** 30, (20), 5973-81.

35. Lundqvist, M.; Stigler, J.; Elia, G.; Lynch, I.; Cedervall, T.; Dawson, K. A., Nanoparticle size and surface properties determine the protein corona with possible implications for biological impacts. *P Natl Acad Sci USA* **2008,** 105, (38), 14265-14270.

36. Norde, W.; Zoungrana, T., Surface-induced changes in the structure and activity of enzymes physically immobilized at solid/liquid interfaces. *Biotechnol Appl Bioc* **1998,** 28, 133-143.

37. Thyparambil, A. A.; Wei, Y.; Wu, Y.; Latour, R. A., Determination of orientation and adsorption-induced changes in the tertiary structure of proteins on material surfaces by chemical modification and peptide mapping. *Acta Biomater* **2014,** 10, (6), 2404-14.

38. Wei, Y.; Thyparambil, A. A.; Wu, Y.; Latour, R. A., Adsorption-induced changes in ribonuclease A structure and enzymatic activity on solid surfaces. *Langmuir* **2014,** 30, (49), 14849-58.

39. Faller, L.; Sturtevant, J. M., The kinetics of the alpha-chymotrypsin-catalyzed hydrolysis of p-nitrophenyl acetate in organic solvent-water mixtures. *J Biol Chem* **1966,** 241, (21), 4825-34.

40. Ghosh, K. K.; Verma, S. K., Kinetics of alpha-chymotrypsin catalyzed hydrolysis of 4-nitrophenyl acetate in ethanolamine surfactants. *Indian J Biochem Bio* **2008,** 45, (5), 350-353.

41. Kezdy, F. J.; Bender, M. L., The kinetics of the α-chymotrypsin-catalyzed hydrolysis of p-nitrophenyl acetate*. *Biochemistry* **1962,** 1, (6), 1097-1106.

42. Butt, H.-J. r.; Graf, K.; Kappl, M., *Physics and chemistry of interfaces*. 2nd., rev. and enl. ed.; Wiley-VCH: Weinheim, 2006; p x, 386 p.

43. Van Oss, C. J., *Interfacial forces in aqueous media*. 2nd ed.; Taylor & Francis: Boca Raton, Fla., 2006; p 438 p.

44. Keesom, W. H., The second viral coefficient for rigid spherical molecules, whose mutual attraction is equivalent to that of a quadruplet placed at their centre. *Proceedings of the Netherlands Academy of Science* **1915,** (18), 636-646.

45. Debye, P., Die van der Waals`schen Kohäsionskräfte. *Nachrichten von der Gesellschaft der Wissenschaften zu Göttingen, Mathematisch-Physikalische Klasse* **1920,** 21, 55-73.

46. London, F., Zur Theorie und Systematik der Molekularkräfte. *Z. Physik* **1930,** 63, (3-4), 245-279.

47. Butt, H.-J. r.; Kappl, M., *Surface and interfacial forces*. Wiley-VCH: Weinheim, 2010; p xv, 421 p.

48. Dörfler, H. D., *Grenzflächen und kolloid-disperse Systeme: Physik und Chemie*. Springer: 2002.

49. Israelachvili, J. N., *Intermolecular and surface forces*. 3rd ed.; Academic Press: Burlington, MA, 2011; p xxx, 674 p.

50. Shaw, D. J., *Introduction to colloid and surface chemistry*. 4th ed.; Butterworth-Heinemann: Oxford ; Boston, 1992; p vi, 306 p.

51. Hamaker, H. C., The London—van der Waals attraction between spherical particles. *Physica* **1937,** 4, (10), 1058-1072.

52. Ackler, H. D.; French, R. H.; Chiang, Y. M., Comparisons of Hamaker constants for ceramic systems with intervening vacuum or water: From force laws and physical properties. *J Colloid Interf Sci* **1996,** 179, (2), 460-469.

53. Gomez-Merino, A. L.; Rubio-Hernandez, F. J.; Velazquez-Navarro, J. F.; Gaiindo-Rosaies, F. J.; Fortes-Quesada, P., The Hamaker constant of anatase aqueous suspensions. *J Colloid Interf Sci* **2007,** 316, (2), 451-456.

54. von Stockar, U.; van der Wielen, L. A. M., *Biothermodynamics: The role of thermodynamics in biochemical engineering*. EFPL Press: 2013.

55. Parsegian, V. A., *Van der Waals forces: A handbook for biologists, chemists, engineers, and physicists*. Cambridge University Press: 2005.

56. John, C. W., Reactions at the oxide-solution interface: chemical and electrostatic models. In *Geochemical Processes at Mineral Surfaces*, American Chemical Society: 1987; Vol. 323, pp 54-78.

57. Kosmulski, M., *Surface charging and points of zero charge*. CRC Press: 2009.

58. Piasecki, W.; Rudziński, W.; Charmas, R., 1-pK and 2-pK protonation models in the theoretical description of simple ion adsorption at the oxide/electrolyte interface: a comparative study of the behavior of the surface charge, the individual isotherms of ions, and the accompanying electrokinetic effects. *The Journal of Physical Chemistry B* **2001,** 105, (40), 9755-9771.

59. Koopal, L. K., Mineral hydroxides: from homogeneous to heterogeneous modelling. *Electrochim Acta* **1996,** 41, (14), 2293-2305.

60. Luuk, K. K., Ion adsorption on homogeneous and heterogeneous surfaces. In *Coagulation and Flocculation, Second Edition*, CRC Press: 2005; pp 217-348.

61. Lagaly, G.; Schulz, O.; Zimehl, R., *Dispersionen und Emulsionen*. Steinkopff: 2013.

62. Hiemenz, P. C.; Rajagopalan, R., *Principles of colloid and surface chemistry*. 3rd ed.; Marcel Dekker: New York, 1997; p xix, 650 p.

63. Ohshima, H., *Electrical phenomena at interfaces and biointerfaces: fundamentals and applications in nano-, bio-, and environmental sciences*. Wiley: 2012.

64. Stern, O., Zur Theorie der elektrolytischen Doppelschicht. *Zeitschrift für Elektrochemie und angewandte physikalische Chemie* **1924,** 30, (21-22), 508-516.

65. Ohshima, H., Surface charge density/surface potential relationship for a spherical colloidal particle in a solution of general electrolytes. *J Colloid Interf Sci* **1995,** 171, (2), 525-527.

66. Devlin, T. M., *Textbook of biochemistry : with clinical correlations*. 6th ed.; Wiley-Liss: Hoboken, N.J., 2006; p xxvii, 1208 p.

67. Horton, H. R., *Biochemie*. Pearson Studium: 2008.

68. Pelley, J. W.; Goljan, E. F., *Biochemistry*. 3rd ed.; Mosby/Elsevier: Philadelphia, PA, 2011; p xi, 186 p.

69. Wilson, K.; Walker, J. M., *Principles and techniques of biochemistry and molecular biology*. 7th ed.; Cambridge University Press: Cambridge, UK New York, 2009; p xvi, 744 p.

70. Humphrey, W.; Dalke, A.; Schulten, K., VMD: Visual molecular dynamics. *J Mol Graph Model* **1996,** 14, (1), 33-38.

71. Stryer, L., *Biochemistry*. 4th ed.; W.H. Freeman: New York, 1995; p xxxiv, 1064 p.

72. Christen, P.; Jaussi, R., *Biochemie: Eine Einführung mit 40 Lerneinheiten*. Springer: 2004.

73. Wiberg, E.; Wiberg, N., *Inorganic chemistry*. Academic Press: 2001.

74. Heimann, R. B., *Classic and advanced ceramics: From fundamentals to applications*. Wiley: 2010.

75. Pourbaix, M., *Atlas of electrochemicai equilibria in aqueous solutions*. 2d English ed.; National Association of Corrosion Engineers: Houston, Tex., 1974; p 644 p.

76. Lee, B. I.; Pope, E. J. A., *Chemical processing of ceramics*. Taylor & Francis: 1994.

77. Franks, G. V.; Gan, Y., Charging behavior at the alumina–water interface and implications for ceramic processing. *J Am Ceram Soc* **2007,** 90, (11), 3373-3388.

78. Kim, H. N.; Lee, S. K., Atomic structure and dehydration mechanism of amorphous silica: Insights from 29Si and 1H solid-state MAS NMR study of SiO2 nanoparticles. *Geochim Cosmochim Ac* **2013,** 120, (0), 39-64.

79. Diebold, U., The surface science of titanium dioxide. *Surf Sci Rep* **2003,** 48, (5–8), 53-229.

80. Hermanson, G. T., Chapter 13 - Silane coupling agents. In *Bioconjugate Techniques (Second Edition)*, Hermanson, G. T., Ed. Academic Press: New York, 2008; pp 562-581.

81. Hermanson, G. T., Chapter 14 - Microparticles and nanoparticles. In *Bioconjugate Techniques (Second Edition)*, Hermanson, G. T., Ed. Academic Press: New York, 2008; pp 582-626.

82. Hermanson, G. T., Chapter 28 - Bioconjugation in the study of protein interactions. In *Bioconjugate Techniques (Second Edition)*, Hermanson, G. T., Ed. Academic Press: New York, 2008; pp 1003-1039.

83. Hanefeld, U., Immobilisation of hydroxynitrile lyases. *Chem Soc Rev* **2013,** 42, (15), 6308-6321.

84. Hermanson, G. T., Chapter 3 - Zero-length crosslinkers. In *Bioconjugate Techniques (Second Edition)*, Hermanson, G. T., Ed. Academic Press: New York, 2008; pp 213-233.

85. Sheehan, J.; Cruickshank, P.; Boshart, G., Notes- a convenient synthesis of water-soluble carbodiimides. *The Journal of Organic Chemistry* **1961,** 26, (7), 2525-2528.

86. Sheehan, J. C.; Preston, J.; Cruickshank, P. A., A rapid synthesis of oligopeptide derivatives without isolation of intermediates. *J Am Chem Soc* **1965,** 87, (11), 2492-2493.

87. Bonfield, T. L.; John, N.; Barna, B. P.; Kavuru, M. S.; Thomassen, M. J.; Yen-Lieberman, B., Multiplexed particle-based anti-granulocyte macrophage colony stimulating factor assay used as pulmonary diagnostic test. *Clin Diagn Lab Immunol* **2005,** 12, (7), 821-4.

88. Staros, J. V., N-hydroxysulfosuccinimide active esters: bis(N-hydroxysulfosuccinimide) esters of two dicarboxylic acids are hydrophilic, membrane-impermeant, protein cross-linkers. *Biochemistry* **1982,** 21, (17), 3950-3955.

89. Carraway, K. L.; Triplett, R. B., Reaction of carbodiimides with protein sulfhydryl groups. *Biochimica et Biophysica Acta (BBA) - Protein Structure* **1970,** 200, (3), 564-566.

90. Carraway, K. L.; Koshland Jr, D. E., Reaction of tyrosine residues in proteins with carbodiimide reagents. *Biochimica et Biophysica Acta (BBA) - Protein Structure* **1968,** 160, (2), 272-274.

91. Lyklema, J., *Fundamentals of interface and colloid science: Soft colloids*. Elsevier Science: 2005.

92. Nakanishi, K.; Sakiyama, T.; Imamura, K., On the adsorption of proteins on solid surfaces, a common but very complicated phenomenon. *J Biosci Bioeng* **2001,** 91, (3), 233-44.

93. Vroman, L.; Adams, A. L., Identification of rapid changes at plasma-solid interfaces. *J Biomed Mater Res* **1969,** 3, (1), 43-67.

94. Adamczyk, Z., *Particles at interfaces : interactions, deposition, structure*. 1st ed.; Elsevier/ Academic Press: Amsterdam ; Boston, 2006; p xiii, 743 p.

95. Gray, C. J.; Weissenborn, M. J.; Eyers, C. E.; Flitsch, S. L., Enzymatic reactions on immobilised substrates. *Chem Soc Rev* **2013,** 42, (15), 6378-6405.

96. Vertegel, A. A.; Siegel, R. W.; Dordick, J. S., Silica nanoparticle size influences the structure and enzymatic activity of adsorbed lysozyme. *Langmuir* **2004,** 20, (16), 6800-7.

97. Puleo, D. A.; Bizios, R., *Biological interactions on materials surfaces : understanding and controlling protein, cell, and tissue responses*. Springer: Dordrecht ; London, 2009; p xx, 429 p.

98. Yang, S. T.; Liu, Y.; Wang, Y. W.; Cao, A., Biosafety and bioapplication of nanomaterials by designing protein-nanoparticle interactions. *Small* **2013,** 9, (9-10), 1635-53.

99. Baszkin, A.; Norde, W., *Physical chemistry of biological interfaces*. M. Dekker: New York, 2000; p ix, 836 p.

100. Rabe, M.; Verdes, D.; Seeger, S., Understanding protein adsorption phenomena at solid surfaces. *Adv Colloid Interface Sci* **2011,** 162, (1-2), 87-106.

101. Atkins, P. W.; De Paula, J., *Atkins' Physical chemistry*. 9th ed.; Oxford University Press: Oxford ; New York, 2010; p xxix, 972 p.

102. Langmuir, I., The adsorption of gases on plane surfaces of glass, mica and platinum. *J Am Chem Soc* **1918,** 40, (9), 1361-1403.

103. Bathen, D.; Breitbach, M., *Adsorptionstechnik*. Springer Berlin Heidelberg: 2001.

104. Feder, J., Random sequential adsorption. *J Theor Biol* **1980,** 87, (2), 237-254.

105. Derr, L.; Steckbeck, S.; Dringen, R.; Colombi Ciacchi, L.; Treccani, L.; Rezwan, K., Assessment of the proteolytic activity of α-chymotrypsin immobilized on colloidal particles by matrix-assisted laser desorption ionization time-of-flight mass spectrometry. *Anal Lett* **2014,** 48, (3), 424-441.

106. Zoungrana, T.; Findenegg, G. H.; Norde, W., Structure, stability, and activity of adsorbed enzymes. *J Colloid Interface Sci* **1997,** 190, (2), 437-48.

107. Gettens, R. T.; Bai, Z.; Gilbert, J. L., Quantification of the kinetics and thermodynamics of protein adsorption using atomic force microscopy. *J Biomed Mater Res A* **2005,** 72, (3), 246-57.

108. Lee, K. G.; Pillai, S. R.; Singh, S. R.; Willing, G. A., The investigation of protein A and salmonella antibody adsorption onto biosensor surfaces by atomic force microscopy. *Biotechnol Bioeng* **2008,** 99, (4), 949-59.

109. Schon, P.; Gorlich, M.; Coenen, M. J.; Heus, H. A.; Speller, S., Nonspecific protein adsorption at the single molecule level studied by atomic force microscopy. *Langmuir* **2007,** 23, (20), 9921-3.

110. Servoli, E.; Maniglio, D.; Aguilar, M. R.; Motta, A.; San Roman, J.; Belfiore, L. A.; Migliaresi, C., Quantitative analysis of protein adsorption via atomic force microscopy and surface plasmon resonance. *Macromol Biosci* **2008,** 8, (12), 1126-34.

111. Sakata, S.; Inoue, Y.; Ishihara, K., Quantitative evaluation of interaction force between functional groups in protein and polymer brush surfaces. *Langmuir* **2014,** 30, (10), 2745-51.

112. Stobiecka, M., Novel plasmonic field-enhanced nanoassay for trace detection of proteins. *Biosens Bioelectron* **2014,** 55, 379-85.

113. Dringen, R.; Koehler, Y.; Derr, L.; Tomba, G.; Schmidt, M. M.; Treccani, L.; Ciacchi, L. C.; Rezwan, K., Adsorption and reduction of glutathione disulfide on alpha-Al2O3 nanoparticles: experiments and modeling. *Langmuir* **2011,** 27, (15), 9449-9457.

114. Fleischer, C. C.; Payne, C. K., Secondary structure of corona proteins determines the cell surface receptors used by nanoparticles. *J Phys Chem B* **2014,** 118, (49), 14017-26.

115. Greenfield, N. J., Using circular dichroism spectra to estimate protein secondary structure. *Nat Protoc* **2006,** 1, (6), 2876-90.

116. Bhakta, S. A.; Evans, E.; Benavidez, T. E.; Garcia, C. D., Protein adsorption onto nanomaterials for the development of biosensors and analytical devices: A review. *Anal Chim Acta* **2015,** 872, 7-25.

117. Holtzhauer, M.; Behlke, J., *Methoden in der Proteinanalytik*. Springer: Berlin ; New York, 1996; p xxiv, 467 p.

118. Dukhin, A. S.; Goetz, P. J., *Studies in interface science*. Elsevier: Amsterdam, 2002; Vol. 15.

119. Dukhin, A. S.; Goetz, P. J., Acoustic and electroacoustic spectroscopy for characterizing concentrated dispersions and emulsions. *Adv Colloid Interface Sci* **2001,** 92, (1-3), 73-132.

120. Takata, Y.; Shimatsu, Y.; Nagahashi, T.; Miyayama, T.; Hyono, A.; Ohshima, H., Effect of ionic surfactants on ion vibration current and colloid vibration current. *Journal of oleo science* **2010,** 59, (8), 401-6.

121. Brien, R. W. O.; Wade, T. A.; Carasso, M. L.; Hunter, R. J.; Rowlands, W. N.; Beattie, J. K., Electroacoustic determination of droplet size and zeta potential in concentrated emulsions. In *Particle Size Distribution III*, American Chemical Society: 1998; Vol. 693, pp 311-319.

122. Dukhin, A. S.; Shilov, V. N.; Ohshima, H.; Goetz, P. J., Electroacoustic phenomena in concentrated dispersions: New theory and CVI experiment. *Langmuir* **1999,** 15, (20), 6692-6706.

123. Lowell, S., *Characterization of porous solids and powders: surface area, pore size and density*. Springer: 2004.

124. Harkins, W. D.; Jura, G.; Loeser, E. H., Surfaces of solids. XVI. adsorbed films of water and normal heptane on the surface of graphite. *J Am Chem Soc* **1946,** 68, (4), 554-557.

125. Brunauer, S.; Emmett, P. H.; Teller, E., Adsorption of gases in multimolecular layers. *J Am Chem Soc* **1938,** 60, (2), 309-319.

126. Smith, P. K.; Krohn, R. I.; Hermanson, G. T.; Mallia, A. K.; Gartner, F. H.; Provenzano, M. D.; Fujimoto, E. K.; Goeke, N. M.; Olson, B. J.; Klenk, D. C., Measurement of protein using bicinchoninic acid. *Anal Biochem* **1985,** 150, (1), 76-85.

127. Bundy, H. F., Chymotrypsin-catalyzed hydrolysis of N-acetyl- and N-benzoyl-l-tyrosine p-nitroanilides. *Archives of Biochemistry and Biophysics* **1963,** 102, (3), 416-422.

128. Dennison, C., *A guide to protein isolation*. Springer Netherlands: 2007.

129. Wiechelman, K. J.; Braun, R. D.; Fitzpatrick, J. D., Investigation of the bicinchoninic acid protein assay - identification of the groups responsible for color formation. *Anal Biochem* **1988,** 175, (1), 231-237.

130. Richter, G., *Praktische Biochemie: Grundlagen und Techniken ; 19 Tabellen*. Thieme: 2003.

131. Kumar, S.; Dar, K.; Ganno, S.; Hatano, H., Modification of isoleucine-16 acetylated delta-chymotrypsin. *J Biol Chem* **1975,** 250, (14), 5393-9.

132. Mekras, C. I.; George, M. H.; Barrie, J. A., Immobilization of alpha-chymotrypsin on poly(urethane-graft-acrylic acid). *Int J Biol Macromol* **1989,** 11, (2), 113-118.

133. Liao, F.; Liu, W. L.; Zhou, Q. X.; Zeng, Z. C.; Zuo, Y. P., Assay of serum arylesterase activity by fitting to the reaction curve with an integrated rate equation. *Clin Chim Acta* **2001,** 314, (1-2), 67-76.

134. Derr, L.; Dringen, R.; Treccani, L.; Hildebrand, N.; Ciacchi, L. C.; Rezwan, K., Physisorption of enzymatically active chymotrypsin on titania colloidal particles. *J Colloid Interf Sci* **2015,** 455, (0), 236-244.

135. Romanova, E. V.; Annangudi, S. P.; Sweedler, J. V., Mass spectroscopy of proteins. In *Encyclopedia of Neuroscience*, Squire, L. R., Ed. Academic Press: Oxford, 2009; pp 681-687.

136. Zenobi, R.; Knochenmuss, R., Ion formation in MALDI mass spectrometry. *Mass Spectrom Rev* **1998,** 17, (5), 337-366.

137. Sreerama, N.; Woody, R. W., Estimation of protein secondary structure from circular dichroism spectra: Comparison of CONTIN, SELCON, and CDSSTR methods with an expanded reference set. *Anal Biochem* **2000,** 287, (2), 252-260.

138. Baker, N. A.; Sept, D.; Joseph, S.; Holst, M. J.; McCammon, J. A., Electrostatics of nanosystems: application to microtubules and the ribosome. *Proc Natl Acad Sci U S A* **2001,** 98, (18), 10037-41.

139. Dolinsky, T. J.; Nielsen, J. E.; McCammon, J. A.; Baker, N. A., PDB2PQR: an automated pipeline for the setup of Poisson–Boltzmann electrostatics calculations. *Nucleic Acids Research* **2004,** 32, (suppl 2), W665-W667.

140. Krenkova, J.; Svec, F., Less common applications of monoliths: IV. Recent developments in immobilized enzyme reactors for proteomics and biotechnology. *Journal of Separation Science* **2009,** 32, (5-6), 706-718.

141. DiCosimo, R.; McAuliffe, J.; Poulose, A. J.; Bohlmann, G., Industrial use of immobilized enzymes. *Chem Soc Rev* **2013,** 42, (15), 6437-6474.

142. Hahn Berg, I. C.; Muller, D.; Arnebrant, T.; Malmsten, M., Ellipsometry and TIRF studies of enzymatic degradation of interfacial proteinaceous layers. *Langmuir* **2001,** 17, (5), 1641-1652.

143. Malmsten, M.; Larsson, A., Immobilization of trypsin on porous glycidyl methacrylate beads: effects of polymer hydrophilization. *Colloids Surf B Biointerfaces* **2000,** 18, (3-4), 277-284.

144. Mansson, R.; Frenning, G.; Malmsten, M., Factors affecting enzymatic degradation of microgel-bound peptides. *Biomacromolecules* **2013,** 14, (7), 2317-25.

145. Gagner, J. E.; Qian, X.; Lopez, M. M.; Dordick, J. S.; Siegel, R. W., Effect of gold nanoparticle structure on the conformation and function of adsorbed proteins. *Biomaterials* **2012,** 33, (33), 8503-8516.

146. Ponomareva, E. A.; Kartuzova, V. E.; Vlakh, E. G.; Tennikova, T. B., Monolithic bioreactors: Effect of chymotrypsin immobilization on its biocatalytic properties. *Journal of Chromatography B* **2010,** 878, (5–6), 567-574.

147. Bess, E.; Cavin, R.; Ma, K.; Ong, J. L., Protein adsorption and osteoblast responses to heat-treated titanium surfaces. *Implant dentistry* **1999,** 8, (2), 126-32.

148. Ellingsen, J. E., A study on the mechanism of protein adsorption to TiO2. *Biomaterials* **1991,** 12, (6), 593-6.

149. Klinger, A.; Steinberg, D.; Kohavi, D.; Sela, M. N., Mechanism of adsorption of human albumin to titanium in vitro. *J Biomed Mater Res* **1997,** 36, (3), 387-92.

150. Tiginyanu, I. M.; Lupan, O.; Ursaki, V. V.; Chow, L.; Enachi, M., 3.11 - Nanostructures of metal oxides. In *Comprehensive Semiconductor Science and Technology*, Kamimura, P. B. F., Ed. Elsevier: Amsterdam, 2011; pp 396-479.

151. Topoglidis, E.; Cass, A. E.; Gilardi, G.; Sadeghi, S.; Beaumont, N.; Durrant, J. R., Protein adsorption on nanocrystalline TiO(2) films: an immobilization strategy for bioanalytical devices. *Anal Chem* **1998,** 70, (23), 5111-3.

152. da Costa, J. P.; Oliveira-Silva, R.; Daniel-da-Silva, A. L.; Vitorino, R., Bionanoconjugation for proteomics applications — an overview. *Biotechnol Adv* **2014,** 32, (5), 952-970.

153. Bardsley, W. G.; Leff, P.; Kavanagh, J.; Waight, R. D., Deviations from Michaelis-Menten kinetics. The possibility of complicated curves for simple kinetic schemes and the computer fitting of

experimental data for acetylcholinesterase, acid phosphatase, adenosine deaminase, arylsulphatase, benzylamine oxidase, chymotrypsin, fumarase, galactose dehydrogenase, beta-galactosidase, lactate dehydrogenase, peroxidase and xanthine oxidase. *Biochem J* **1980,** 187, (3), 739-65.

154. Grime, J. K.; Lockhart, K.; Tan, B., The enthalpimetric determination of the Michaelis constant of the alpha-chymotrypsin-catalysed hydrolysis of N-acetyl-l-tyrosine ethyl ester based on the integrated Michaelis--Menten equation. *Anal Chim Acta* **1977,** 91, (2), 245-50.

155. Shimamoto, N.; Fukutome, H., Substituent effects on substrate activation and Michaelis-Menten Kinetic parameters in the alpha-chymotrypsin-catalyzed hydrolysis of phenyl acetates. *J Biochem* **1975,** 78, (4), 663-71.

156. Liu, P.; Shang, L.; Li, H.; Cui, Y.; Qin, Y.; Wu, Y.; Hiltunen, J. K.; Chen, Z.; Shen, J., Synthesis of fluorescent [small alpha]-chymotrypsin A-functionalized gold nanoclusters and their application to blot-based technology for Hg2+ detection. *Rsc Adv* **2014,** 4, (60), 31536-31543.

157. Kim, D.; Herr, A. E., Protein immobilization techniques for microfluidic assays. *Biomicrofluidics* **2013,** 7, (4), 41501.

158. Meder, F.; Daberkow, T.; Treccani, L.; Wilhelm, M.; Schowalter, M.; Rosenauer, A.; Madler, L.; Rezwan, K., Protein adsorption on colloidal alumina particles functionalized with amino, carboxyl, sulfonate and phosphate groups. *Acta Biomater* **2012,** 8, (3), 1221-1229.

159. Hidber, P. C. Zusammenhang von Struktur und Wirkung von Carbonsäuren als Verflüssiger für wässrige α-Aluminiumoxidsuspensionen. ETH Zurich Switzerland, Zurich, 1993.

160. Lowell, S., *Characterization of porous solids and powders surface area, pore size, and density*. Kluwer Academic Publishers: Dordrecht; Boston, 2004.

161. Demaneche, S.; Chapel, J. P.; Monrozier, L. J.; Quiquampoix, H., Dissimilar pH-dependent adsorption features of bovine serum albumin and alpha-chymotrypsin on mica probed by AFM. *Colloid Surface B* **2009,** 70, (2), 226-231.

162. Caldararu, H.; Timmins, G. S.; Davies, M. J.; Gilbert, B. C., Dynamics of spin-labelled alpha-chymotrypsin in reverse micelles of differently charged surfactants. *J Chem Soc Faraday T* **1996,** 92, (17), 3151-3155.

163. Ui, N., Isoelectric points and conformation of proteins .2. Isoelectric focusing of alpha-chymotrypsin and its inactive derivative. *Biochimica Et Biophysica Acta* **1971,** 229, (3), 582-&.

164. Cole, D. J.; Payne, M. C.; Ciacchi, L. C., Water structuring and collagen adsorption at hydrophilic and hydrophobic silicon surfaces. *Phys Chem Chem Phys* **2009,** 11, (48), 11395-9.

165. Schneider, J.; Ciacchi, L. C., Specific material recognition by small peptides mediated by the interfacial solvent structure. *J Am Chem Soc* **2012,** 134, (4), 2407-13.

166. Hildebrand, N.; Köppen, S.; Derr, L.; Li, K.; Koleini, M.; Rezwan, K.; Colombi Ciacchi, L., Adsorption orientation and binding motifs of lysozyme and chymotrypsin on amorphous silica. *The Journal of Physical Chemistry C* **2015,** 119, (13), 7295-7307.

167. Wei, J.; Igarashi, T.; Okumori, N.; Maetani, T.; Liu, B.; Yoshinari, M., Influence of surface wettability on competitive protein adsorption and initial attachment of osteoblasts. *Biomed Mater* **2009,** 4, (4), 045002.

168. Kondo, A.; Higashitani, K., Adsorption of model proteins with wide variation in molecular properties on colloidal particles. *J Colloid Interf Sci* **1992,** 150, (2), 344-351.

169. Lele, B. S.; Russell, A. J., Rational protein modification leading to resistance of enzymes to TiO2-UV irradiation-induced inactivation. *Biomacromolecules* **2004,** 5, (5), 1947-55.

170. Lele, B. S.; Russell, A. J., Enhancing enzyme stability against TiO2-UV induced inactivation. *Biomacromolecules* **2005,** 6, (1), 475-82.

171. Ju, H. Y.; Kuo, C. H.; Too, J. R.; Huang, H. Y.; Twu, Y. K.; Chang, C. M. J.; Liu, Y. C.; Shieh, C. J., Optimal covalent immobilization of alpha-chymotrypsin on Fe3O4-chitosan nanoparticles. *J Mol Catal B-Enzym* **2012,** 78, 9-15.

172. Rao, R. S.; Borkar, P. S.; Khobragade, C. N.; Sagar, A. D., Enzymatic activities of proteases immobilized on tri(4-formyl phenoxy) cyanurate. *Enzyme Microb Tech* **2006,** 39, (4), 958-962.

173. Specht, B. U.; Brendel, W., Preparation and properties of trypsin and chymotrysin coupled covalently to poly (N-vinylpyrrolidone). *Biochim Biophys Acta* **1977,** 484, (1), 109-14.

174. Tanizawa, K.; Bender, M. L., The application of insolubilized alpha-chymotrypsin to kinetic studies on the effect of aprotic dipolar organic solvents. *J Biol Chem* **1974,** 249, (7), 2130-4.

175. Shtelzer, S.; Rappoport, S.; Avnir, D.; Ottolenghi, M.; Braun, S., Properties of trypsin and of acid phosphatase immobilized in sol-gel glass matrices. *Biotechnol Appl Bioc* **1992,** 15, (3), 227-235.

176. Saha, B.; Saikia, J.; Das, G., Correlating enzyme density, conformation and activity on nanoparticle surfaces in highly functional bio-nanocomposites. *Analyst* **2015,** 140, (2), 532-542.

177. Wei, Y.; Thyparambil, A. A.; Latour, R. A., Quantification of the influence of protein-protein interactions on adsorbed protein structure and bioactivity. *Colloids and Surfaces B: Biointerfaces* **2013,** 110, (0), 363-371.

178. Li, J.; Wang, J. Q.; Gavalas, V. G.; Atwood, D. A.; Bachas, L. G., Alumina-pepsin hybrid nanoparticles with orientation-specific enzyme coupling. *Nano Lett.* **2003,** 3, (1), 55-58.

179. Xiao, P.; Lv, X. F.; Deng, Y. L., Immobilization of chymotrypsin on silica beads based on high affinity and specificity aptamer and its applications. *Anal Lett* **2012,** 45, (10), 1264-1273.

180. Ansari, S. A.; Husain, Q., Potential applications of enzymes immobilized on/in nano materials: A review. *Biotechnol Adv* **2012,** 30, (3), 512-523.

181. Guisan, J. M.; Bastida, A.; Cuesta, C.; Fernandezlafuente, R.; Rosell, C. M., Immobilization stabilization of alpha-chymotrypsin by covalent attachment to aldehyde agarose gels. *Biotechnol Bioeng* **1991,** 38, (10), 1144-1152.

182. Prikryl, P.; Lenfeld, J.; Horak, D.; Ticha, M.; Kucerova, Z., Magnetic bead cellulose as a suitable support for immobilization of alpha-chymotrypsin. *Appl Biochem Biotech* **2012,** 168, (2), 295-305.

183. Sustrova, B.; Novotna, L.; Kucerova, Z.; Ticha, M., Immobilization of alpha-chymotrypsin to magnetic particles and their use for proteolytic cleavage of porcine pepsin A. *J Mol Catal B-Enzym* **2009,** 60, (1-2), 22-28.

184. Rabe, M.; Verdes, D.; Seeger, S., Understanding cooperative protein adsorption events at the microscopic scale: A comparison between experimental data and Monte Carlo simulations. *Journal of Physical Chemistry B* **2010,** 114, (17), 5862-5869.

185. Rabe, M.; Verdes, D.; Seeger, S., Understanding protein adsorption phenomena at solid surfaces. *Adv Colloid Interfac* **2011,** 162, (1-2), 87-106.

186. Meder, F.; Hintz, H.; Koehler, Y.; Schmidt, M. M.; Treccani, L.; Dringen, R.; Rezwan, K., Adsorption and orientation of the physiological extracellular peptide glutathione disulfide on surface functionalized colloidal alumina particles. *J Am Chem Soc* **2013,** 135, (16), 6307-6316.

187. Schmidt, M. M.; Koehler, Y.; Derr, L.; Treccani, L.; Rezwan, K.; Dringen, R., Interaction of the physiological tripeptide glutathione with colloidal alumina particles. *The Journal of Physical Chemistry C* **2012,** 116, (43), 23136-23142.

188. Keighron, J. D.; Keating, C. D., Enzyme:nanoparticle bioconjugates with two sequential enzymes: stoichiometry and activity of malate dehydrogenase and citrate synthase on Au nanoparticles. *Langmuir* **2010,** 26, (24), 18992-19000.

189. Rusmini, F.; Zhong, Z.; Feijen, J., Protein immobilization strategies for protein biochips. *Biomacromolecules* **2007,** 8, (6), 1775-89.

190. Hermanson, G. T., *Bioconjugate techniques*. 2nd edition ed.; Elsevier: 2008.

191. Brash, J. L.; Wojciechowski, P. W., *Interfacial phenomena and bioproducts*. Marcel Dekker: New York, 1996; p xi, 510 p.

192. Chen, D. H.; Caruso, R. A., Recent progress in the synthesis of spherical titania nanostructures and their applications. *Adv Funct Mater* **2013,** 23, (11), 1356-1374.

193. De, M.; Ghosh, P. S.; Rotello, V. M., Applications of nanoparticles in biology. *Adv Mater* **2008,** 20, (22), 4225-4241.

194. Elaissari, A., *Colloidal nanoparticles in biotechnology*. Wiley-Interscience: Hoboken, N.J., 2008; p xiii, 358 p., 8 p. of plates.

195. Tehrani, F. M. K.; Rashidzadeh, M.; Nemati, A.; Irandoukht, A.; Faridnia, B., Characterization and photocatalytic activities of nanosized titanium dioxide thin films. *Int J Environ Sci Te* **2011,** 8, (3), 545-552.

196. An, S.; Lee, M. W.; Joshi, B. N.; Jo, A.; Jung, J.; Yoon, S. S., Water purification and toxicity control of chlorophenols by 3D nanofiber membranes decorated with photocatalytic titania nanoparticles. *Ceram Int* **2014,** 40, (2), 3305-3313.

197. Das, S. K.; Khan, M. M. R.; Parandhaman, T.; Laffir, F.; Guha, A. K.; Sekarana, G.; Mandal, A. B., Nano-silica fabricated with silver nanoparticles: antifouling adsorbent for efficient dye removal, effective water disinfection and biofouling control. *Nanoscale* **2013,** 5, (12), 5549-5560.

198. Likodimos, V.; Dionysiou, D. D.; Falaras, P., CLEAN WATER: water detoxification using innovative photocatalysts. *Rev Environ Sci Bio* **2010,** 9, (2), 87-94.

199. Liu, J. B.; Wang, Z. M.; Luo, Z. P.; Bashir, S., Effective bactericidal performance of silver-decorated titania nano-composites. *Dalton T* **2013,** 42, (6), 2158-2166.

200. Sharif, A.; Koolivand, H.; Khanbabaie, G.; Hemmati, M.; Aalaie, J.; Kashani, M. R.; Gheshlaghi, A., Improvement of CO2/CH4 separation characteristics of polyethersulfone by modifying with polydimethylsiloxane and nano-silica. *J Polym Res* **2012,** 19, (7).

201. De Persiis, F.; La Mesa, C.; Pons, R., Protein-covered silica nano-particles adsorbing onto synthetic vesicles. *Soft Matter* **2012,** 8, (5), 1361-1368.

202. He, Q. J.; Shi, J. L., Mesoporous silica nanoparticle based nano drug delivery systems: synthesis, controlled drug release and delivery, pharmacokinetics and biocompatibility. *J Mater Chem* **2011,** 21, (16), 5845-5855.

203. Jang, H. D.; Kil, D. S.; Chang, H.; Cho, K.; Kim, S. K.; Oh, K. J.; Choi, J. H., Preparation of nanoporous SiO2 particles and their application in drug release control. *J Nanosci Nanotechno* **2011,** 11, (5), 4169-4173.

204. Norde, W.; Giacomelli, C. E., BSA structural changes during homomolecular exchange between the adsorbed and the dissolved states. *J Biotechnol* **2000,** 79, (3), 259-268.

205. Ammann, R. W.; Tagwecher, E.; Kashiwagi, H.; Rosenmund, H., Diagnostic value of fecal chymotrypsin and trypsin assessment for detection of pancreatic disease. A comparative study. *The American journal of digestive diseases* **1968,** 13, (2), 123-46.

206. Remtulla, M. A.; Durie, P. R.; Goldberg, D. M., Stool chymotrypsin activity measured by a spectrophotometric procedure to identify pancreatic disease in infants. *Clin Biochem* **1986,** 19, (6), 341-7.

207. Wald, M.; Olejar, T.; Sebkova, V.; Zadinova, M.; Boubelik, M.; Pouckova, P., Mixture of trypsin, chymotrypsin and papain reduces formation of metastases and extends survival time of C57Bl6 mice with syngeneic melanoma B16. *Cancer Chemother Pharmacol* **2001,** 47 S16-22.

208. Zhu, R. R.; Wang, W. R.; Sun, X. Y.; Liu, H.; Wang, S. L., Enzyme activity inhibition and secondary structure disruption of nano-TiO2 on pepsin. *Toxicol in Vitro* **2010,** 24, (6), 1639-47.

209. Thyparambil, A. A.; Wei, Y.; Latour, R. A., Experimental characterization of adsorbed protein orientation, conformation, and bioactivity. *Biointerphases* **2015,** 10, (1), 019002.

210. Norde, W., Adsorption of proteins from solution at the solid-liquid interface. *Adv Colloid Interfac* **1986,** 25, (4), 267-340.

211. Maffre, P.; Nienhaus, K.; Amin, F.; Parak, W. J.; Nienhaus, G. U., Characterization of protein adsorption onto FePt nanoparticles using dual-focus fluorescence correlation spectroscopy. *Beilstein Journal of Nanotechnoiogy* **2011,** 2, 374-383.

212. Rocker, C.; Potzl, M.; Zhang, F.; Parak, W. J.; Nienhaus, G. U., A quantitative fluorescence study of protein monolayer formation on colloidal nanoparticles. *Nat Nano* **2009,** 4, (9), 577-580.

213. Welzel, P. B., Investigation of adsorption-induced structural changes of proteins at solid/liquid interfaces by differential scanning calorimetry. *Thermochim Acta* **2002,** 382, (1–2), 175-188.

214. Compton, S. J.; Jones, C. G., Mechanism of dye response and interference in the Bradford protein assay. *Anal Biochem* **1985,** 151, (2), 369-374.

215. Reisner, A. H.; Nemes, P.; Bucholtz, C., Use of Coomassie Brilliant Blue G250 perchloric-acid solution for staining in electrophoresis and isoelectric focusing on polyacrylamide gels. *Anal Biochem* **1975,** 64, (2), 509-516.

216. Serro, A. P.; Degiampietro, K.; Colaco, R.; Saramago, B., Adsorption of albumin and sodium hyaluronate on UHMWPE: A QCM-D and AFM study. *Colloid Surface B* **2010,** 78, (1), 1-7.

217. Jones, E.; Oliphant, E.; Peterson, P. SciPy: Open source scientific tools for Python. (09-24),

218. Case, D. A.; Cheatham, T. E.; Darden, T.; Gohlke, H.; Luo, R.; Merz, K. M.; Onufriev, A.; Simmerling, C.; Wang, B.; Woods, R. J., The Amber biomolecular simulation programs. *Journal of Computational Chemistry* **2005,** 26, (16), 1668-1688.

219. Frey, P. A.; Whitt, S. A.; Tobin, J. B., A low-barrier hydrogen-bond in the catalytic triad of serine proteases. *Science* **1994,** 264, (5167), 1927-1930.

220. Jorgensen, W. L.; Chandrasekhar, J.; Madura, J. D.; Impey, R. W.; Klein, M. L., Comparison of simple potential functions for simulating liquid water. *The Journal of Chemical Physics* **1983,** 79, (2), 926-935.

221. Cole, D. J.; Payne, M. C.; Csanyi, G.; Spearing, S. M.; Colombi Ciacchi, L., Development of a classical force field for the oxidized Si surface: application to hydrophilic wafer bonding. *J Chem Phys* **2007,** 127, (20), 204704.

222. Butenuth, A.; Moras, G.; Schneider, J.; Koleini, M.; Köppen, S.; Meißner, R.; Wright, L. B.; Walsh, T. R.; Ciacchi, L. C., Ab initio derived force-field parameters for molecular dynamics simulations of deprotonated amorphous-SiO2/water interfaces. *physica status solidi (b)* **2012,** 249, (2), 292-305.

223. The surface properties of silicas. In Legrand, A. P., Ed. John Wiley & Sons: Chichester :, 1998.

224. Dove, P. M.; Craven, C. M., Surface charge density on silica in alkali and alkaline earth chloride electrolyte solutions. *Geochim Cosmochim Ac* **2005,** 69, (21), 4963-4970.

225. Kobayashi, M.; Juillerat, F.; Galletto, P.; Bowen, P.; Borkovec, M., Aggregation and charging of colloidal silica particles: effect of particle size. *Langmuir* **2005,** 21, (13), 5761-9.

226. Sonnefeld, J.; Göbel, A.; Vogelsberger, W., Surface charge density on spherical silica particles in aqueous alkali chloride solutions. *Colloid Polym Sci* **1995,** 273, (10), 926-931.

227. Salameh, S.; Schneider, J.; Laube, J.; Alessandrini, A.; Facci, P.; Seo, J. W.; Ciacchi, L. C.; Madler, L., Adhesion mechanisms of the contact interface of TiO2 nanoparticles in films and aggregates. *Langmuir* **2012,** 28, (31), 11457-64.

228. Hiemstra, T.; De Wit, J. C. M.; Van Riemsdijk, W. H., Multisite proton adsorption modeling at the solid/solution interface of (hydr)oxides: A new approach: II. Application to various important (hydr)oxides. *J Colloid Interf Sci* **1989,** 133, (1), 105-117.

229. Köppen, S.; Langel, W., Simulation of the interface of (100) rutile with aqueous ionic solution. *Surf Sci* **2006,** 600, (10), 2040-2050.

230. Schneider, J.; Ciacchi, L. C., First principles and classical modeling of the oxidized titanium (0001) surface. *Surf Sci* **2010,** 604, (13–14), 1105-1115.

231. Schneider, J.; Ciacchi, L. C., A classical potential to model the adsorption of biological molecules on oxidized titanium surfaces. *Journal of Chemical Theory and Computation* **2010,** 7, (2), 473-484.

232. Onufriev, A.; Bashford, D.; Case, D. A., Exploring protein native states and large-scale conformational changes with a modified generalized born model. *Proteins* **2004,** 55, (2), 383-94.

233. Pronk, S.; Páll, S.; Schulz, R.; Larsson, P.; Bjelkmar, P.; Apostolov, R.; Shirts, M. R.; Smith, J. C.; Kasson, P. M.; van der Spoel, D.; Hess, B.; Lindahl, E., GROMACS 4.5: a high-throughput and highly parallel open source molecular simulation toolkit. *Bioinformatics* **2013,** 29, (7), 845-854.

234. Hess, B., P-LINCS: A parallel linear constraint solver for molecular simulation. *Journal of Chemical Theory and Computation* **2007,** 4, (1), 116-122.

235. Bussi, G.; Donadio, D.; Parrinello, M., Canonical sampling through velocity rescaling. *J Chem Phys* **2007,** 126, (1), 014101.

236. Kabsch, W.; Sander, C., Dictionary of protein secondary structure - pattern-recognition of hydrogen-bonded and geometrical features. *Biopolymers* **1983,** 22, (12), 2577-2637.

237. Li, S.; Wan, Q.; Qin, Z.; Fu, Y.; Gu, Y., Understanding Stober silica's pore characteristics measured by gas adsorption. *Langmuir* **2015,** 31, (2), 824-32.

238. Mitra, A.; Bhaumik, A.; Imae, T., Synthesis and characterization of nanoporous silica using dendrimer molecules. *J Nanosci Nanotechno* **2004,** 4, (8), 1052-1055.

239. Chan, B. M. C.; Brash, J. L., Conformational change in fibrinogen desorbed from glass-surface. *J Colloid Interf Sci* **1981,** 84, (1), 263-265.

240. Brash, J. L.; Samak, Q. M., Dynamics of interactions between human-albumin and polyethylene surface. *J Colloid Interf Sci* **1978,** 65, (3), 495-504.

241. Schneider, J.; Colombi Ciacchi, L., Specific material recognition by small peptides mediated by the interfacial solvent structure. *J Am Chem Soc* **2012,** 134, (4), 2407-2413.

242. Bentaleb, A.; Ball, V.; Haikel, Y.; Voegel, J. C.; Schaaf, P., Kinetics of the homogeneous exchange of lysozyme adsorbed on a titanium oxide surface. *Langmuir* **1997,** 13, (4), 729-735.

243. Felsovalyi, F.; Mangiagalli, P.; Bureau, C.; Kumar, S. K.; Banta, S., Reversibility of the adsorption of lysozyme on silica. *Langmuir* **2011,** 27, (19), 11873-82.

244. Chiti, F.; Dobson, C. M., Amyloid formation by globular proteins under native conditions. *Nat Chem Biol* **2009,** 5, (1), 15-22.

245. Haynes, C. A.; Norde, W., Structures and stabilities of adsorbed proteins. *J Colloid Interf Sci* **1995,** 169, (2), 313-328.

246. Kleijn, M.; Norde, W., The adsorption of proteins from aqueous solution on solid surfaces. *Heterogen Chem Rev* **1995,** 2, (3), 157-172.

247. Nakanishi, K.; Sakiyama, T.; Imamura, K., On the adsorption of proteins on solid surfaces, a common but very complicated phenomenon. *J Biosci Bioeng* **2001,** 91, (3), 233-244.

248. Roach, P.; Farrar, D.; Perry, C. C., Interpretation of protein adsorption: Surface-induced conformational changes. *J Am Chem Soc* **2005,** 127, (22), 8168-8173.

249. Sigler, P. B.; Blow, D. M.; Matthews, B. W.; Henderson, R., Structure of crystalline - chymotrypsin. II. A preliminary report including a hypothesis for the activation mechanism. *J Mol Biol* **1968,** 35, (1), 143-64.

250. Martin, C. J.; Marini, M. A., Spectral detection of the reaction of formaldehyde with the histidine residues of alpha-chymotrypsin. *J Biol Chem* **1967,** 242, (24), 5736-43.

251. Barquero-Quiros, M.; Dominguez-Renedo, O.; Alonso-Lomillo, M. A.; Arcos-Martinez, M. J., Biosensor for aluminium(III) based on its inhibition of alpha-chymotrypsin immobilized on a screen-printed carbon electrode modified with gold nanoparticles. *Microchim Acta* **2012,** 179, (1-2), 65-70.

252. Bhat, M. K., Cellulases and related enzymes in biotechnology. *Biotechnol Adv* **2000,** 18, (5), 355-383.

253. Meyer, A. S.; Isaksen, A., Application of enzymes as food antioxidants. *Trends Food Sci Tech* **1995,** 6, (9), 300-304.

254. Vellard, M., The enzyme as drug: application of enzymes as pharmaceuticals. *Curr Opin Biotech* **2003,** 14, (4), 444-450.

255. Sheldon, R. A., Enzyme immobilization: The quest for optimum performance. *Adv Synth Catal* **2007,** 349, (8-9), 1289-1307.

256. Rivera, J. G.; Messersmith, P. B., Polydopamine-assisted immobilization of trypsin onto monolithic structures for protein digestion. *Journal of Separation Science* **2012,** 35, (12), 1514-1520.

257. Yamaguchi, H.; Miyazaki, M.; Kawazumi, H.; Maeda, H., Multidigestion in continuous flow tandem protease-immobilized microreactors for proteomic analysis. *Anal Biochem* **2010,** 407, (1), 12-18.

258. Celikbicak, O.; Atakay, M.; Guler, U.; Salih, B., A trypsin immobilized sol-gel for protein identification in MALDi-MS application. *Anal Lett* **2013,** 47, (4), 707-719.

259. Jeng, J. Y.; Lin, M. F.; Cheng, F. Y.; Yeh, C. S.; Shiea, J. T., Using high-concentration trypsin-immobilized magnetic nanoparticles for rapid in situ protein digestion at elevated temperature. *Rapid Commun Mass Sp* **2007,** 21, (18), 3060-3068.

260. Lin, S.; Yun, D. J.; Qi, D.; Deng, C.; Li, Y.; Zhang, X., Novel microwave-assisted digestion by trypsin-immobilized magnetic nanoparticles for proteome ananlysis. *Journal of Proteome Research* **2007,** 7, 1297-1307.

261. Xu, X. Q.; Deng, C. H.; Yang, P. Y.; Zhang, X. M., Immobilization of trypsin on superparamagnetic nanoparticles for rapid and effective proteolysis. *J Proteome Res* **2007,** 6, (9), 3849-3855.

262. Bergmeyer, H. U., *Methods of enzymatic analysis*. 2d English ed.; Verlag Chemie ; Academic Press: Weinheim New York, 1974; p 4 v.

263. Daberkow, T.; Meder, F.; Treccani, L.; Schowalter, M.; Rosenauer, A.; Rezwan, K., Fluorescence labeling of colloidal core-shell particles with defined isoelectric points for in vitro studies. *Acta Biomater* **2012,** 8, (2), 720-727.

264. Walker, J. M., *The protein protocols handbook*. 2nd ed.; Humana Press: Totowa, N.J., 2002; p xxiv, 1146 p.

265. Xiao, P.; Lv, X. F.; Man, Y.; Qing, H.; Li, Q.; Deng, Y. L., Rapid and efficient proteolysis for protein analysis by an aptamer-based immobilized chymotrypsin microreactor. *Anal Lett* **2013,** 46, (5), 868-878.

266. Hong, J.; Gong, P. J.; Xu, D. M.; Dong, L.; Yao, S. D., Stabilization of alpha-chymotrypsin by covalent immobilization on amine-functionalized superparamagnetic nanogel. *J Biotechnol* **2007,** 128, (3), 597-605.

267. Switzar, L.; Giera, M.; Niessen, W. M., Protein digestion: an overview of the available techniques and recent developments. *J Proteome Res* **2013,** 12, (3), 1067-77.

268. Temporini, C.; Calleri, E.; Campese, D.; Cabrera, K.; Felix, G.; Massolini, G., Chymotrypsin immobilization on epoxy monolithic silica columns: development and characterization of a bioreactor for protein digestion. *J Sep Sci* **2007,** 30, (17), 3069-76.

269. Silva, A. M. N.; Marcal, S. L.; Vitorino, R.; Domingues, M. R. M.; Domingues, P., Characterization of in vitro protein oxidation using mass spectrometry: A time course study of oxidized alpha-amylase. *Archives of Biochemistry and Biophysics* **2013,** 530, (1), 23-31.

270. Liu, A. L.; Zhou, T.; He, F. Y.; Xu, J. J.; Lu, Y.; Chen, H. Y.; Xia, X. H., Off-line form of the Michaelis-Menten equation for studying the reaction kinetics in a polymer microchip integrated with enzyme microreactor. *Lab Chip* **2006,** 6, (6), 811-818.

271. Jiang, H. H.; Zou, H. F.; Wang, H. L.; Ni, J. Y.; Zhang, Q.; Zhang, Y. K., On-line characterization of the activity and reaction kinetics of immobilized enzyme by high-performance frontal analysis. *J Chromatogr A* **2000,** 903, (1-2), 77-84.

272. Abd El-Ghaffar, M. A.; Hashem, M. S., Calcium alginate beads encapsulated PMMA-g-CS nano-particles for alpha-chymotrypsin immobilization. *Carbohyd Polym* **2013,** 92, (2), 2095-2102.

273. Bizzozero, S. A.; Baumann, W. K.; Dutler, H., Kinetic investigation of the alpha-chymotrypsin-catalyzed hydrolysis of peptide-ester substrates. The relationship between the structure of the peptide moiety and reactivity. *Eur J Biochem* **1975,** 58, (1), 167-76.

274. Farmer, D. A.; Hageman, J. H., Use of N-benzoyl-L-tyrosine thiobenzyl ester as a protease substrate - hydrolysis by alpha-chymotrypsin and subtilisin bpn'. *J Biol Chem* **1975,** 250, (18), 7366-7371.

275. Hortin, G. L., The MALDI-TOF mass spectrometric view of the plasma proteome and peptidome. *Clin Chem* **2006,** 52, (7), 1223-1237.

276. Anderson, E.; Sze, K. W. C.; Sathe, S. K., New colorimetric method for the detection and quantitation of proteolytic-enzyme activity. *J Agr Food Chem* **1995,** 43, (6), 1530-1534.

277. Fan, H. L.; Jiang, X. H.; Zhang, T.; Jin, Q. H., Peptide-induced fluorescence quenching of conjugated polyelectrolyte for label-free, ultrasensitive and selective assay of protease activity. *Biosens Bioelectron* **2012,** 34, (1), 221-226.

278. Stuart, B. H., *Infrared spectroscopy: Fundamentals and applications*. Wiley: 2004.

279. Meder, F.; Brandes, C.; Treccani, L.; Rezwan, K., Controlling protein-particle adsorption by surface tailoring colloidal alumina particles with sulfonate groups. *Acta Biomater* **2013,** 9, (3), 5780-7.

# Curriculum vitae

| | |
|---|---|
| First name: | Ludmilla |
| Surname: | Derr |
| Date of birth: | March 25th 1984 |
| Place of birth: | Koktschetaw, Kazakhstan |

## *Education*

| | |
|---|---|
| 10/2004 - 09/2009 | Dipl.-Chem., Chemistry Studies, University of Technology Carolo-Wilhelmina zu Braunschweig, Braunschweig, Germany |
| 08/2001 - 06/2004 | German Highschool Graduation, Raabeschule Gymnasium, Braunschweig, Germany |
| 09/1998 - 06/2001 | Realschule Schöppenstedt, Schöppenstedt, Germany |
| 09/1991 - 05/1998 | Integrated school no. 1 in Koktschetaw, Kazakhstan |

## *Research Experience*

| | |
|---|---|
| 02/2010 - current | PhD student, University of Bremen, Department of Production Engineering, Advanced Ceramics Group, Head: Prof. K. Rezwan, Bremen, Germany |
| 04/2009 - 09/2009 | Diploma thesis "Funktionelle Partikelmodifizierung und Charakterisierung", Fraunhofer Institute for Wood Research Wilhelm-Klauditz Institute, Head: Prof. Dr. Marutzky, Braunschweig, Germany |
| 12/2001 - 01/2010 | Research Assistant, Fraunhofer Institute for Wood Research Wilhelm-Klauditz Institute in the Departments "Surface Technology" and "Building & Construction", Braunschweig, Germany |

# Online-Buchshop für Ingenieure

**VDI nachrichten** **BUCHSHOP**

Online-Shops

**Fachliteratur und mehr - jetzt bequem online recherchieren & bestellen unter: www.vdi-nachrichten.com/Der-Shop-im-Ueberblick**


**Täglich aktualisiert: Neuerscheinungen VDI-Schriftenreihen**

Im Buchshop von vdi-nachrichten.com finden Ingenieure und Techniker ein speziell auf sie zugeschnittenes, umfassendes Literaturangebot.

Mit der komfortablen Schnellsuche werden Sie in den VDI-Schriftenreihen und im Verzeichnis lieferbarer Bücher unter 1.000.000 Titeln garantiert fündig.

Im Buchshop stehen für Sie bereit:

**VDI-Berichte** und die Reihe **Kunststofftechnik:**

Berichte nationaler und internationaler technischer Fachtagungen der VDI-Fachgliederungen

**Fortschritt-Berichte VDI:**

Dissertationen, Habilitationen und Forschungsberichte aus sämtlichen ingenieurwissenschaftlichen Fachrichtungen

**Newsletter „Neuerscheinungen":**

Kostenfreie Infos zu aktuellen Titeln der VDI-Schriftenreihen bequem per E-Mail

**Autoren-Service:**

Umfassende Betreuung bei der Veröffentlichung Ihrer Arbeit in der Reihe Fortschritt-Berichte VDI

**Buch- und Medien-Service:**

Beschaffung aller am Markt verfügbaren Zeitschriften, Zeitungen, Fortsetzungsreihen, Handbücher, Technische Regelwerke, elektronische Medien und vieles mehr – einzeln oder im Abo und mit weltweitem Lieferservice

## Die Reihen der Fortschritt-Berichte VDI:

1 Konstruktionstechnik/Maschinenelemente
2 Fertigungstechnik
3 Verfahrenstechnik
4 Bauingenieurwesen
5 Grund- und Werkstoffe/Kunststoffe
6 Energietechnik
7 Strömungstechnik
8 Mess-, Steuerungs- und Regelungstechnik
9 Elektronik/Mikro- und Nanotechnik
10 Informatik/Kommunikation
11 Schwingungstechnik
12 Verkehrstechnik/Fahrzeugtechnik
13 Fördertechnik/Logistik
14 Landtechnik/Lebensmitteltechnik
15 Umwelttechnik
16 Technik und Wirtschaft
17 Biotechnik/Medizintechnik
18 Mechanik/Bruchmechanik
19 Wärmetechnik/Kältetechnik
20 Rechnerunterstützte Verfahren (CAD, CAM, CAE CAQ, CIM ...)
21 Elektrotechnik
22 Mensch-Maschine-Systeme
23 Technische Gebäudeausrüstung

ISBN 978-3-18-3**76005**-3